NASA CONTRACTOR REPORT

NASA CR-2334

NASA CR-2334

CORRELATION OF FULL-SCALE DRAG PREDICTIONS WITH FLIGHT MEASUREMENTS ON THE C-141A AIRCRAFT - PHASE II, WIND TUNNEL TEST, ANALYSIS, AND PREDICTION TECHNIQUES

Volume 2 - Wind Tunnel Test and Basic Data

by D. G. MacWilkinson, W. T. Blackerby, and J. H. Paterson

Prepared by
LOCKHEED-GEORGIA COMPANY
Marietta, Ga. 30063
for Langley Research Center

NATIONAL AERONAUTICS AND SPACE ADMINISTRATION • WASHINGTON, D. C. • FEBRUARY 1974

1. Report No.	2. Government Accession No.	3. Recipient's Catalog No.
NASA CR-2334		

4. Title and Subtitle	5. Report Date
CORRELATION OF FULL-SCALE DRAG PREDICTIONS WITH FLIGHT MEASUREMENTS ON THE C-141A AIRCRAFT - PHASE II, WIND TUNNEL TEST, ANALYSIS, AND PREDICTION TECHNIQUES VOLUME 2. WIND TUNNEL TEST AND BASIC DATA	February 1974
	6. Performing Organization Code

7. Author(s)	8. Performing Organization Report No.
D. G. MacWilkinson, W. T. Blackerby and J. H. Paterson	LG73ER0058
	10. Work Unit No. 501-06-09-01

9. Performing Organization Name and Address	11. Contract or Grant No.
Lockheed-Georgia Company Marietta, Georgia	NAS1-10045
	13. Type of Report and Period Covered
12. Sponsoring Agency Name and Address	Contractor Report
National Aeronautics and Space Administration Washington, D. C.	14. Sponsoring Agency Code

15. Supplementary Notes

This is one of two final reports.

16. Abstract

A research program has been conducted to determine the degree of cruise drag correlation on the C-141A aircraft between predictions based on wind-tunnel test data, and flight test results. Volume 2 contains information on the wind-tunnel test program and basic aerodynamic data on the C-141A wind-tunnel model used in the correlation studies described in Volume 1. The model was tested in the NASA Langley 8-foot transonic wind tunnel.

17. Key Words (Suggested by Author(s))	18. Distribution Statement
C-141A Wind-Tunnel Test Langley 8-Foot Transonic Tunnel	Unclassified-Unlimited

19. Security Classif. (of this report)	20. Security Classif. (of this page)	21. No. of Pages	22. Price*
Unclassified	Unclassified	185	Domestic, $5.25 Foreign, $7.75

*For sale by the National Technical Information Service, Springfield, Virginia 22151

CONTENTS

	Page
INTRODUCTION	1
WIND TUNNEL TEST	1
Facility	1
Model and Instrumentation	1
Model Support Configurations	2
Test Conditions and Program	3
Data Reduction and Corrections	4
BASIC AERODYNAMIC DATA	5
General	5
Flow Angularity. Test 617	5
Repeatability. Test 617	5
Complete Model Baseline Data. Test 617	6
Support Tare and Interference Data. Test 617	6
Basic Data. Test 591	6
Aft Located Transition. Test 617	6
Miscellaneous Data. Test 617	7
Afterbody Pressure Data	7
REFERENCES	8

INTRODUCTION

This volume contains information on the wind tunnel test program and basic aerodynamic data on the C-141A configuration used in the correlation studies described in Volume 1. The Lockheed-Georgia Company was contracted to prepare an existing C-141A high-speed wind tunnel model for installation and test in the NASA Langley 8-foot transonic tunnel. This program was divided into two principal phases, and due to scheduling requirements at the Langley facility, the acquisition and analysis of data from both tests was conducted at intervals over a period from June 1971 to March 1973.

WIND TUNNEL TEST

Facility

The investigation of the C-141A model was made in the NASA Langley 8-foot transonic pressure wind tunnel. This is a single-return closed-circuit tunnel. The test section is square in a cross section whose sides measure 7.1 feet (2.16m). The upper and lower walls are axially slotted to permit a variable test section Mach number from about 0.20 to 1.30, with negligible effects of choking and blockage. The total pressure can be varied from a minimum value of about 0.2 atmosphere (0.2×10^5 N/m^2) at all test Mach numbers, to a maximum value of 1.5 atmospheres (1.52×10^5 N/m^2) at transonic Mach numbers. The stagnation temperature of the air is automatically controlled and is usually held constant at 120°F (49°C). The tunnel air is dried until the dew point temperature in the test section is reduced sufficiently to avoid condensation effects. The resulting maximum Reynolds number available was approximately 6×10^6 per foot (19.7×10^6 per meter) for this program.

Model and Instrumentation

An existing 0.0275-scale C-141A model was used for the wind tunnel investigation. This was modified to accommodate a new support system, in which the model was supported by a thin load-bearing blade from the lower fuselage and attached to a support sting below the model. In addition, adaptor blocks were designed and fabricated to locate the NASA strain gaged balance, and two fuselage afterbody fairings of identical geometries were available to meet the requirements for testing with the NASA dorsal support system and the blade/sting system. In other respects, the principal model components were the same as those that were manufactured and tested during the C-141A design and development program in the early 1960s. Details of the model dimensions are given in table 1.

The Langley Research Center provided a 2.0 inch (5.08 cm) balance (No. 837) for measuring six-component total model loads. In addition, a secondary 1.5-inch (3.81 cm) balance was used to measure blade loads. The standard fuselage afterbody contained two scanivalves for measuring pressures from 67 static orifices on the external afterbody surface, and from 16 orifices inside the fuselage. The layout of these orifices is shown in figures 1 (a) and 1 (b). The alternative configuration with a dorsal support measured a total of 44 static pressures on the afterbody, and 18 internal pressures through one scanivalve located in the afterbody and one inside a wheelwell fairing.

The model angle-of-attack was measured by two servo-accelerometers during both test phases. A Kearfott servo accelerometer was located in the model nose and was the principal instrumentation from which the final force data was computed. A back-up system was provided by an Endevco servo-accelerometer located in the wheelwell fairing.

Model Support Configurations

Details of the principal model configurations are given in figures 2 through 6. Figure 2 shows the model mounted on the live blade and sting combination of support configuration 1. This configuration measured the model loads plus the mutual aerodynamic interference effects of the blade/sting combination and the model. Configurations 2, 3 and 4, (not shown) were obtained by locating the blade at the three alternative sets of holes indicated in figure 2, thus giving an increasing model-to-sting displacement for evaluation of the sting interference effects on the model. The vertical displacements of the sting center line from the model fuselage reference line were as follows: Sting position 1, 10.79 inches (0.274 m), position 2, 14.20 inches (0.361 m), position 3, 18.49 inches (0.47 m) and position 4, 22.79 inches (0.578 m). Figure 3 gives details of configuration 5. In this case, the model was mounted on the dorsal strut, and the blade attached directly to the balance so that model and blade loads and mutual interference effects between the model and blade could be measured. Configuration 6 (not shown) was defined as this same configuration, but with the blade removed.

In order to measure the load on the blade separately on configuration 7 (figure 4), the model was attached directly to the dorsal strut and the blade attached to the smaller balance. In addition to the blade load, the interference of the model on the blade is included in this measurement.

In configuration 8 (figure 5), the model was supported by the dorsal strut, and the dummy blade and sting attached as in configurations 1 through 4, but with the blade positioned in a cavity on the fuselage underside with a small gap between the blade and model. Tests were conducted with different seal configurations in the cavity. Configuration 9, (figure 6), was included in the test program to evaluate the effects of the 12-inch (0.305 m) offset fairing on the model. This offset was part of the standard configuration for the main test program. In configuration 9, the support sting was located with its center-line along

the tunnel center-line, and the bullet fairing was therefore not required.

An additional configuration was included during the test program, and designated No. 10. This was obtained from configuration 8 by removing the blade so that measurements could be made with the lower sting only in position.

Test Conditions and Program

Transition was fixed on all model surfaces by 0.05-inch (0.125 cm) bands of ballotini glass beads set into a thin layer of lacquer. The choice of bead size was based on previous extensive experience on transition fixing for high speed drag evaluation during the C-5A development program.

Work by Braslow (reference 1) at NASA Langley has shown that it is possible to obtain essentially a zero-drag penalty due to the transition strip providing narrow, sparsely distributed bands of roughness are used. The roughness size for a given Reynolds number is determined according to the criterion $R_k \geq 600$, the critical roughness Reynolds number based on roughness height, k, the velocity at the top of the roughness, u_k, and the kinematic viscosity at the top of the roughness, ν_k.

Results for the C-5A tests, reference 2, showed that for a Reynolds number $\geq 3 \times 10^6$ per foot (10×10^6 per meter) and a corresponding range of R_x values from 0.2×10^6 to 0.4×10^6 ((bead size 0.0021 inches (0.0053 cm) to 0.0045 inches (0.0114 cm)) no measurable increase in drag was obtained with transition of the boundary layer occuring immediately downstream of the roughness at all conditions. These results suggested that for the C-141A testing over a Reynolds number range from 3×10^6 per foot (10×10^6 per meter) to 5×10^6 per foot (16.4×10^6 per meter), and for a chosen value of R_x based on ten percent wing MAC, a bead size of 0.0038 inches (0.00965 cm) was required. Further, it was concluded that no evaluation of drag due to transition fixing was necessary as a result of the C-5A data. Transition strips were placed on all C-141A model components, except the fuselage and wheel well fairings, at a distance of 0.73 streamwise inches (1.855 cm) back from the leading-edges. The transition strips on the fuselage and wheel well fairings were placed 2 inches (5.08 cm) and 1.5 inches (3.80 cm) respectively from the nose of those components.

Additional tests were completed with transition located further aft on the wing upper surface and approximately ten percent local chord ahead of the wing shock wave at cruise conditions. The roughness size was 0.0054 inches (0.0137 cm). This technique was included in order to improve the simulation of the interaction of shock and boundary layer at high Mach number drag-rise conditions, where forward transition is known to induce a premature rear separation at low Reynolds numbers for this wing design. Flow visualization tests, wing upper surface transition free, were conducted to locate the main shock position for this investigation.

The tests, in general, covered the Mach number range from M = 0.600 to 0.825. In most cases, the Reynolds Number was 5.0×10^6/foot (16.4×10^6/meter) or 3.05×10^6/MAC.

Scale effects were obtained on some configurations by testing also at 3.0 and 4.0 x 10^6/ foot (10 x 10^6 and 13.12 x 10^6/meter). Six-component force measurements were obtained at zero yaw over an angle-of-attack range from -4° (-0.0619 rad) to +4° (0.0619 rad). Selected configurations also included measurements of the fuselage afterbody and balance cavity pressures.

A summary of the test program is given in table 2. Examples of two model configurations, Nos. 4 and 8, showing the installation in the Langley 8 foot tunnel, are given in the photographs of figures 7 and 8.

Data Reduction and Corrections

Force balance data was reduced to coefficient form in the stability axis system using a reference wing area of 2.44 square feet (0.227 square meters), and a mean aerodynamic chord of 7.328 inches (18.62 cm). Pitching moment was referred to a c.g. position of 25 percent MAC.

The accuracy of the strain gaged balance measurements was based on the manufacturers quoted figure of ±0.5% of the full-scale rating of the balance. The estimated accuracy of the C-141A model force data based on maximum balance loads is

$$C_A = \pm 0.0005$$

$$C_N = \pm 0.0060$$

$$C_M = \pm 0.0011$$

Subsequent test results, however, have suggested somewhat better accuracy levels than these figures. For example, repeatability of drag in a given test series is shown to be of the order of 0.0001 to 0.0002 in C_D. The accuracy of the angle-of-attack measurements is estimated to be ±0.01 degrees (0.0001745 rad).

Corrections have been made to the data for test section flow angularity ((0.065° (0.001135 rad) downflow)) and wall constraint interference on lift, given as:

$$\Delta\alpha = 0.074\, C_N, \text{ degrees}$$

A set of empty tunnel buoyancy corrections were applied to the final correlation results in volume 1 of this report. These had the effect of increasing the final drag data from $\Delta C_D = 0.00036$ at $M = 0.700$ to 0.00032 at $M = 0.825$. All basic data presented in volume 2 of this report have been corrected for angularity and wall constraint effects only, but not for bouyancy.

Blockage effects were assumed to be negligible for this installation, based on experience gained by NASA personnel at the Langley 8-foot facility, and consequently no corrections were applied to the test data.

BASIC AERODYNAMIC DATA

General

The presentation of basic aerodynamic data includes results from two principal test phases. Test 591 was conducted in June 1971 and Test 617 in September 1972. A further short series of tests was completed in March 1973, and designated as a continuation of the previous 617 series.

During testing in the 591 series, some doubt arose concerning the validity of the absolute drag level from the basic tail-off configurations due to suspected model fouling. This was confirmed during the 617 series, when it was found that the drag levels of the tail-on and off baseline configuration were approximately $\Delta C_D = 0.0010$ and 0.0006, respectively, lower than the 591 data. As a final check on the validity of the initial 617 data, the retest of the model tail-off configuration during March 1973 confirmed these results. It should be noted that the basic data given in this volume indicate these discrepancies from both test series. However, the subsequent analysis used only some limited component drag and trim drag increments from the 591 test, and the main analysis was concentrated on the test 617 results.

Flow Angularity. Test 617

Lift, pitching moment and drag data for model upright and inverted runs are shown in figures 9 (a), (b) and (c). These data have been corrected for the flow angularity and indicate good agreement over the full Mach number range of the tests.

Repeatability. Test 617

Examples of the degree of test data repeatability during the 617 series are given in figures 10 (a-d). In general, values of drag are repeated within $\Delta C_D = 0.0001$ to 0.0002. Figure 10 (d) shows the repeatability of the afterbody pressures by a comparison of integrated results from both tests.

Complete Model Baseline Data. Test 617

Figures 11 (a-d) present some of the complete model baseline data which was used in the analysis and drag correlation studies in volume 1. These data were obtained after the model wing surface finish was prepared to a high degree of smoothness and a new transition strip applied prior to this main series of runs. Comparison of these data indicates only a small change in drag level of the order of $\Delta C_D = 0.0001$ for this configuration. The full set of results for the model baseline is given in figures 20 (a-d).

Support Tare and Interference Data. Test 617

Test results for configuration 7, the blade load measurements, are presented in figures 12 (a) and (b). Results from the tests with the dorsal sting arrangement, configurations 8, 6, 5 and 10 are given in figures 13 through 16. The sting interference evaluation tests results are given in figures 17 through 20, for configurations 1, 2, 3 and 4 respectively. Results for the central sting configuration, No. 9 are contained in figures 21 through 24.

Basic Data. Test 591

Selected results from the 591 series are presented in figures 25 through 33. Data for three horizontal tail settings are contained in figures 25, 26 and 27. Scale effects over a Reynolds number range from 1.83×10^6/MAC to 3.05×10^6/MAC are given in figures 28 through 30 for the complete model configuration, and those for tail-off data are shown in figures 31 and 32. The pylon-nacelle effects can be derived from the data given in Figures 33 and 34.

Aft Located Transition. Test 617

Results for the tests with wing upper surface transition moved back from the standard location to a position ten percent local chord ahead of the shock at cruise conditions, are given in figures 35, 36 and 37.

Miscellaneous Data. Test 617

The basic data from which pylon-nacelle and wing increment are derived are given in figures 34 and 38.

The effects of sting position on the aerodynamic data, tail-off, are given in figures 39 through 42.

Afterbody Pressure Data

Selected polar plots giving static pressure variation with fuselage station are shown in figures 43 through 54. These, in general, have been selected to support the discussion of afterbody pressure drag effects, for the different model support configurations, given in volume 1.

REFERENCES

1. Braslow, A. L.; Hicks, R. M.; and Harris, R. V. Jr.: Use of Grit-Type Boundary-Layer-Transition Trips on Wind-Tunnel Models. NASA TN D-3579, 1966.

2. Palfery, J. G.: C-5A High Speed Drag Reduction Study and Investigation of Fixed Boundary Layer Transition on a 0.0226 Scale Model in the NASA-Ames 11 Foot Wind Tunnel. High Speed Series 4C and 4D. Lockheed- Georgia Company Report LG1T6-1-40, April 1968.

TABLE I

MODEL DIMENSIONAL DATA

		0.0275 Scale
Fuselage, B^9		
Length, inches		43.656
Maximum diameter, inches		4.675
Fineness ratio		9.362
Fuselage reference line	WL	5.500
Nose location	FS	6.336
Bullet Fairing, b^8		
Nose location	FS	45.902
Aft end location	FS	54.148
Length, inches		8.246
Fineness ratio ($1/D_{MAX}$)		6.842
Dorsal, D^4		
Area, square feet		0.017
Root chord leading edge	FS	37.998
Horizontal Stabilizer, H^8		
Area, square feet		0.365
Span, inches		16,554
Mean aerodynamic chord, inches		3.401
Aspect ratio		5.210
Taper ratio		0.370
Sweep of 25% chord, degrees		25.000
Tail length, inches		23.885
Tail volume coefficient		0.488
Airfoil section NACA 64A(010)010.5		

MODEL DIMENSIONAL DATA (CONT.)

Nacelle Pylon, K[19]		0.0275 Scale
Inboard area, square feet		0.035
Inboard span, inches		0.916
Inboard chord, inches		5.500
Outboard area, square inches		0.036
Outboard span, inches		0.948
Outboard chord, inches		5.500
Sweep of leading edge, degrees		73.000
Thickness, percent chord		8.000
Nacelles, N[7]		
Length, inches		5.189
Inlet diameter, inches		1.403
Exit diameter, inches		1.211
Inboard Leading edge location	FS	18.195
	BL	7.813
	WL	5.300
Outboard leading edge location	FS	20.538
	BL	12.638
	WL	5.102
Inboard toe-in, degrees		2.00
Outboard toe-in, degrees		1.00
Vertical Stabilizer, V[6]		
Area, square feet		0.301
Span, inches		7.235
Mean aerodynamic chord, inches		6.102

MODEL DIMENSIONAL DATA (CONT.)

Vertical Stabilizer (Cont.)		0.0275 Scale
Aspect ratio		1.208
Taper ratio		0.617
Sweep of 25% chord, degrees		35.000
Tail length, inches		21.065
Vertical tail volume coefficient		0.049
Airfoil section	NACA 64A(012)013	

Wing, W^{12}		
Area, square feet		2.440
Span, inches		52.689
Mean aerodynamic chord, inches		7.328
Aspect ratio		7.900
Taper ratio		0.373
Sweep of 25% chord, degrees (inboard)		23.734
25% mean aerodynamic chord location	FS	25.378
	WL	7.268
	BL	10.818
Sweep of 25% chord, degrees (outboard)		25.025
Incidence, degrees		4.891
Twist, degrees		-5.584
Dihedral of 25% chord, degrees (inboard)		0.941
Dihedral of 25% chord, degrees (outboard)		1.195
Root chord, inches		10.911
Break station chord, inches (inboard)		6.619
Break station chord, inches (outboard)		6.487
Break station location (inboard)	WS	11.138
Break station location (outboard)	WS	11.734

MODEL DIMENSIONAL DATA (CONT.)

Wing (Cont.) — 0.0275 Scale

Airfoil section

Root NACA 0013.0-1.10-40/1.575 (MOD) $a_o = 0.8$ (MOD) $C_{l_i} = 0.153$

Inboard break NACA 0011.2-1.10-40/1.575 (MOD) $a_o = 0.8$ (MOD) $C_{l_i} = 0.194$

Outboard break NACA 0011.0-1.10-40/1.575 (MOD) $a_o = 0.8$ (MOD) $C_{l_i} = 0.201$

Tip NACA 0010.0-2.20-40/1.575 (MOD) mean line 1/2 (NACA 66 at C_{l_i} = 1.0-NACA 230 at $C_l = 1.0$ $C_{l_i} = 0.452$)

Antenna Fairing, Z^{a1}

Leading edge location	FS	26.208
Trailing edge location	FS	33.468

Wheelwell Fairing, Z^{G2I}

Length, inches		11.110
Maximum frontal area per side, square inches		2.922
Fineness ratio		5.760
Leading edge location	FS	21.835

Wing-Fuselage Fillet, Z^{W7}

Leading edge location	FS	15.286
Trailing edge location	FS	30.970

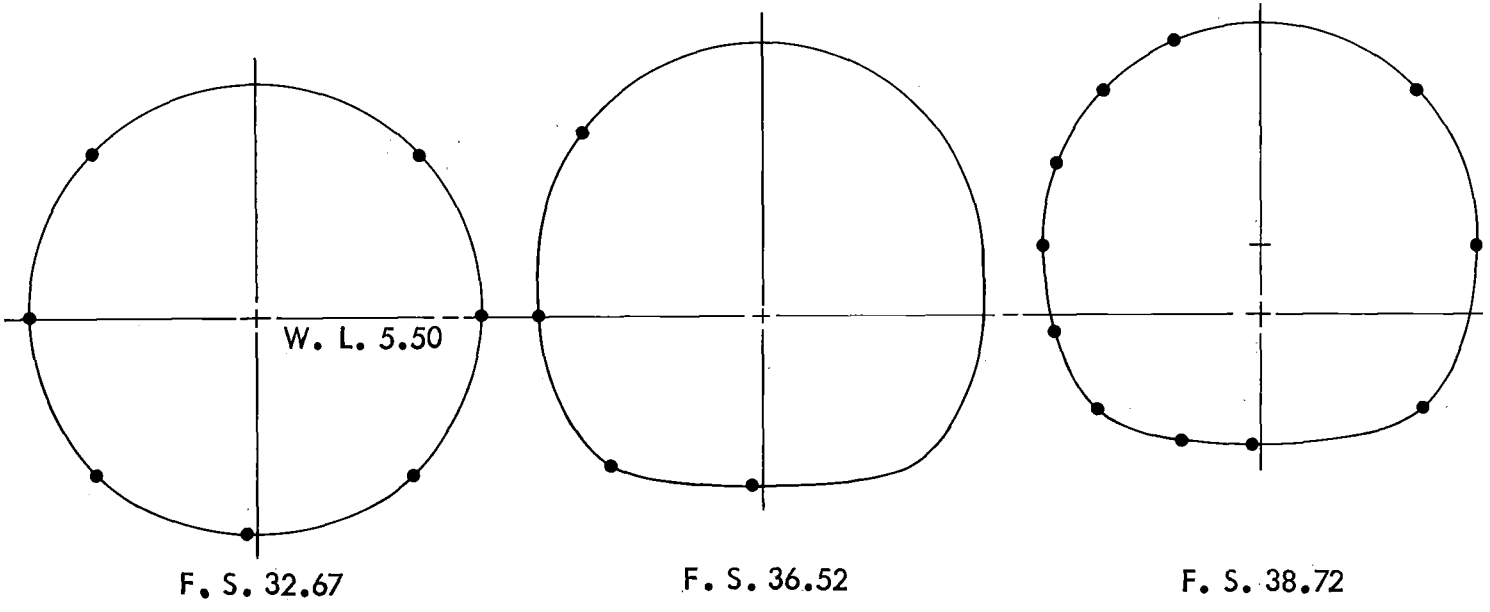


Figure 1(a). Layout of External Static Pressure Orifices on Afterbody. Configurations 1,2,3,4,9.

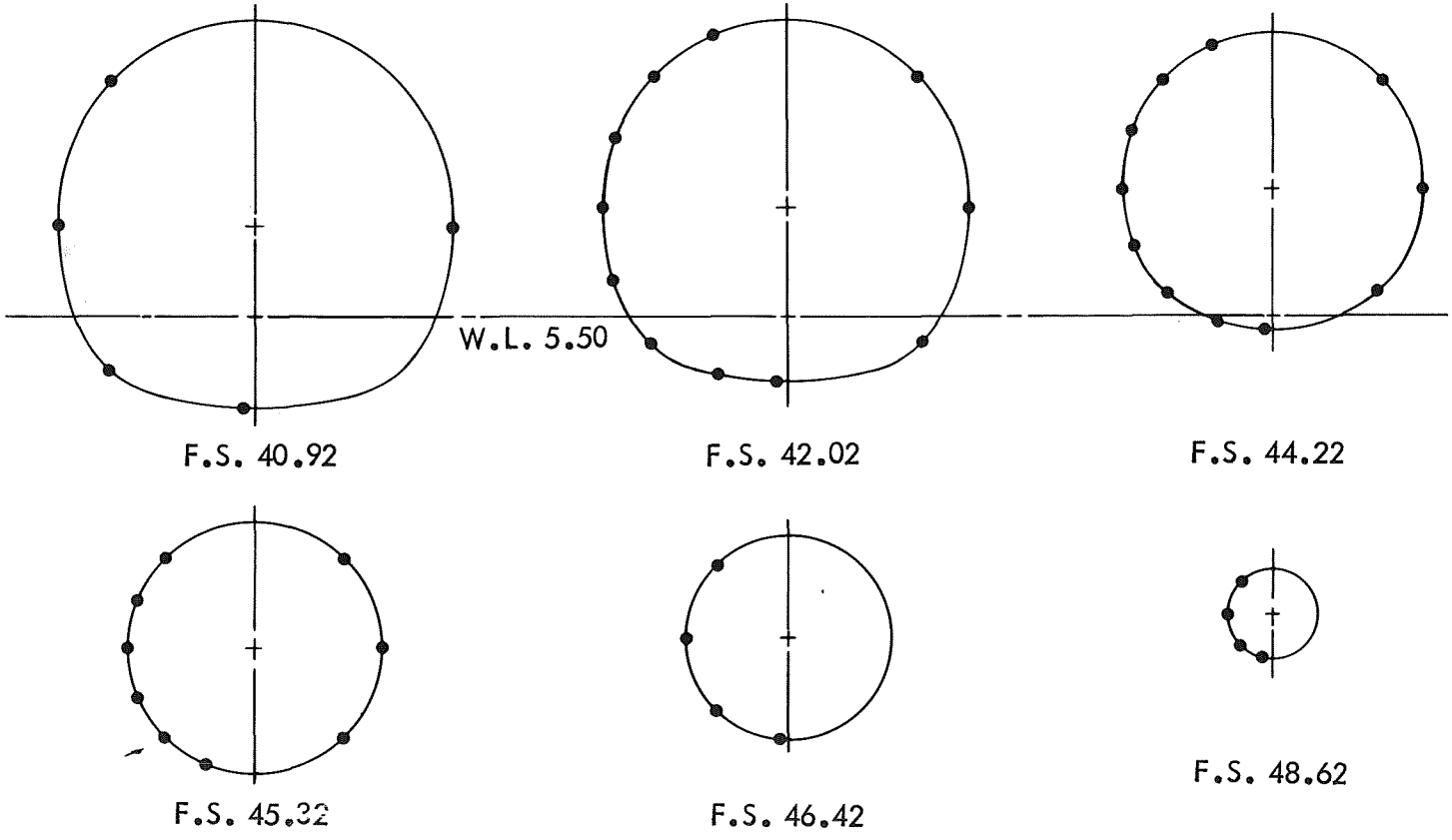


Figure 1(b). Concluded

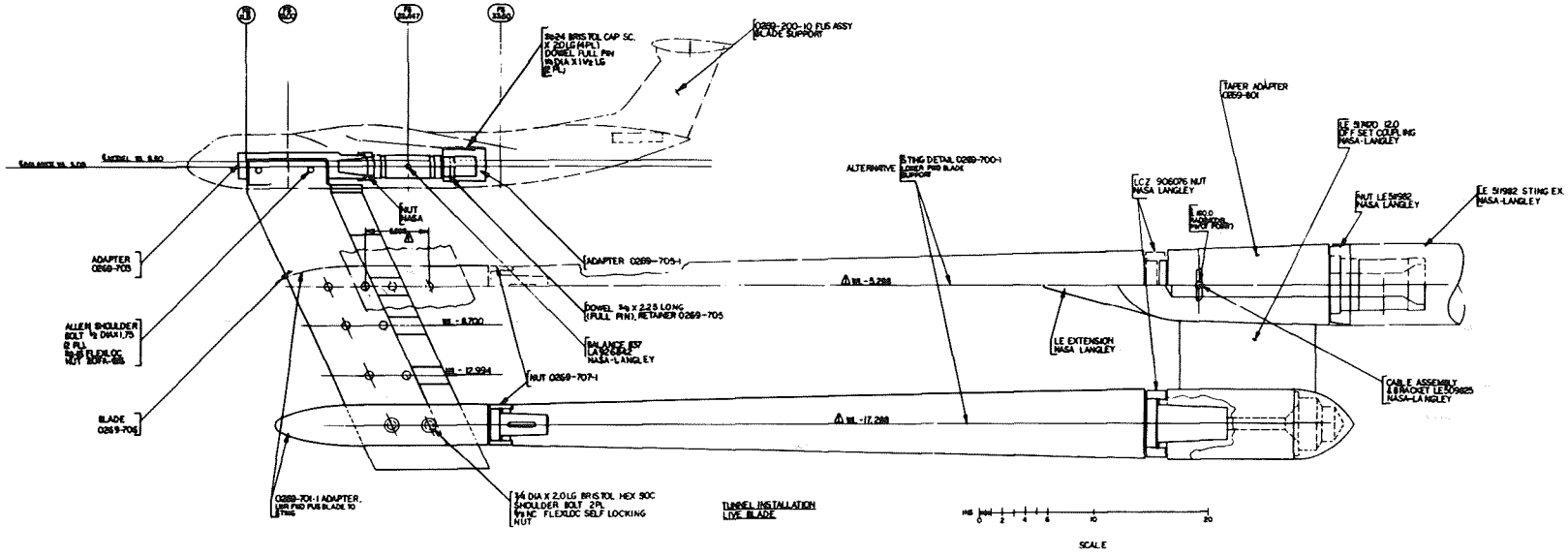


Figure 2. Model Support Configuration 1,2,3 or 4

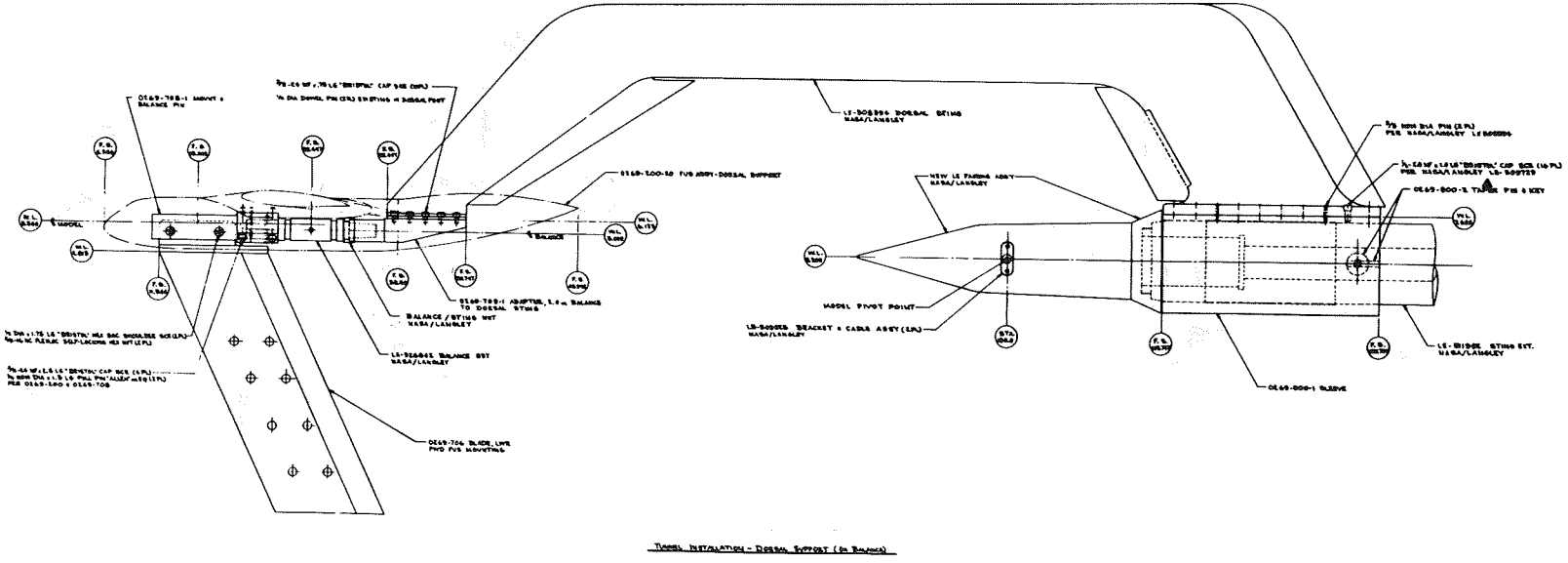


Figure 3. Model Support Configuration 5

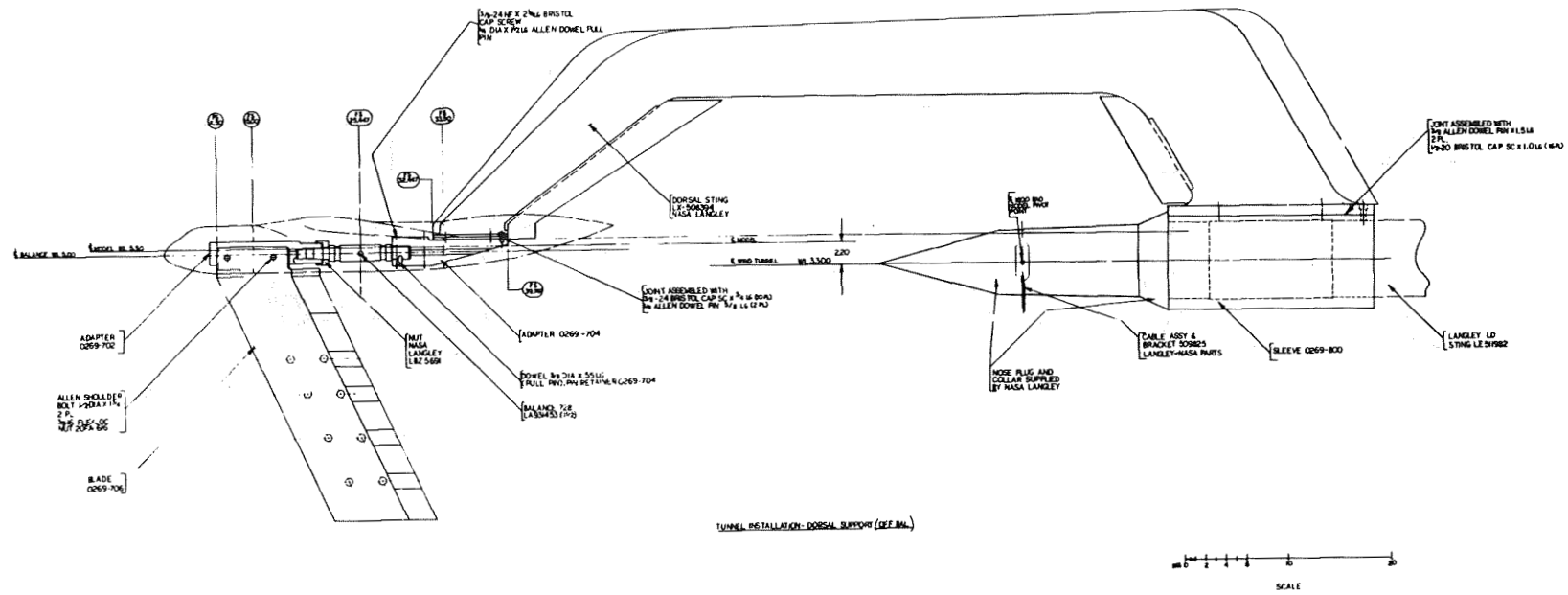


Figure 4. Model Support Configuration 7

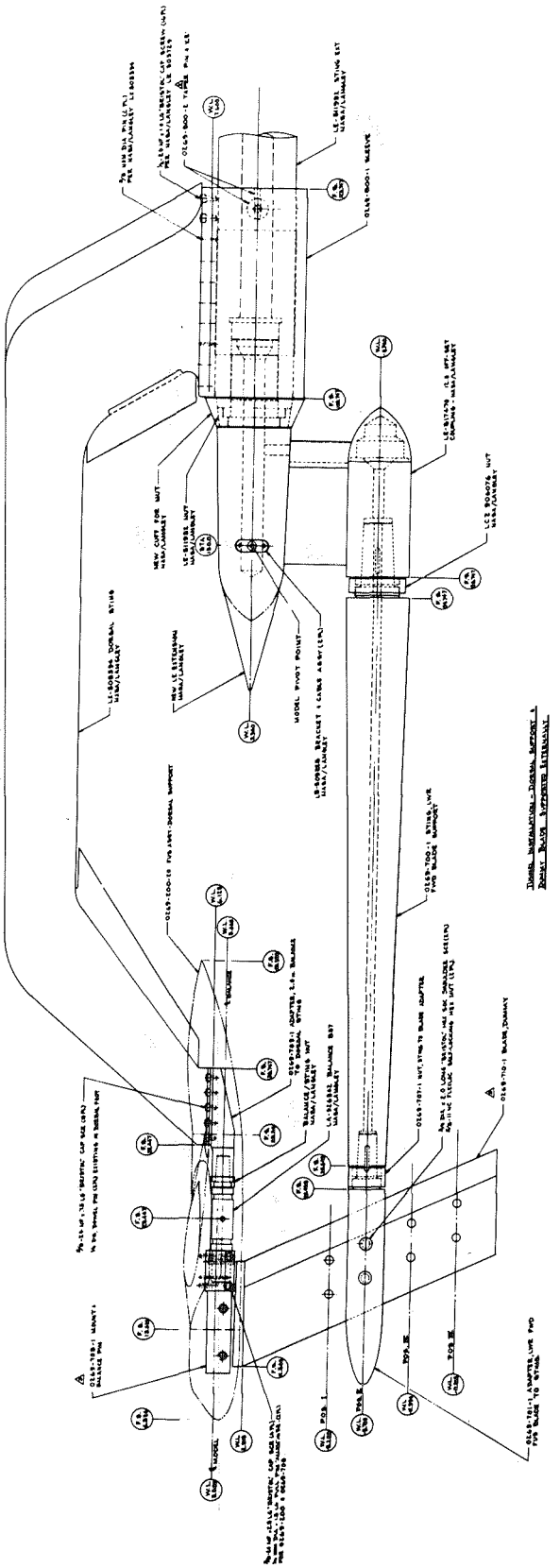


Figure 5. Model Support Configuration 8

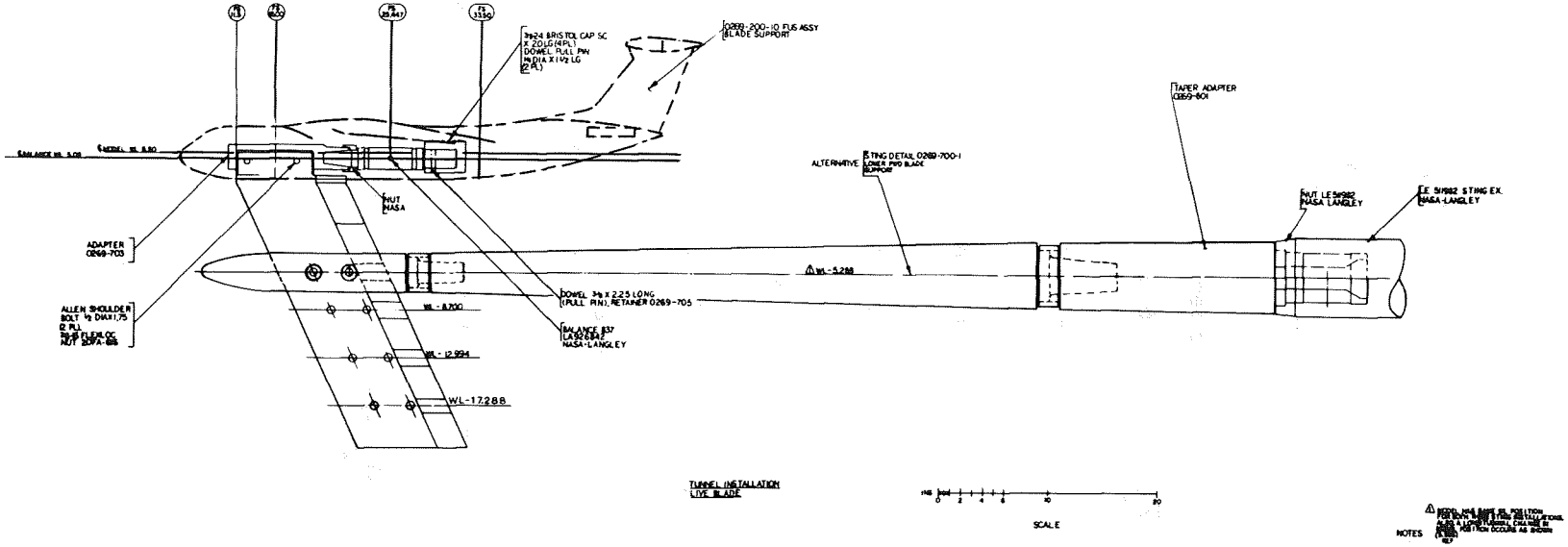


Figure 6. Model Support Configuration 9

TABLE 2

WIND TUNNEL TEST SCHEDULES

(A) TEST 591

Description	Support Config.	R_N/Ft x 10^{-6}	Run Nº At Mach Nº .600	.700	.750	.775	.785	.800	.825
$B^9W^{12}_ZW7K^{19}N^7Z^{a1}_ZG21$	2	5.0	1/8	7	6	5	4	3	2
" " " " " " " (Inverted)	2	5.0	16	15	14	13	12	11	10
$B^9W^{12}_ZW7K^{19}N^7Z^{a1}_ZG21D^4V^6H^8_{-1}b^8$	1	5.0	-	34	33	31	32	30	29
" " " " " " " " " " "	2	5.0	28	27	24	23	26	25	22
" " " " " " " " " " "	3	5.0	41	40	39	38	37	36	35
" " " " " " " " " " "	4	5.0	48	47	46	45	44	43	42
$B^9W^{12}_ZW7K^{19}N^7Z^{a1}_ZG21D^4V^6H^8_0b^8$	4	5.0	55	54	53	52	51	50	49
" " " " " " " " " " H^8_{+1} "	4	5.0	62	61	60	59	58	57	56
" " " " " " " " " " H^8_{-1} "	4	5.0	69	68	67	66	65	64	63
$B^9W^{12}_ZW7K^{19}N^7Z^{a1}_ZG21D^4V^6H^8_{-1}b^8$	4	5.0	73	72	-	71	70	-	-
" " " " " " " " " " "	4	4.0	74	75	-	76	77	-	-
" " " " " " " " " " "	4	3.0	81	80	-	79	78	-	-
$B^9W^{12}_ZW7K^{19}N^7Z^{a1}_ZG21$	4	3.0	85	84	-	83	82	-	-
" " " " " " "	4	5.0	86	87	-	88	89	-	-
$B^9W^{12}_ZW7Z^{a1}_ZG21$	4	5.0	93	92	-	91	90	-	-
B^9Z^{G21}	4	5.0	97	96	-	95	94	-	-

(B) TEST 617

Description	Support Config.	$R_N/Ft \times 10^{-6}$	Run Nº At Mach Nº .600	.700	.750	.775	.785	.800	.825
$B^9W^{12}K^{19}N^7Z^{a1}{}_ZG^{21}{}_ZW^7$ (Inverted)	2	5.0	-	45	44	43	-	42	-
" " " " " " "	2	5.0	-	51	50	49	48	47	46
$B^9W^{12}K^{19}N^7Z^{a1}{}_ZG^{21}{}_ZW^7$ Blade Seal	7	5.0	7	6	5	4	3	2	1
" " " " " " " " No Seal	7	5.0	12	-	11	-	10	-	9
" " " " " " " " "	8	5.0	19	18	17	16	15	14	13
" " " " " " " " "	6	5.0	26	25	24	23	22	21	20
" " " " " " " " "	5	5.0	33	32	31	30	29	28	27
" " " " " " " " Blade Seal	5	5.0	-	35	-	-	34	-	36
" " " " " " " " "	10	5.0	-	39	40	-	38	41	37
$B^9W^{12}K^{19}N^7Z^{a1}{}_ZG^{21}{}_ZW^7D^4V^6H^8_{-1}b^8$	4	5.0	-	60	59	58	57	56	55
" " " " " " " " " " " H^8_{+2} "	4	5.0	-	69	68	67	66	65	64
$B^9W^{12}Z^{a1}{}_ZG^{21}{}_ZW^7$	4	3.0	73	72	-	71	70	-	-
B^9Z^{G21}	4	3.0	77	76	-	75	74	-	-
B^9	4	3.0	82	81	-	80	79	-	-
B^9	4	5.0	86	85	-	84	83	-	-
$B^9W^{12}K^{19}N^7Z^{a1}{}_ZG^{21}{}_ZW^7D^4V^6H^8_{-1}$ b^8	4	5.0	-	93	92	91	90	89	-
" " " " " " " " " " " "	3	5.0	-	126	125	124	123	122	-
" " " " " " " " " " " "	2	5.0	-	121	120	119	118	117	-
" " " " " " " " " " " "	1	5.0	-	116	115	114	113	112	-

(B) TEST 617 CONTINUED

Description	Support Config.	$R_N/Ft \times 10^{-6}$	Run Nº At Mach Nº .600	.700	.750	.775	.785	.800	.825
$B^9W^{12}K^{19}N^7Z^{a1}_{Z}G^{21}_{Z}W^7D^4V^6H^8_{-1}b^8$	4	*5.0	-	99	98	97	96	95	94
" " " " " " " " " " H^8_0 "	4	*5.0	-	105	104	103	102	101	100
" " " " " " " " " " H^8_{+1} "	4	*5.0	-	111	110	109	108	107	106
$B^9W^{12}K^{19}N^7Z^{a1}_{Z}G^{21}_{Z}W^7D^4V^6H^8_{-1}b^8$	9-1 ≠	5.0	-	134	133	132	131	130	-
" " " " " " " " " " "	9-2 ≠	5.0	-	137	-	136	-	135	-
" " " " " " " " " " "	9-3 ≠	5.0	-	140	-	139	-	138	-
" " " " " " " " " " "	9-4 ≠	5.0	-	143	-	142	-	141	-
$B^9W^{12}K^{19}N^7Z^{a1}_{Z}G^{21}_{Z}W^7$	1	5.0	-	178	177	176	175	174	173
" " " " " " " "	2	5.0	-	172	171	170	169	168	167
" " " " " " " "	3	5.0	-	166	165	164	163	162	161
" " " " " " " "	4	5.0	-	160	159	158	157	156	155

* Transition Strip Moved Back to 10% Local Chord Ahead of Shock.
≠ Central Sting - No Offset.

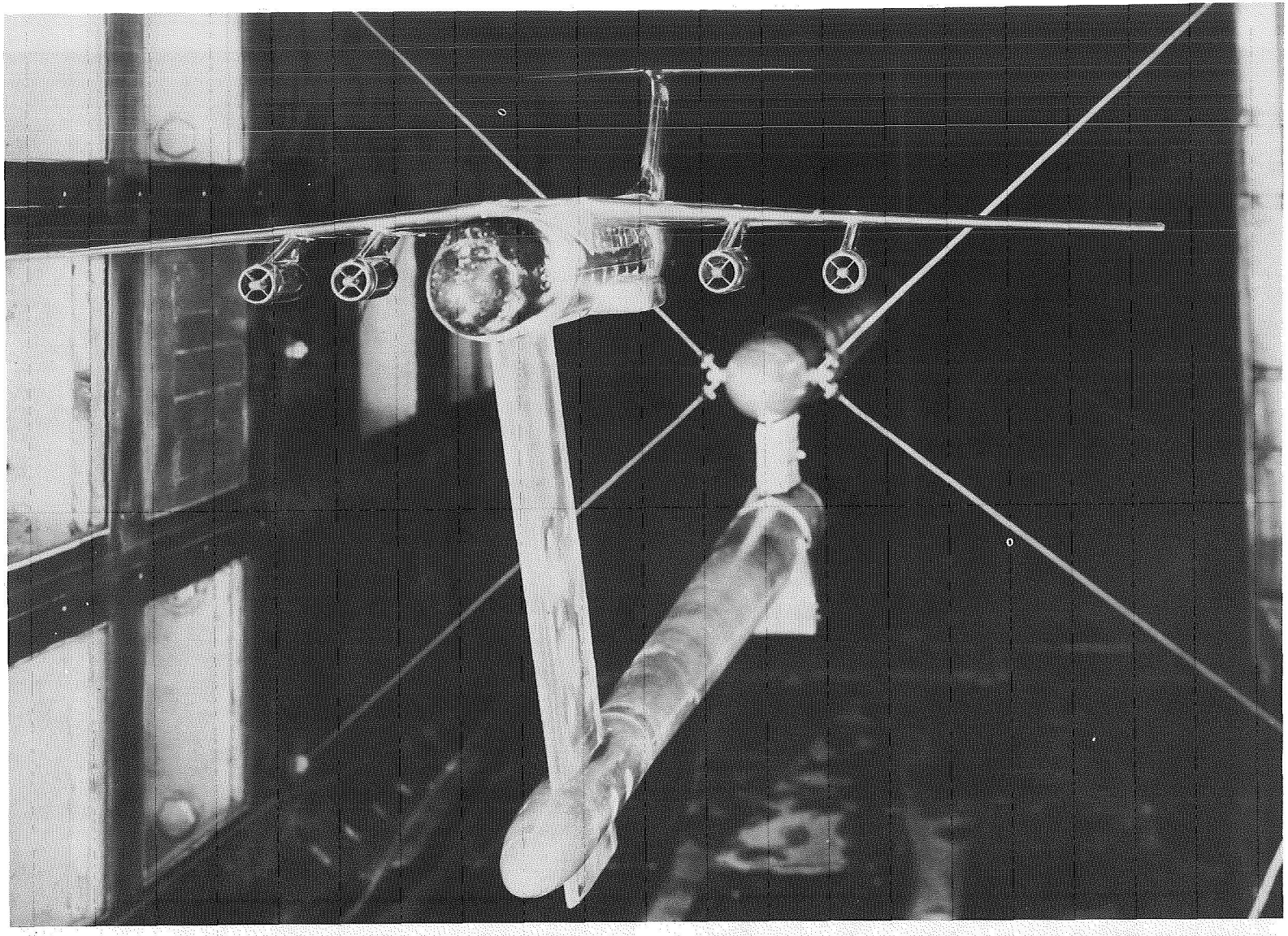


Figure 7. Model Installed in Langley 8-Foot Tunnel. Configuration 4

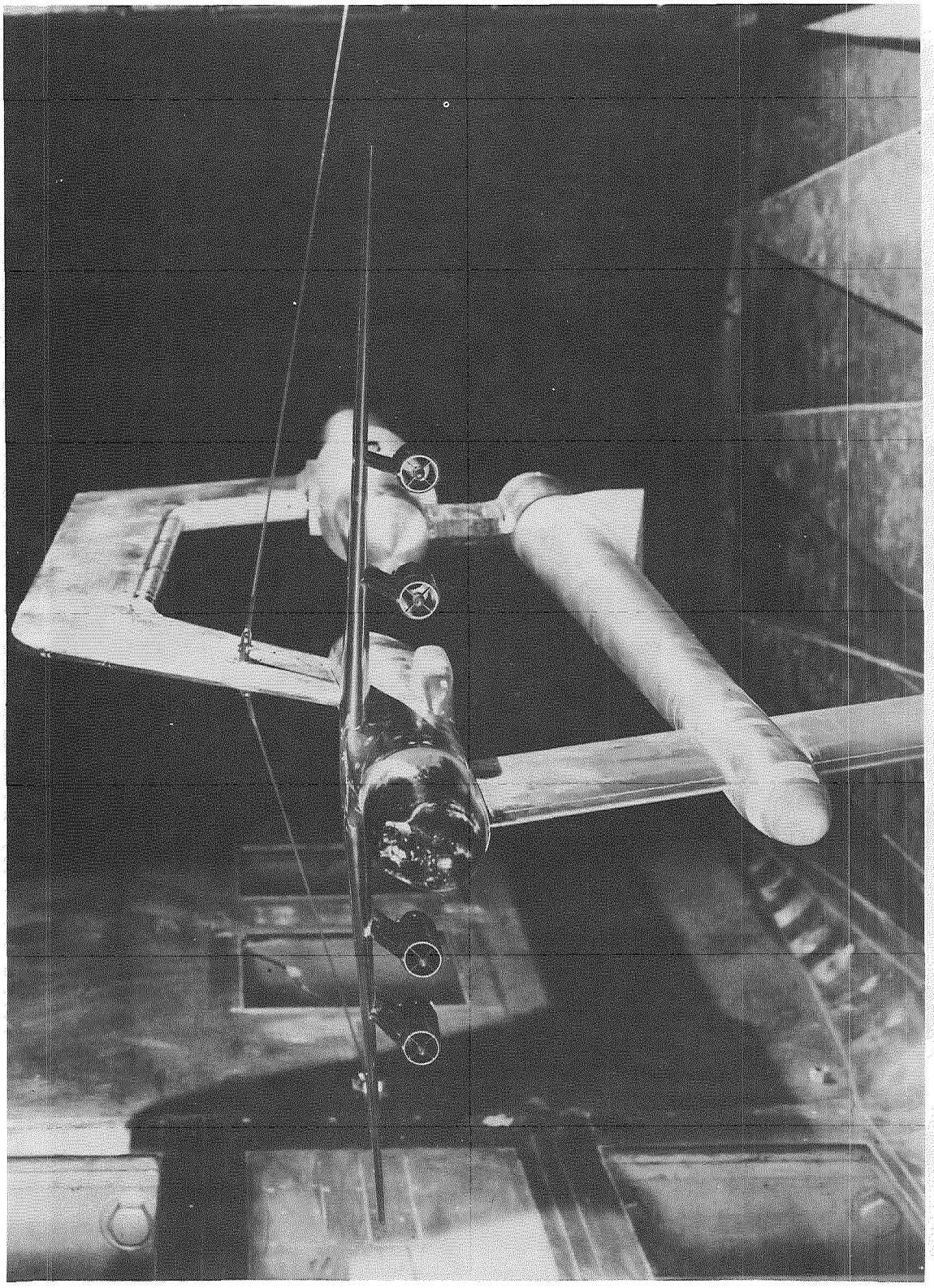
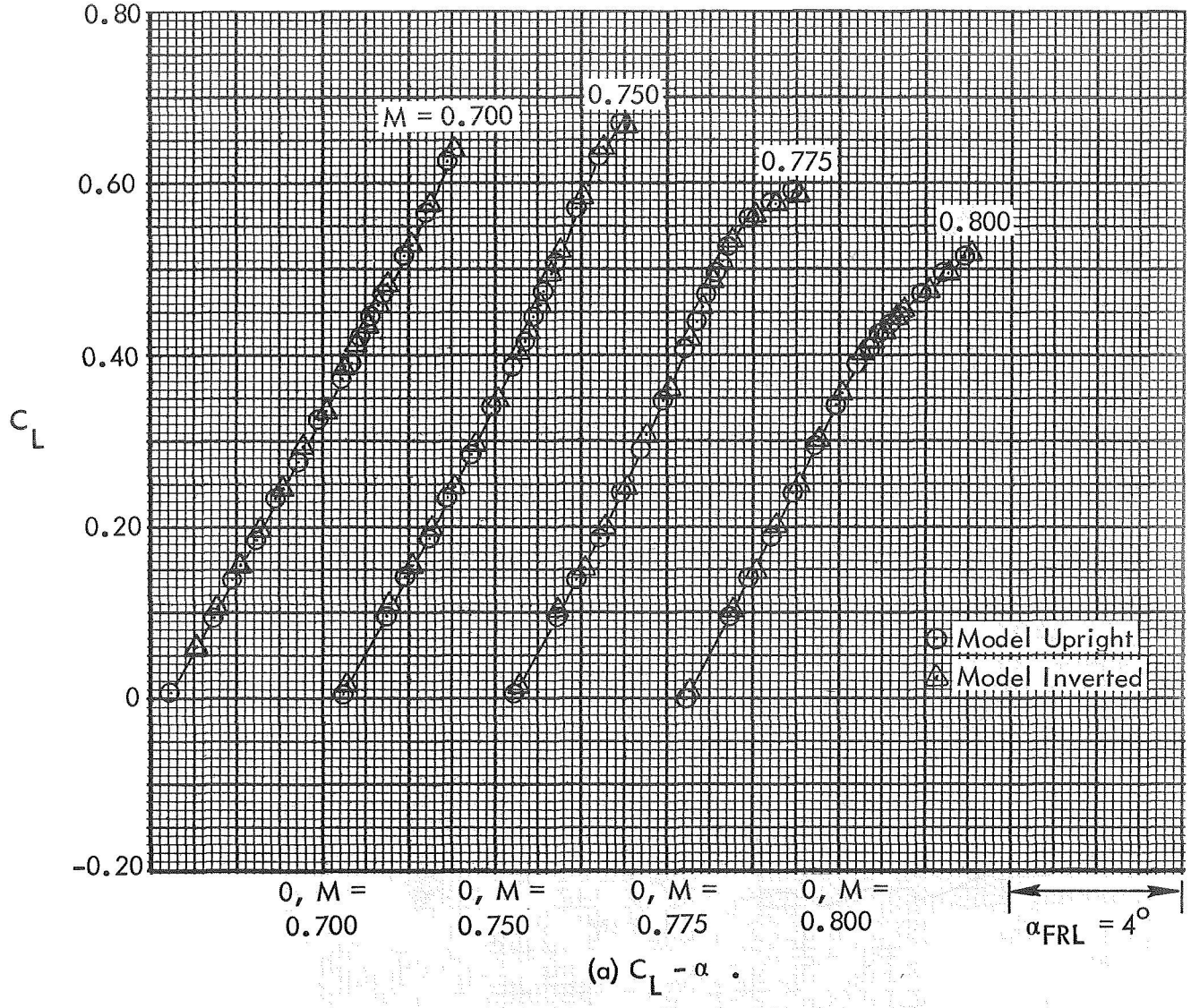
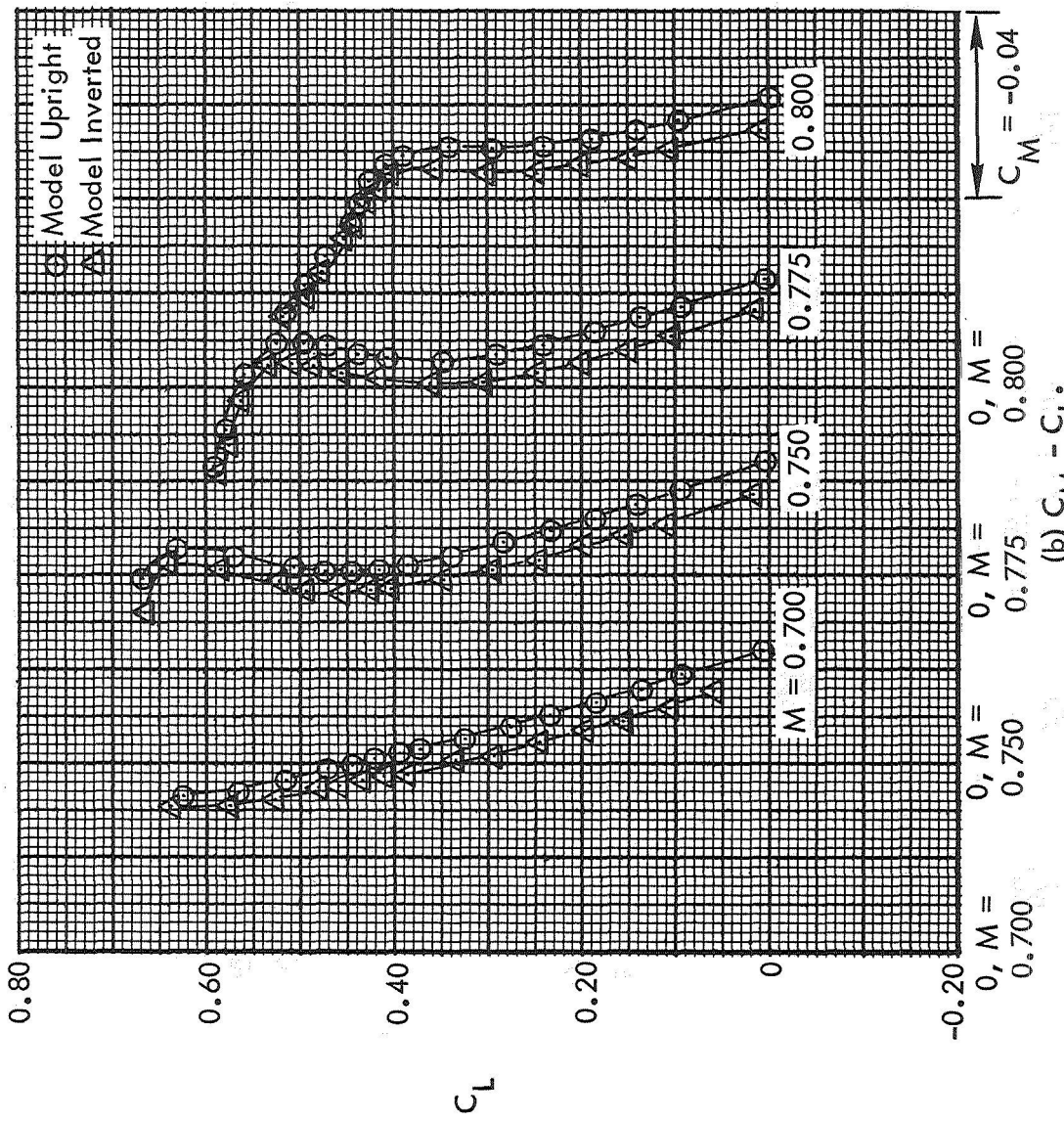


Figure 8. Model Installed in Langley 8-Foot Tunnel. Configuration 8



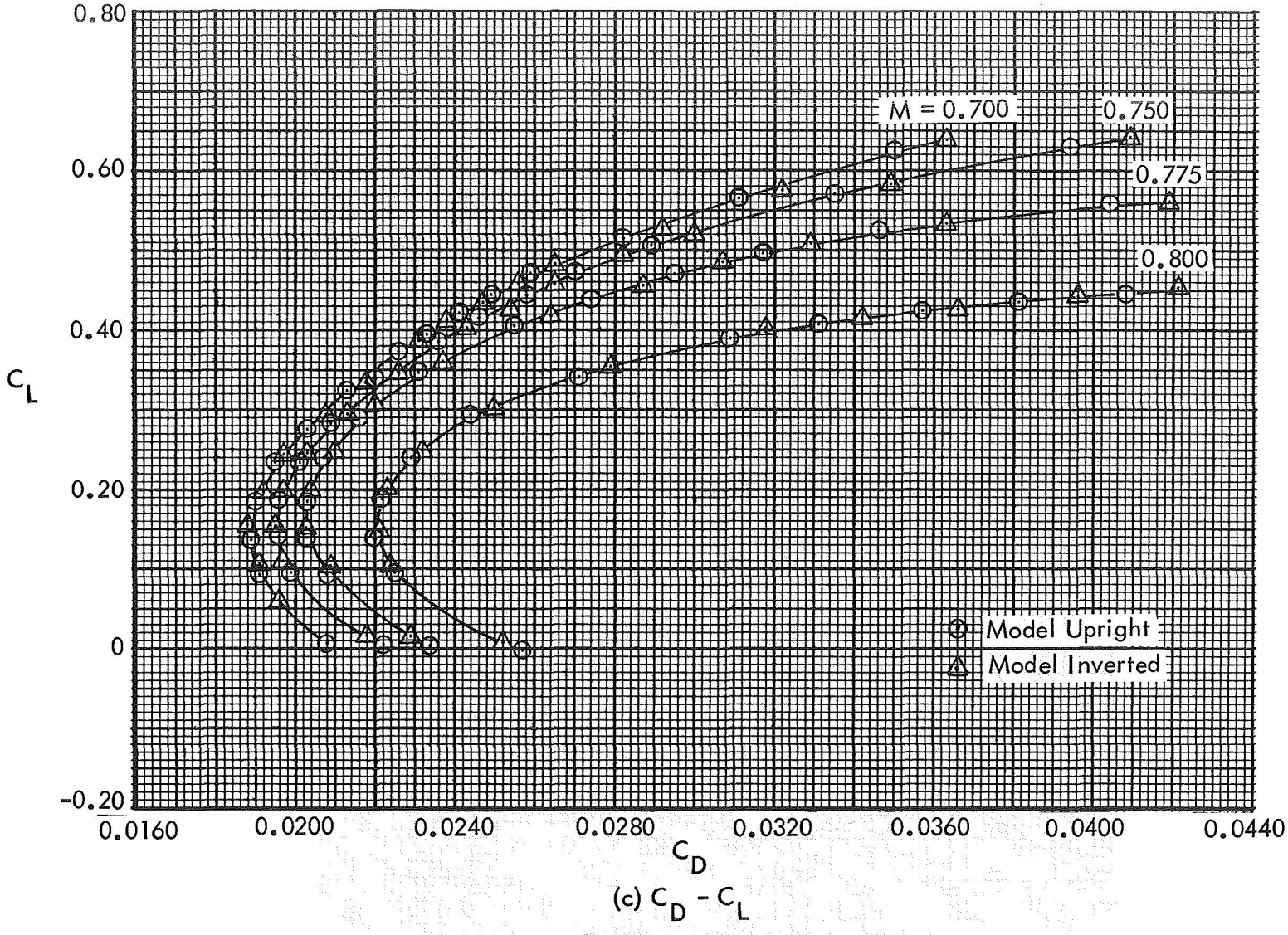
(a) $C_L - \alpha$.

Figure 9. Comparison of Model Upright & Inverted Test Data. Test 617.



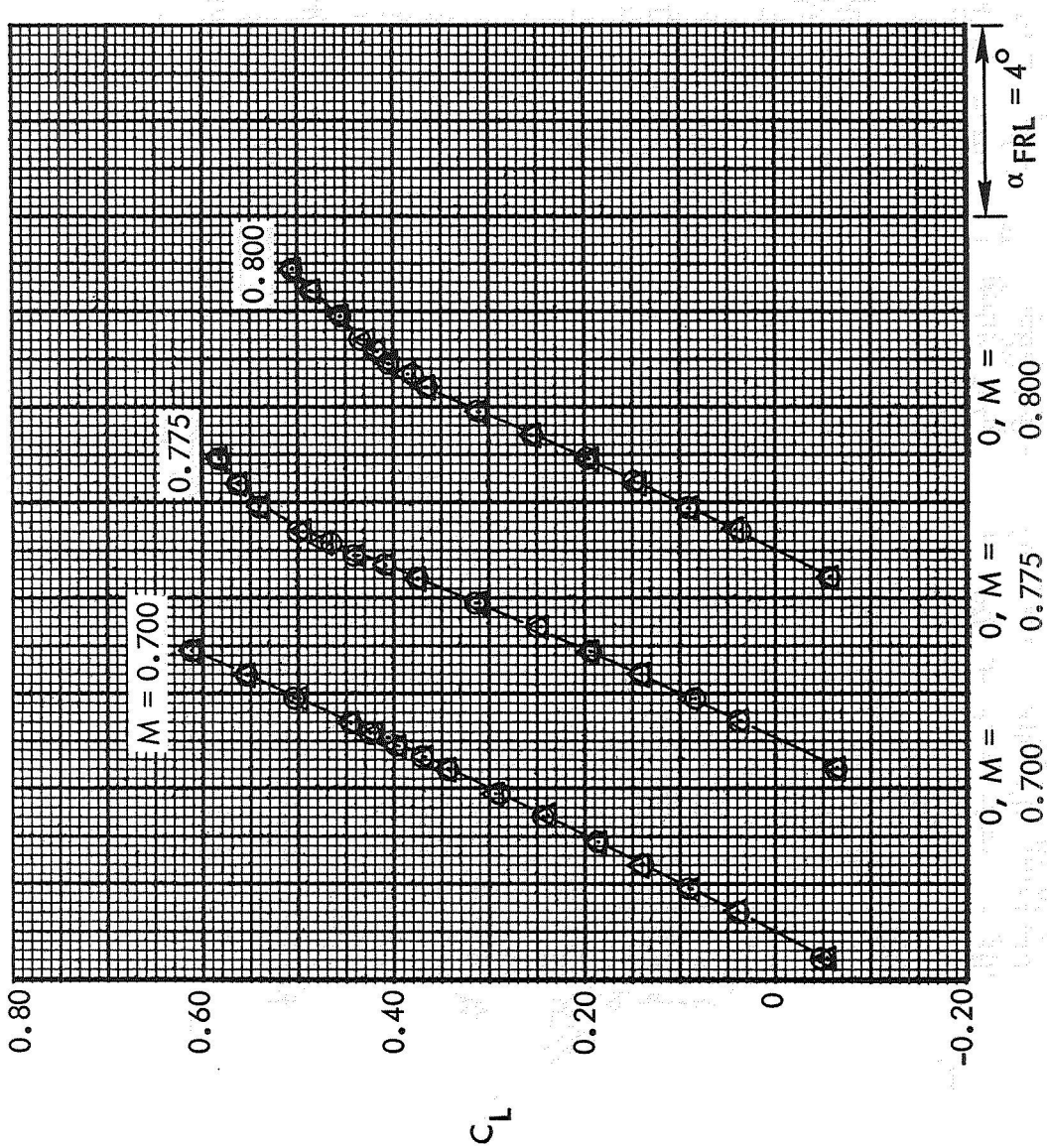
(b) $C_M - C_L$.

Figure 9. Continued.



(c) $C_D - C_L$

Figure 9. Concluded.



(a) $C_L - \alpha$.

Figure 10. Data Repeatability. Test 617.

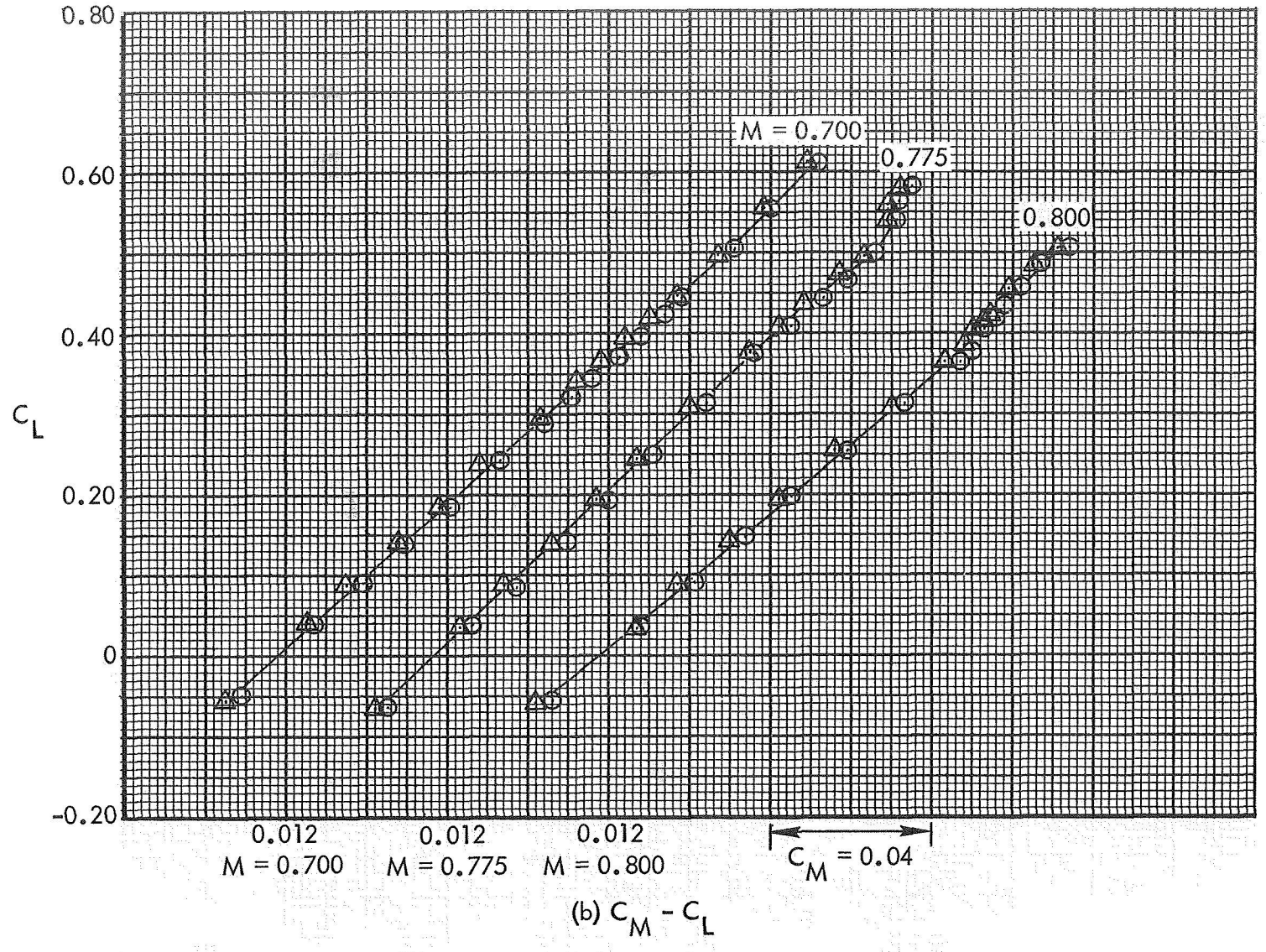
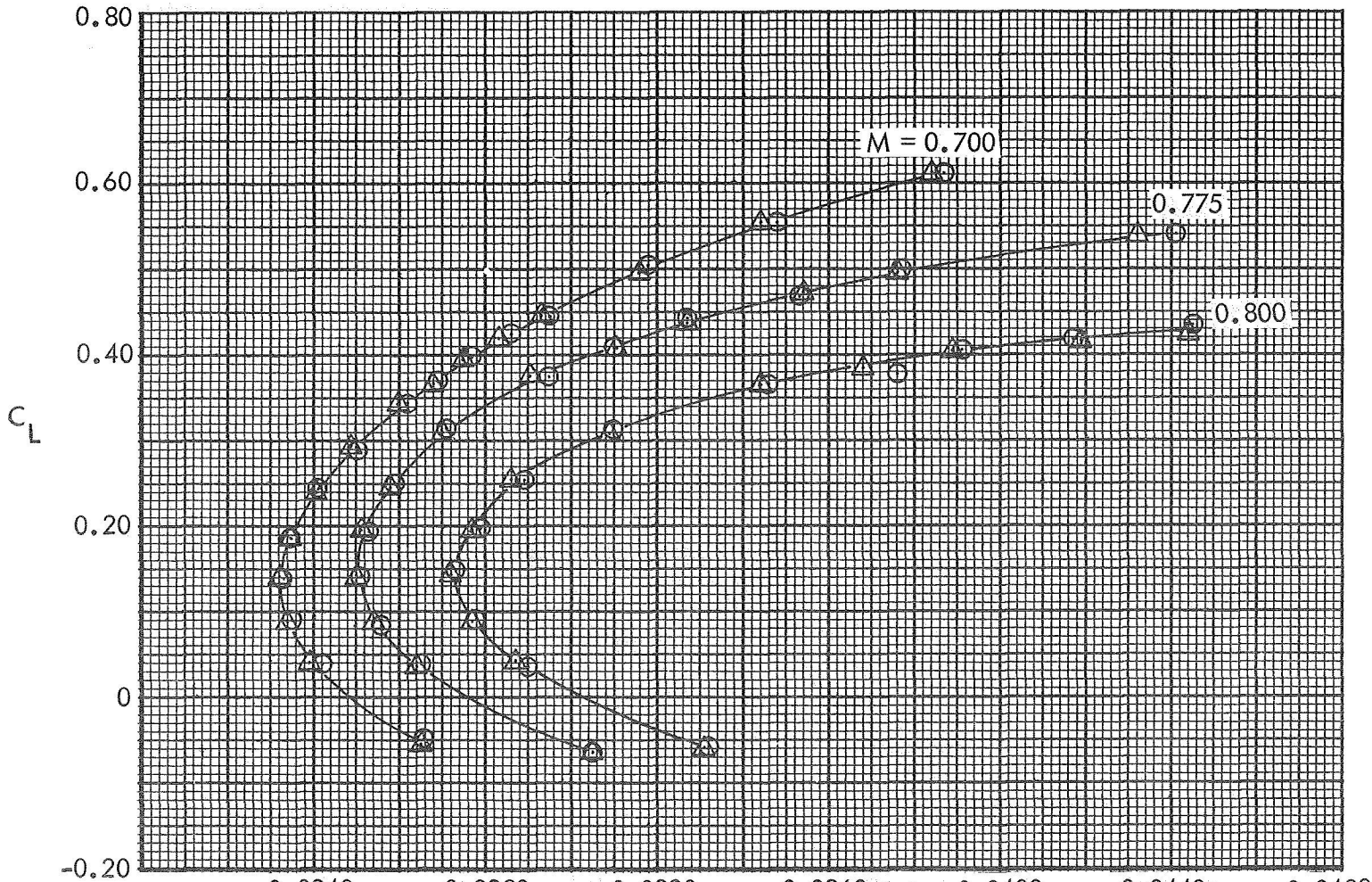
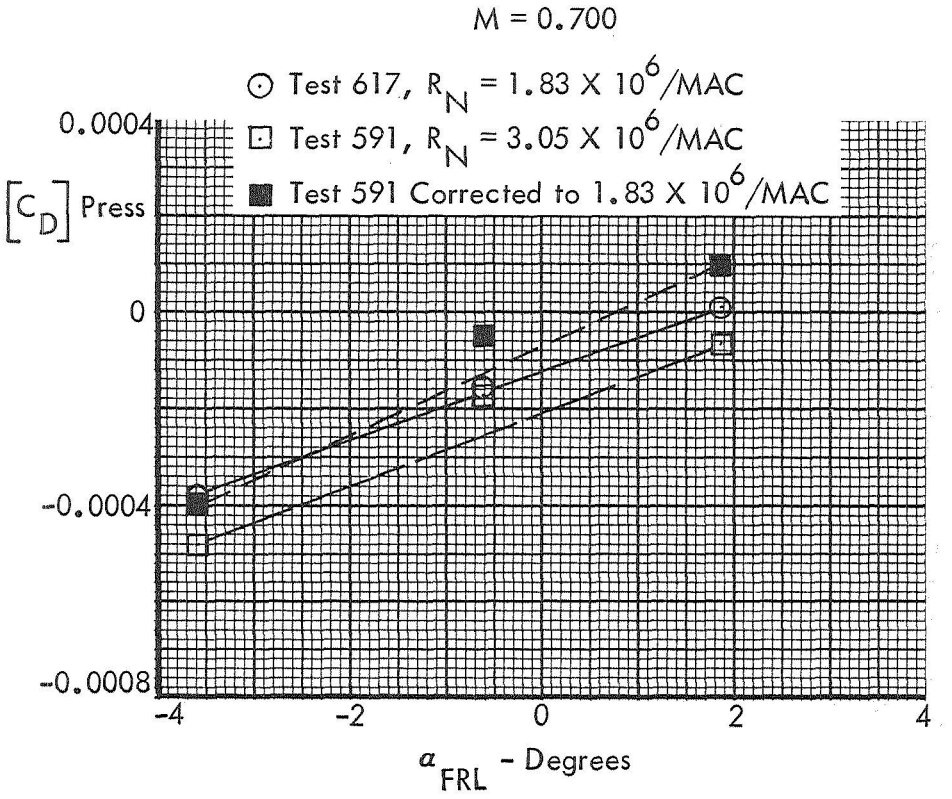


Figure 10. Continued.



(c) $C_D - C_L$

Figure 10. Continued.



(d) Comparison of Test 591 and 617 Afterbody Pressure Drag

Figure 10. Concluded

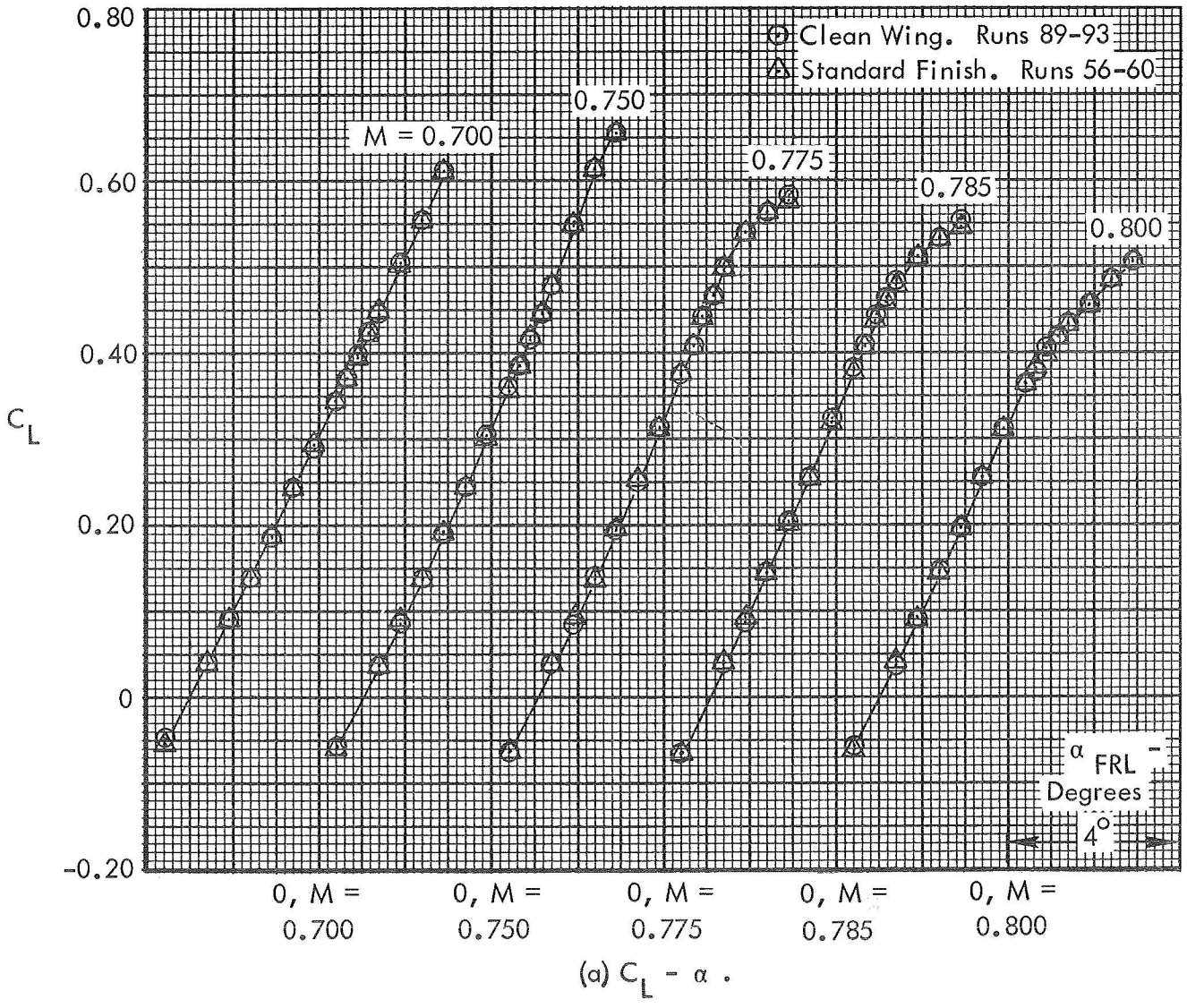
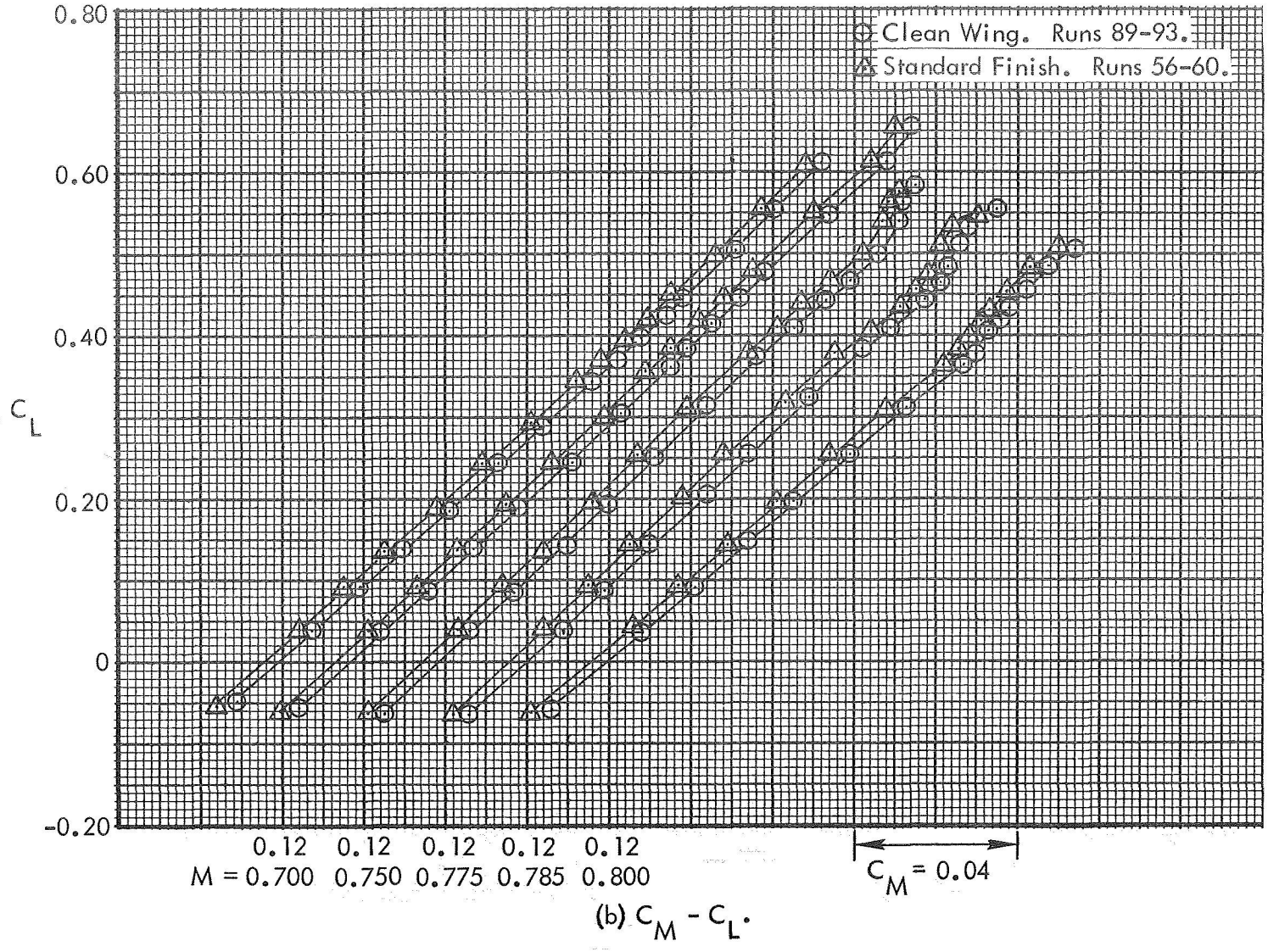
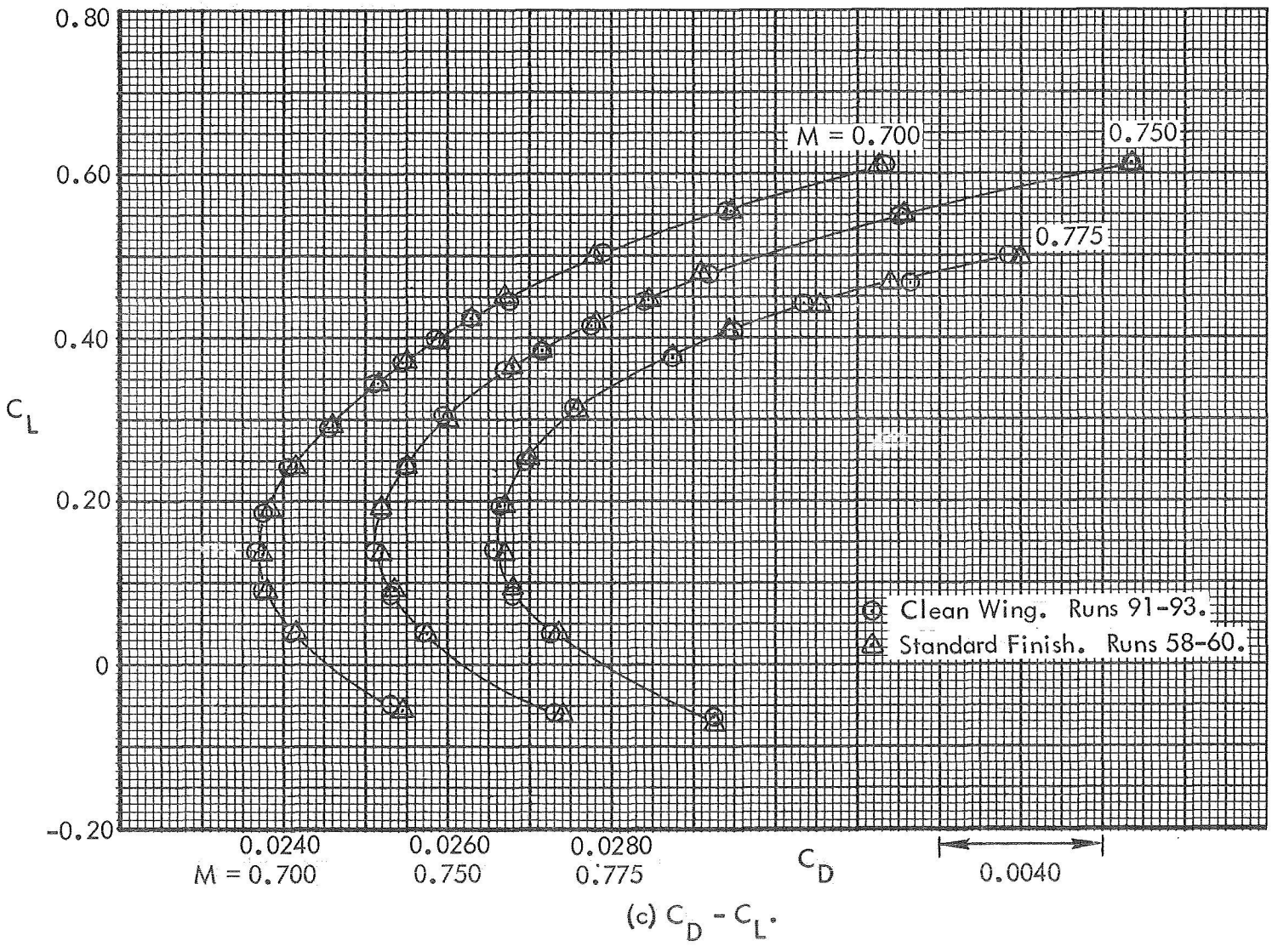


Figure 11. Effect of Wing Surface Finish on Basic Data. Test 617.



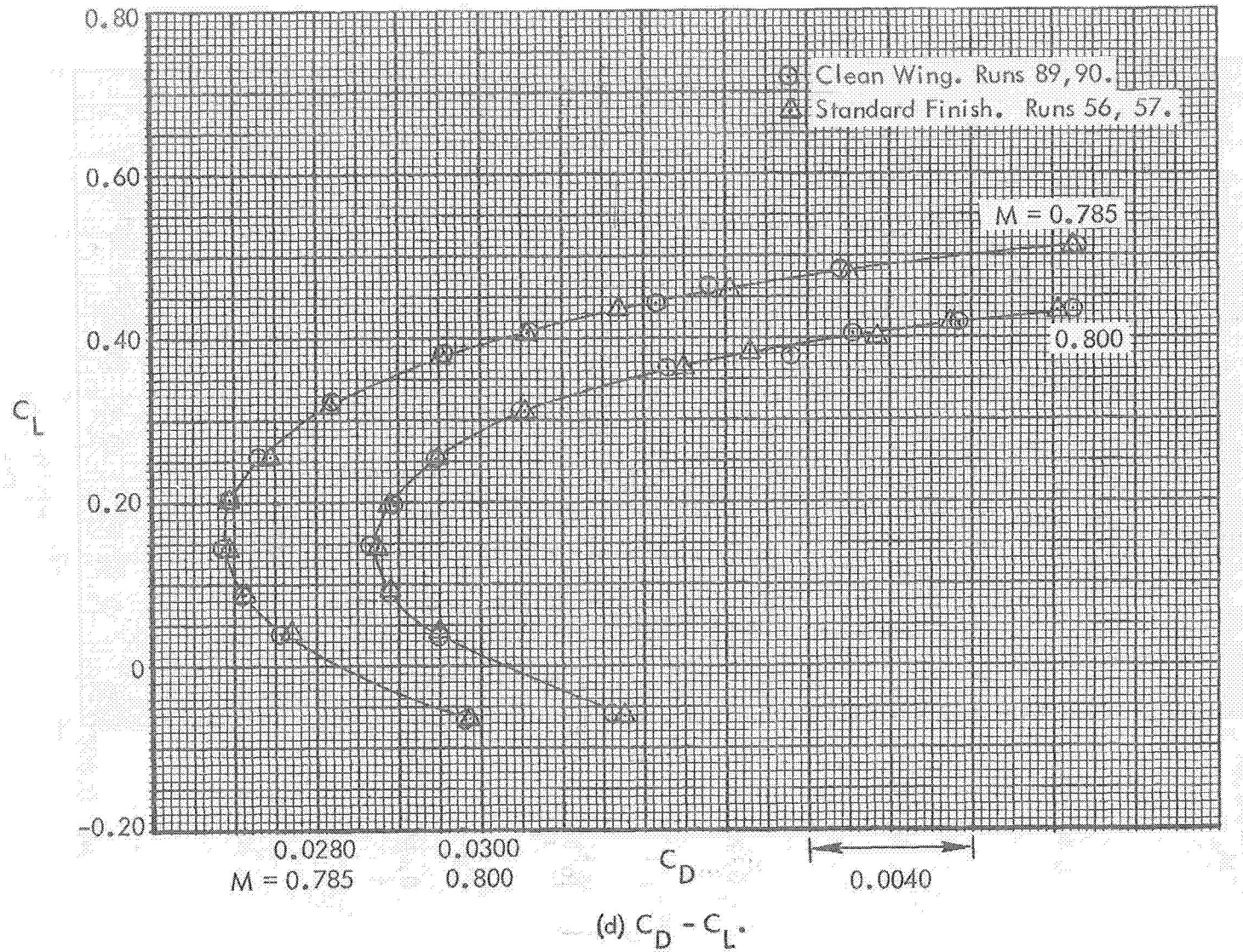
(b) $C_M - C_L$.

Figure 11. Continued.



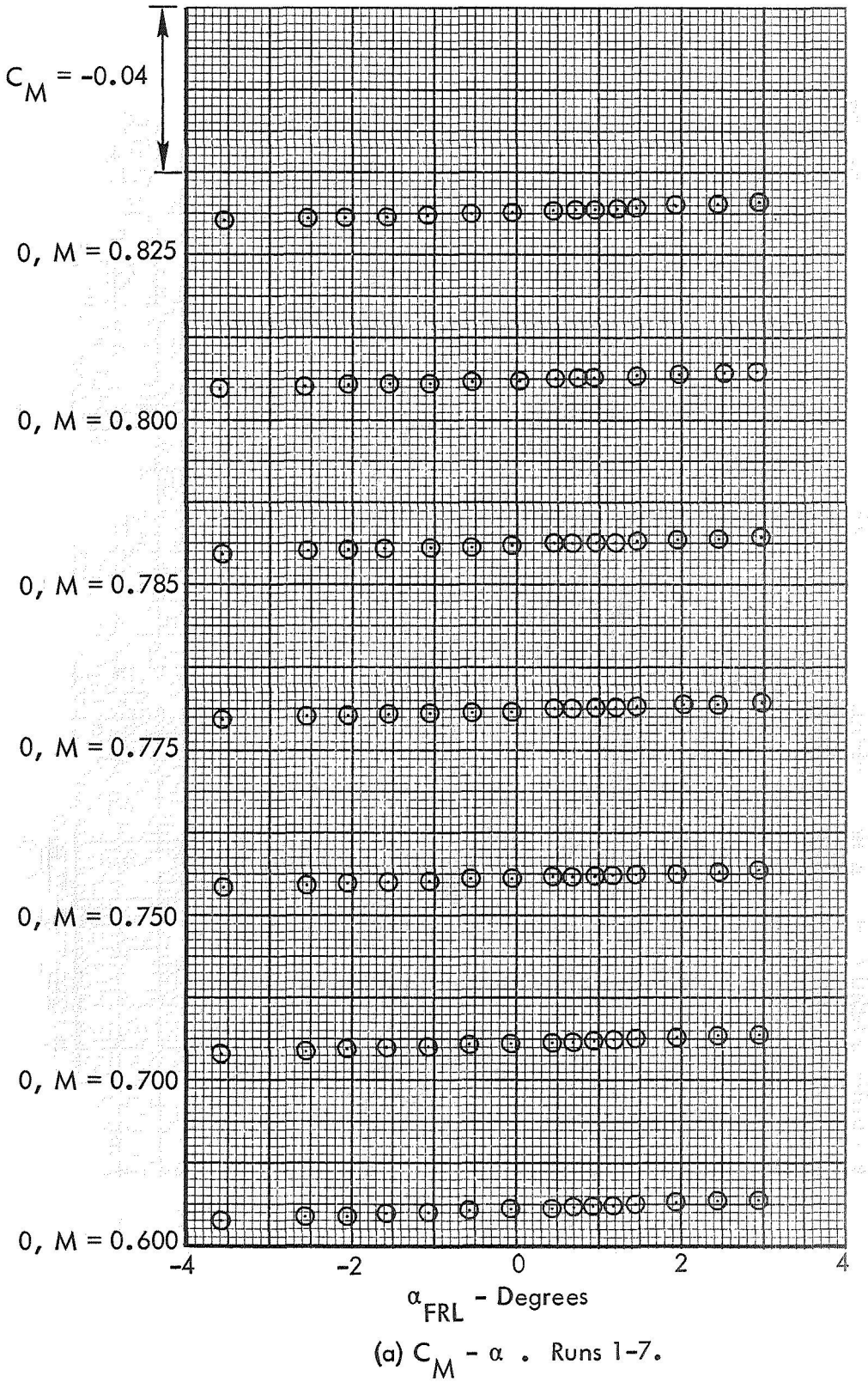
(c) $C_D - C_L$.

Figure 11. Continued.



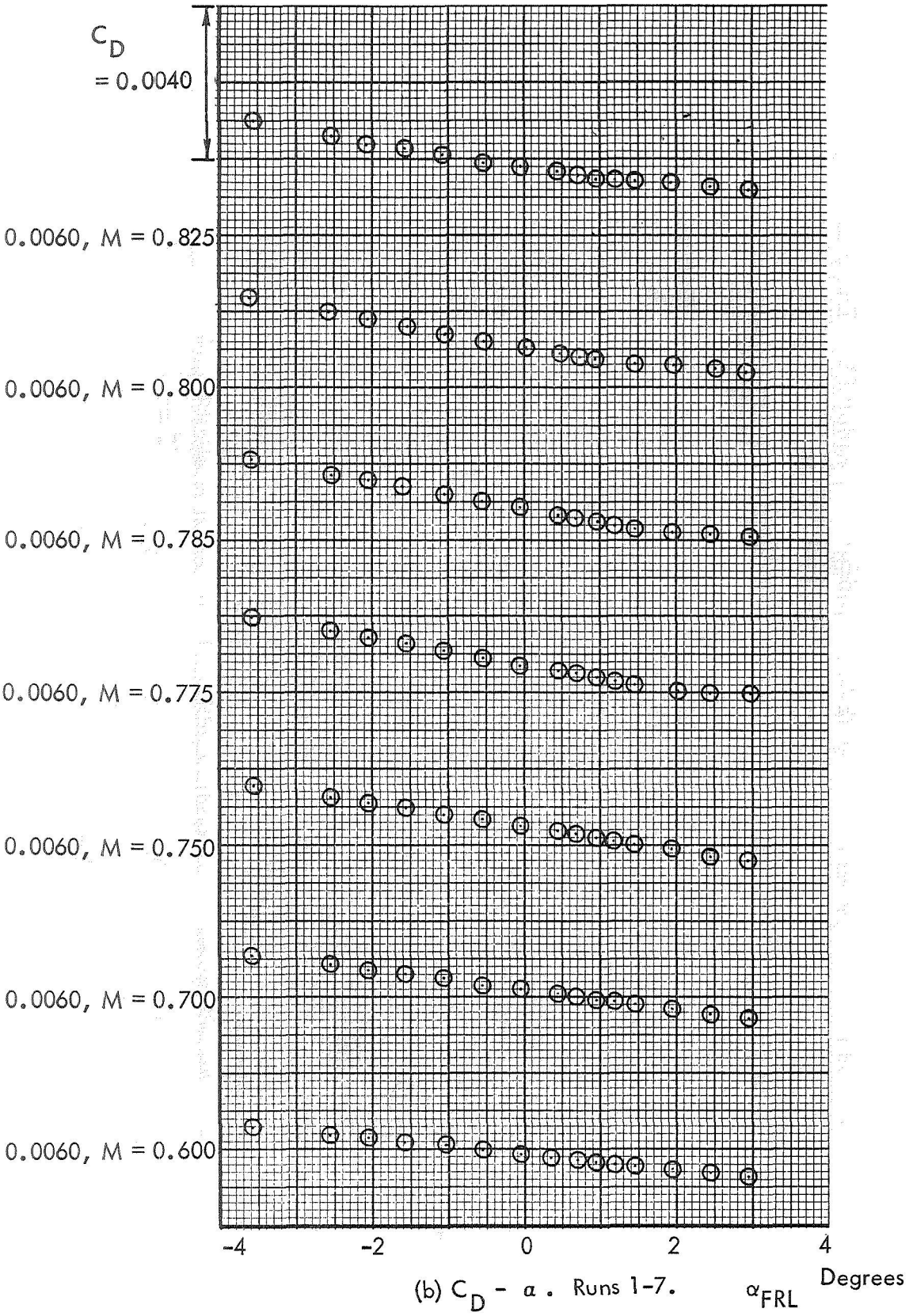
(d) $C_D - C_L$.

Figure 11. Concluded.



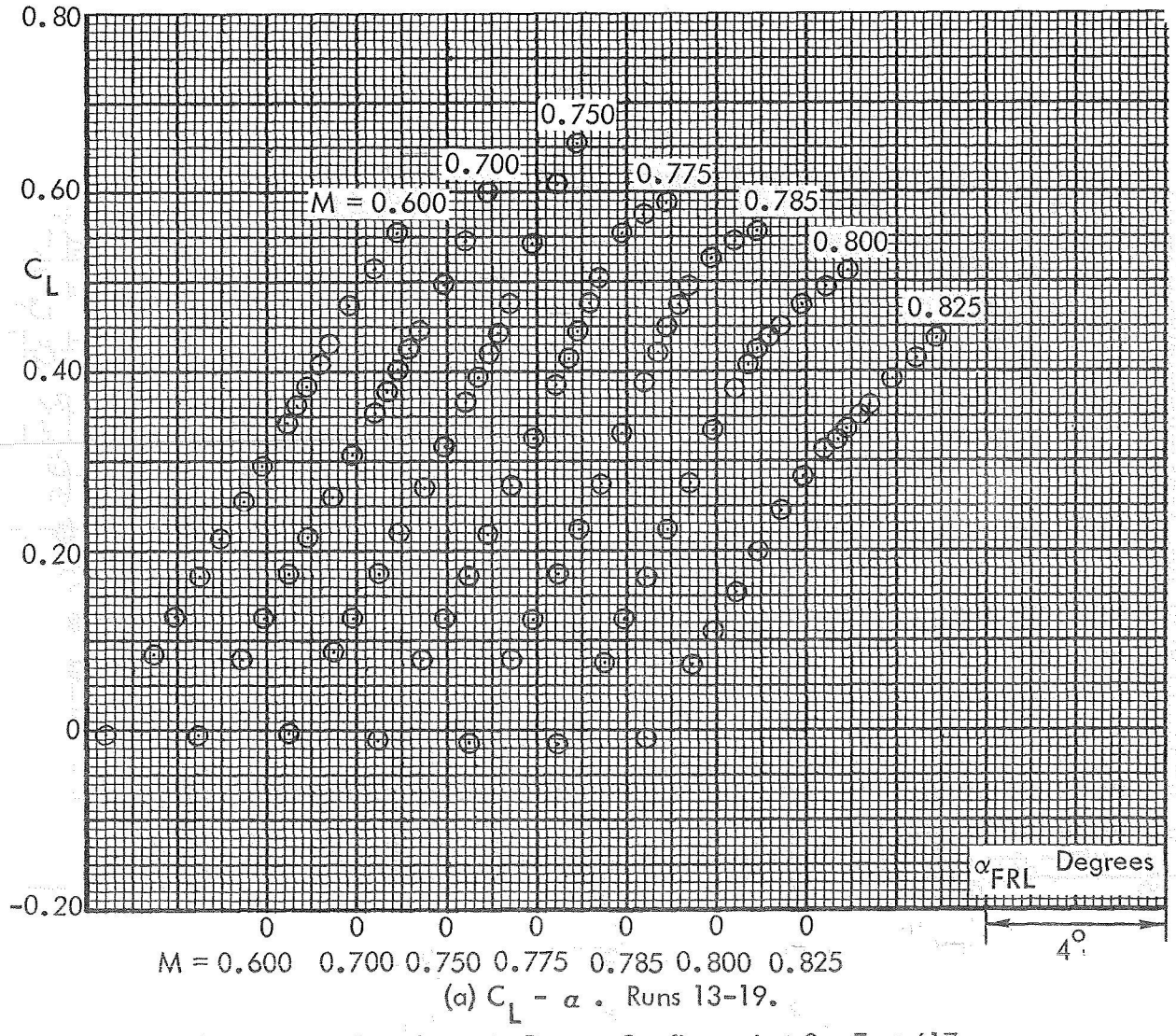
(a) $C_M - \alpha$. Runs 1-7.

Figure 12. Blade Load Data. Configuration 7. Test 617.



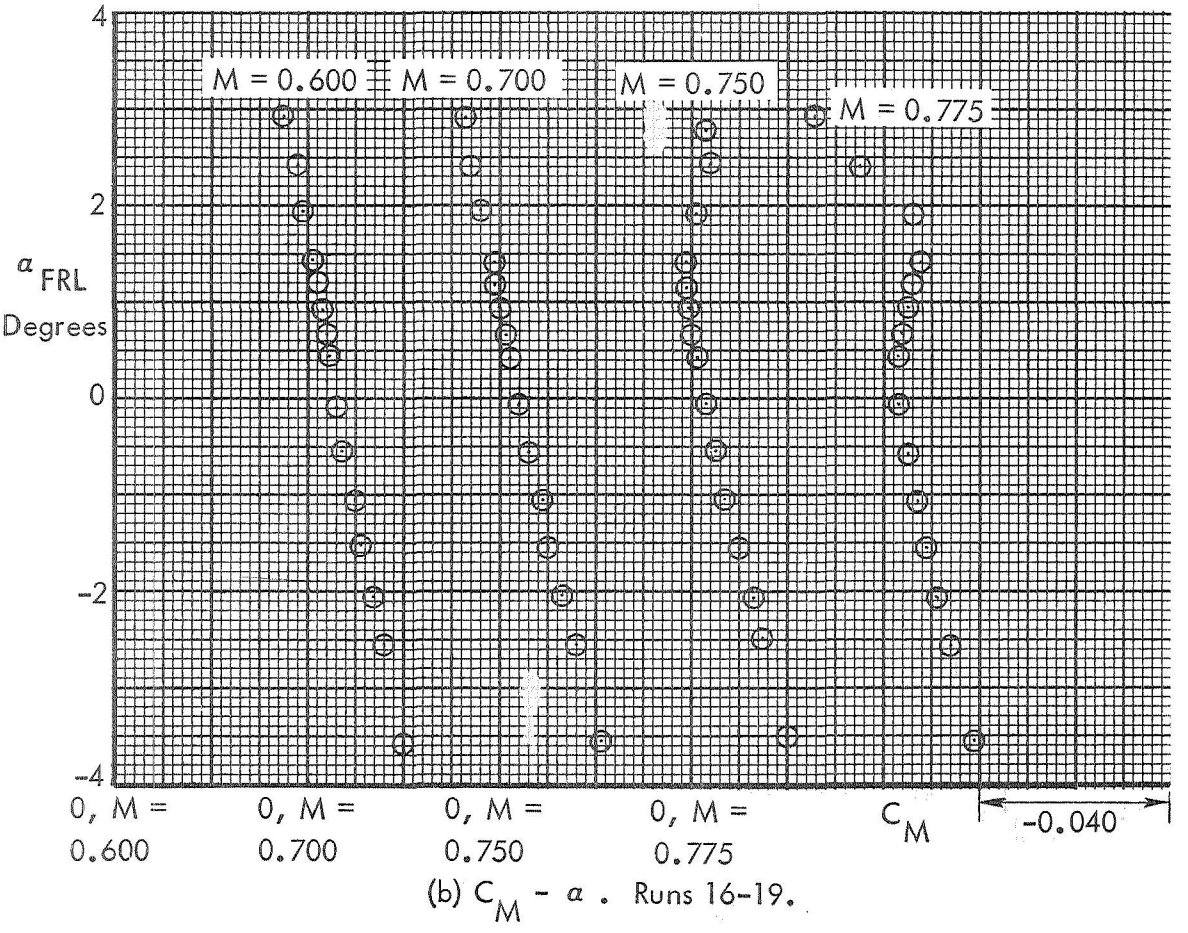
(b) $C_D - \alpha$. Runs 1-7.

Figure 12. Concluded.



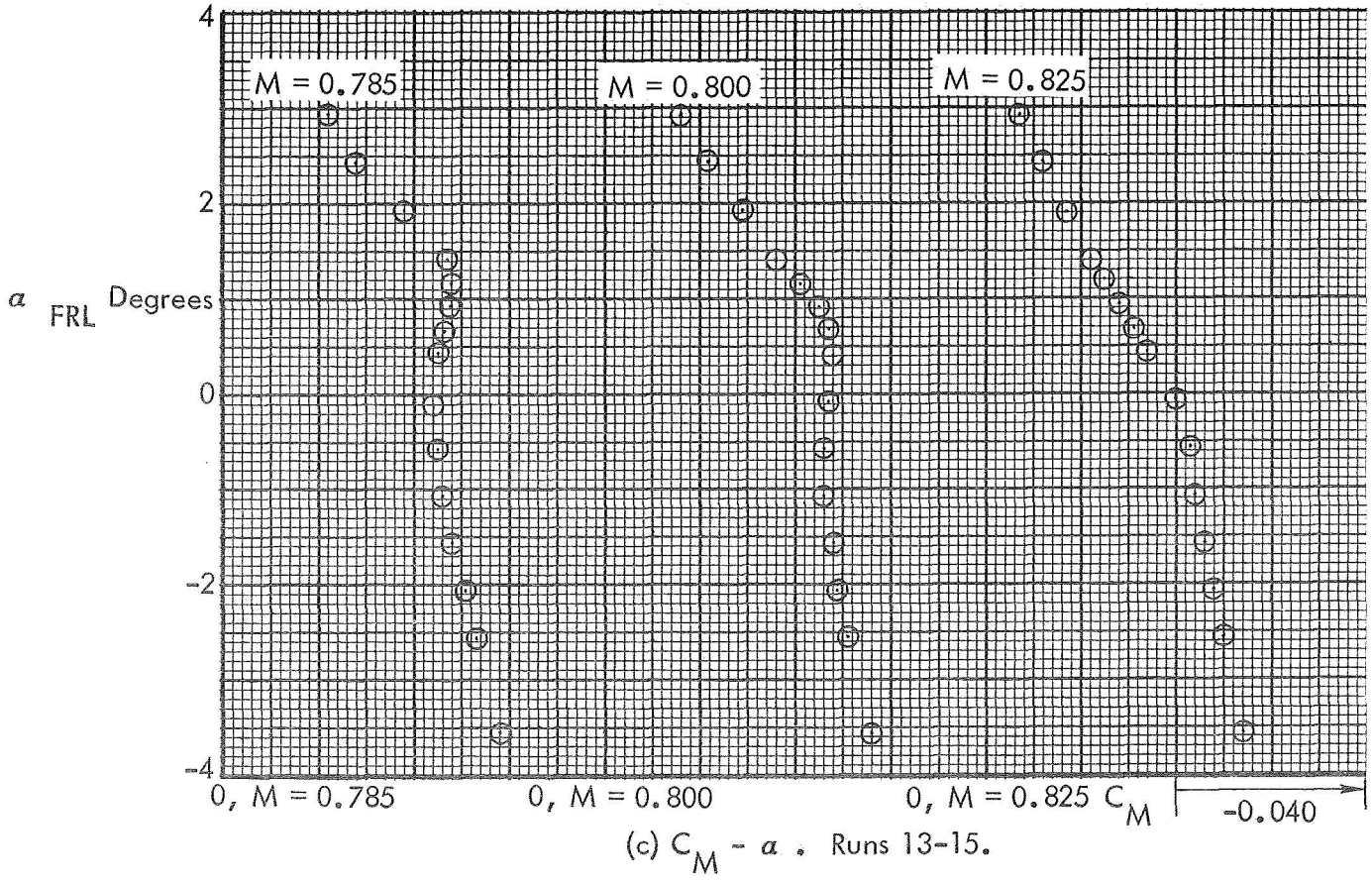
(a) $C_L - \alpha$. Runs 13-19.

Figure 13. Basic Aerodynamic Data. Configuration 8. Test 617.



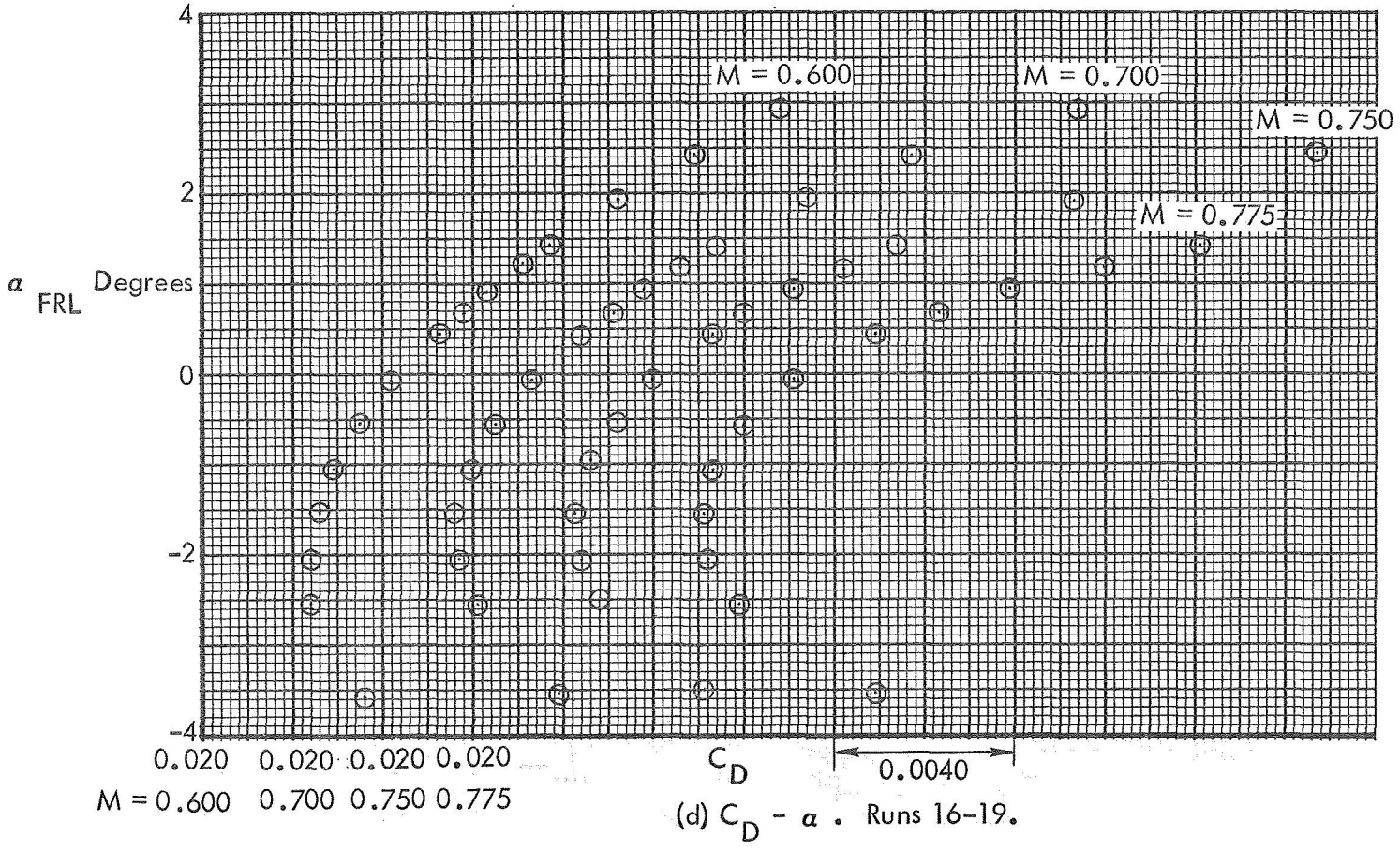
(b) C_M - α . Runs 16-19.

Figure 13. Continued.



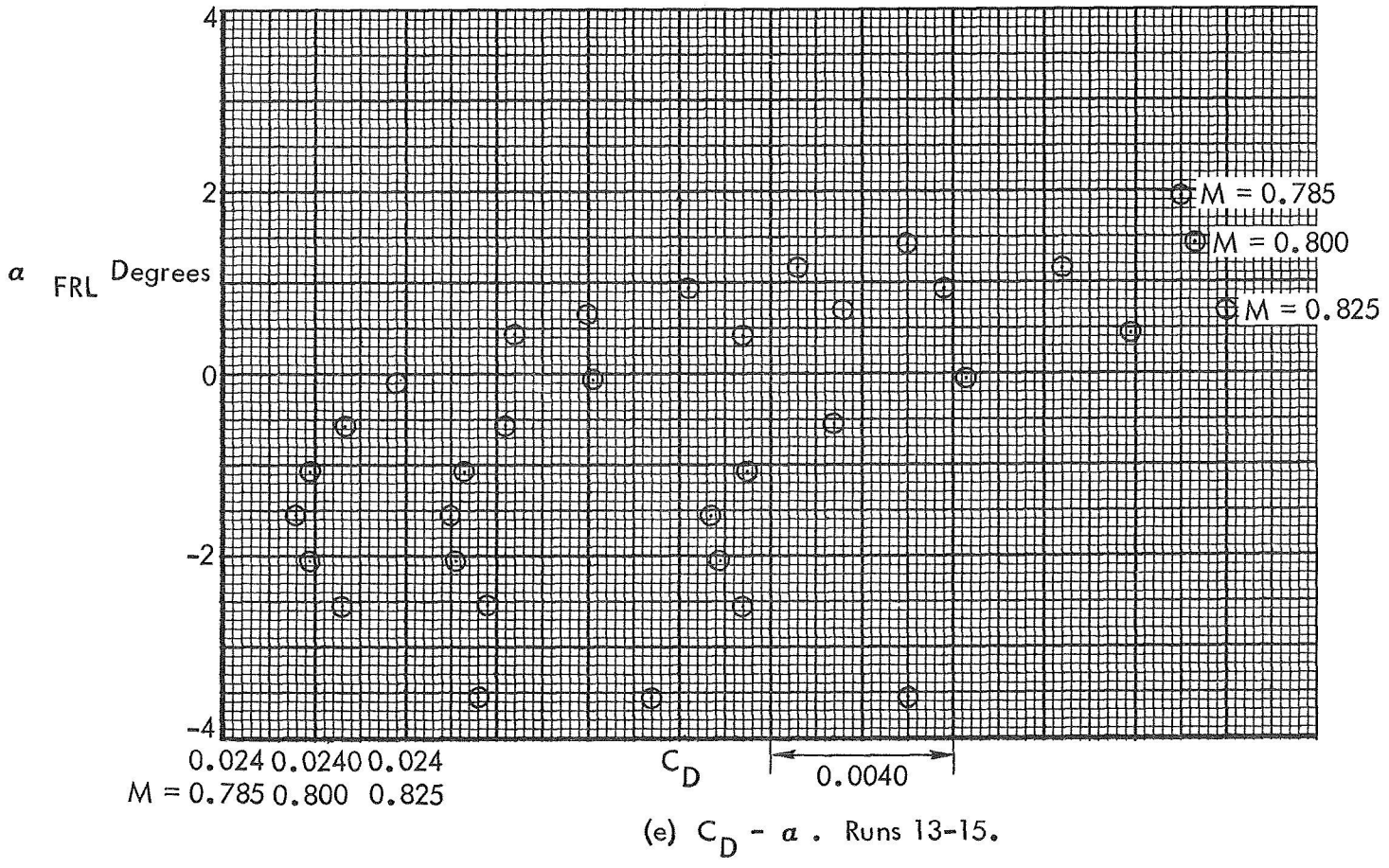
(c) $C_M - \alpha$. Runs 13-15.

Figure 13. Continued.



(d) C_D - α . Runs 16-19.

Figure 13. Continued.



(e) C_D - α . Runs 13-15.

Figure 13. Concluded.

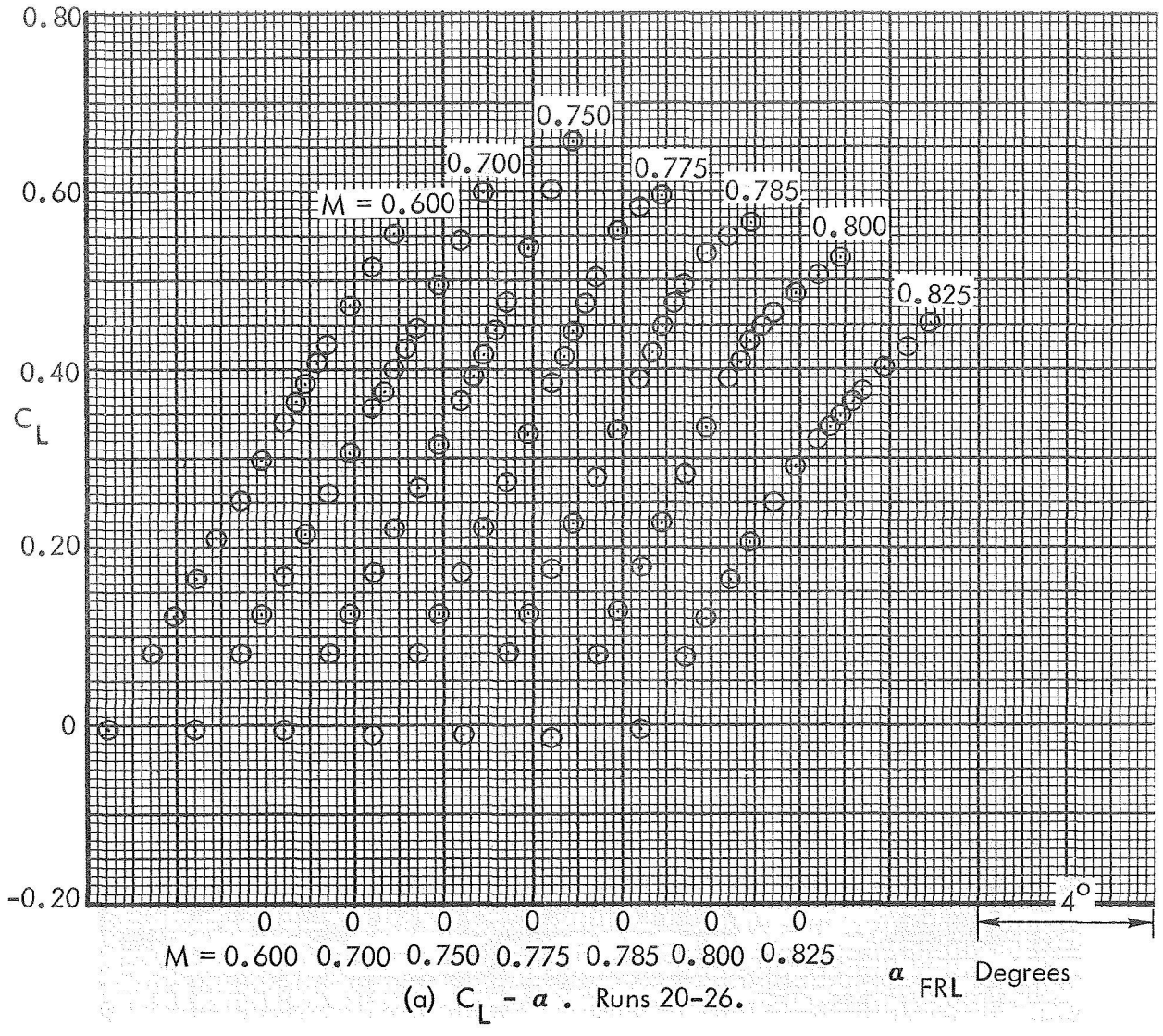
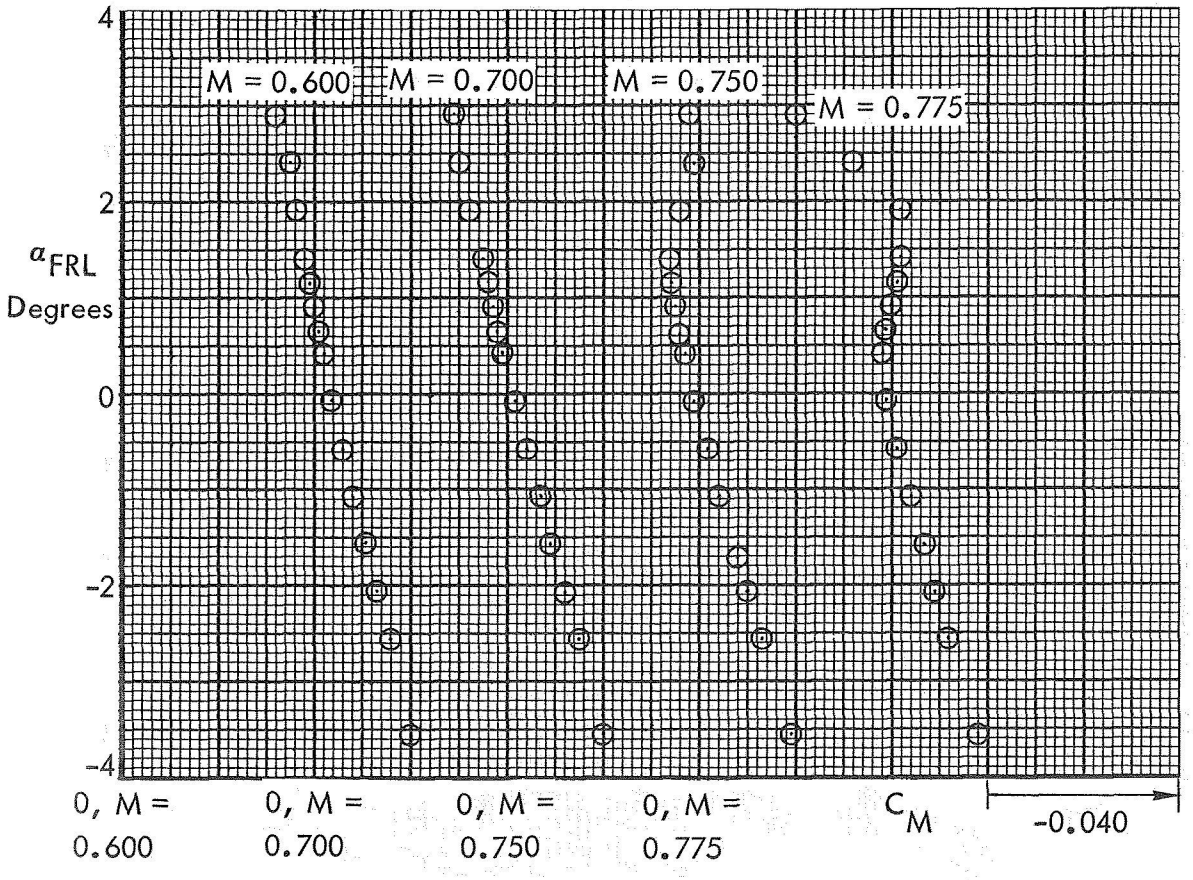
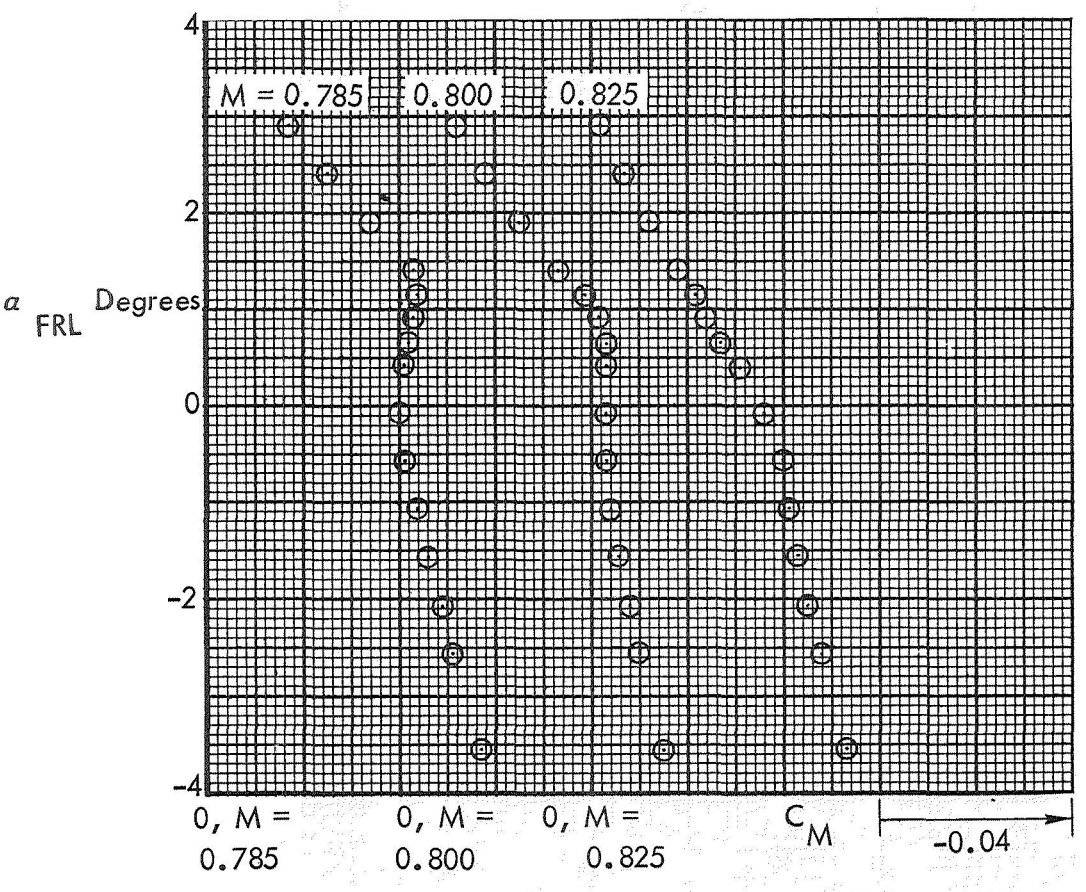


Figure 14. Basic Aerodynamic Data. Configuration 6. Test 617.



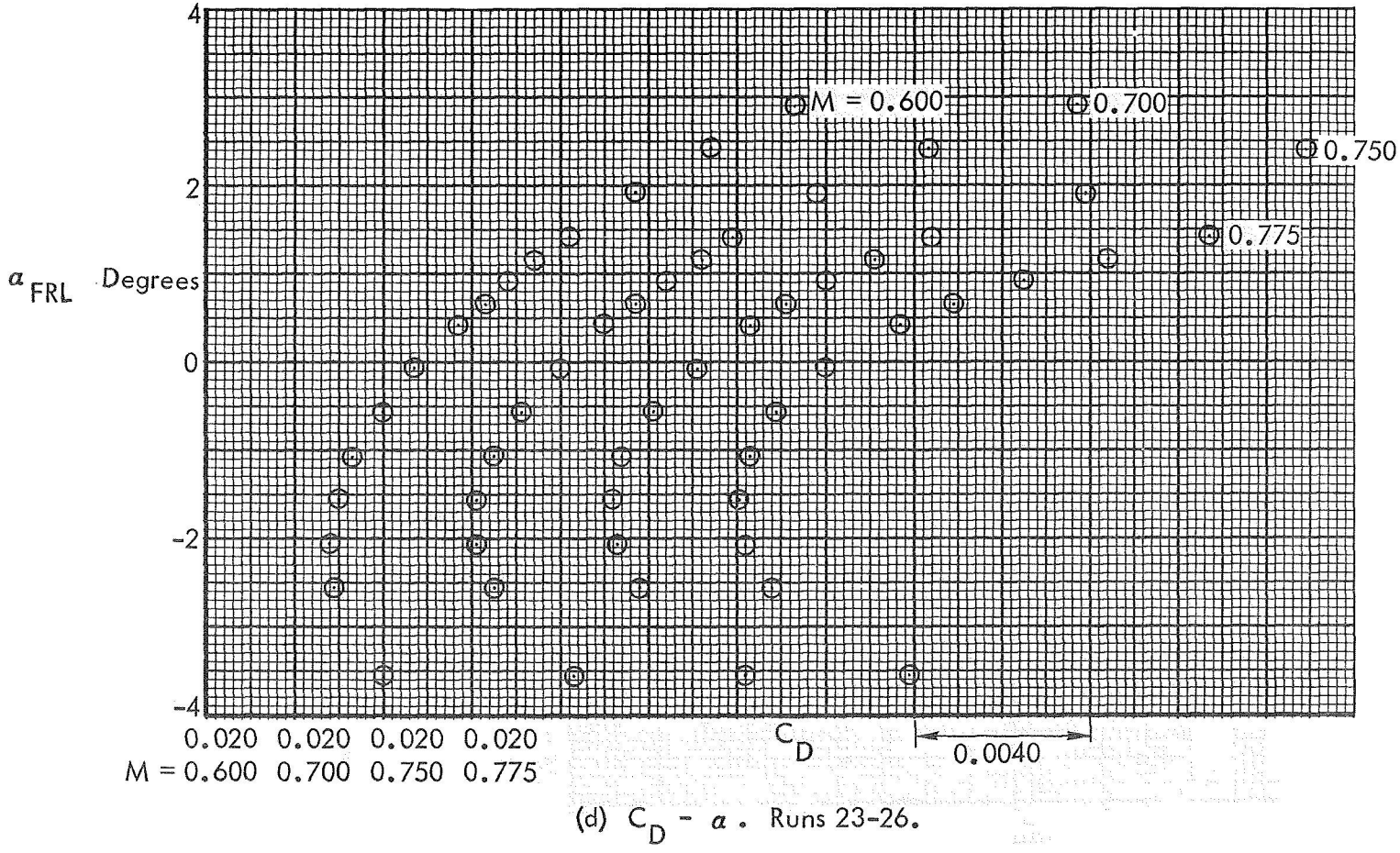
(b) C_M - α . Runs 23-26.

Figure 14. Continued.



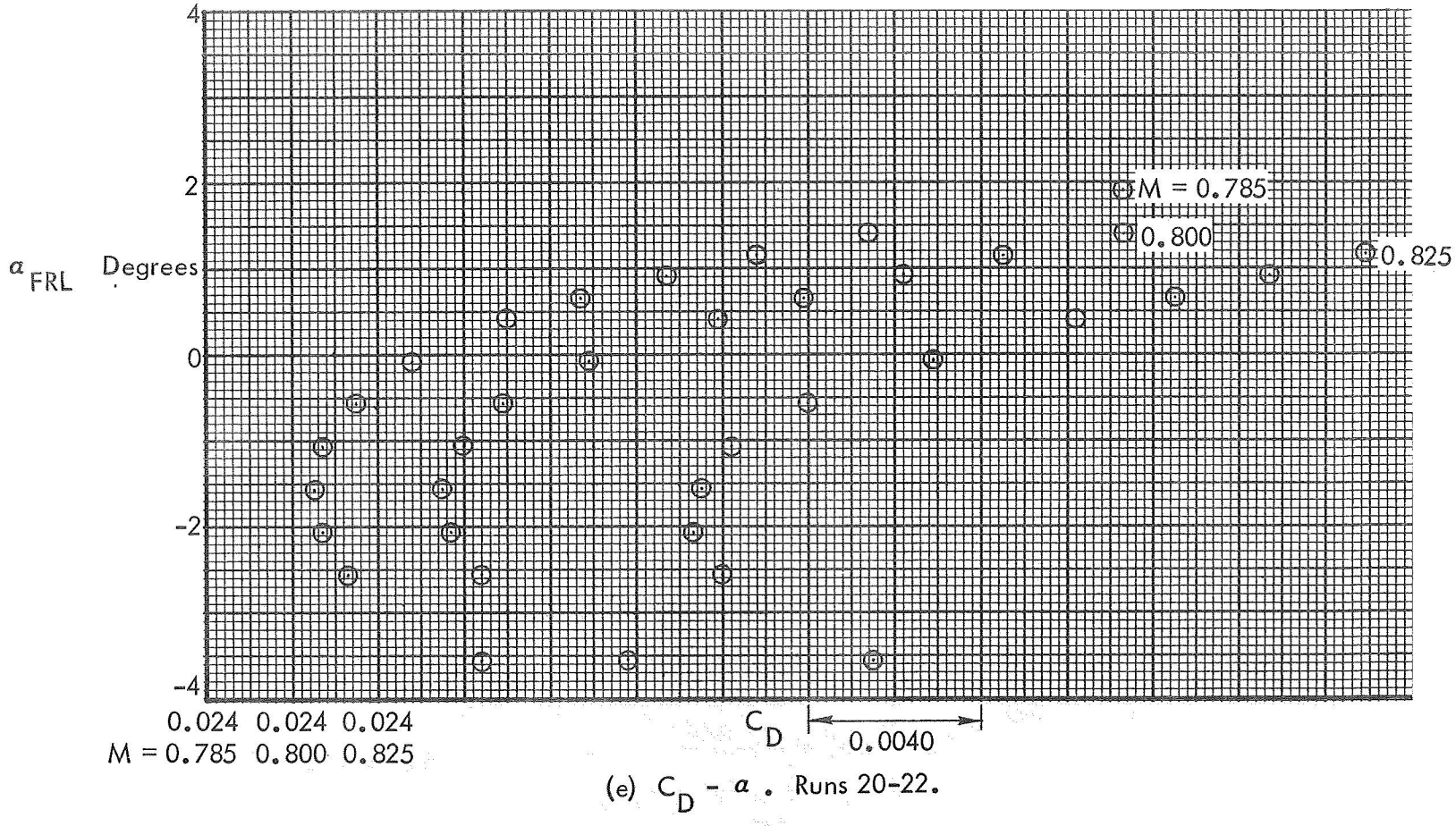
(c) C_M - α . Runs 20-22.

Figure 14. Continued.



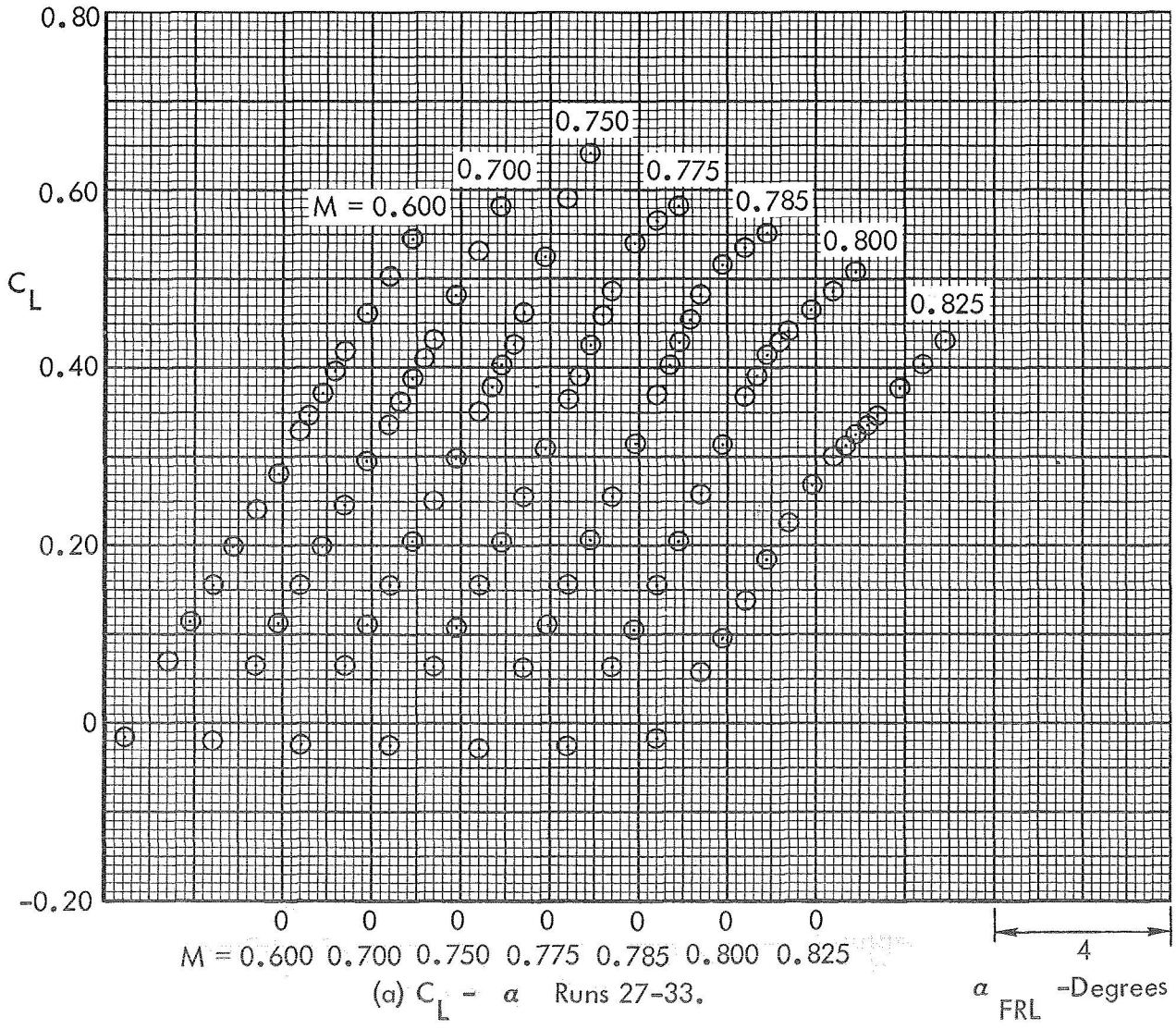
(d) C_D - α . Runs 23-26.

Figure 14. Continued.



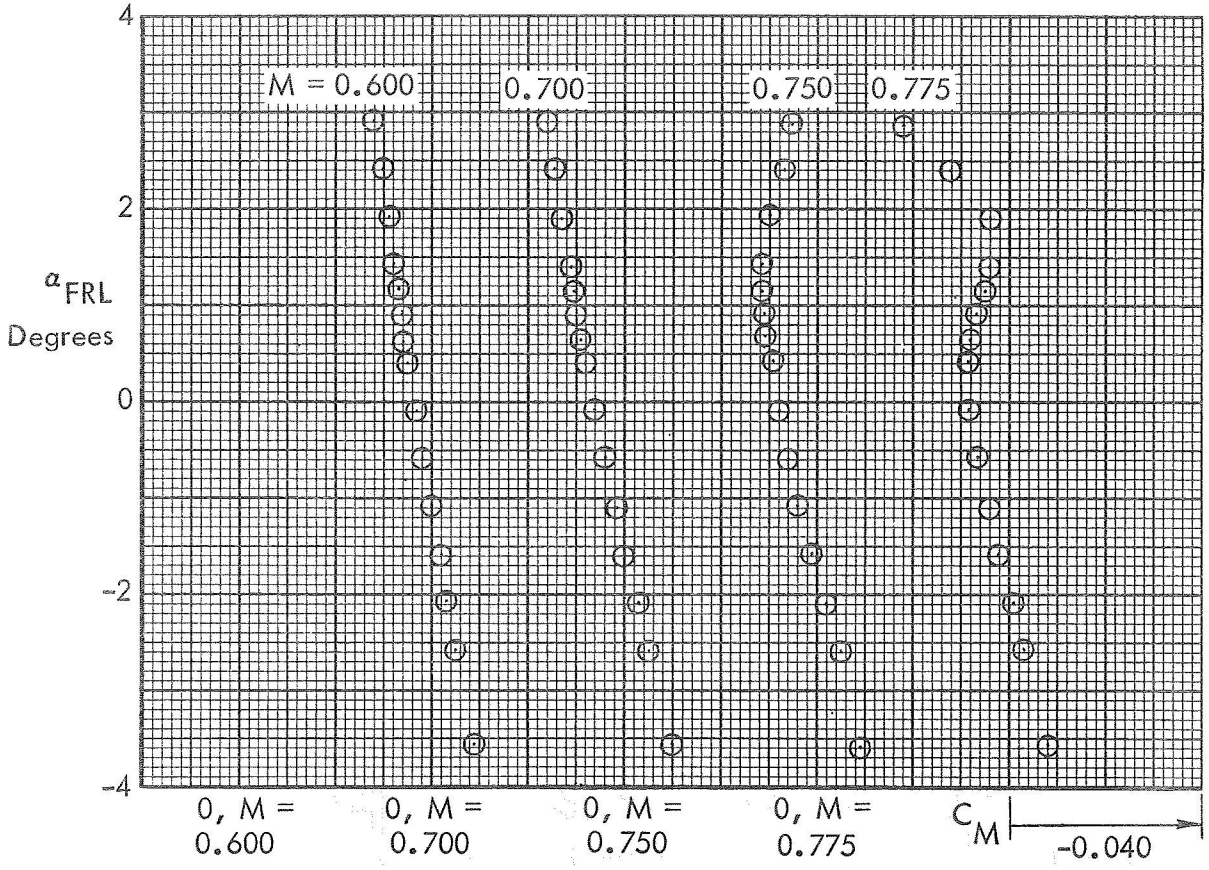
(e) $C_D - \alpha$. Runs 20-22.

Figure 14. Concluded.



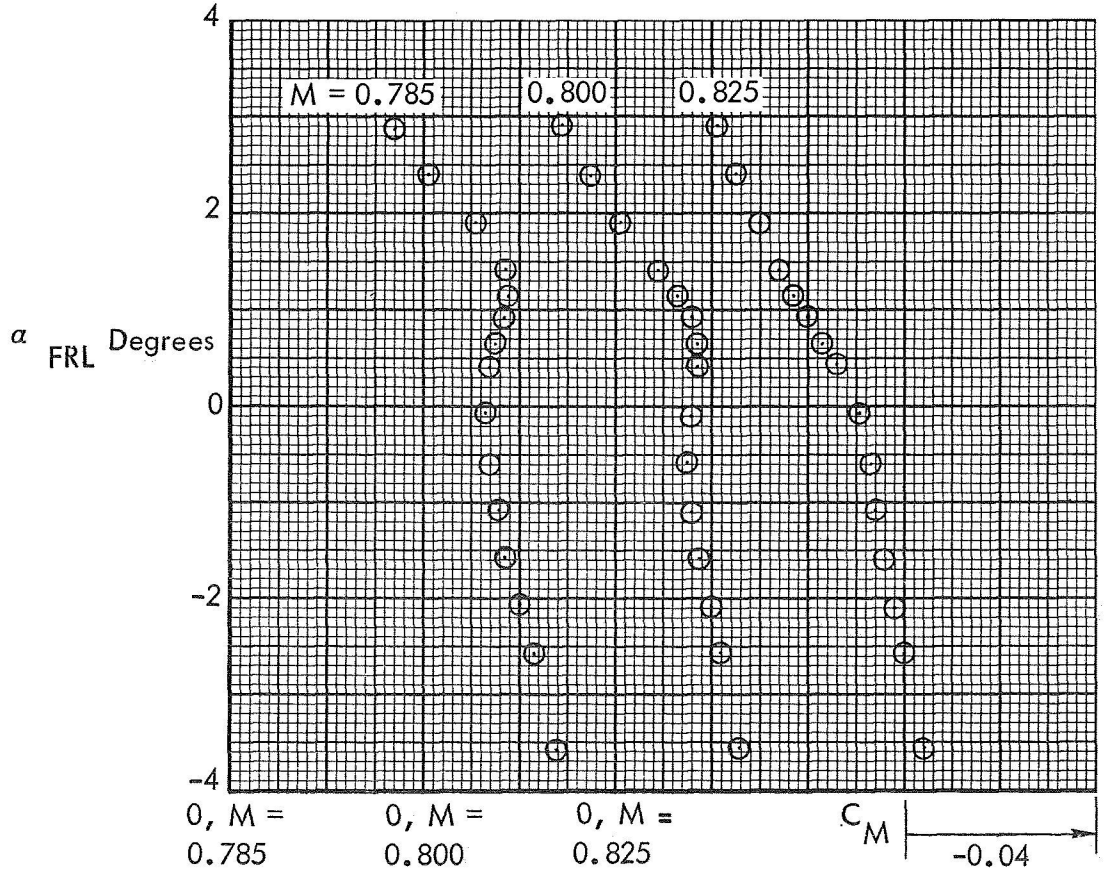
(a) C_L - α Runs 27-33.

Figure 15. Basic Aerodynamic Data. Configuration 5. Test 617.



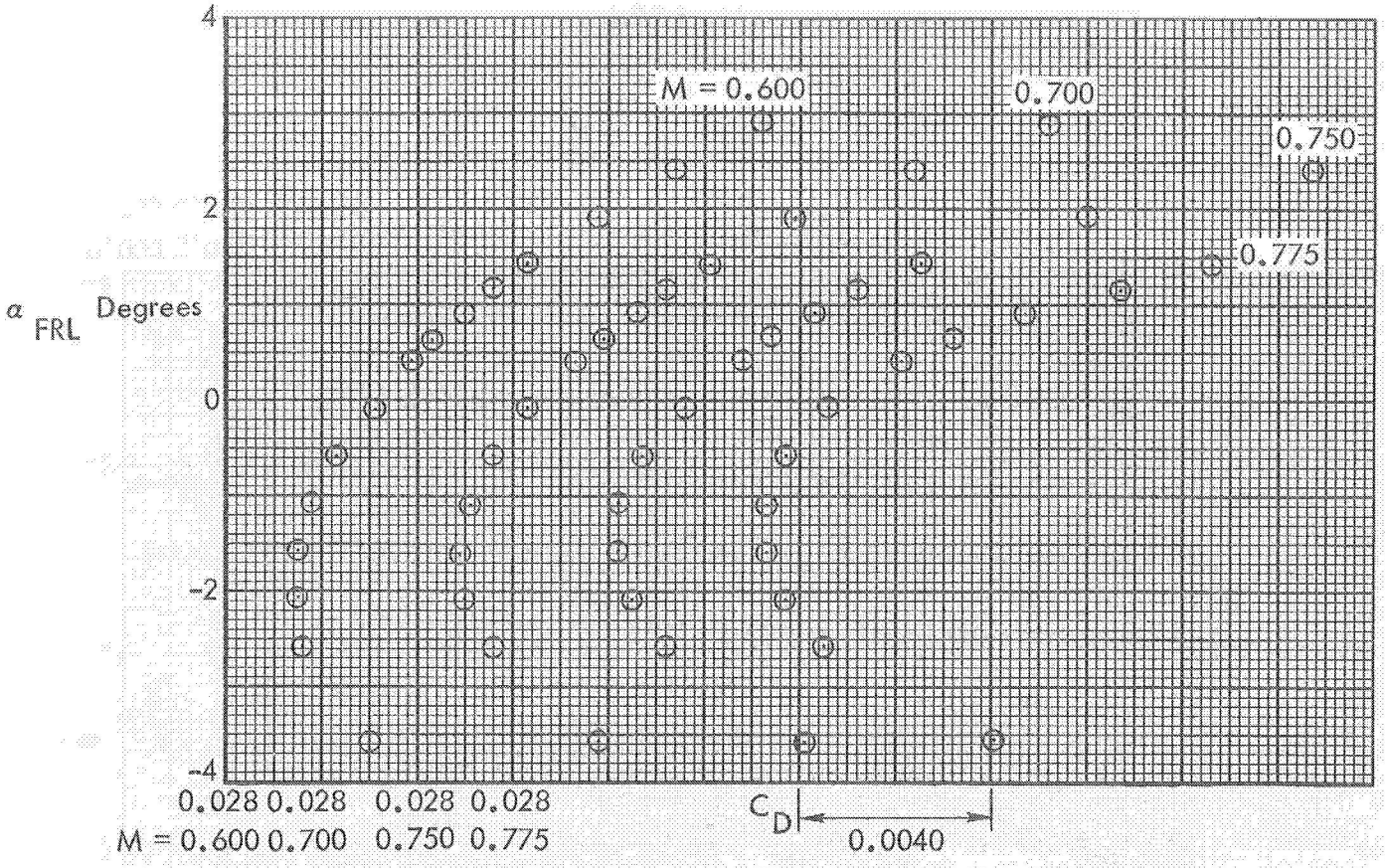
(b) C_M - α Runs 30-33.

Figure 15. Continued.



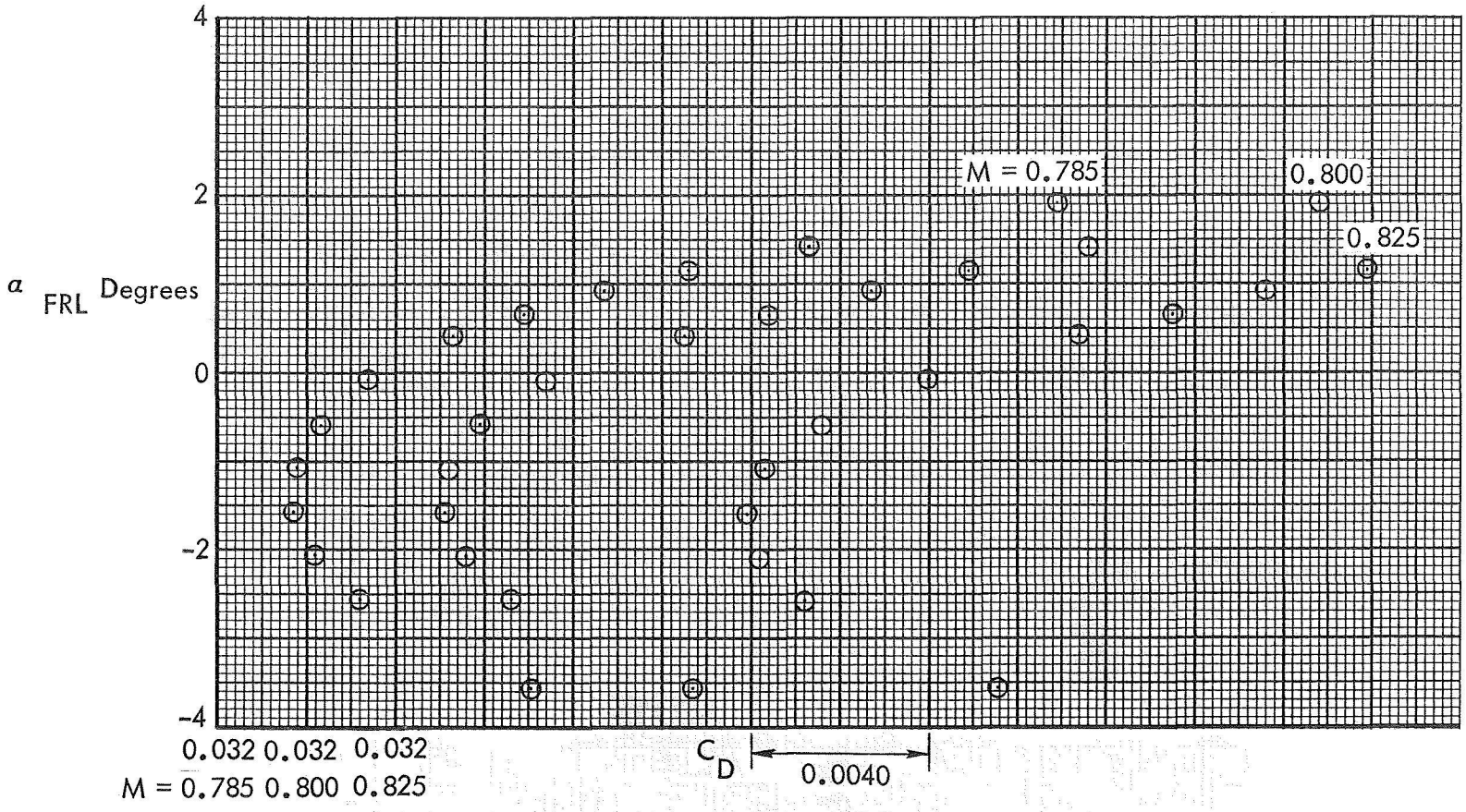
(c) C_M - α Runs 27-29.

Figure 15. Continued.



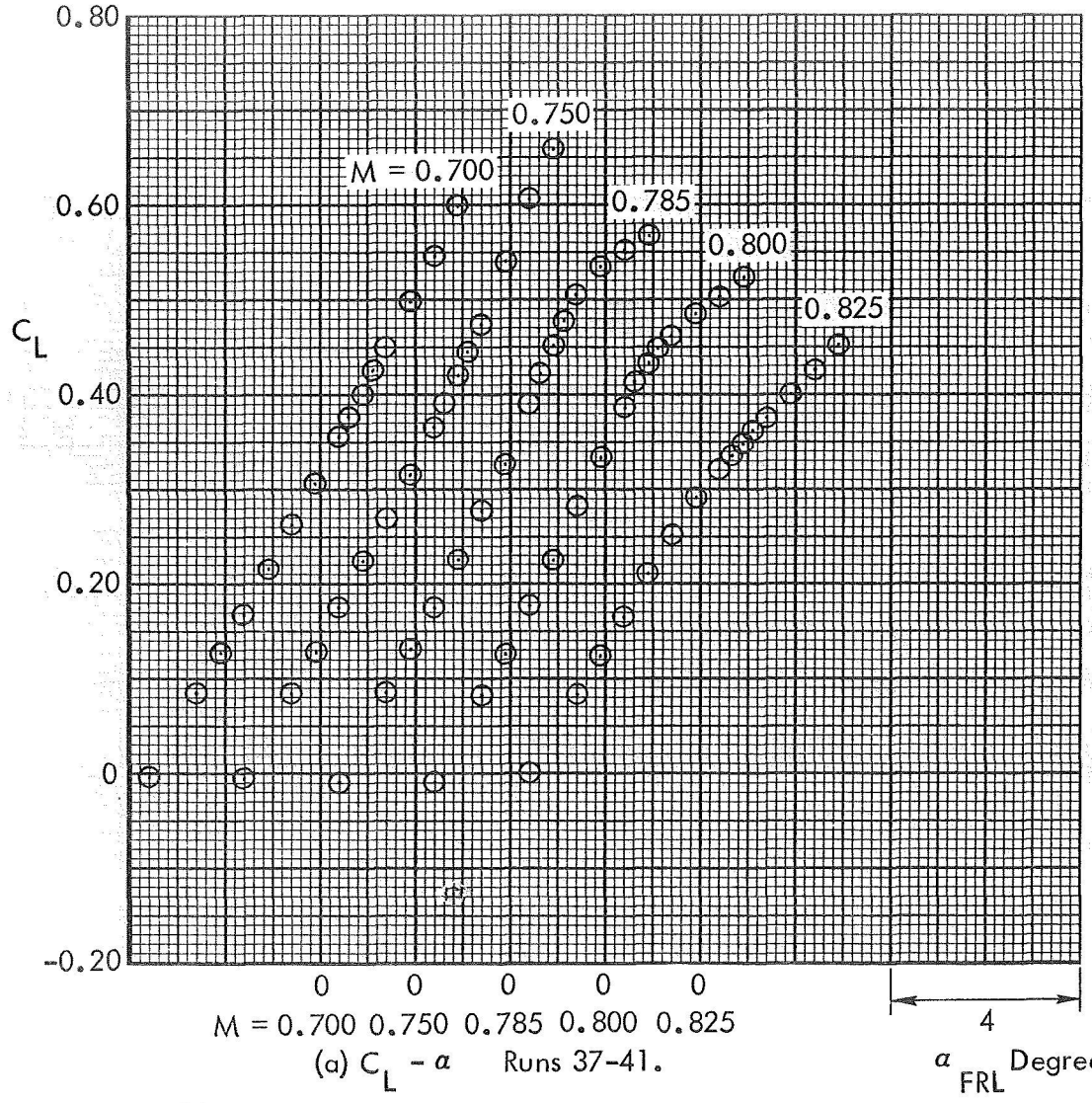
(d) $C_D - \alpha$ Runs 30-33.

Figure 15. Continued.



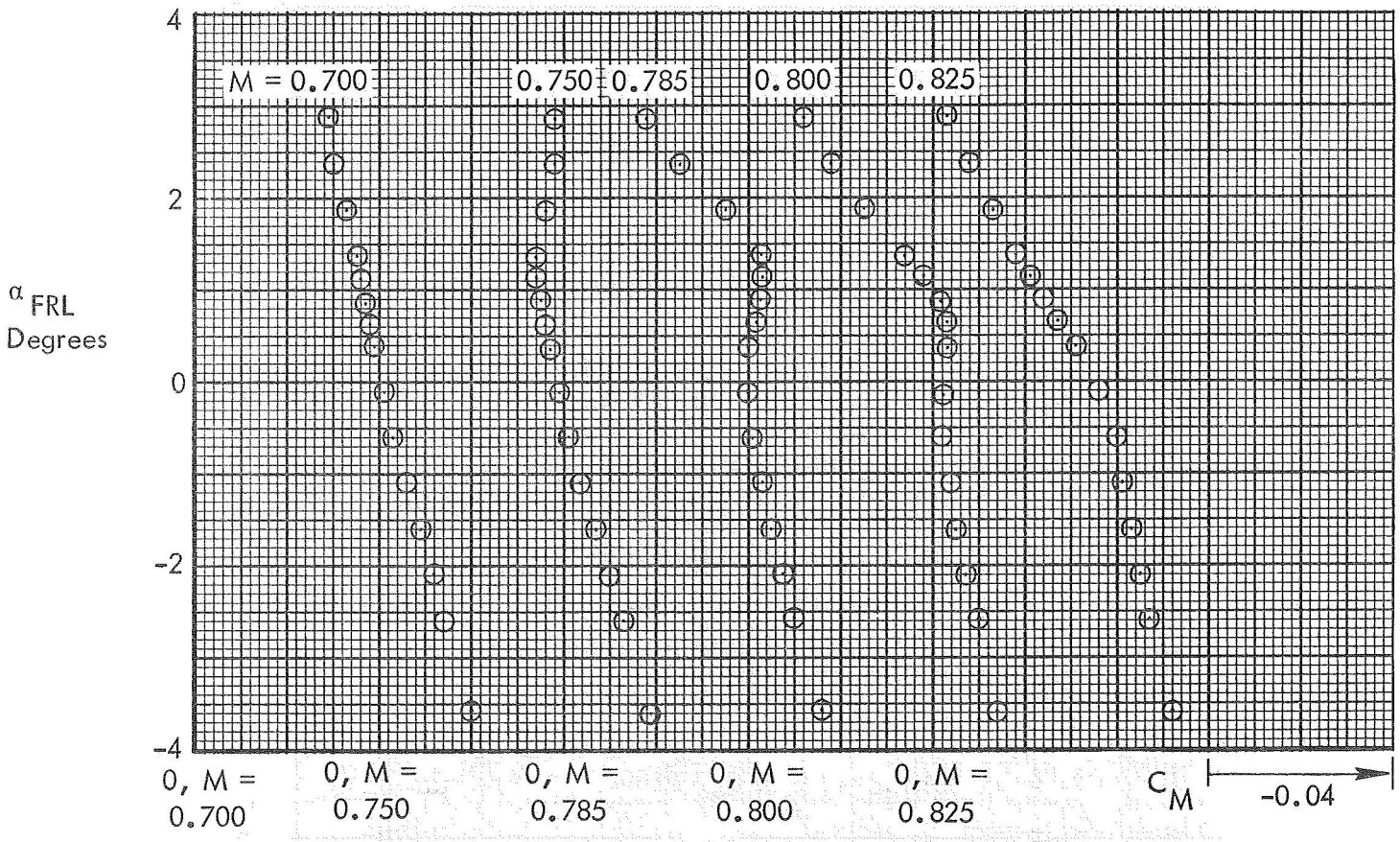
(e) $C_D - \alpha$ Runs 27-29.

Figure 15. Concluded.



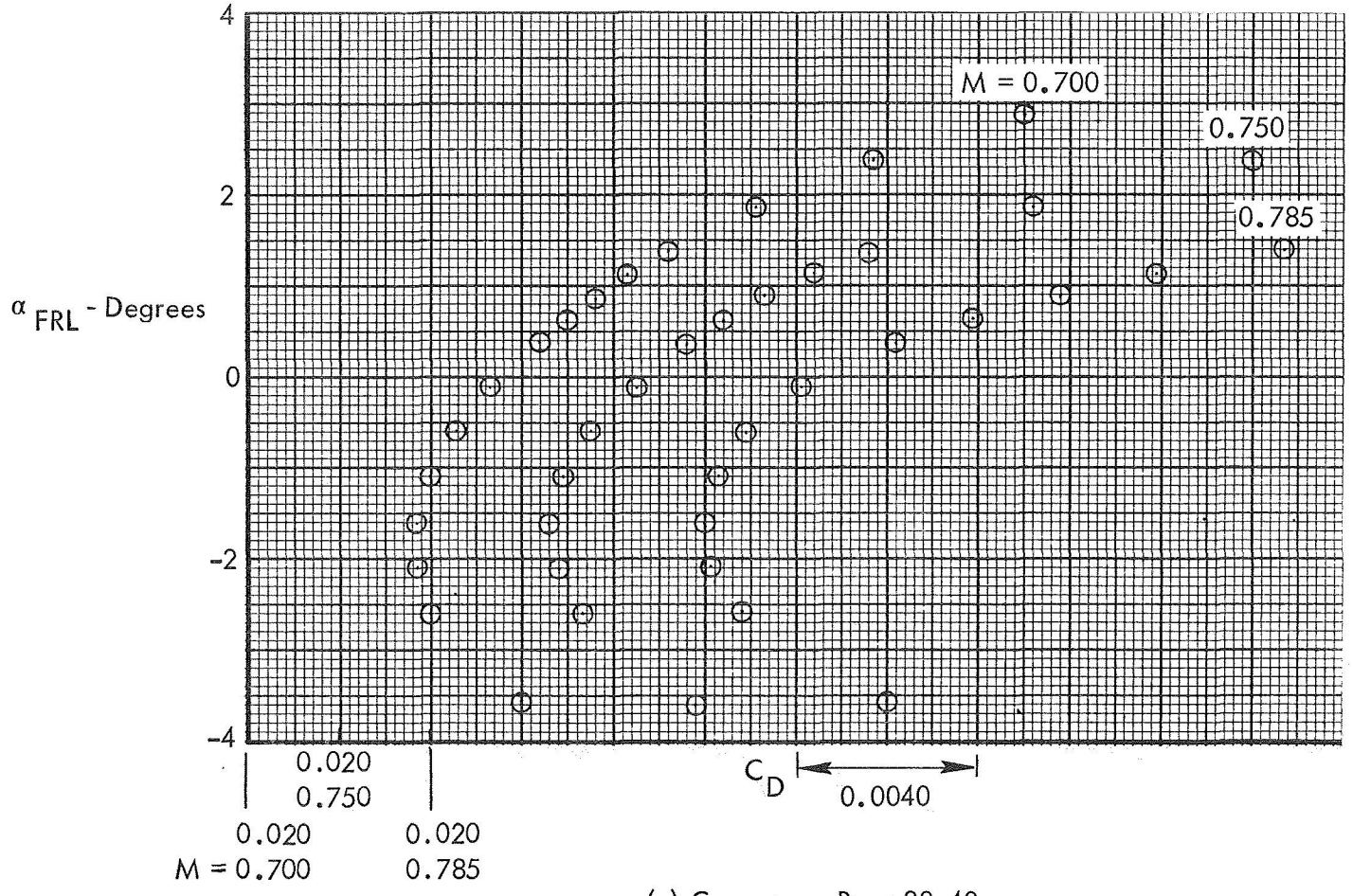
(a) $C_L - \alpha$ Runs 37-41.

Figure 16. Basic Aerodynamic Data. Configuration 10. Test 617.



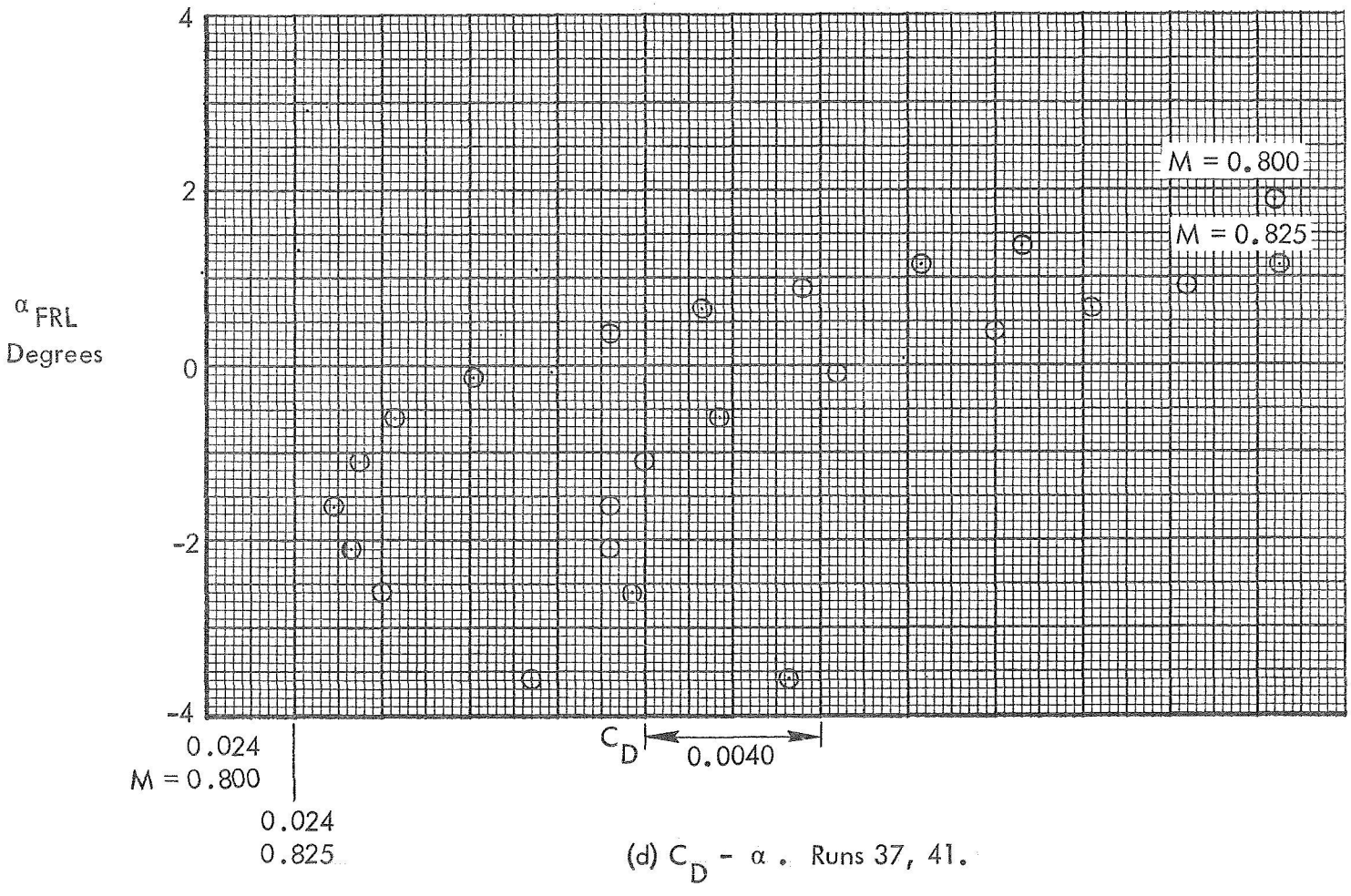
(b) $C_M - \alpha$. Runs 37-41.

Figure 16. Continued.



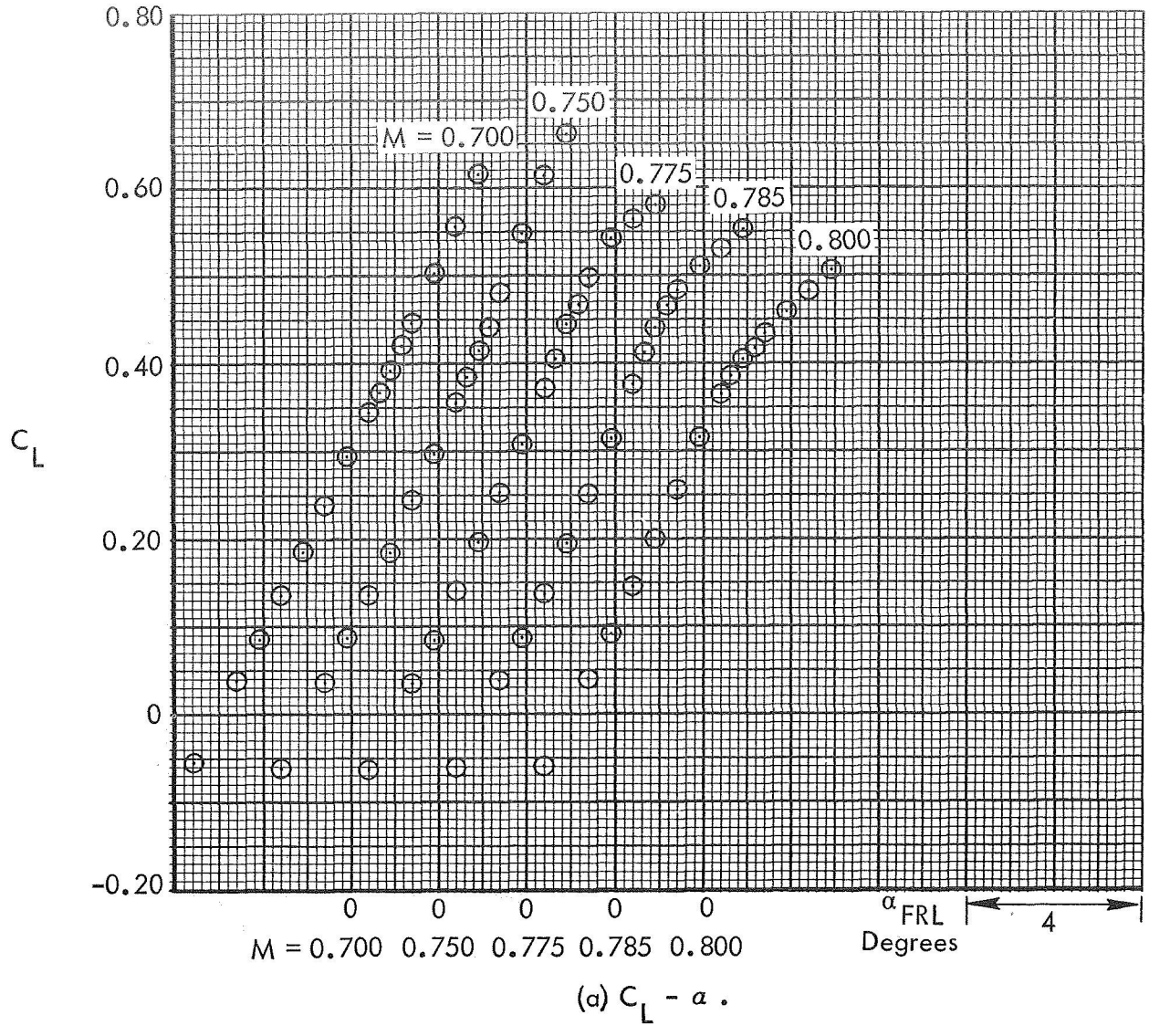
(c) $C_D - \alpha$. Runs 38-40.

Figure 16. Continued.



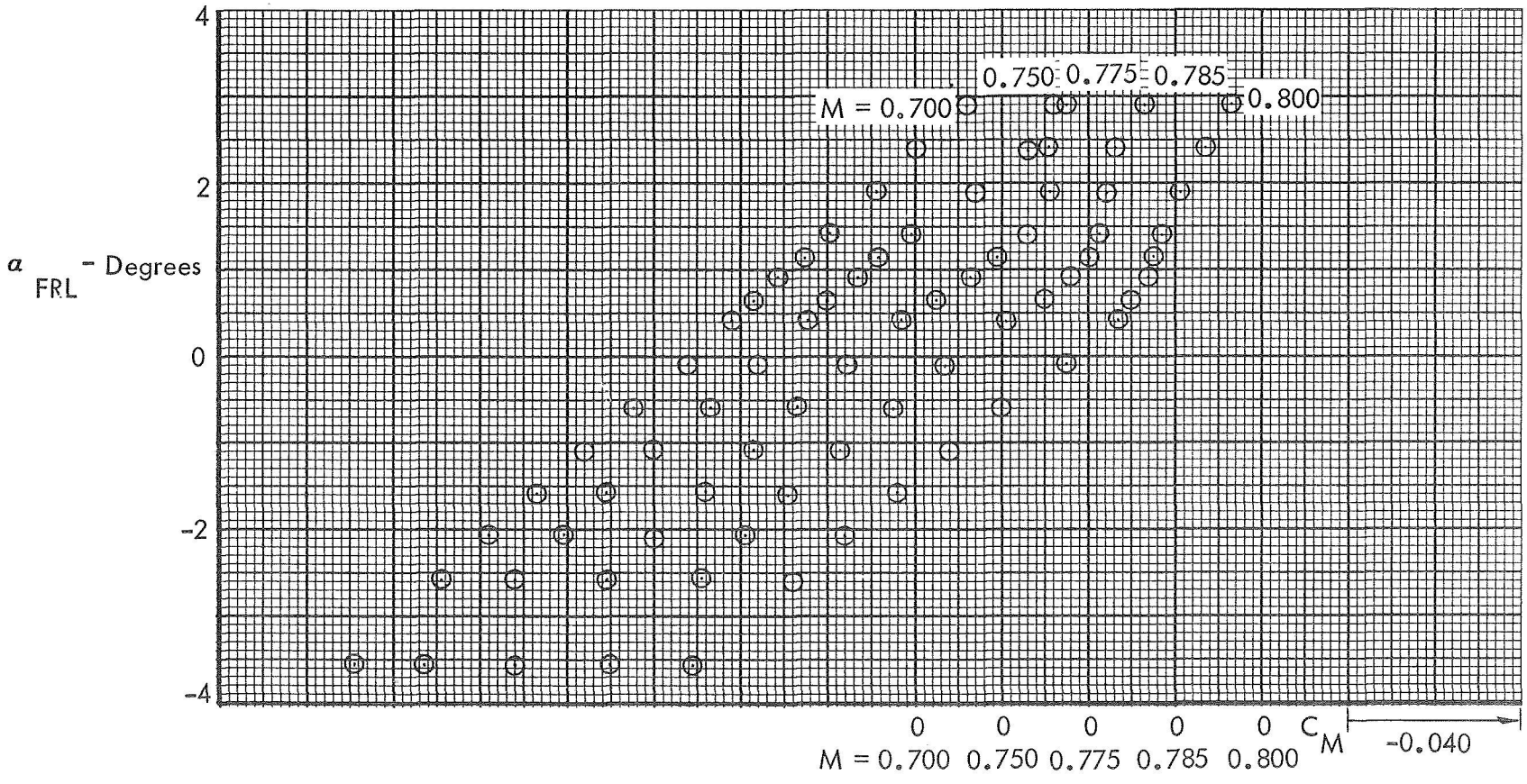
(d) $C_D - \alpha$. Runs 37, 41.

Figure 16. Concluded.



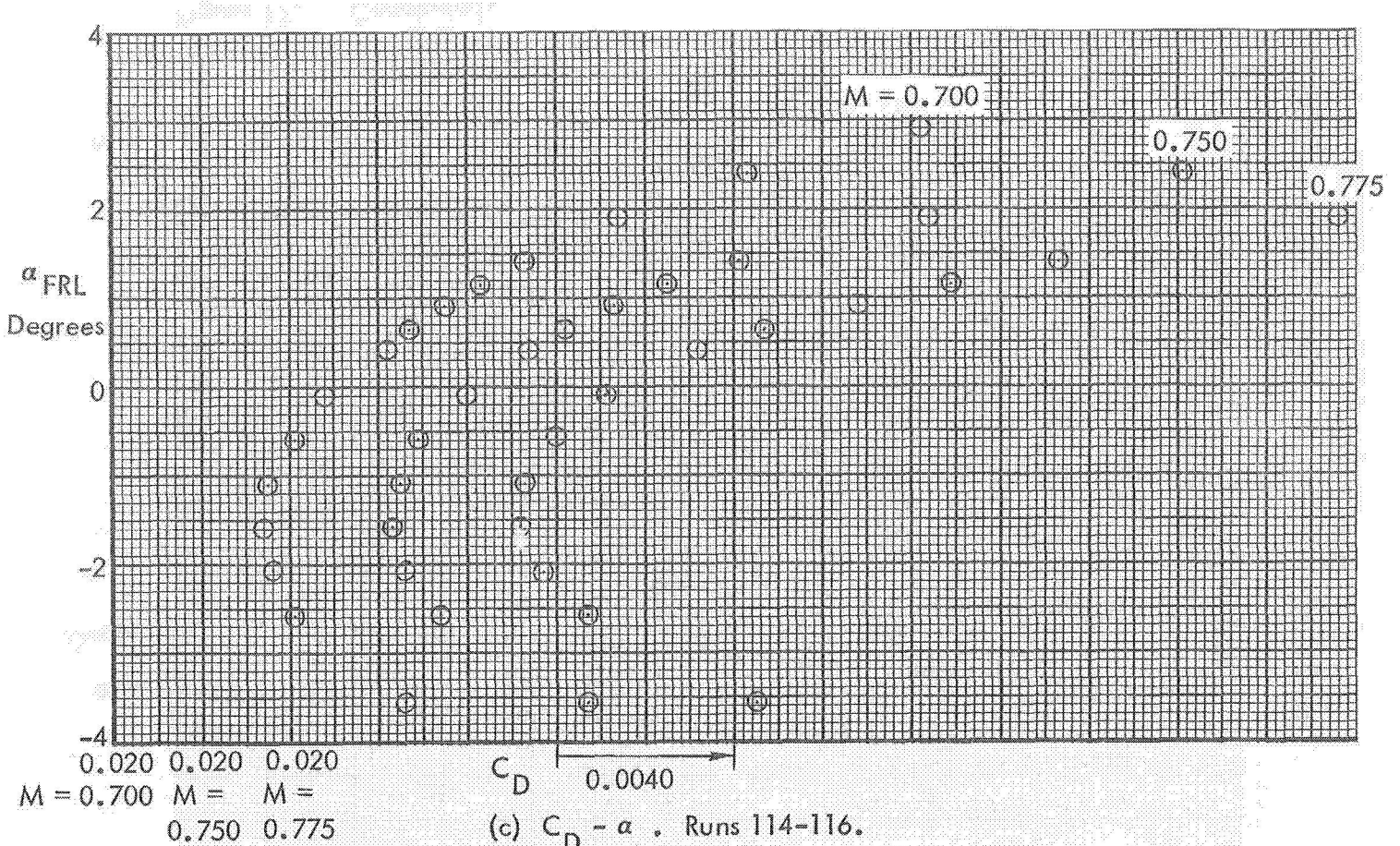
(a) $C_L - \alpha$.

Figure 17. Basic Aerodynamic Data. Sting Configuration 1. Test 617.



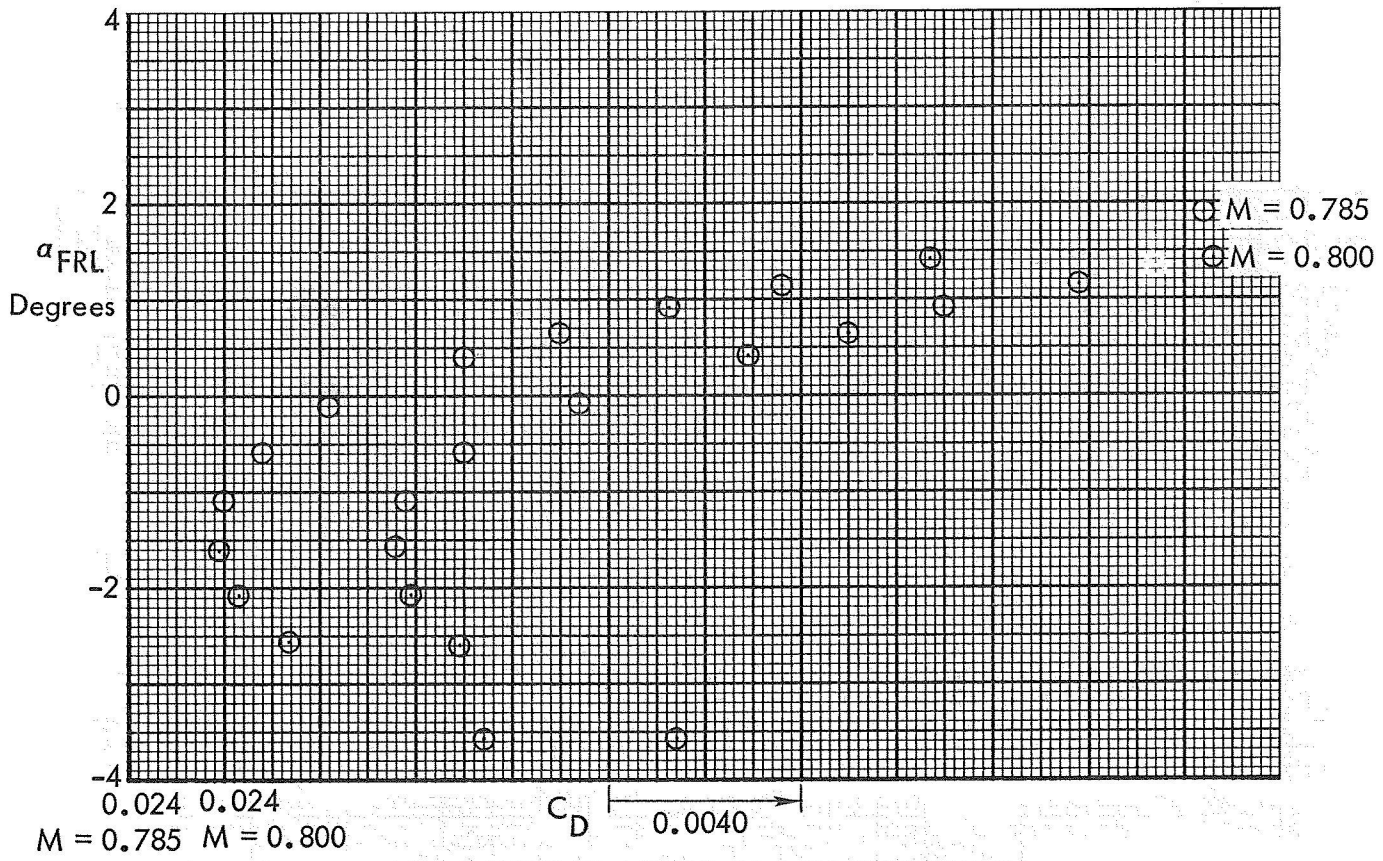
(b) C_M - α . Runs 112-116.

Figure 17. Continued.



(c) $C_D - \alpha$. Runs 114-116.

Figure 17. Continued.



(d) $\alpha - C_D$. Runs 112, 113.

Figure 17. Concluded.

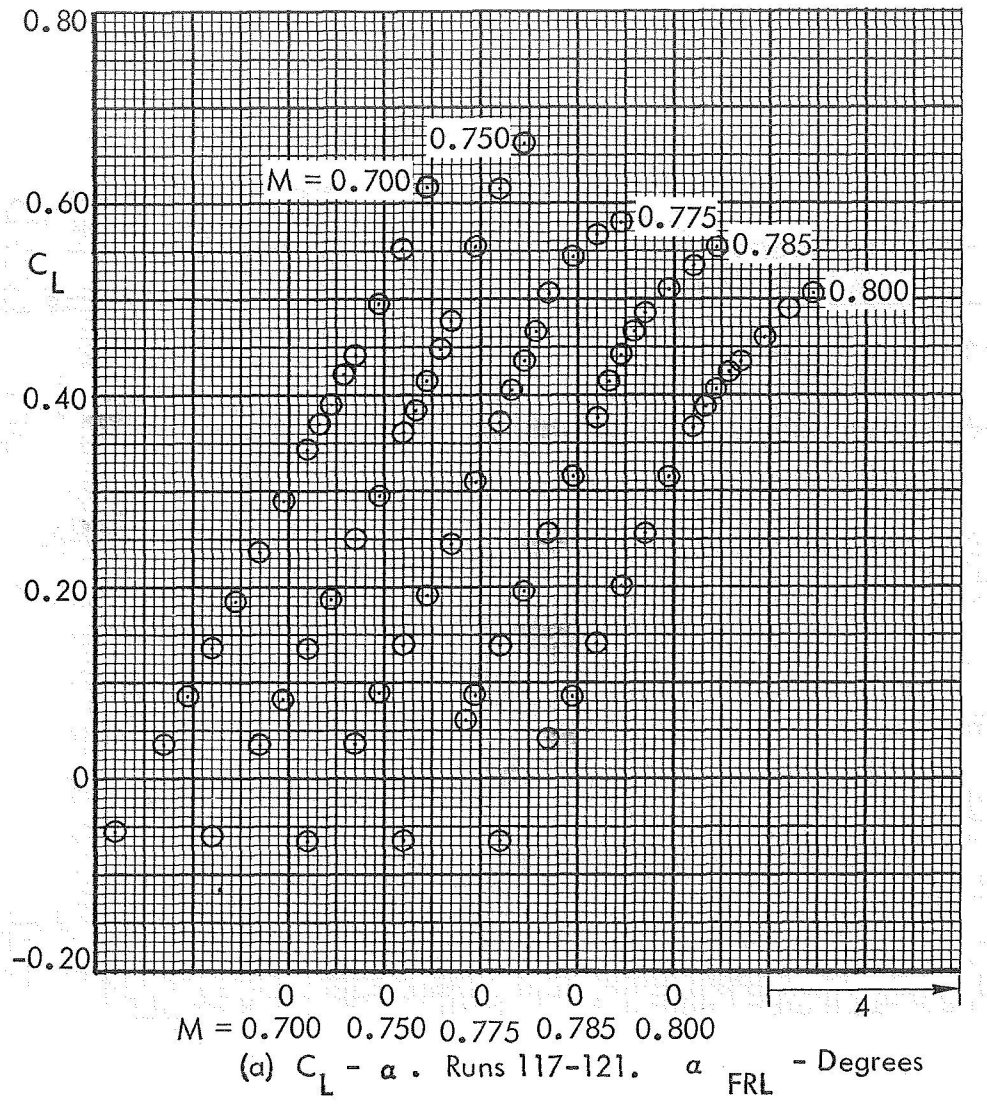
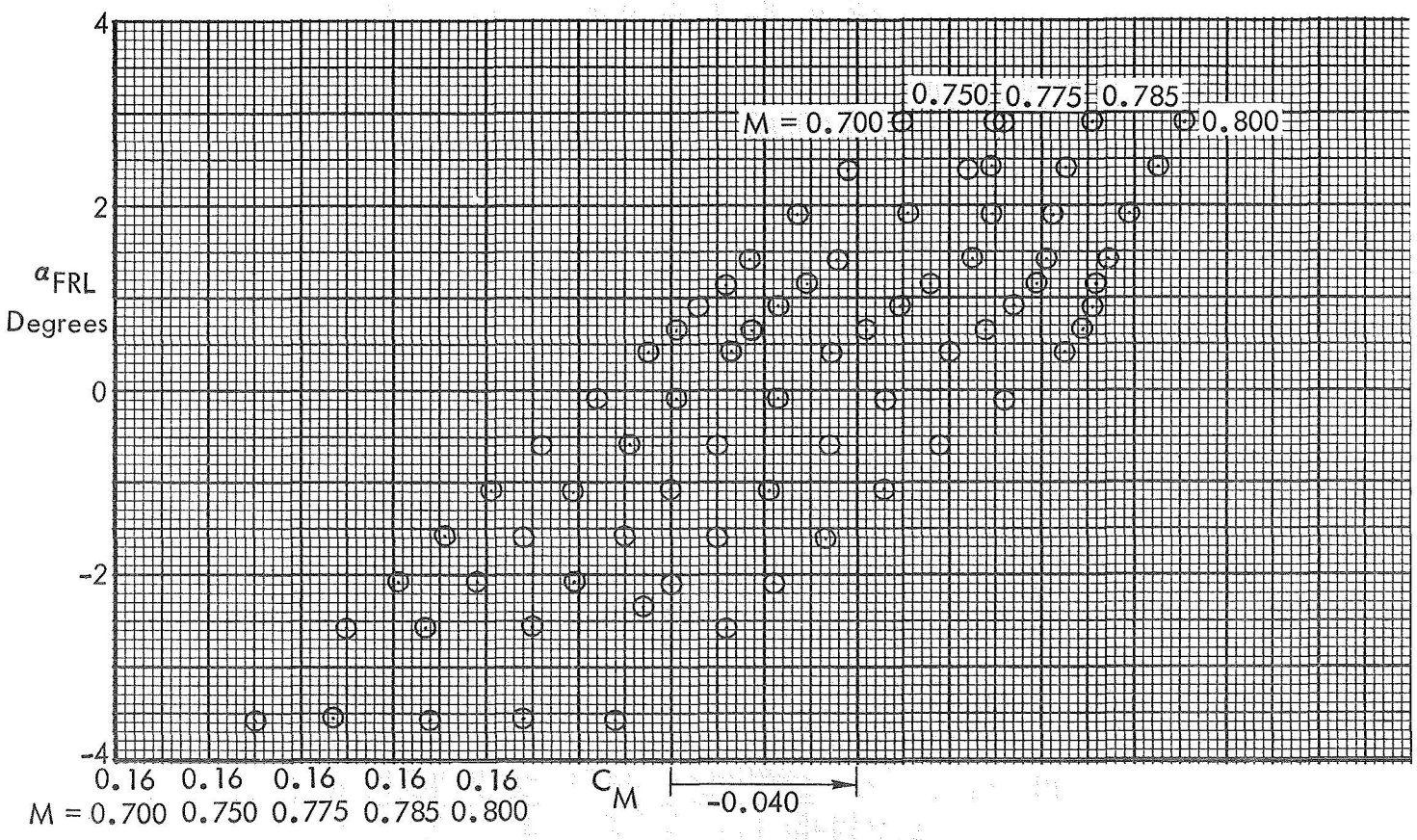
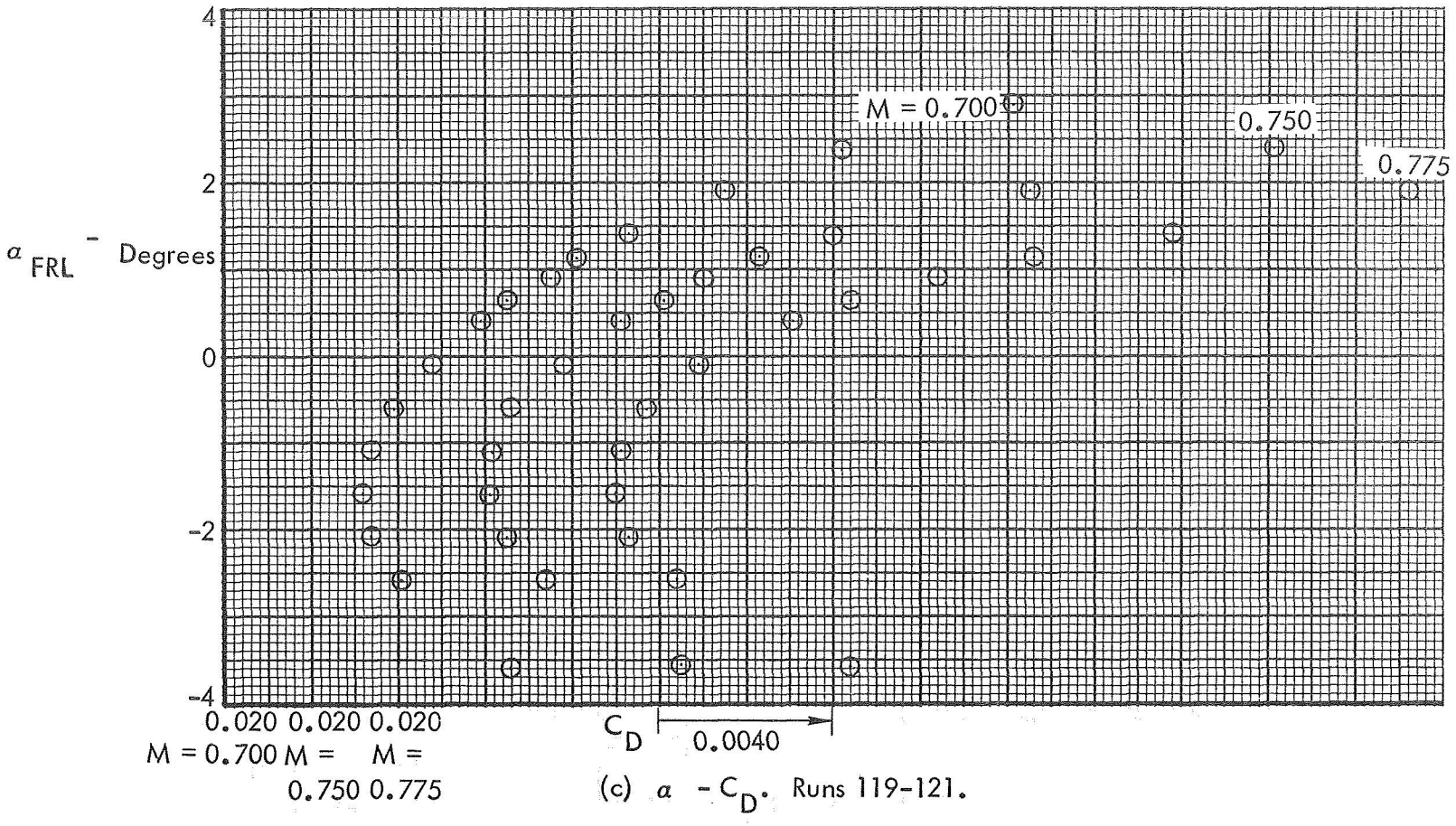


Figure 18. Sting Configuration 2. Test 617.



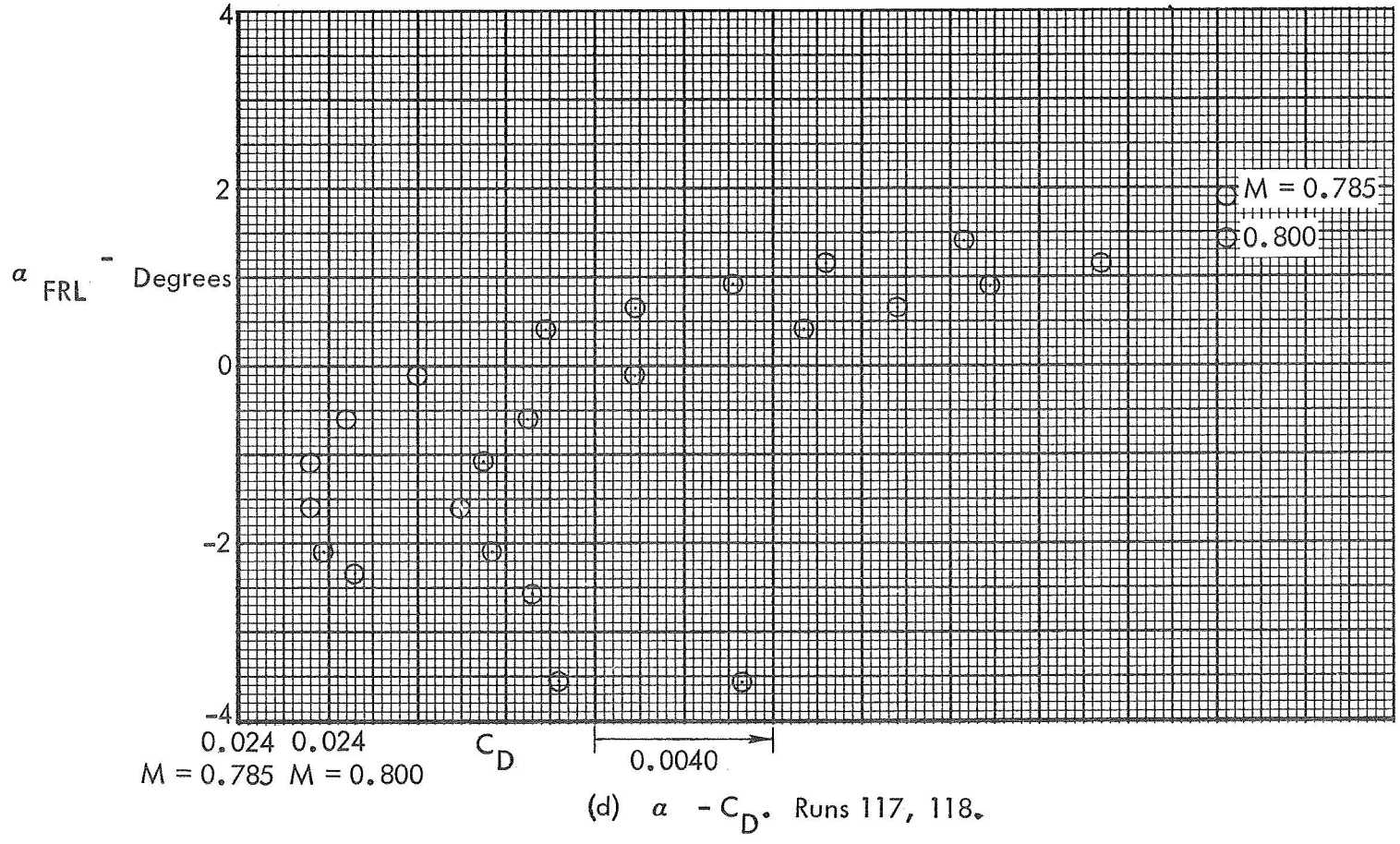
(b) $C_M - \alpha$. Runs 117-121.

Figure 18. Continued.



(c) α - C_D. Runs 119-121.

Figure 18. Continued.



(d) α - C_D. Runs 117, 118.

Figure 18. Concluded.

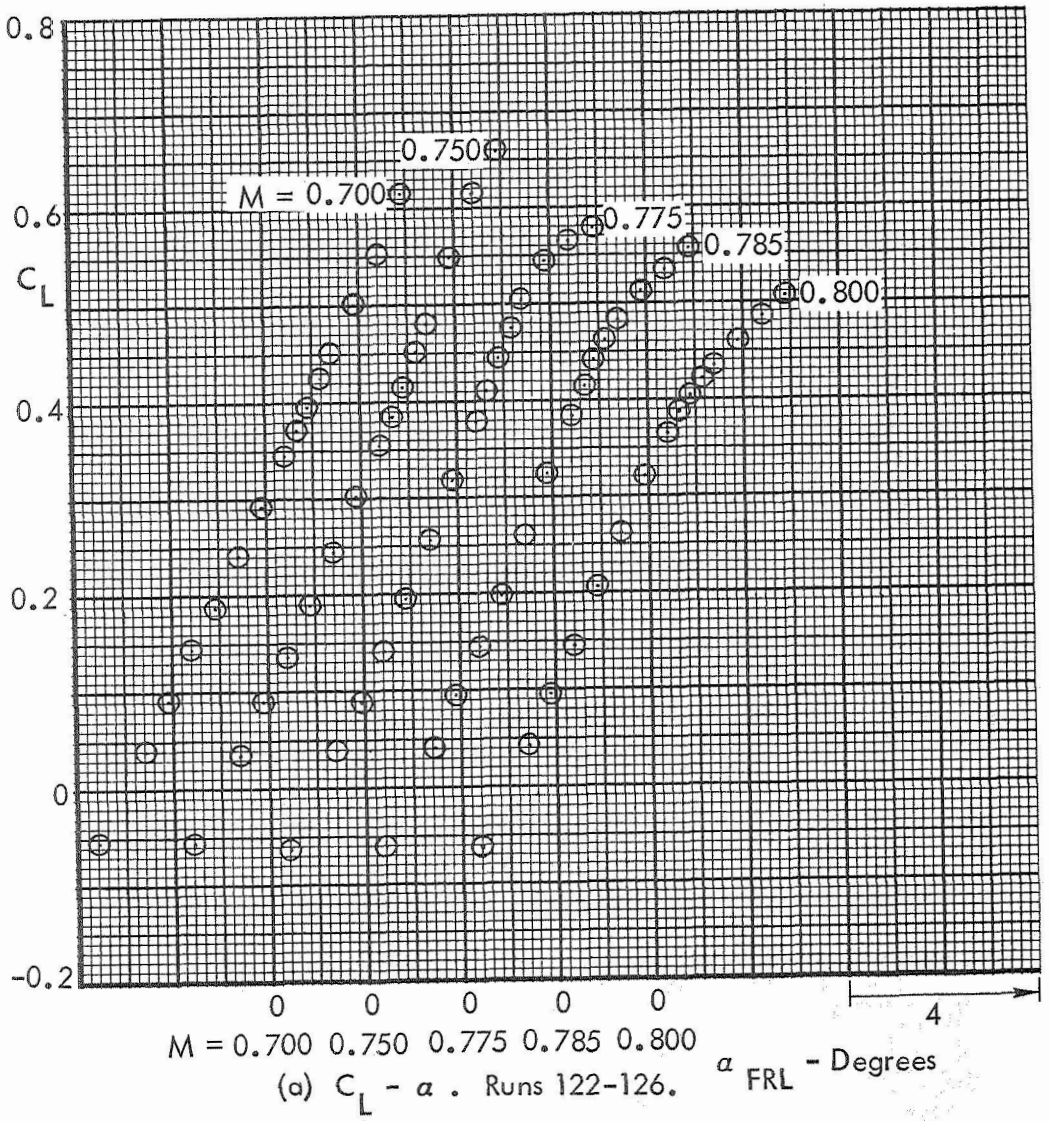
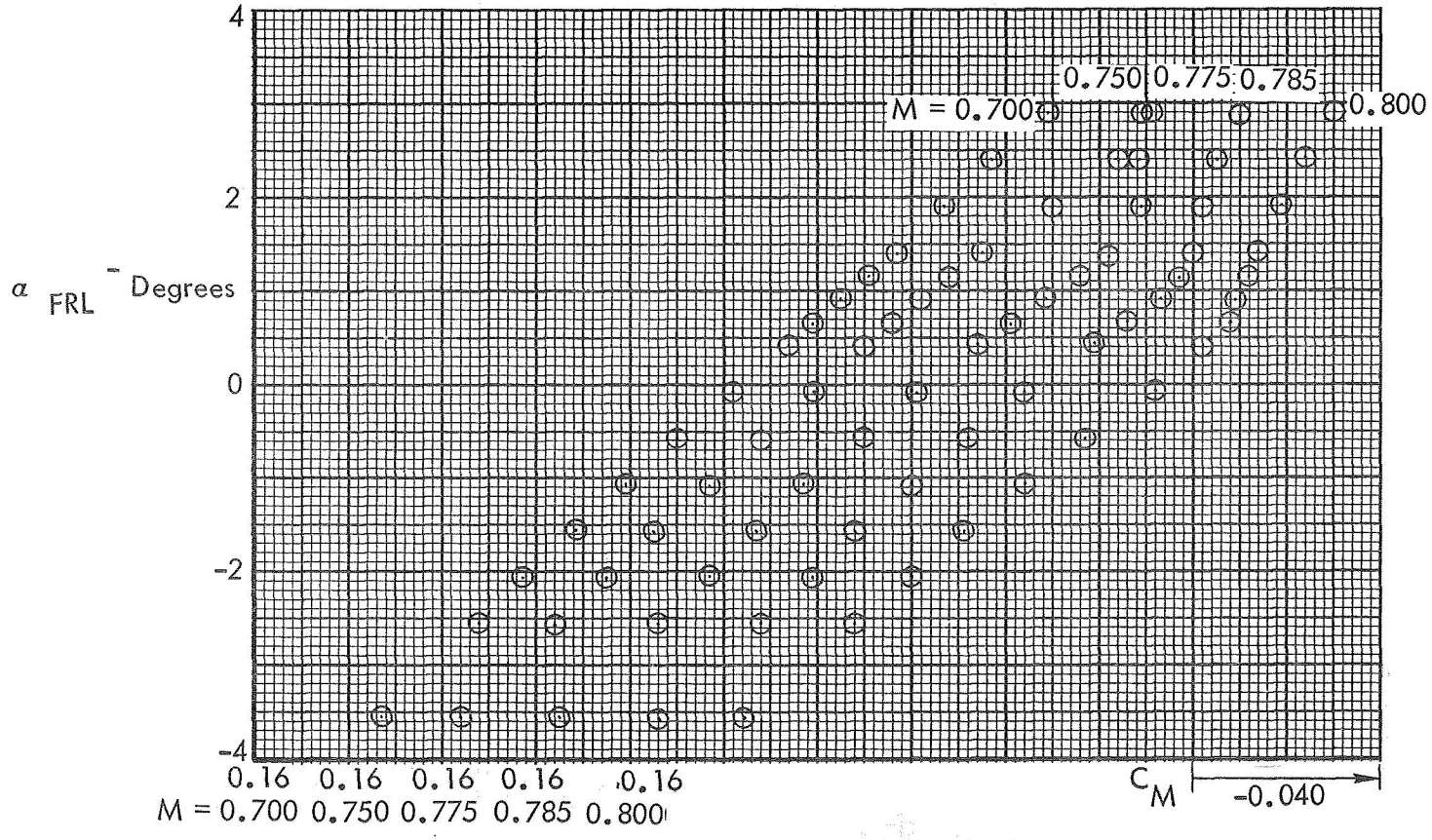
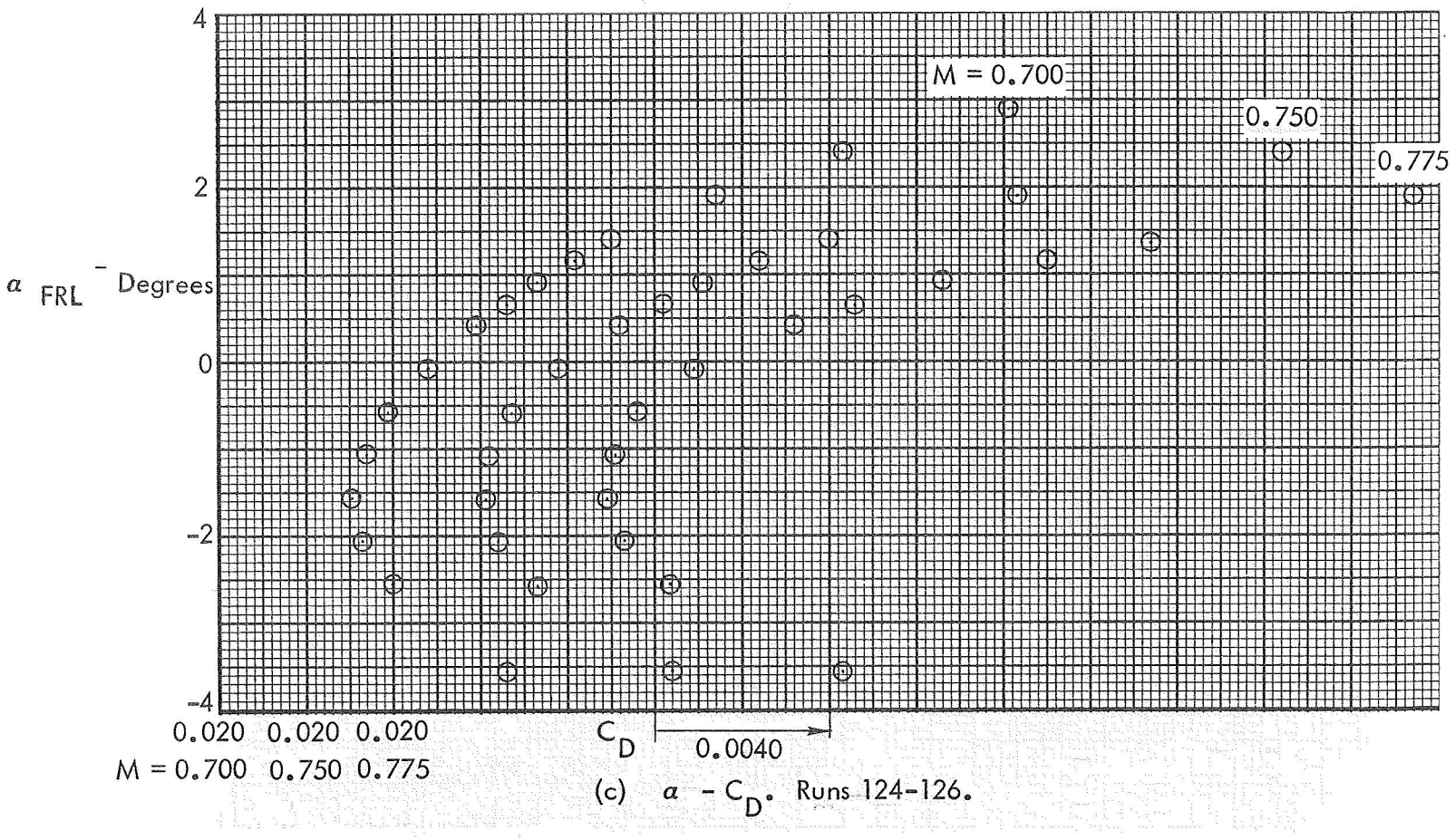


Figure 19. Sting Configuration 3. Test 617.



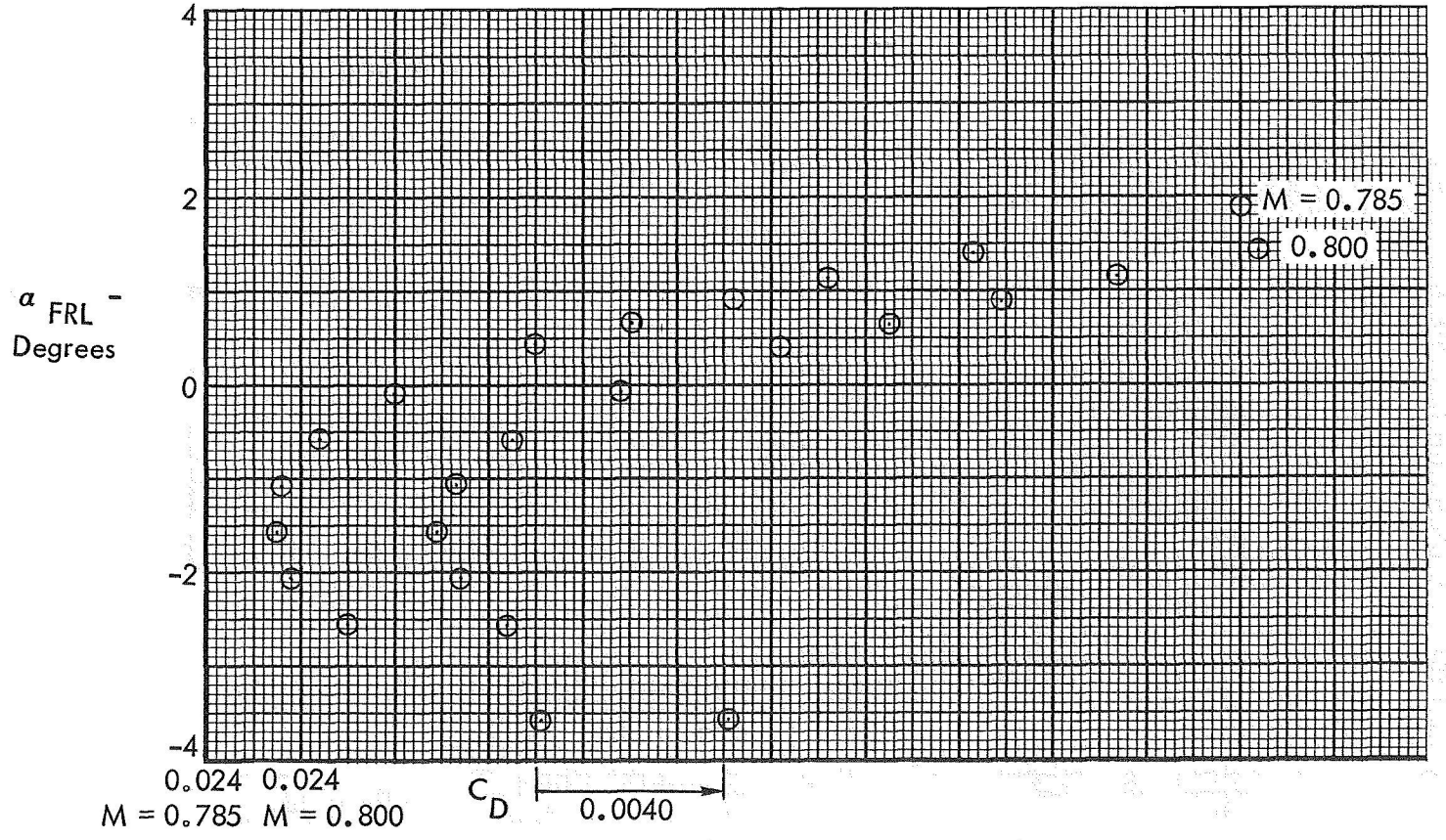
(b) $C_M - \alpha$. Runs 122-126.

Figure 19. Continued.



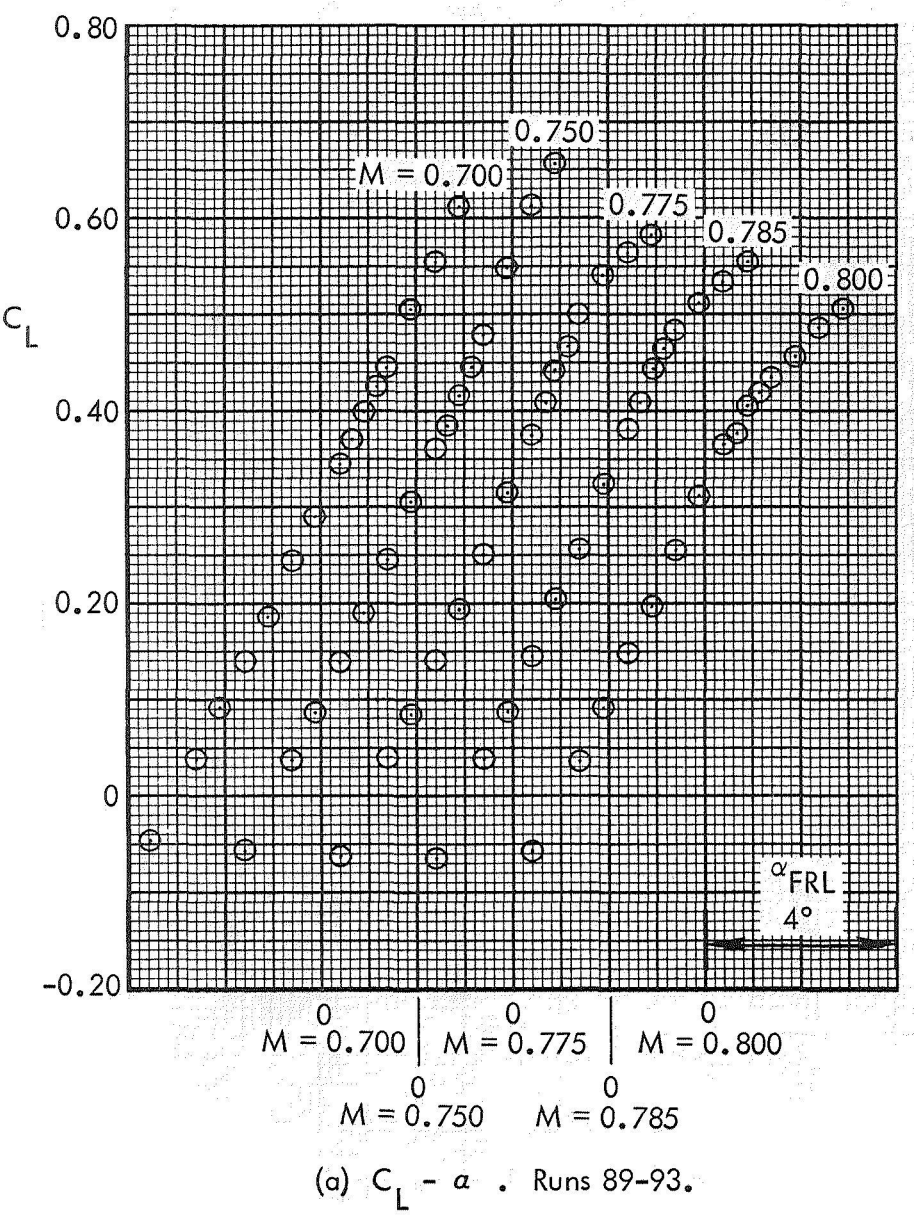
(c) α - C_D. Runs 124-126.

Figure 19. Continued.



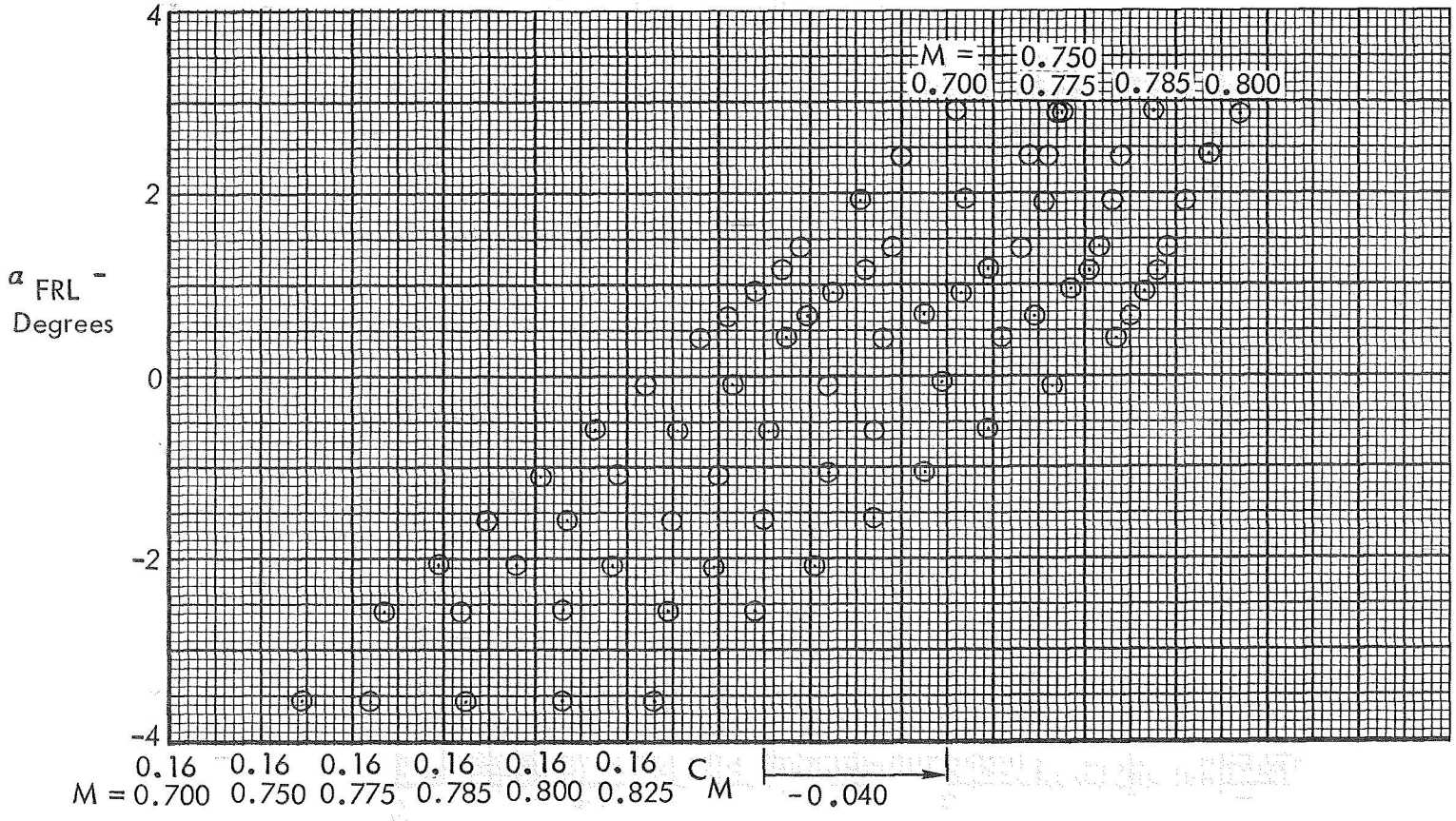
(d) $\alpha - C_D$. Runs 122, 123.

Figure 19. Concluded



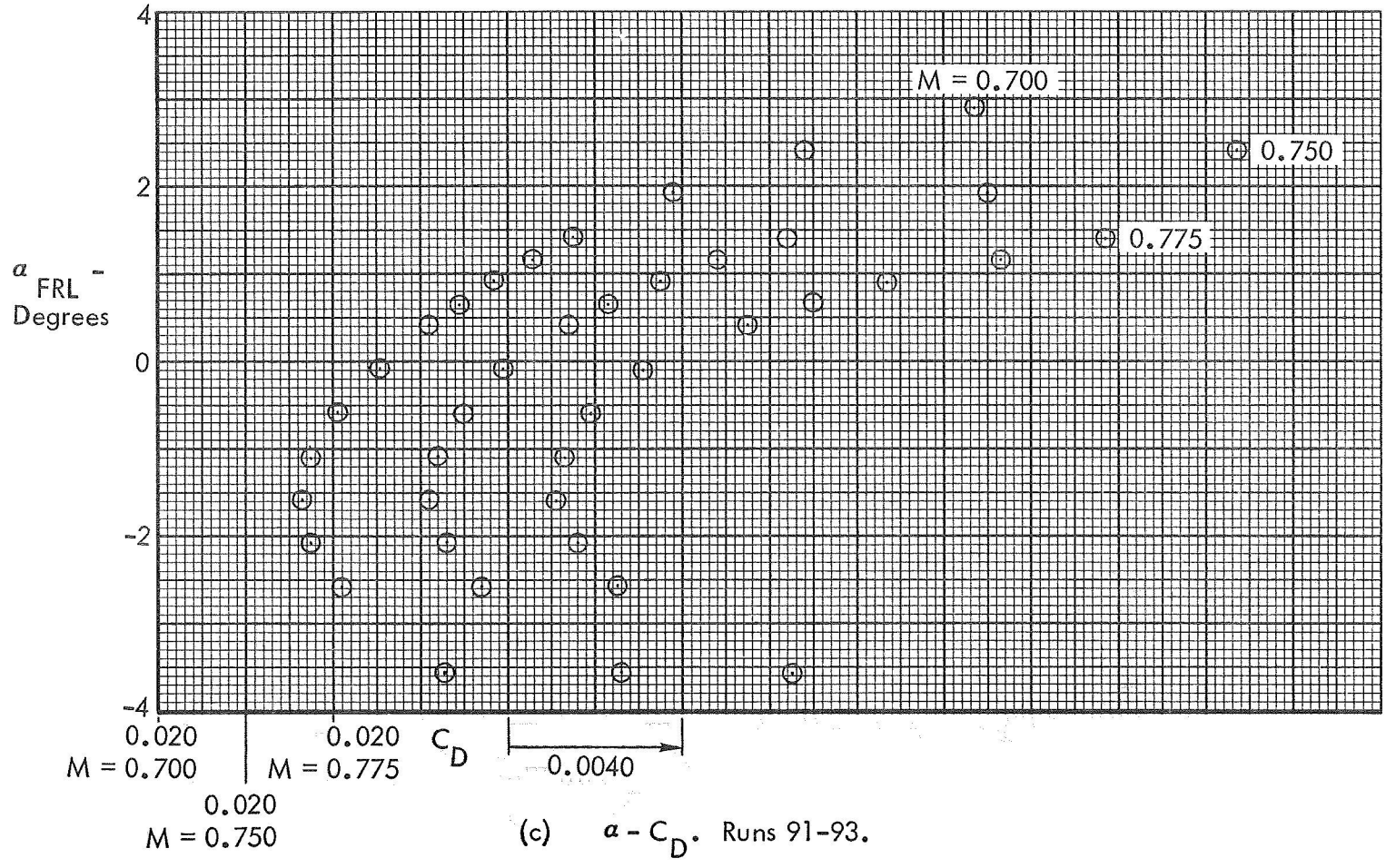
(a) $C_L - \alpha$. Runs 89-93.

Figure 20. Sting Configuration 4. Test 617.



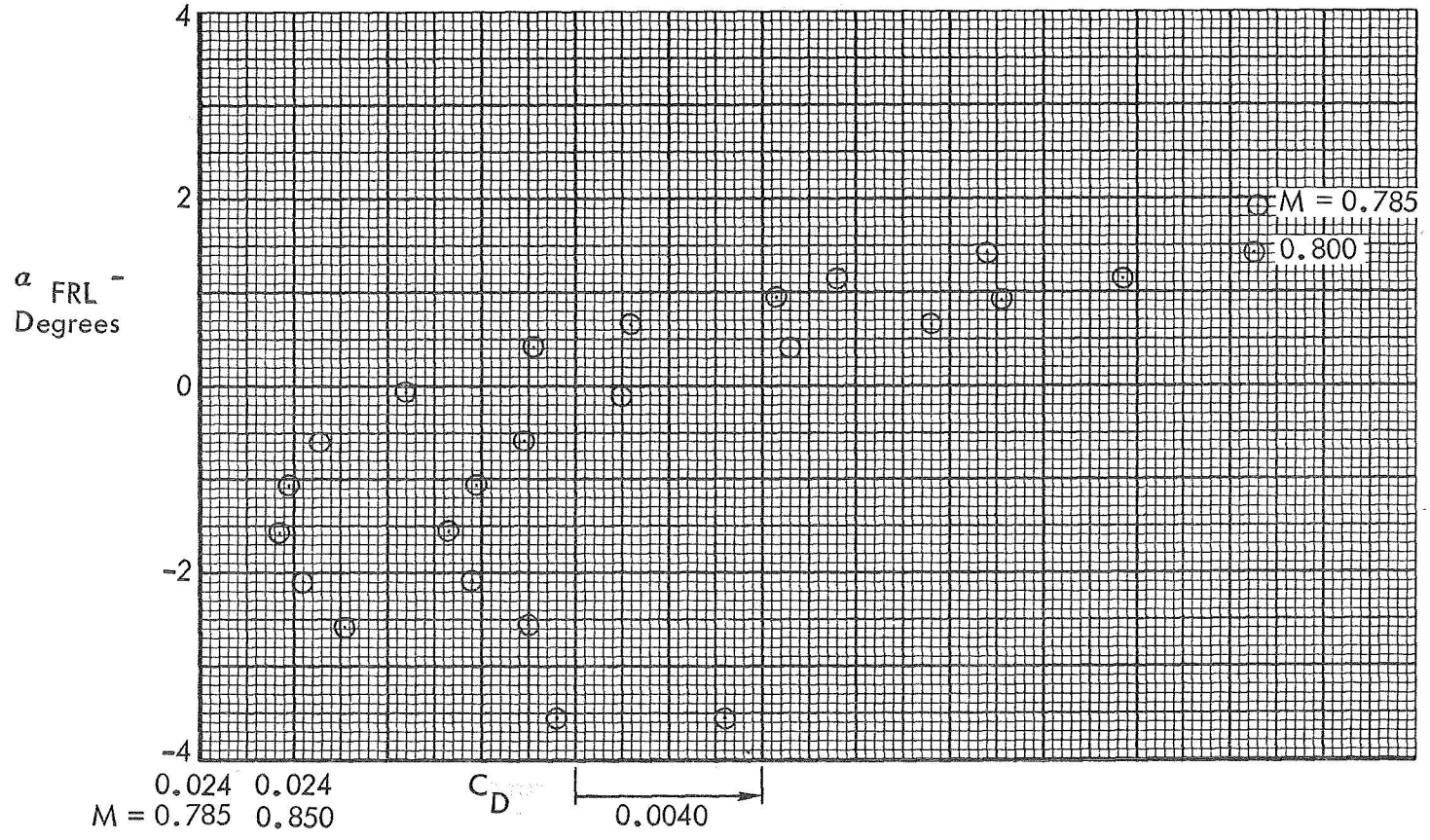
(b) $C_M - \alpha$. Runs 89-93.

Figure 20. Continued.



(c) $\alpha - C_D$. Runs 91-93.

Figure 20. Continued.



(d) $\alpha - C_D$. Runs 89, 90

Figure 20. Concluded.

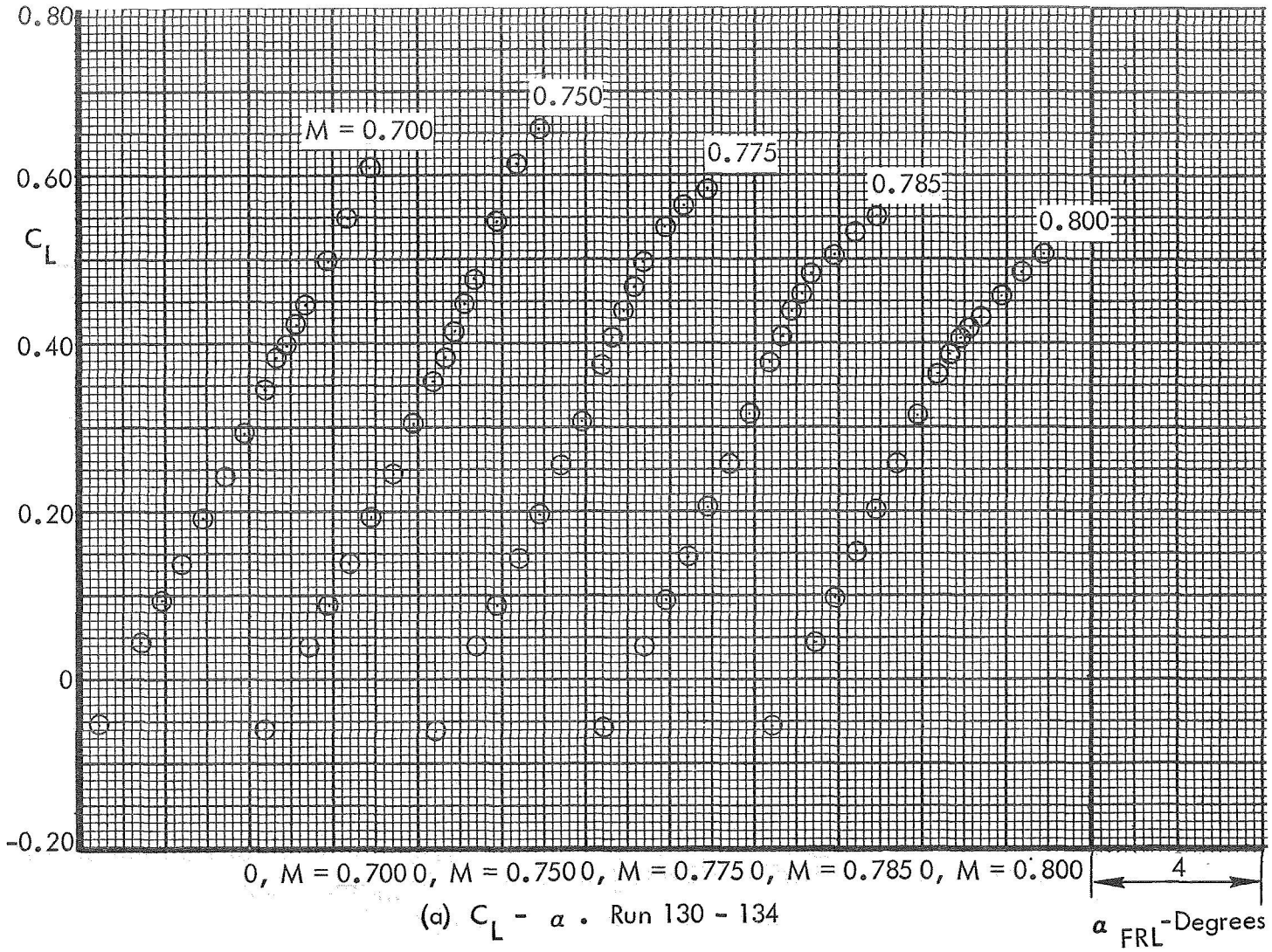
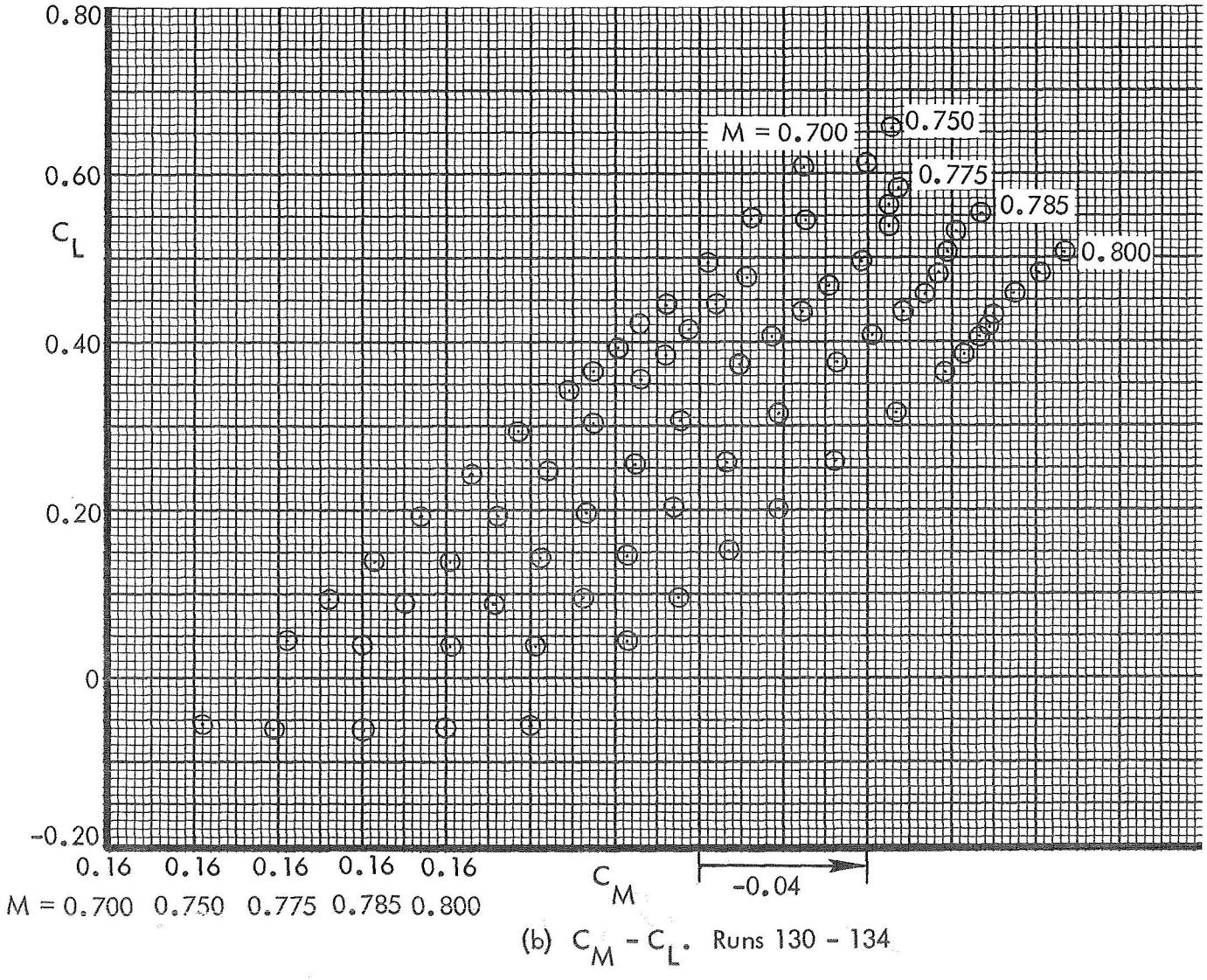


Figure 21. Basic Aerodynamic Data. No Offset Fairing Sting Position 1. Test 617.



(b) $C_M - C_L$. Runs 130 - 134

Figure 21. Continued.

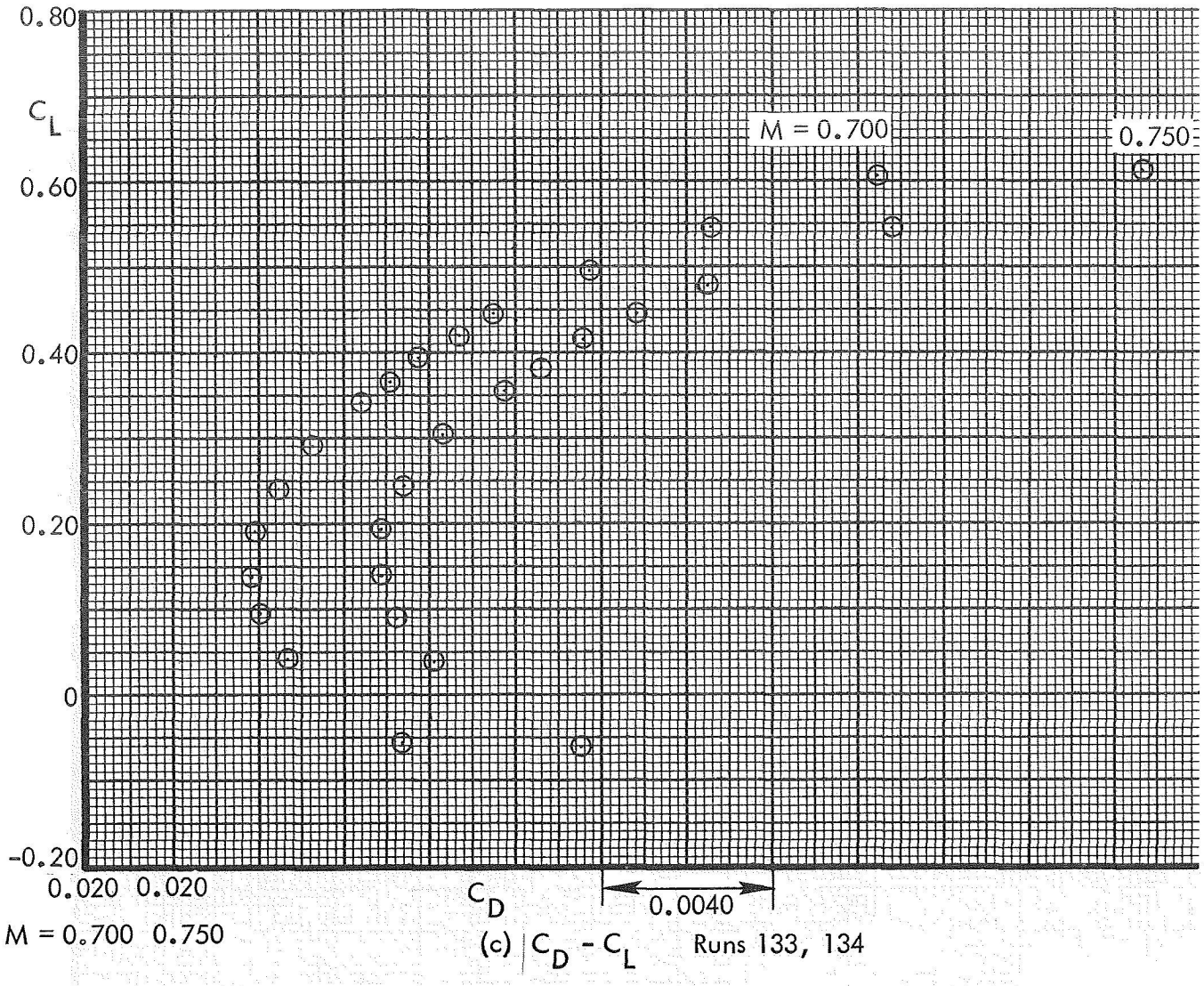
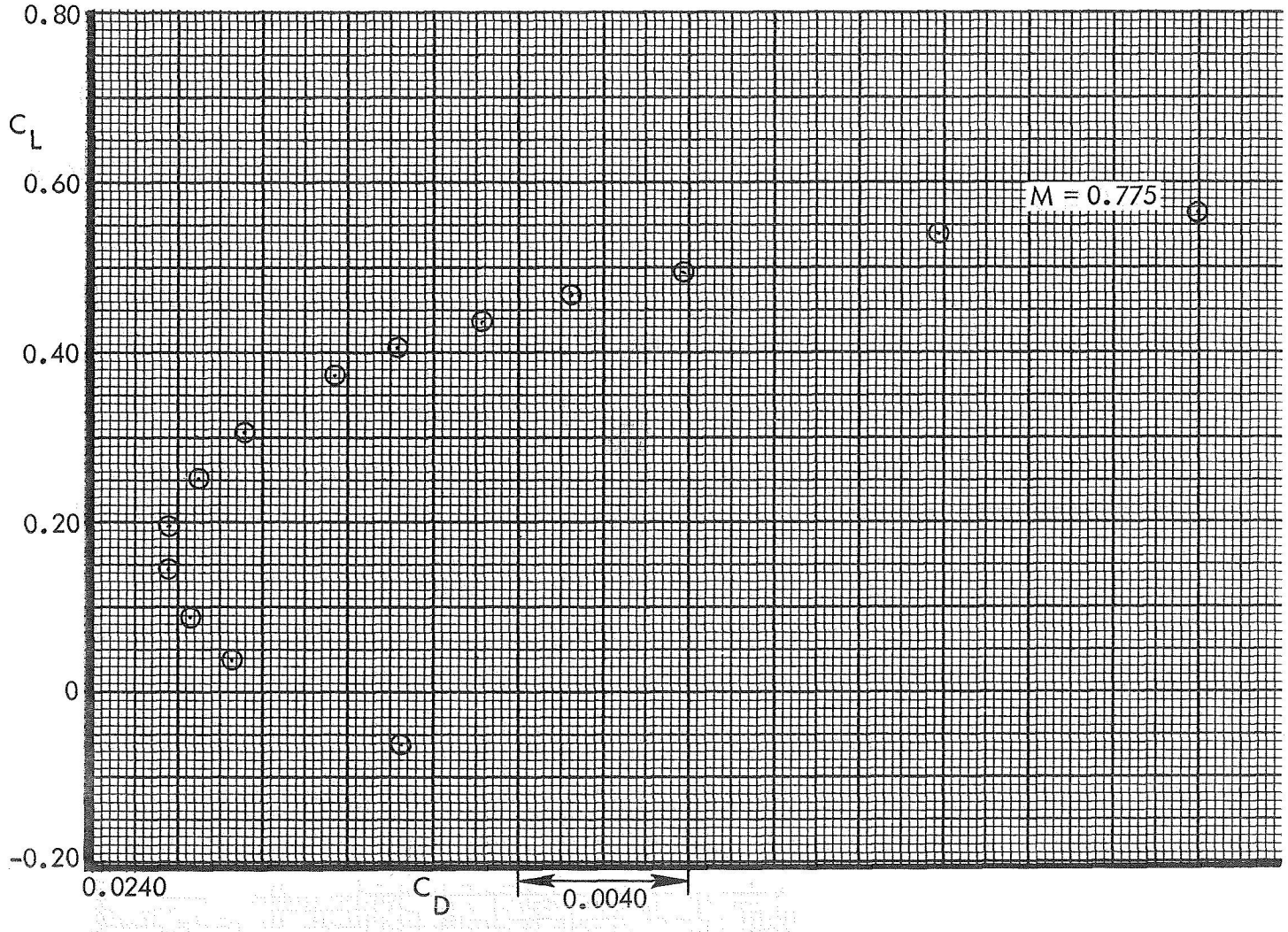
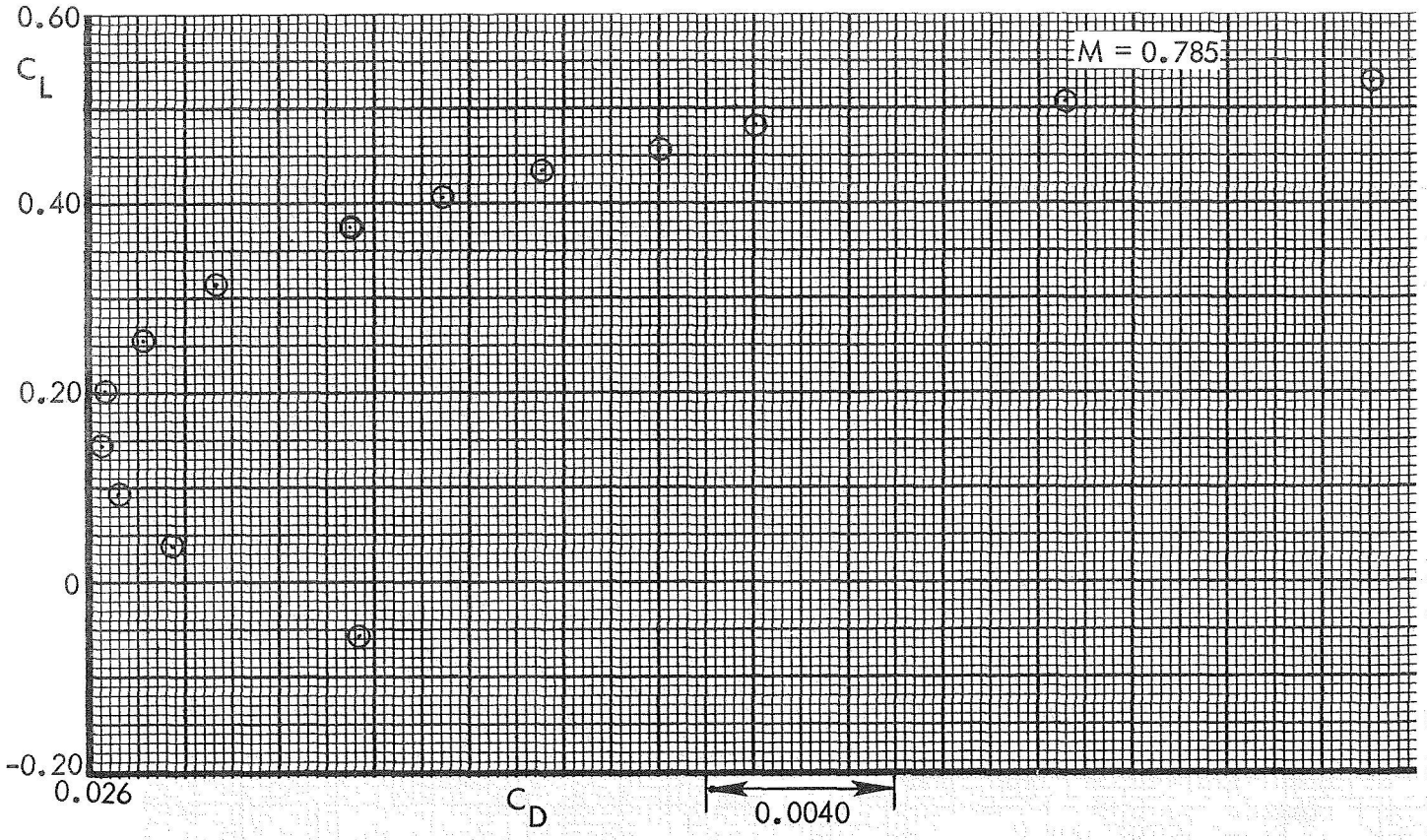


Figure 21. Continued.



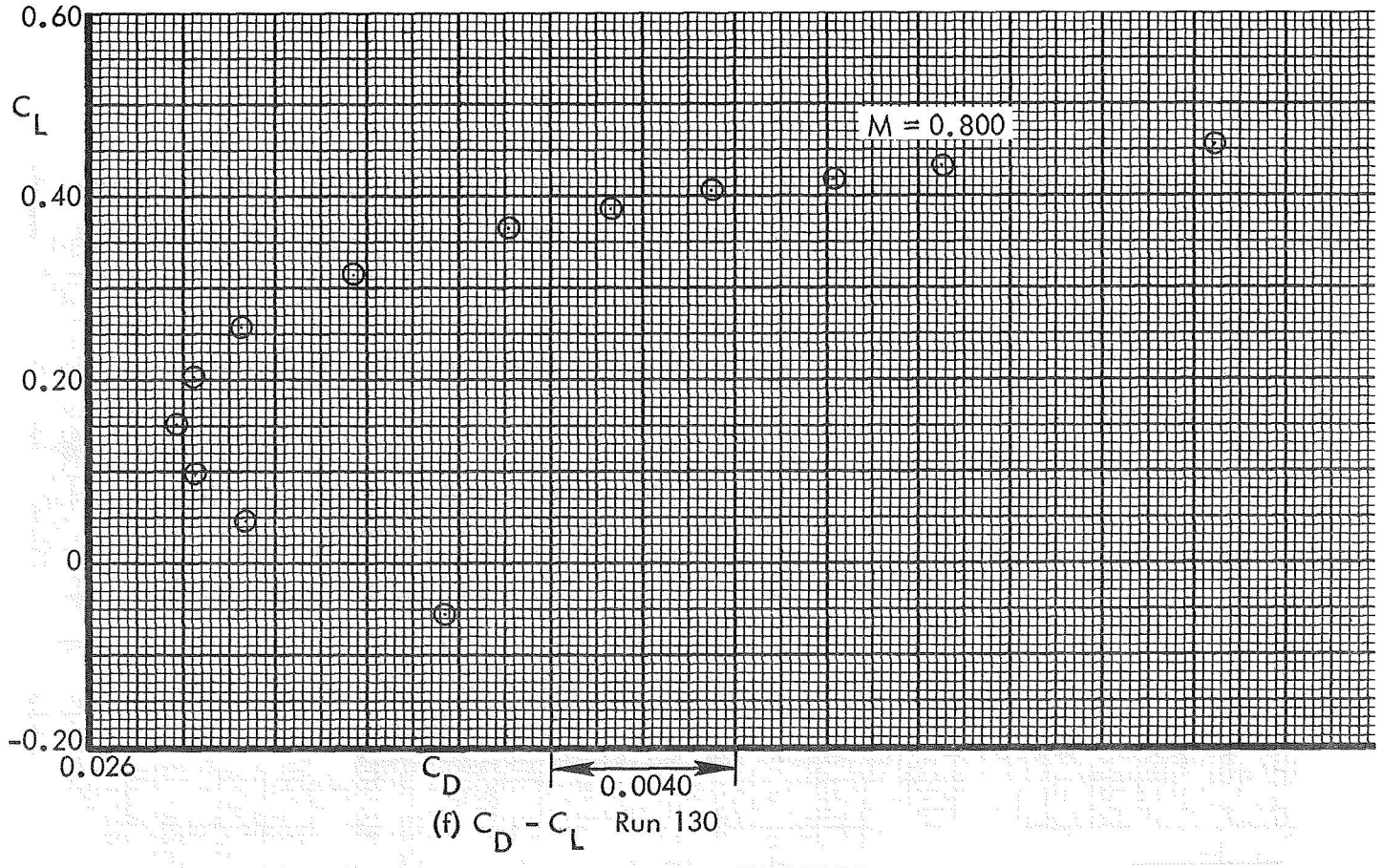
(d) $C_D - C_L$ Run 132

Figure 21. Continued.



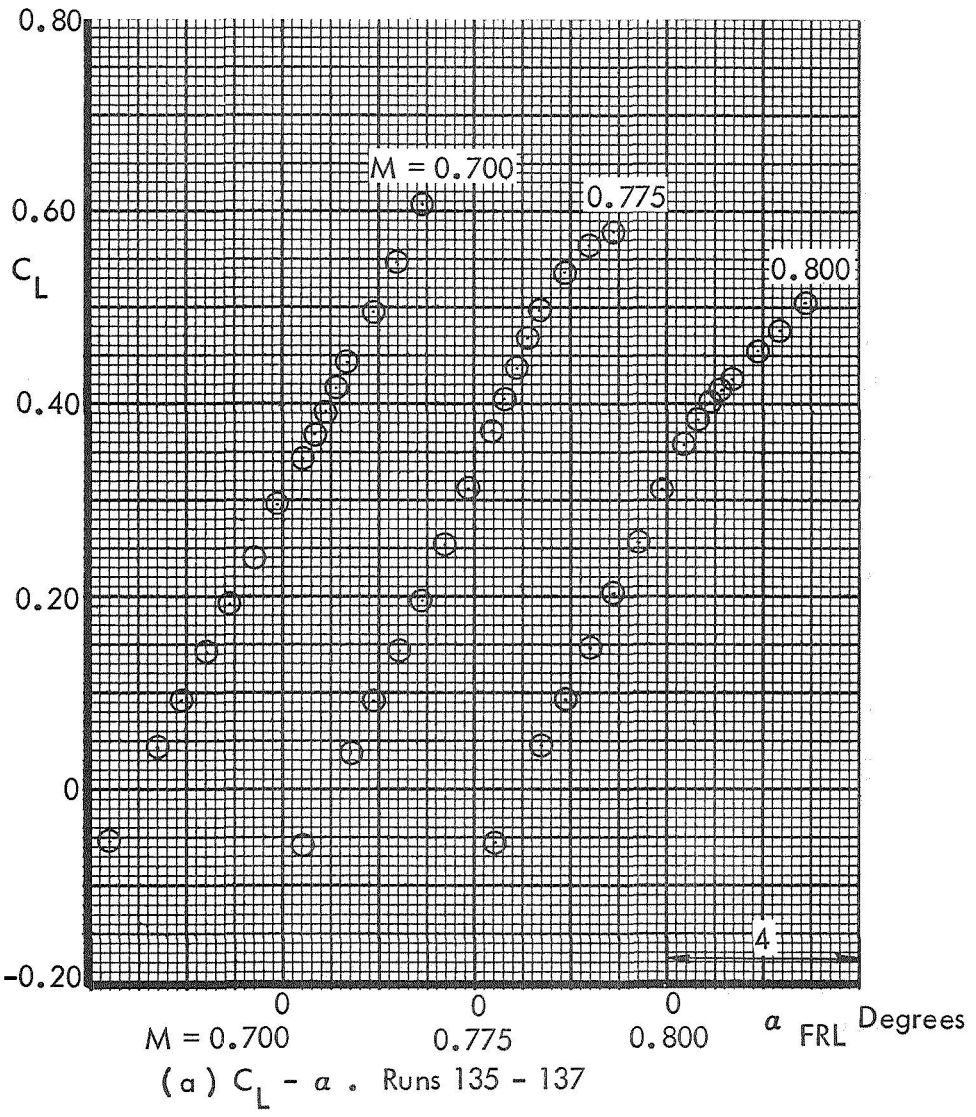
(e) $C_D - C_L$. Run 131

Figure 21. Continued.



(f) $C_D - C_L$ Run 130

Figure 21. Concluded.



(a) C_L - α . Runs 135 - 137

Figure 22. Basic Aerodynamic Data. No Offset Fairing. Sting Position 2. Test 617.

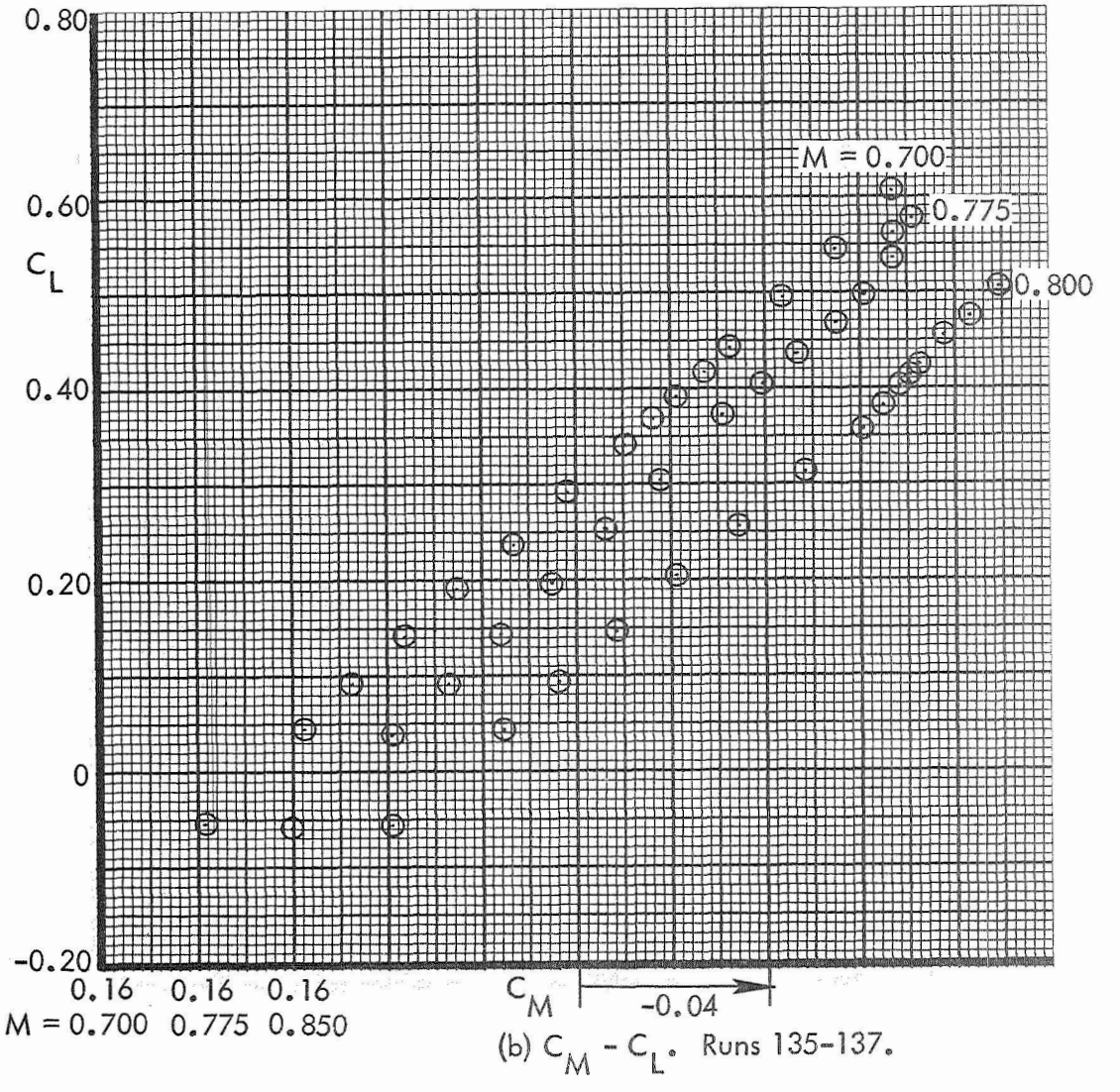
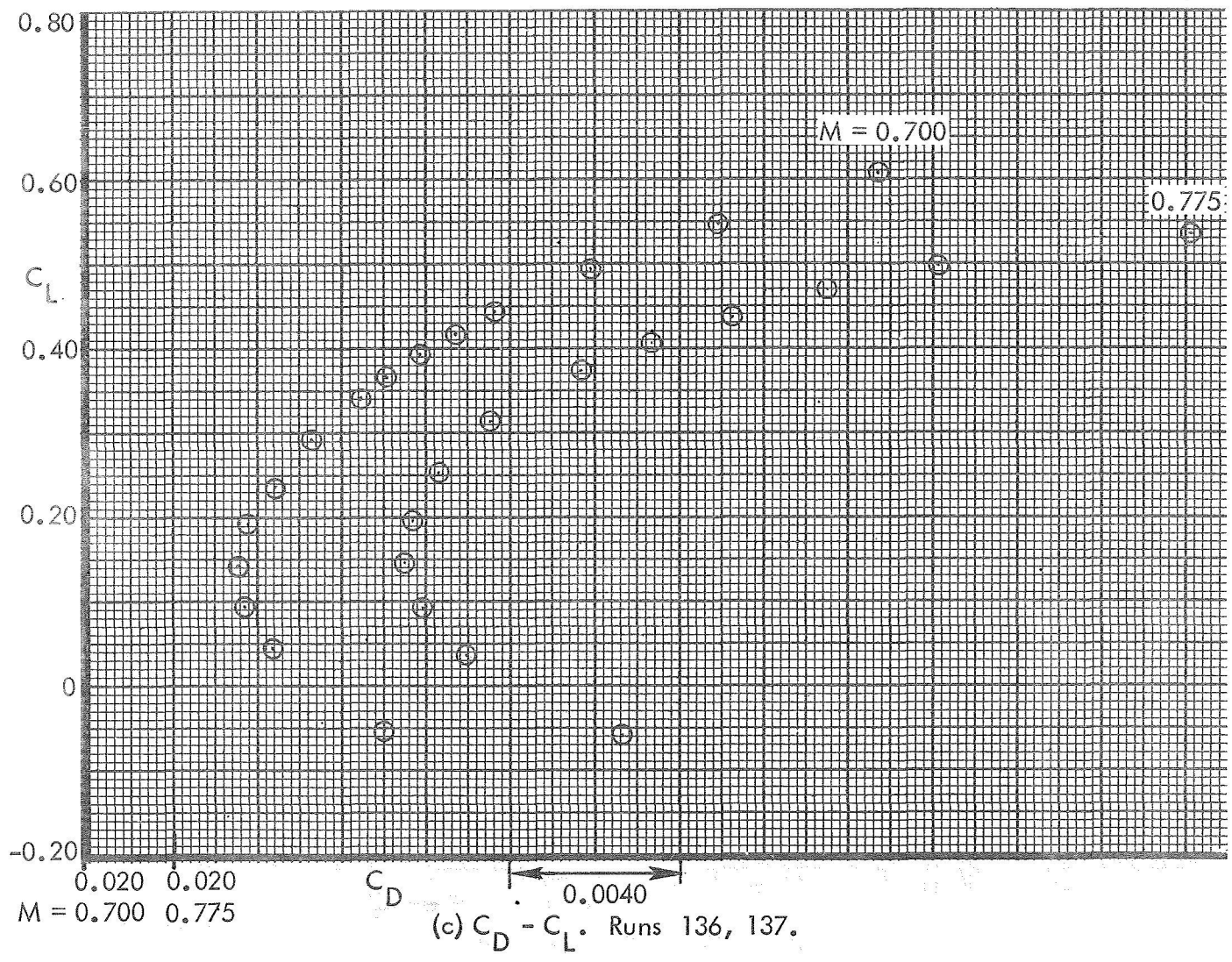
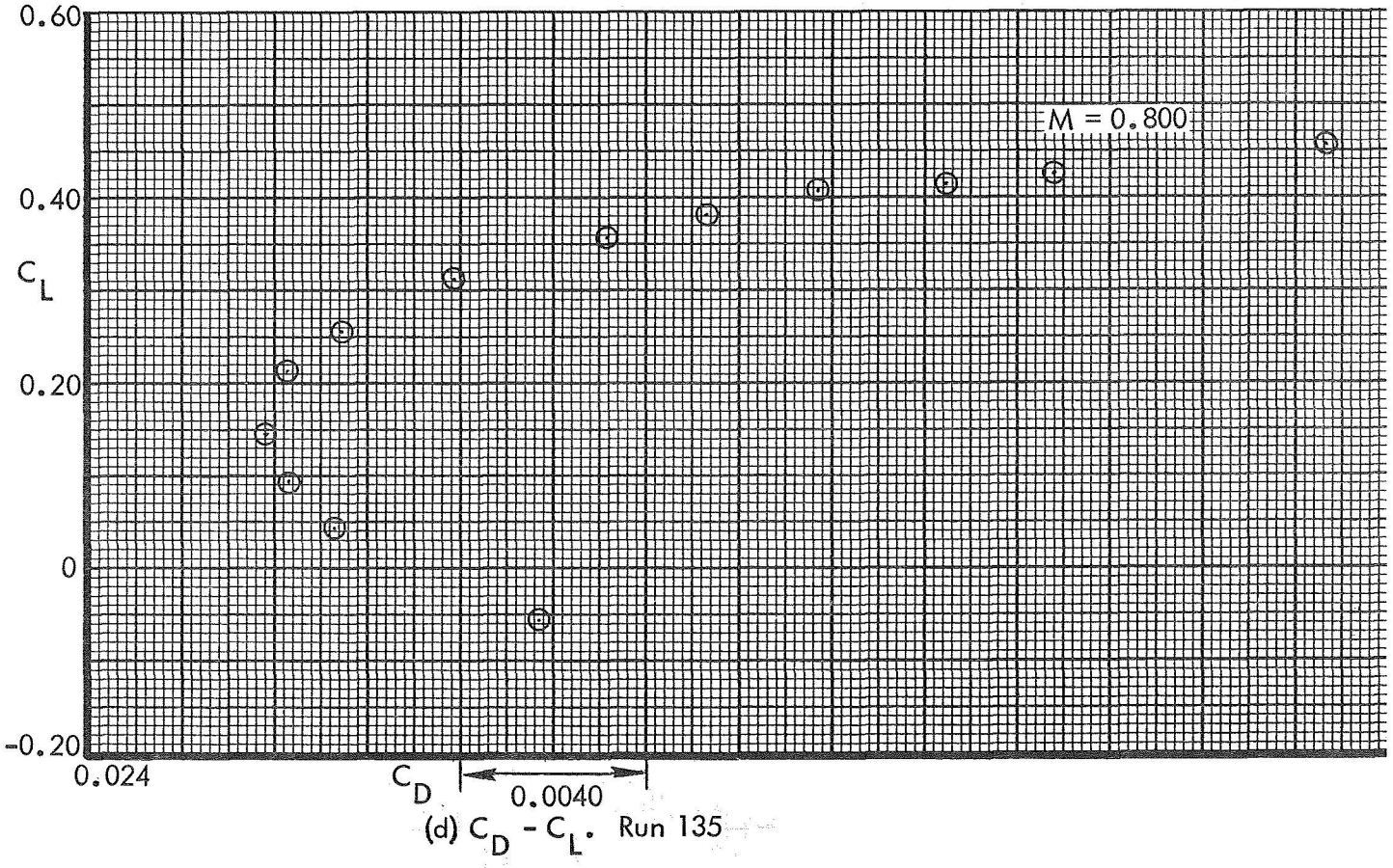


Figure 22. Continued.



(c) $C_D - C_L$. Runs 136, 137.

Figure 22. Continued.



(d) $C_D - C_L$. Run 135

Figure 22. Concluded.

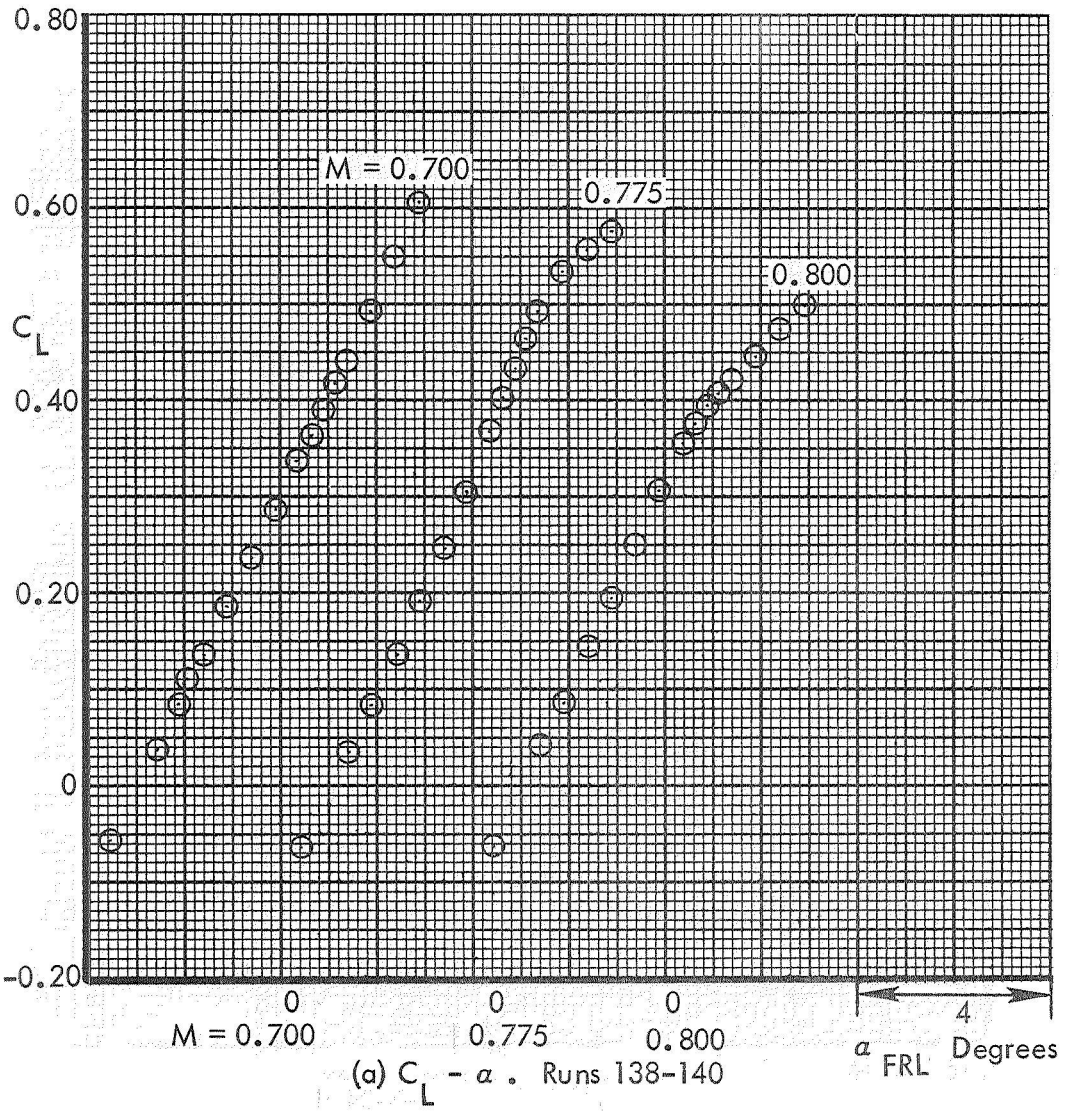


Figure 23. Basic Aerodynamic Data. No Offset Fairing. Sting Position 3. Test 617.

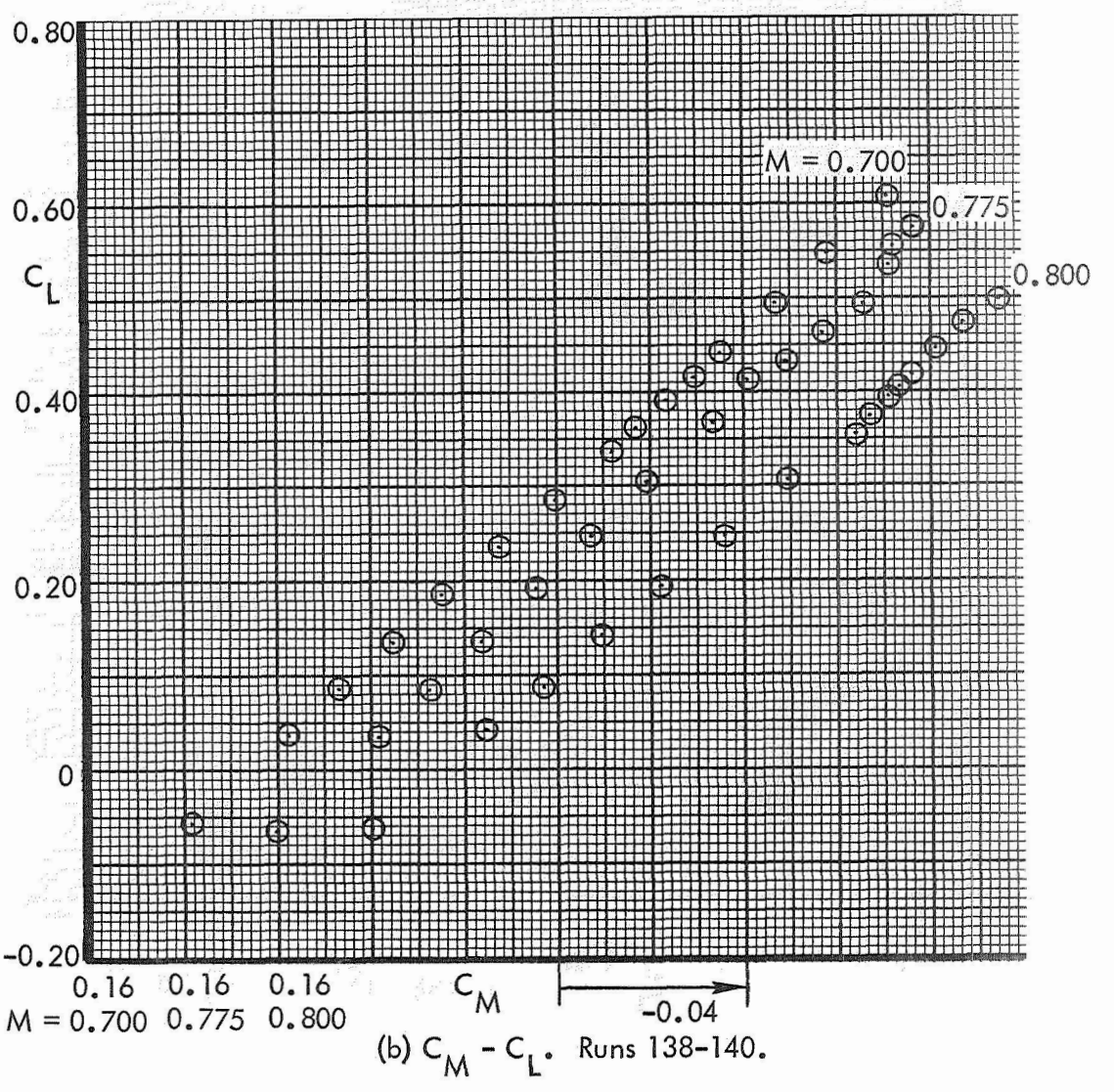
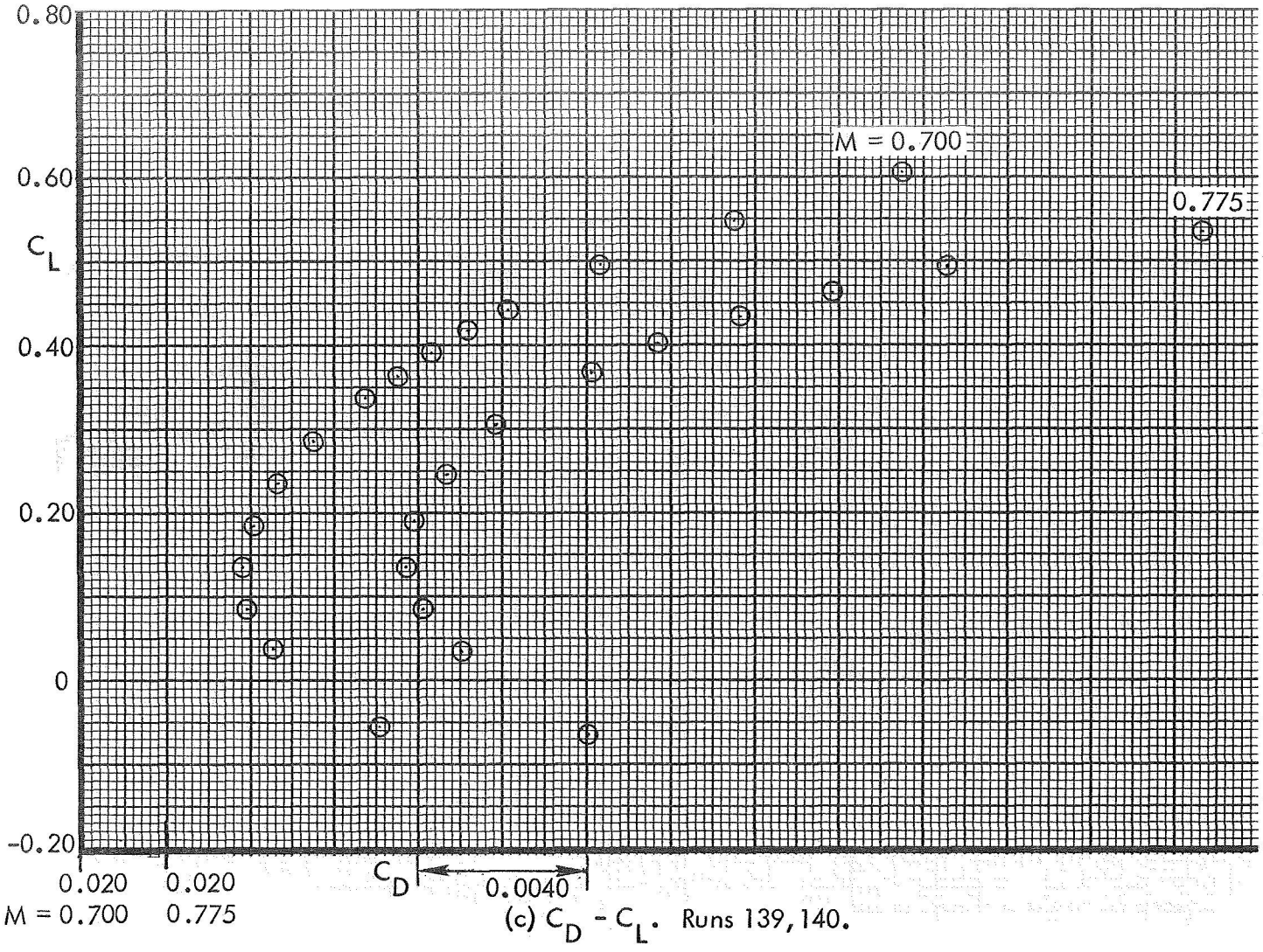
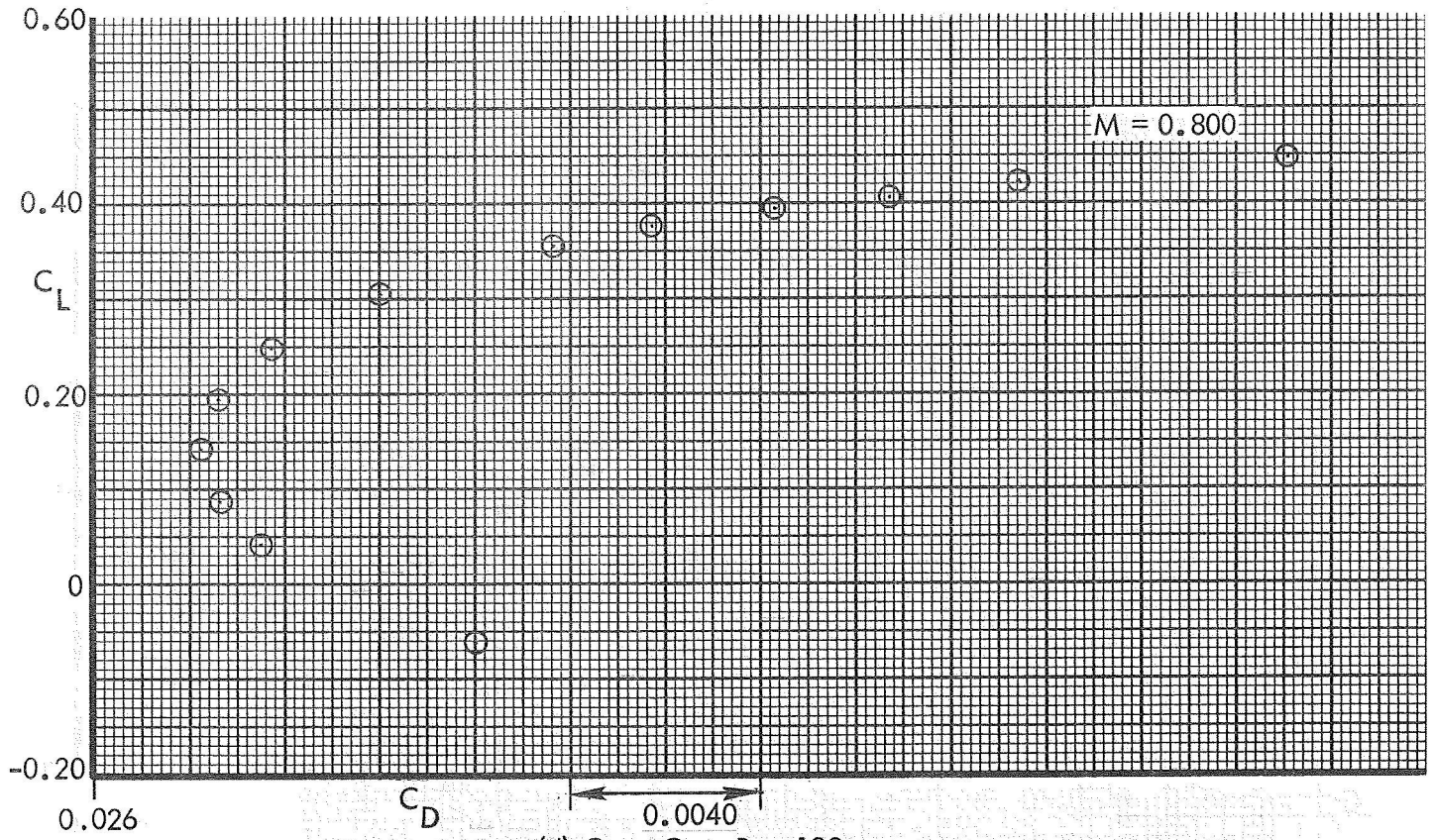


Figure 23. Continued.



(c) C_D - C_L. Runs 139, 140.

Figure 23. Continued.



(d) $C_D - C_L$. Run 138.

Figure 23. Concluded.

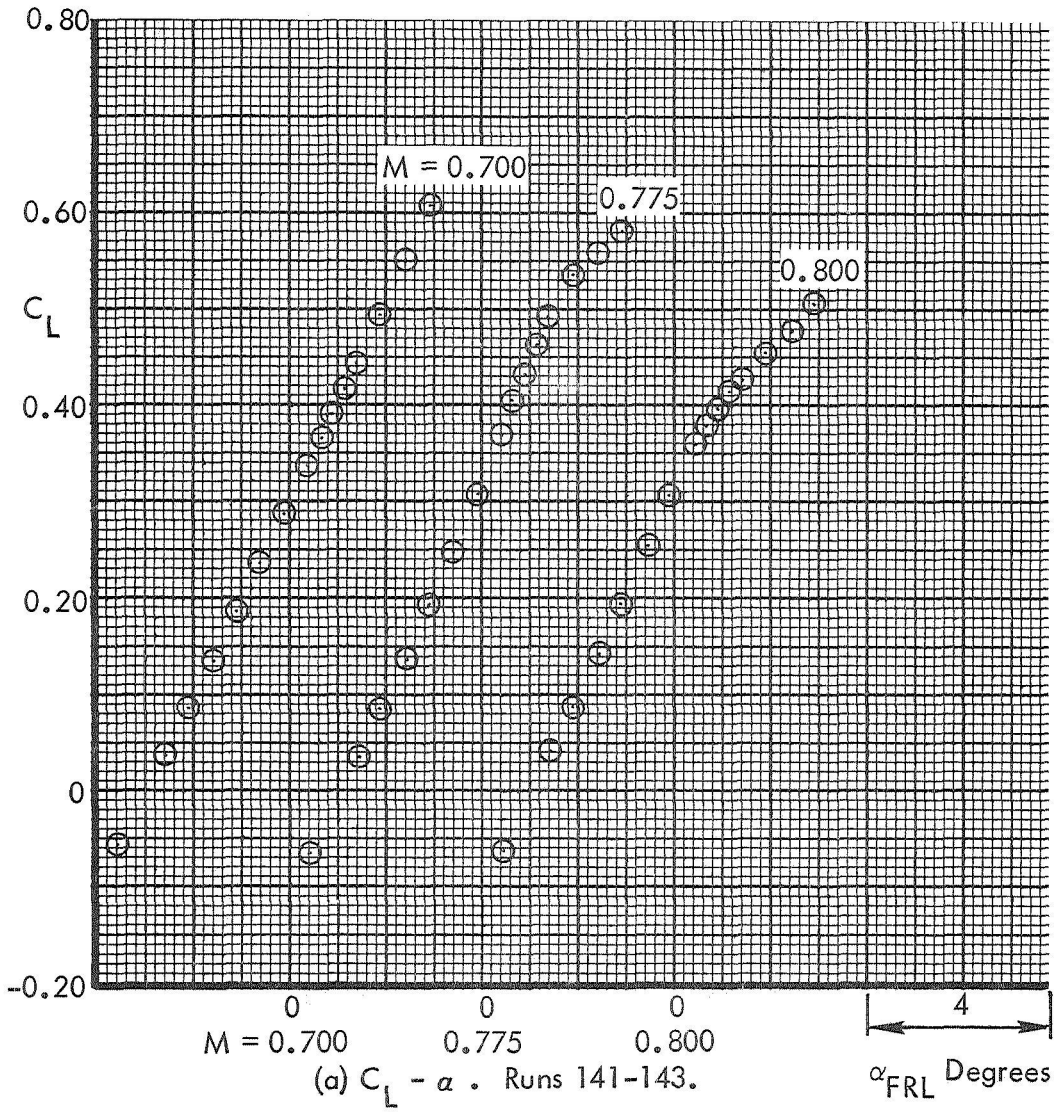
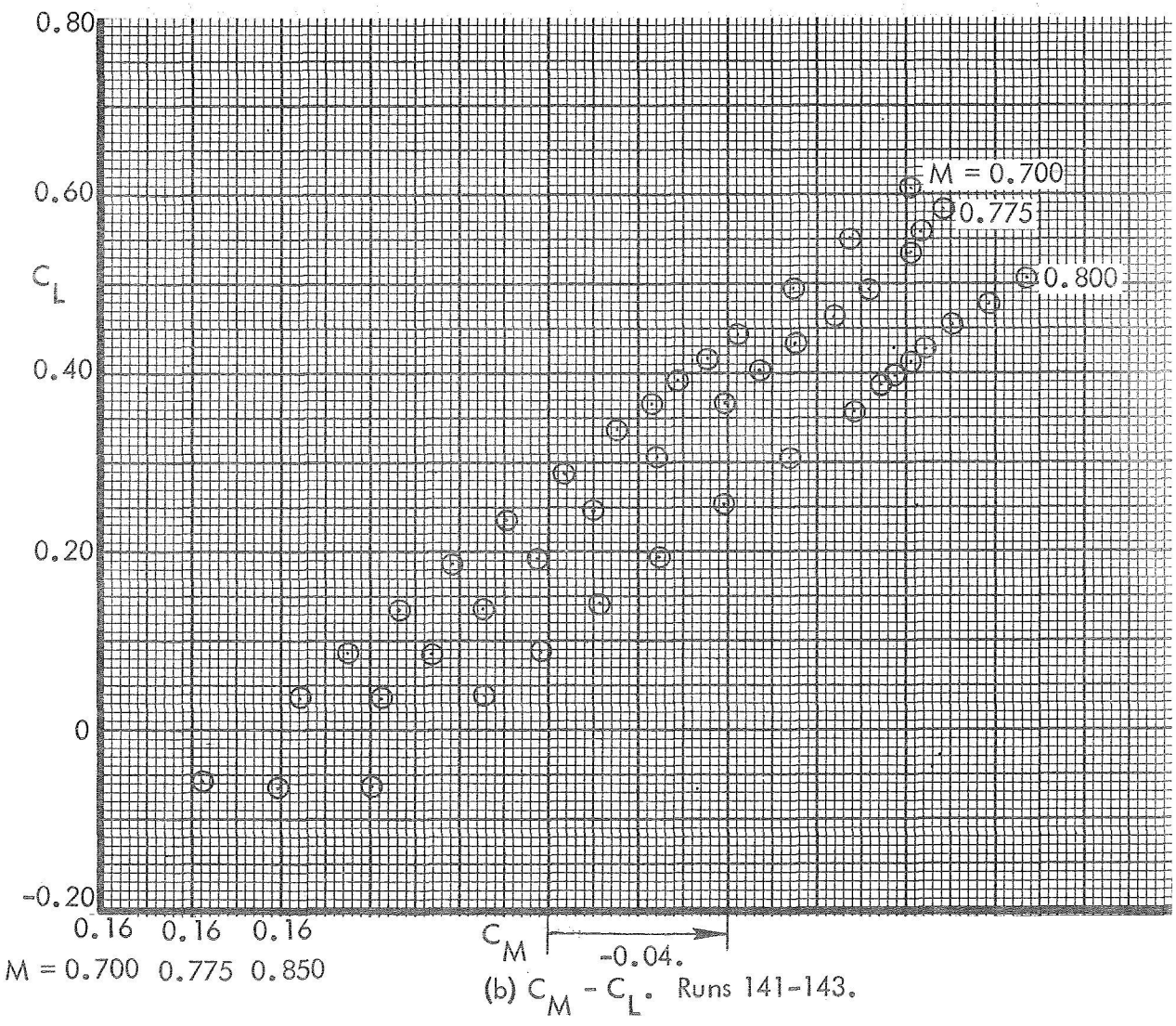
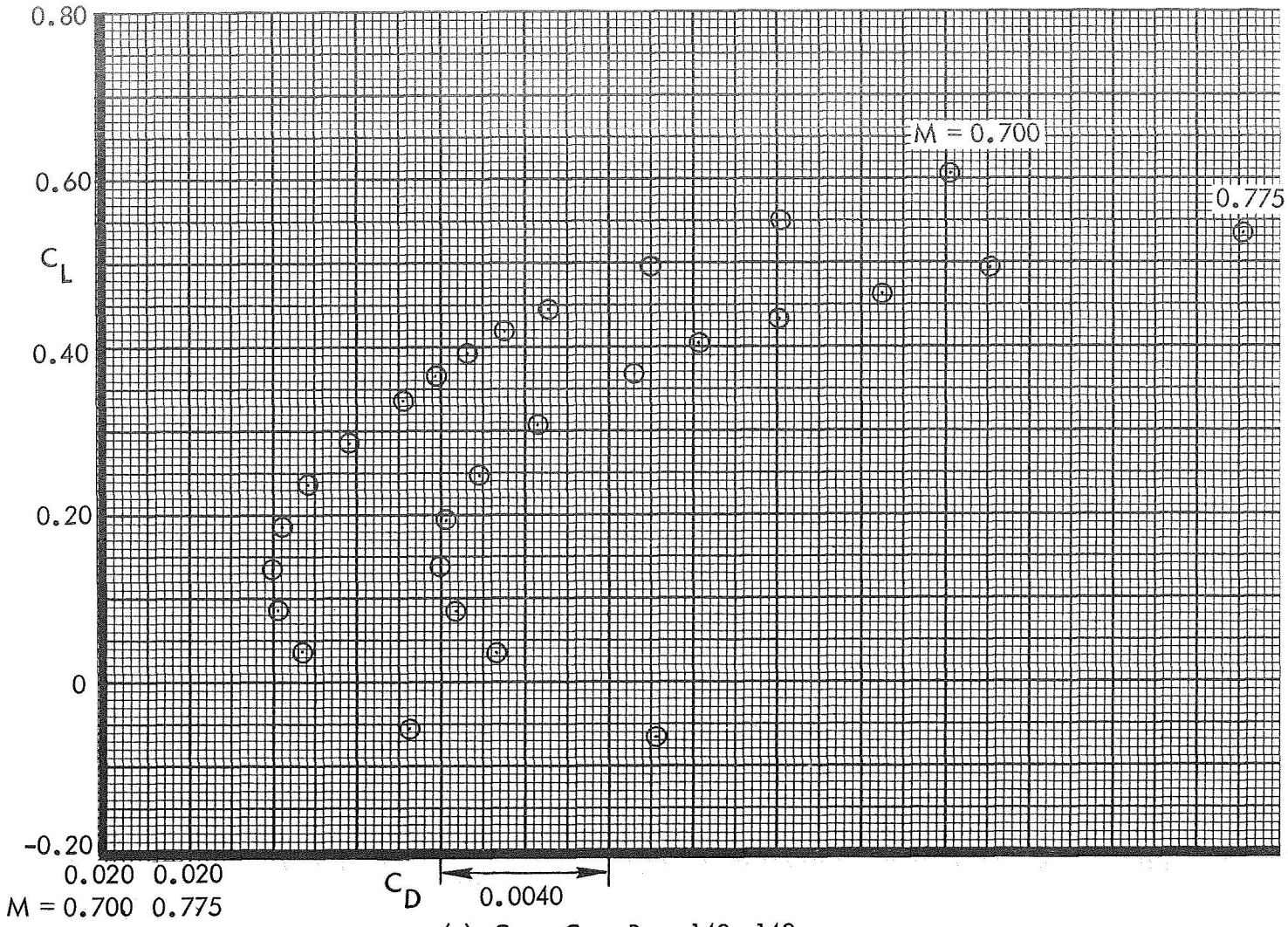


Figure 24. Basic Aerodynamic Data. No Offset Fairing. Sting Position 4. Test 617.



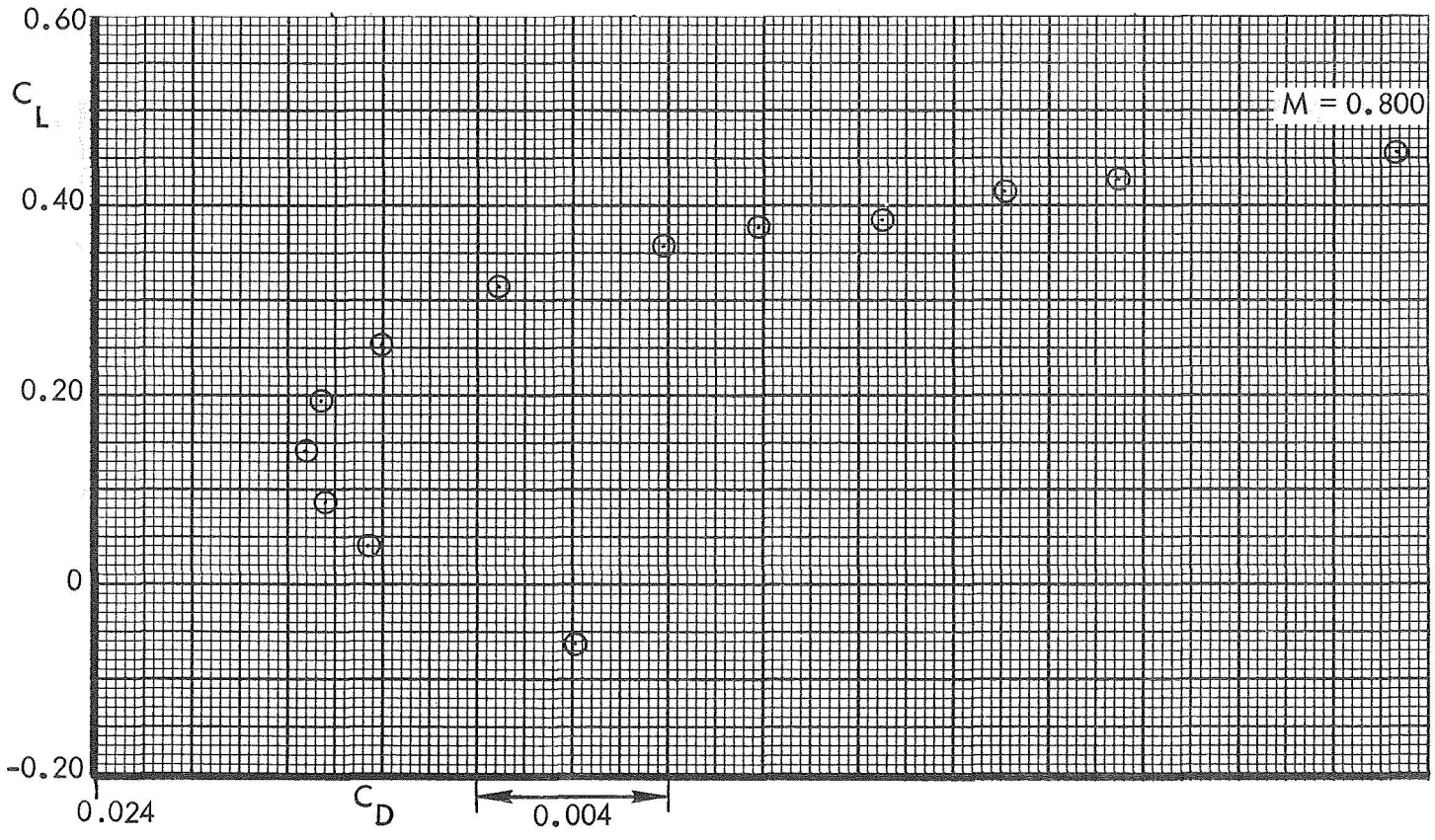
(b) $C_M - C_L$. Runs 141-143.

Figure 24. Continued.



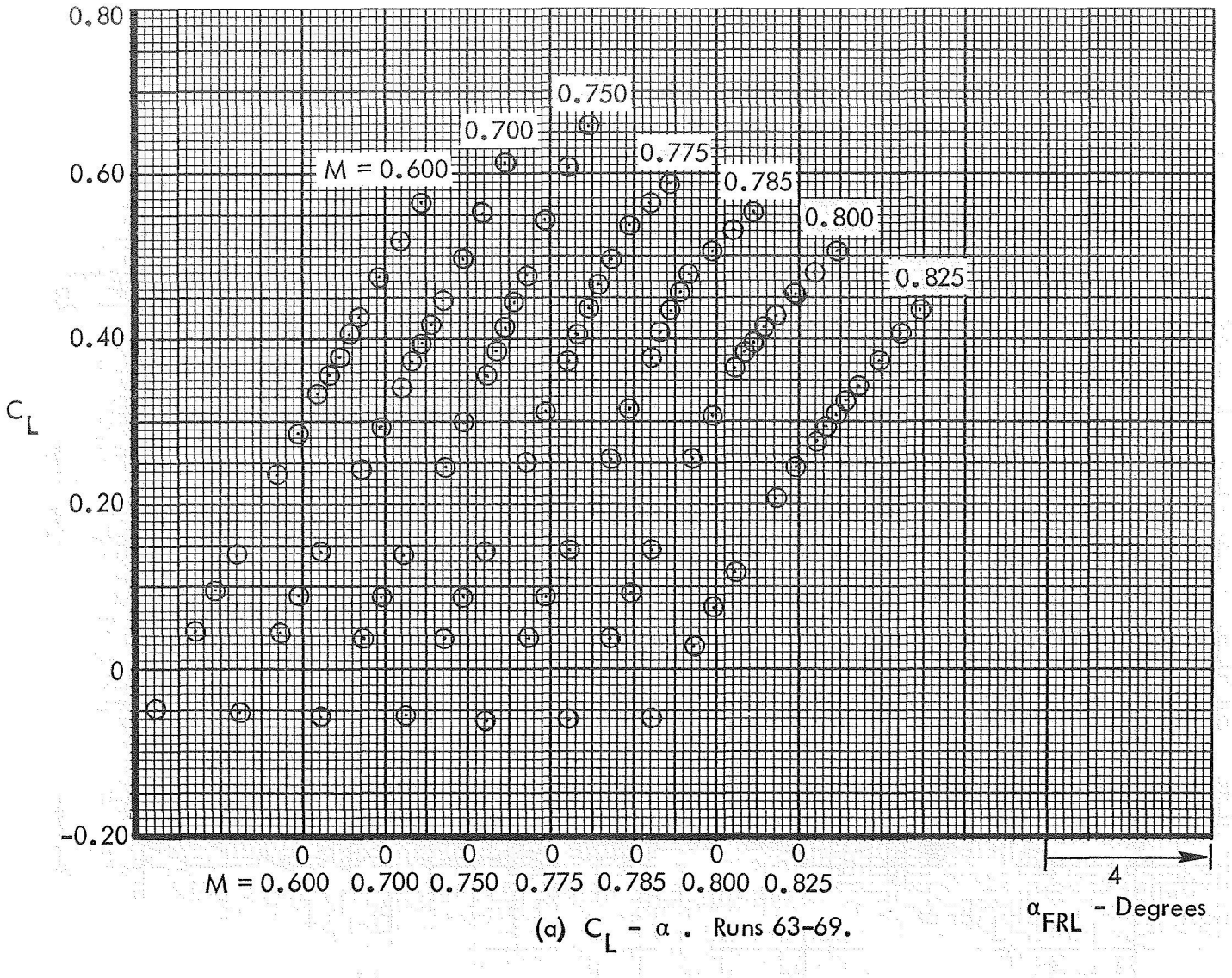
(c) $C_D - C_L$. Runs 142, 143.

Figure 24. Continued.



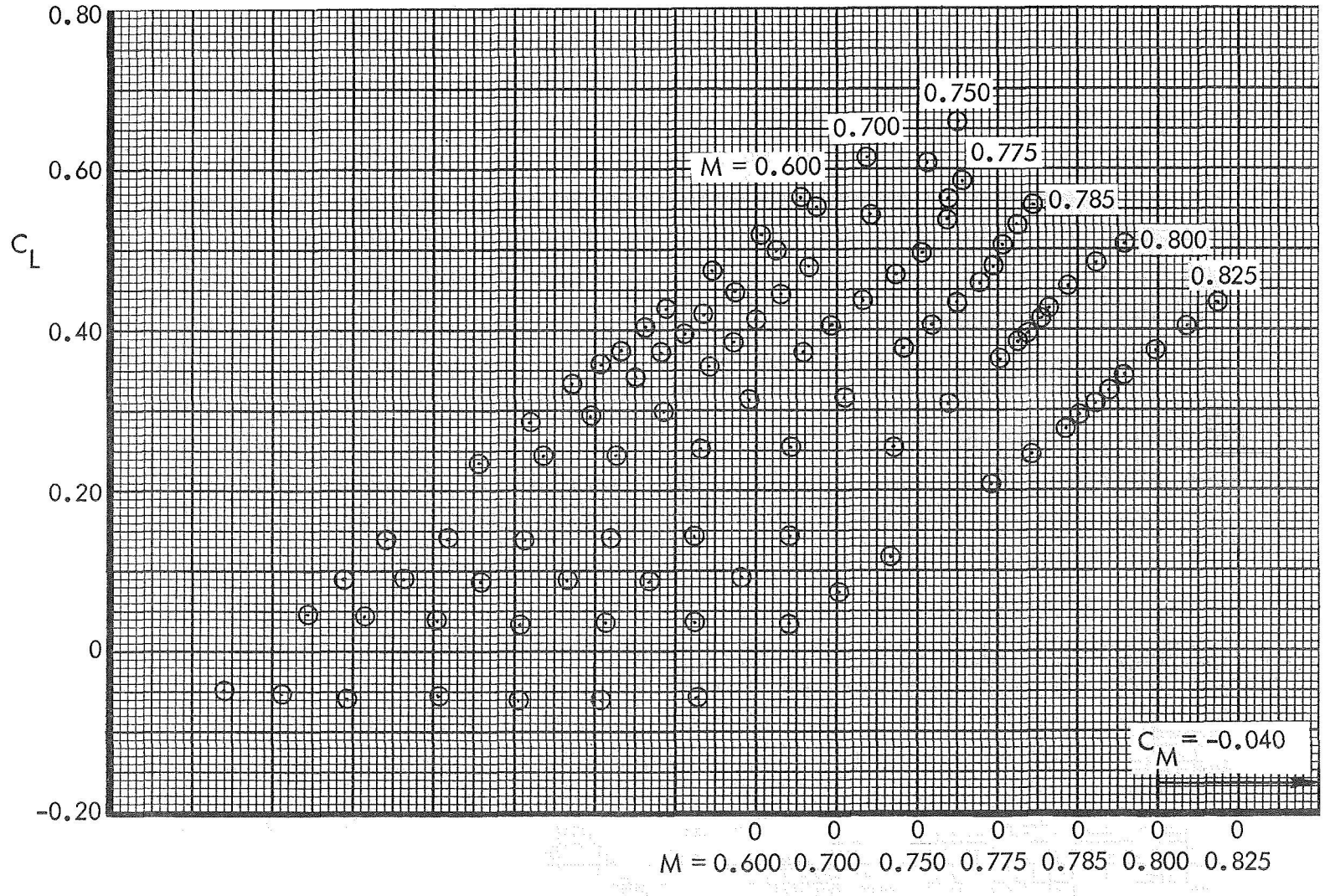
(d) $C_D - C_L$. Runs 141.

Figure 24. Concluded.



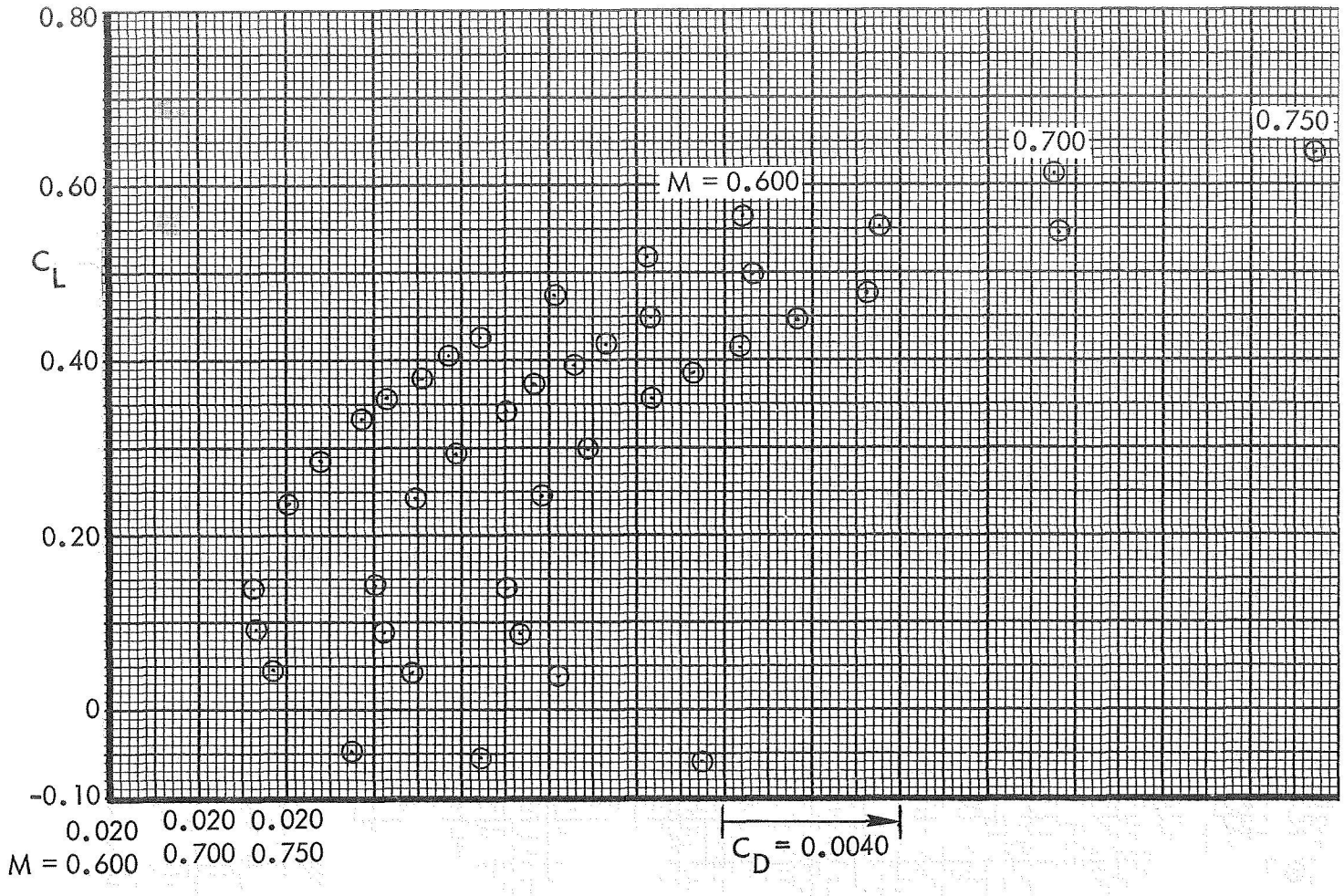
(a) C_L - α . Runs 63-69.

Figure 25. Basic Aerodynamic Data. $i_H = 1^\circ$. Test 591.



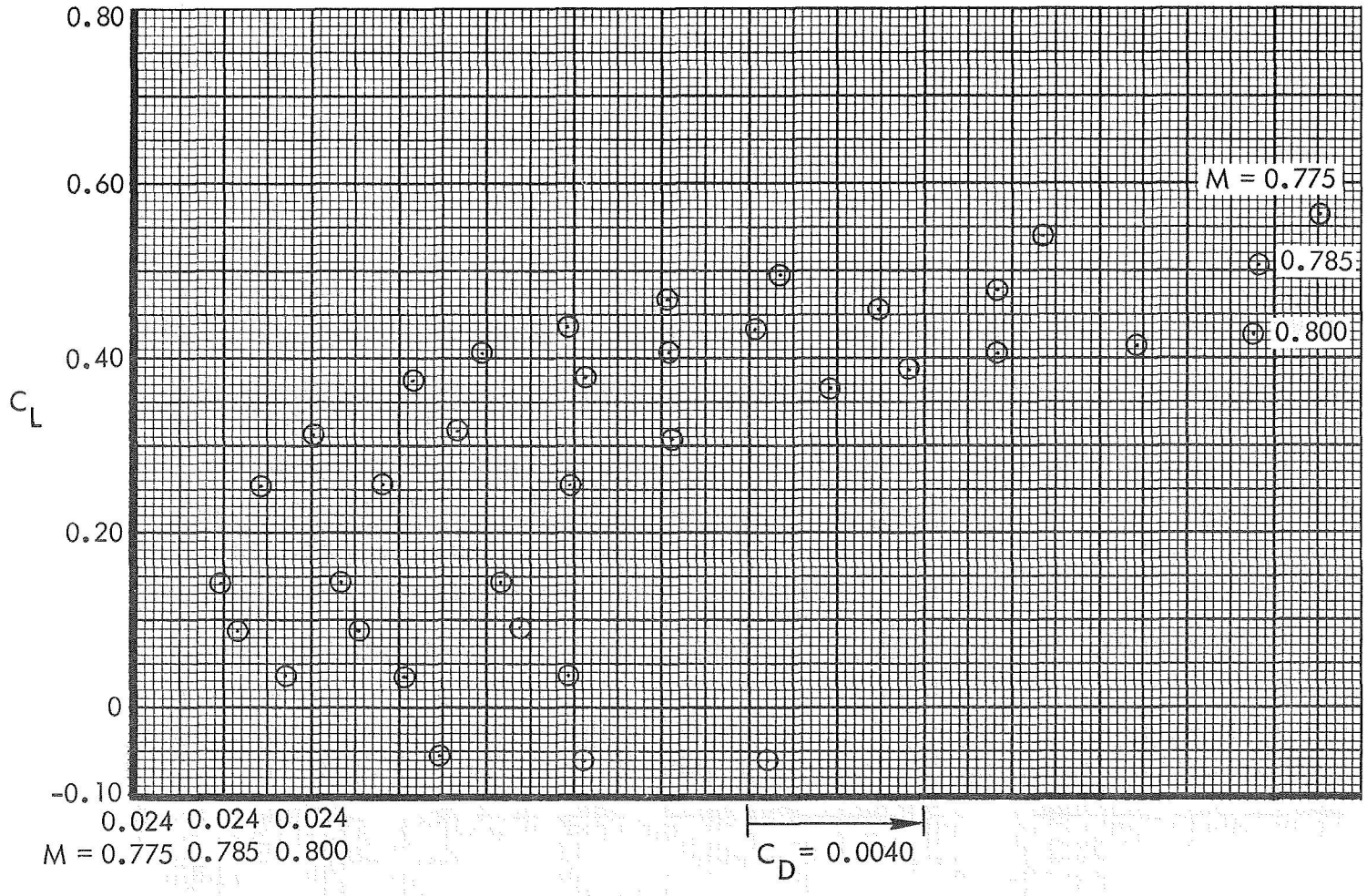
(b) $C_M - C_L$. Runs 63-69.

Figure 25. Continued.



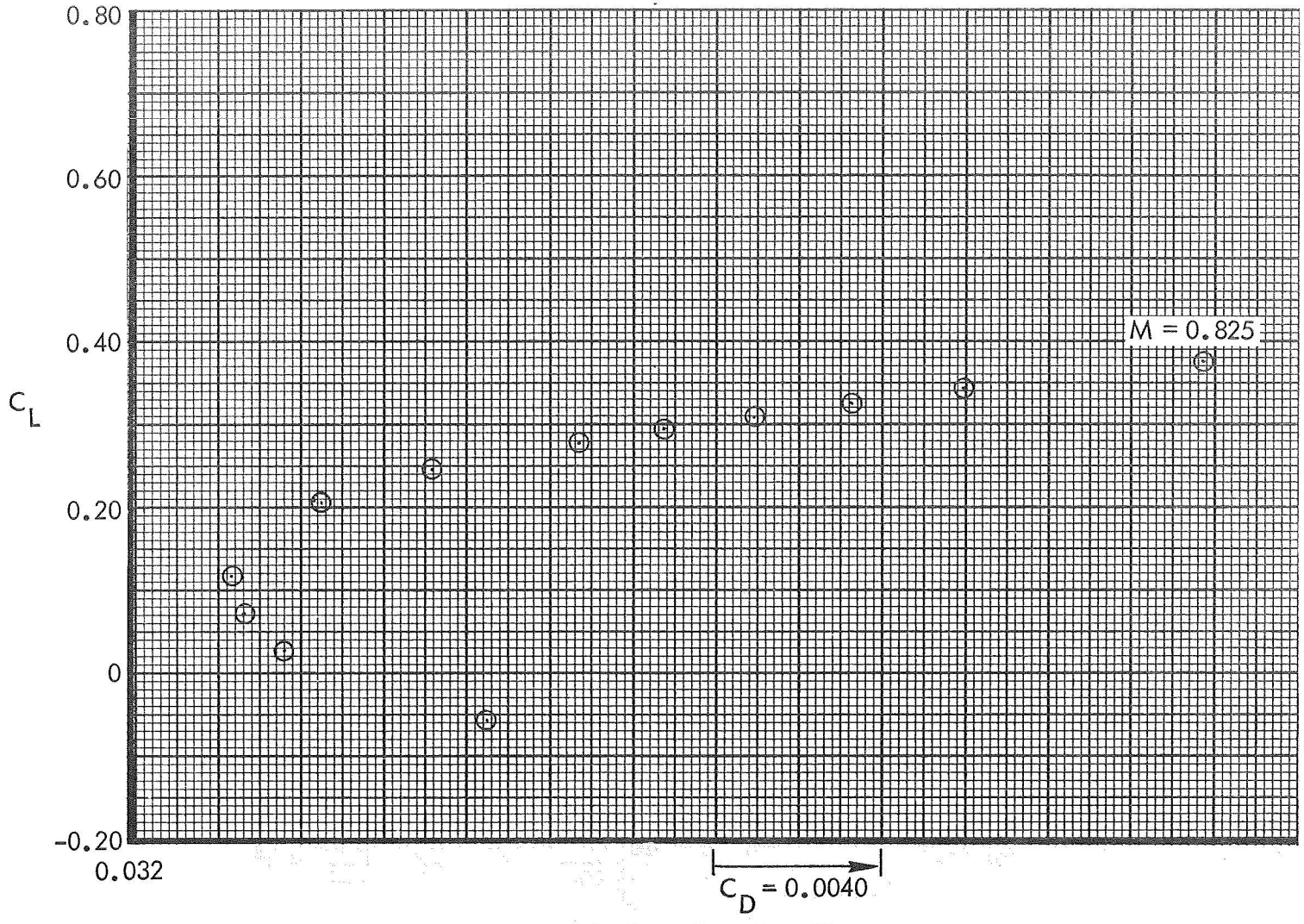
(c) $C_L - C_D$. Runs 67-69.

Figure 25. Continued.



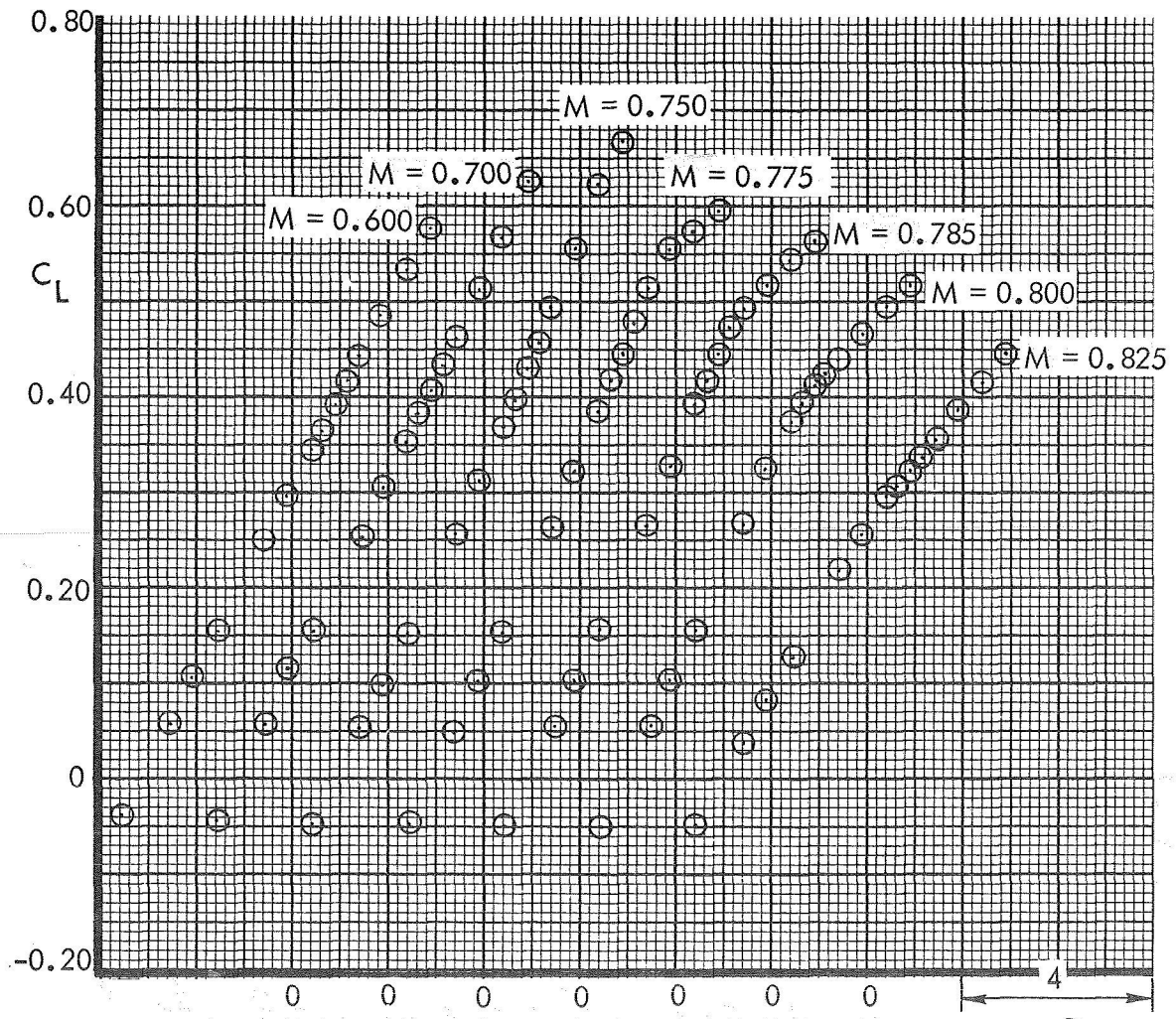
(d) $C_L - C_D$. Runs 64-66.

Figure 25. Continued.



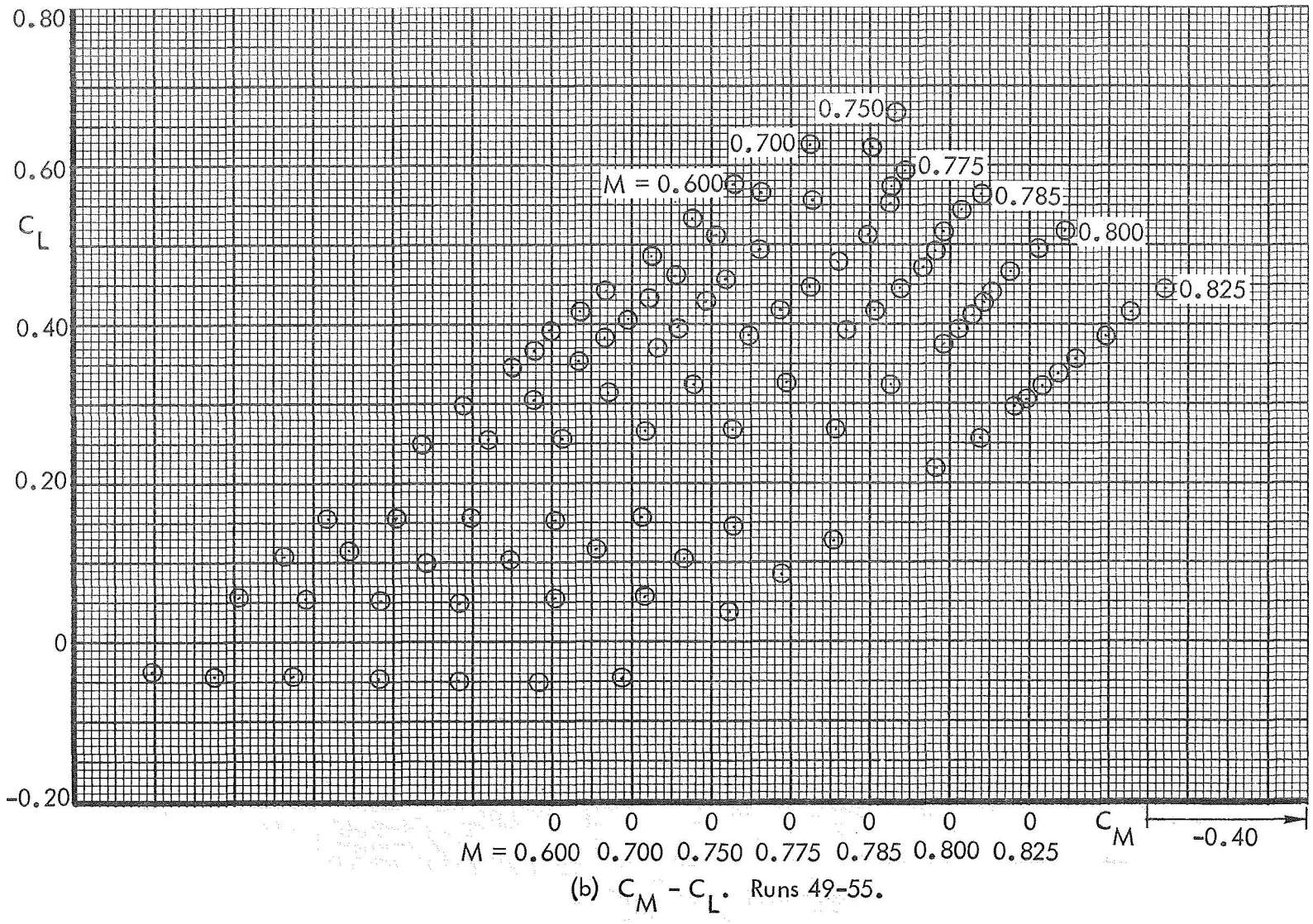
(e) C_L - C_D. Run 63.

Figure 25. Concluded.



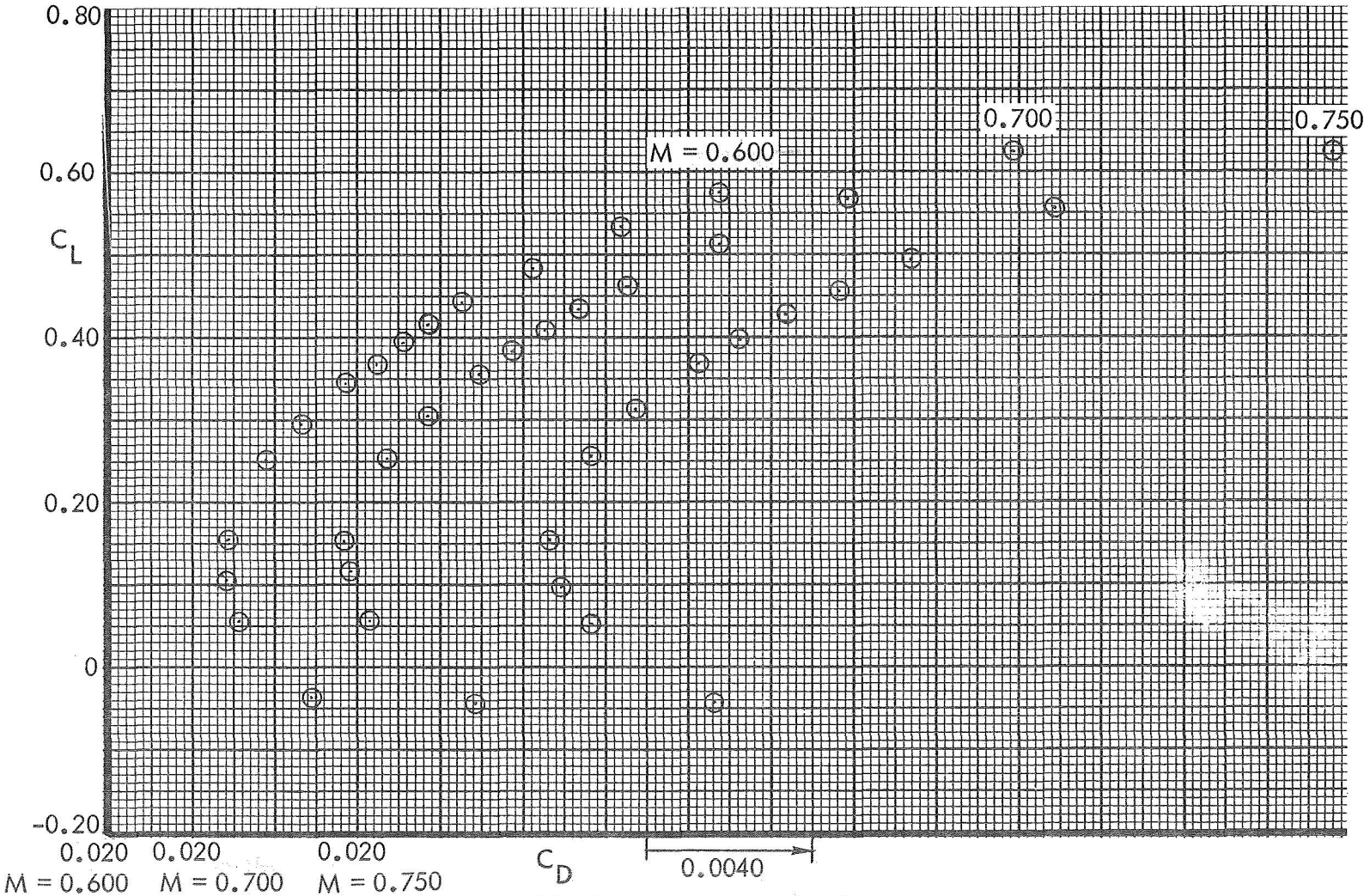
(a) $C_L - \alpha$. Runs 49-55.

Figure 26. Basic Aerodynamic Data. $i_H = 0^\circ$. Test 591.



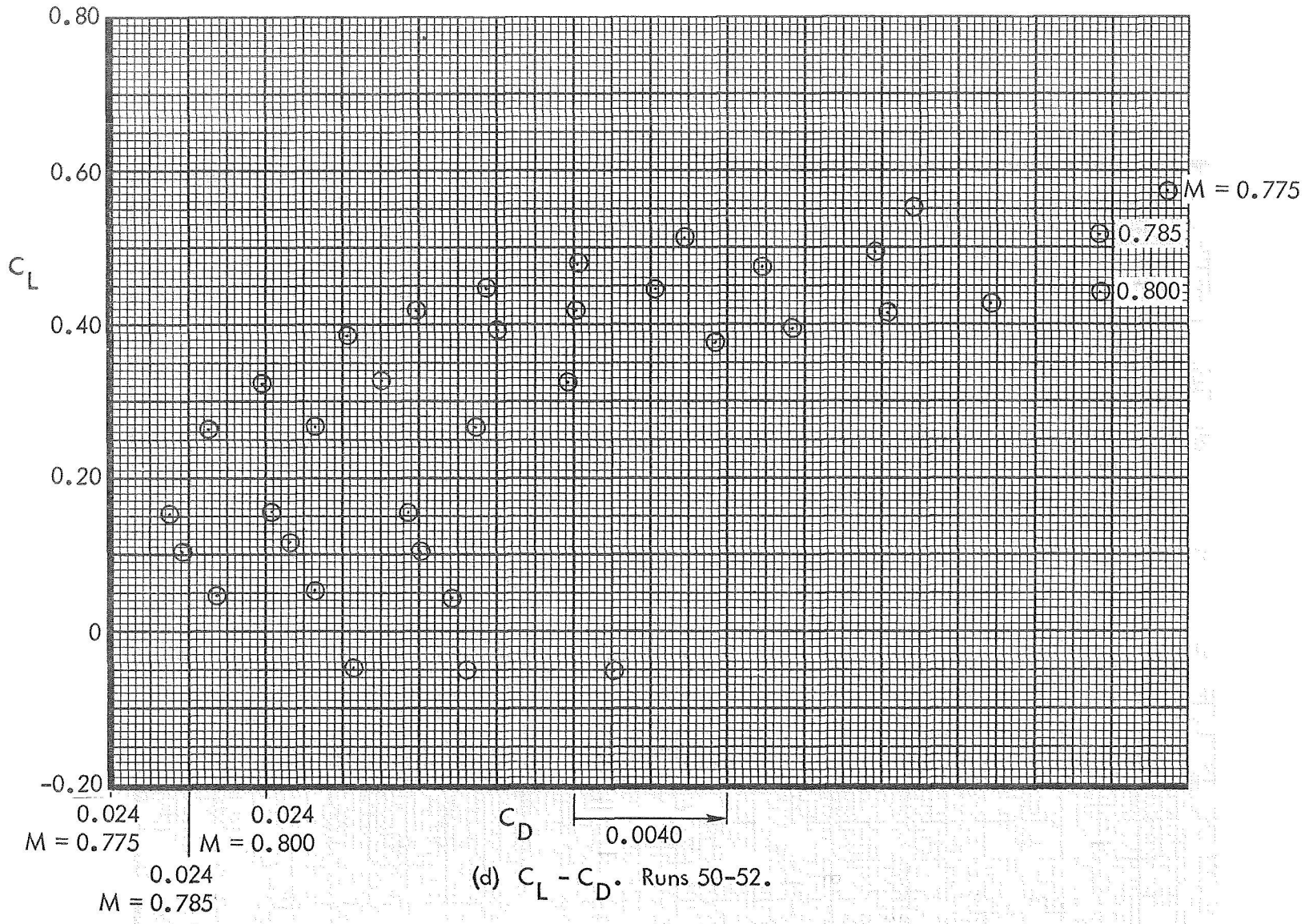
(b) $C_M - C_L$. Runs 49-55.

Figure 26. Continued.



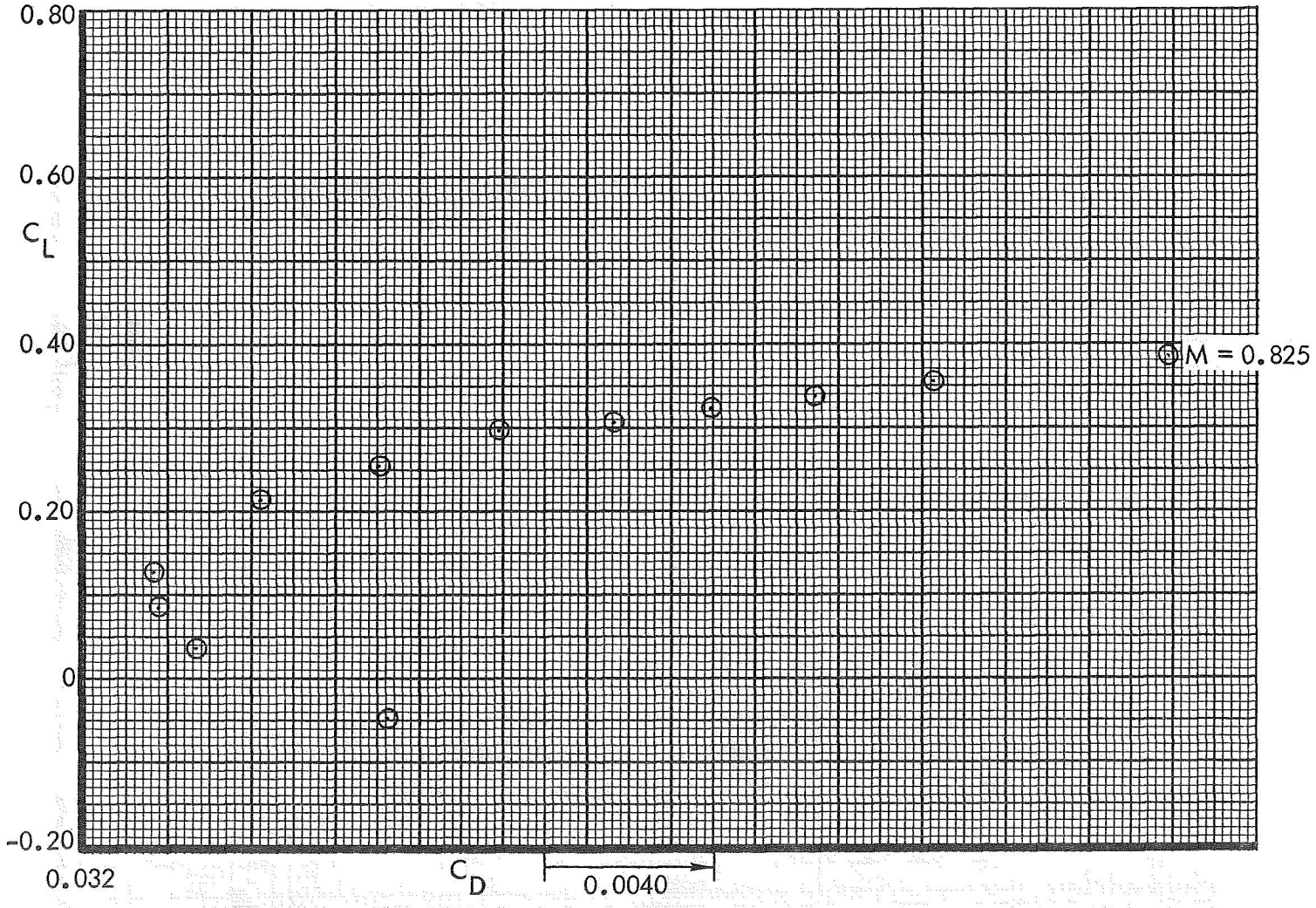
(c) $C_L - C_D$. Runs 53-55.

Figure 26. Continued.



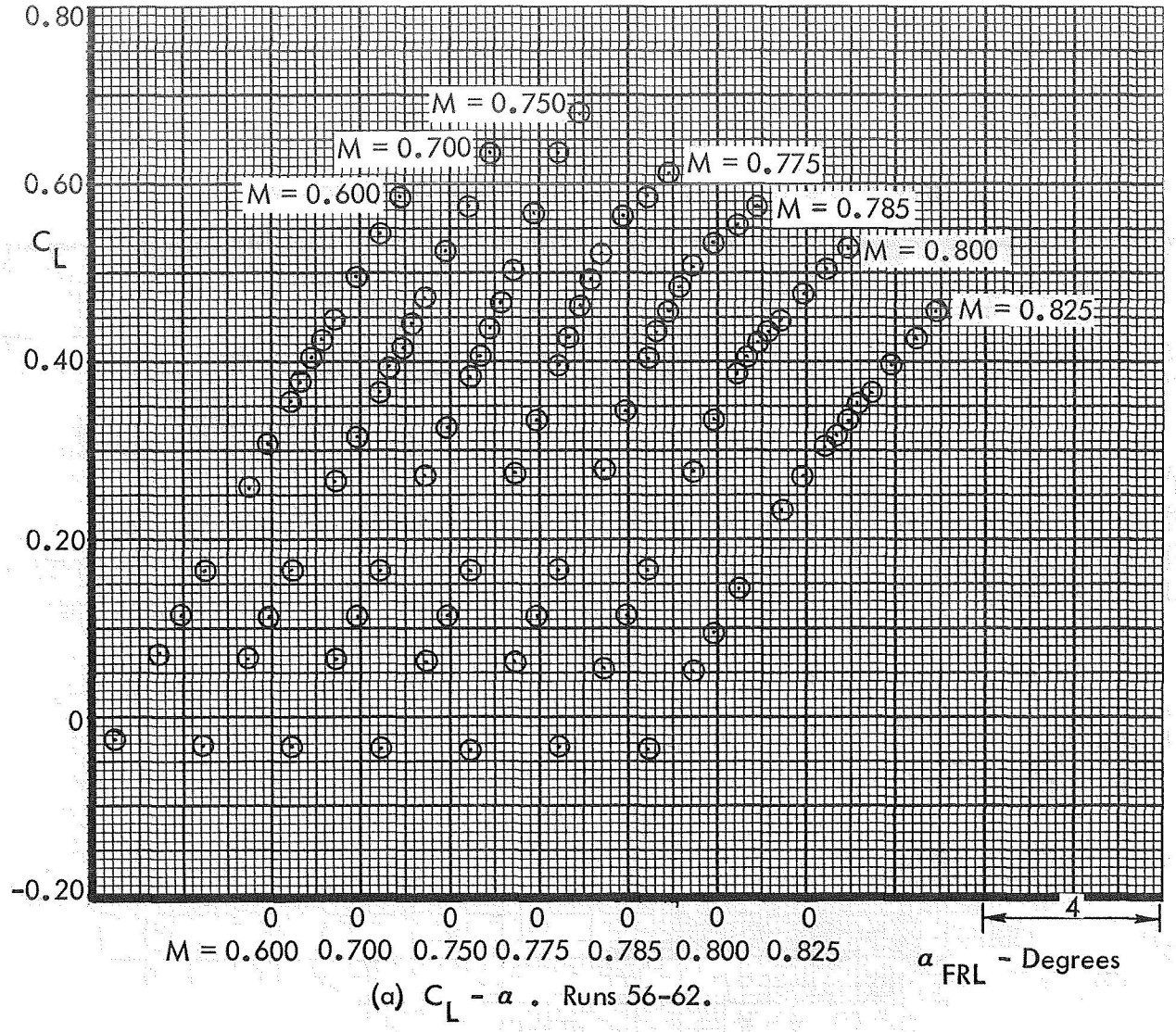
(d) $C_L - C_D$. Runs 50-52.

Figure 26. Continued.



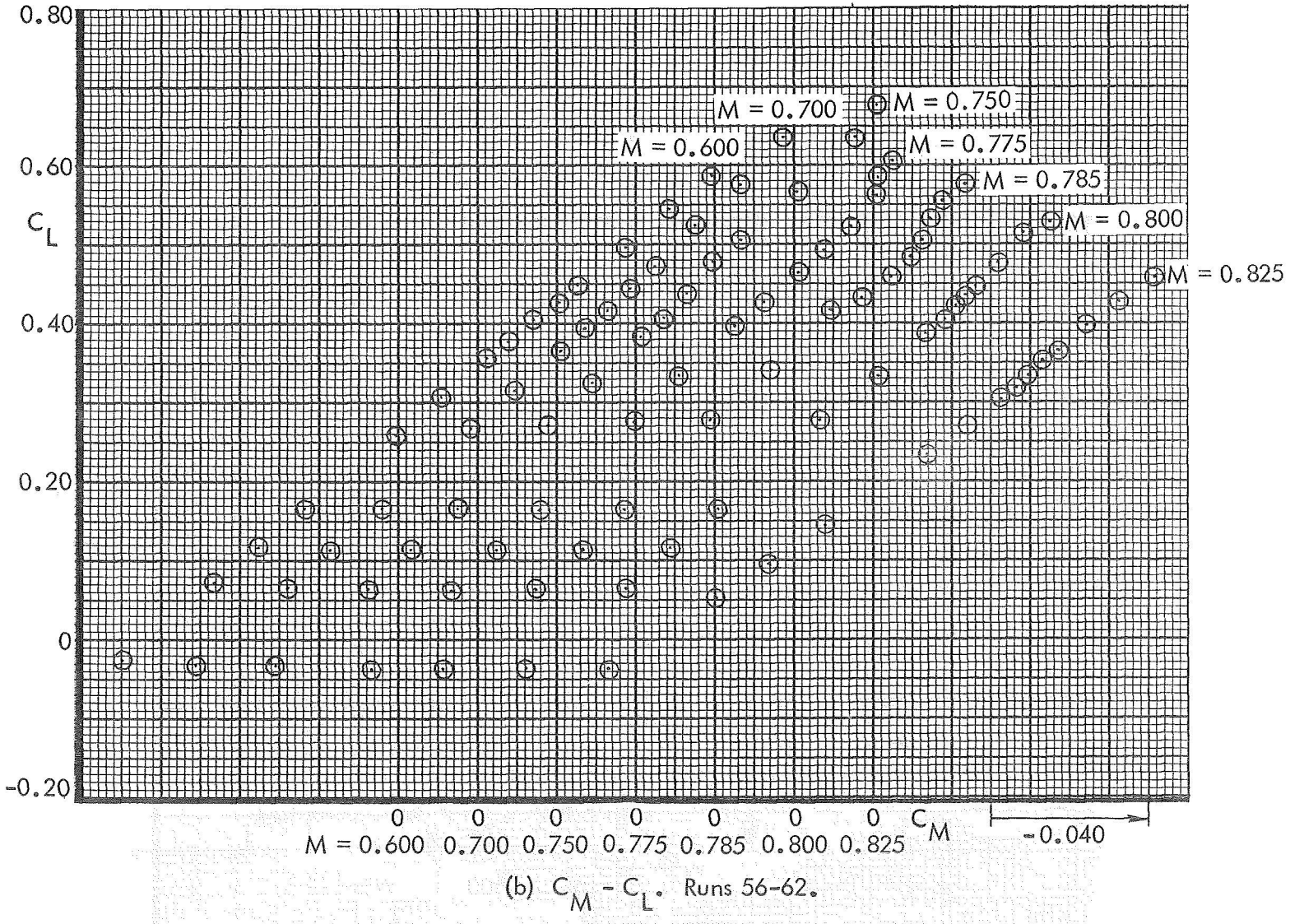
(e) C_L - C_D. Run 49.

Figure 26. Concluded.



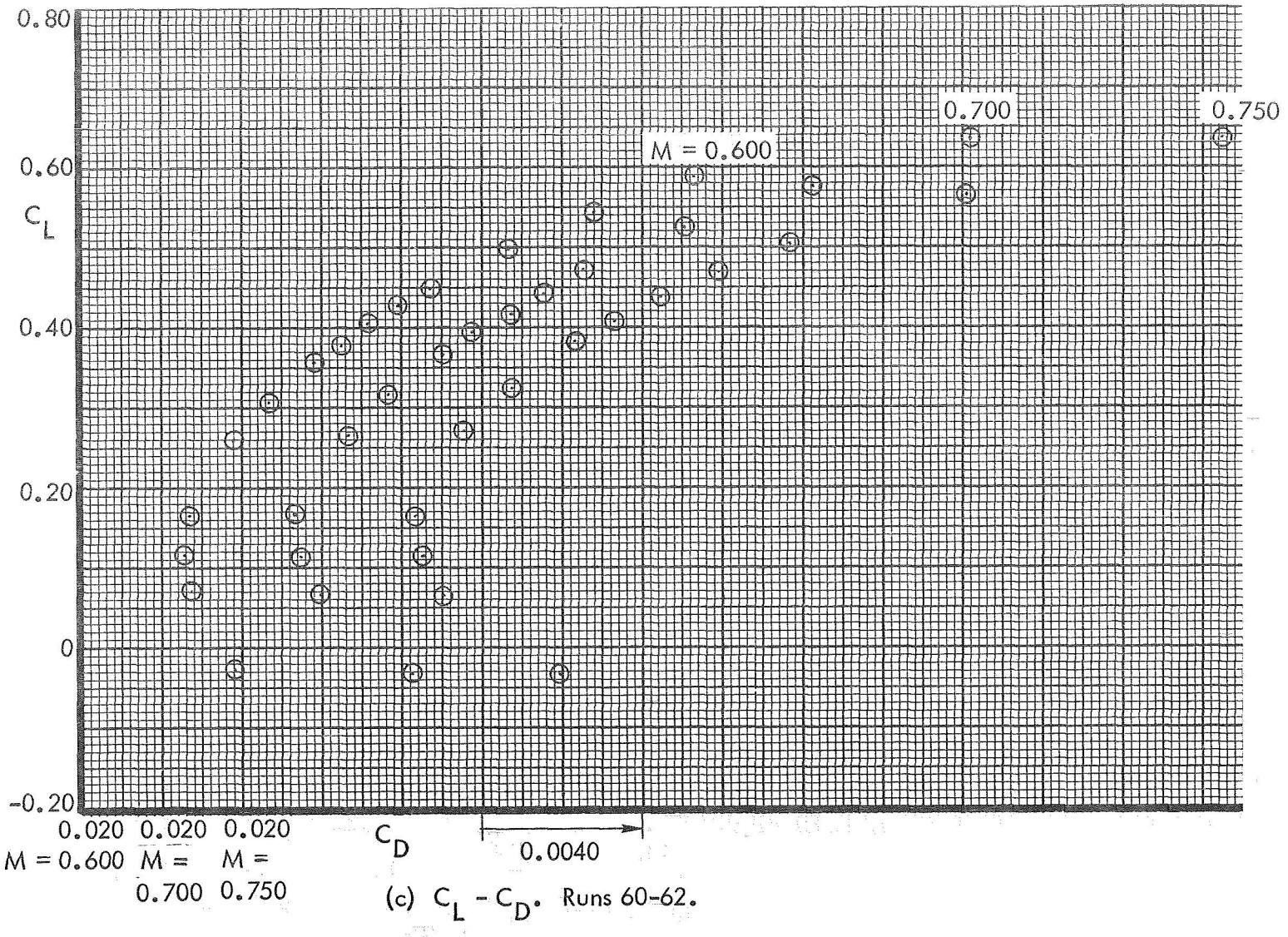
(a) $C_L - \alpha$. Runs 56-62.

Figure 27. Basic Aerodynamic Data. $i_H = +1^\circ$. Test 591.



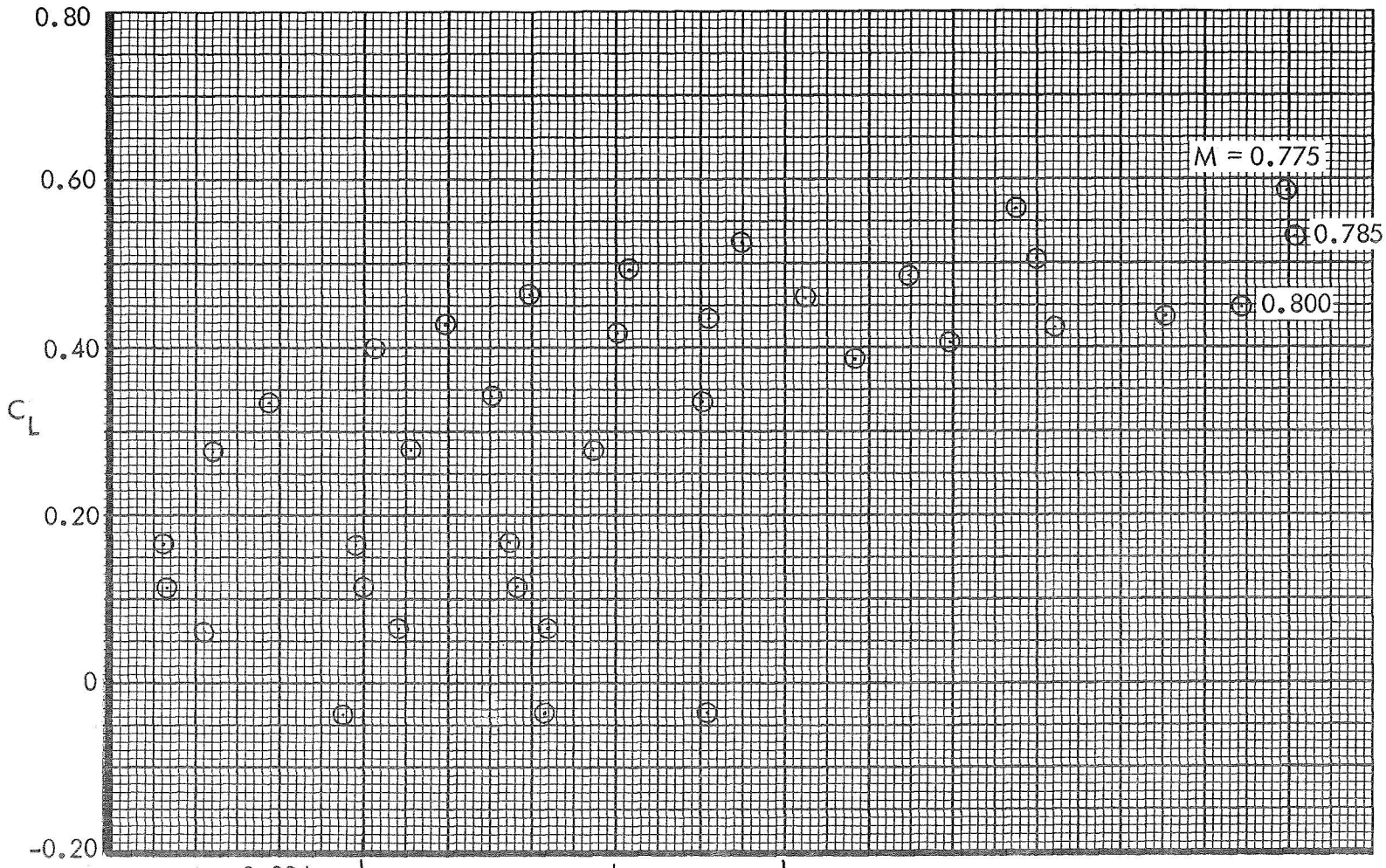
(b) $C_M - C_L$. Runs 56-62.

Figure 27. Continued.



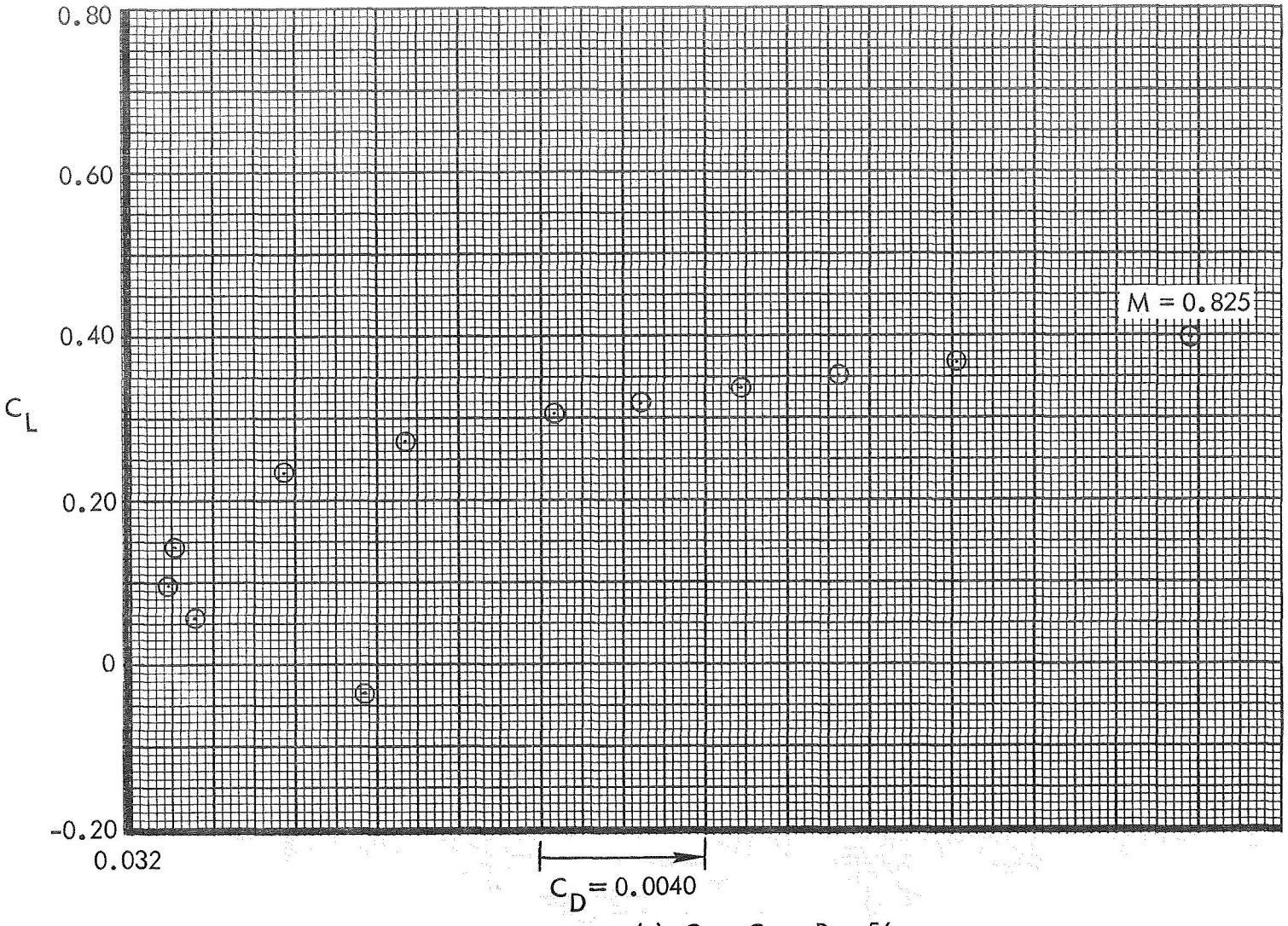
(c) $C_L - C_D$. Runs 60-62.

Figure 27. Continued.



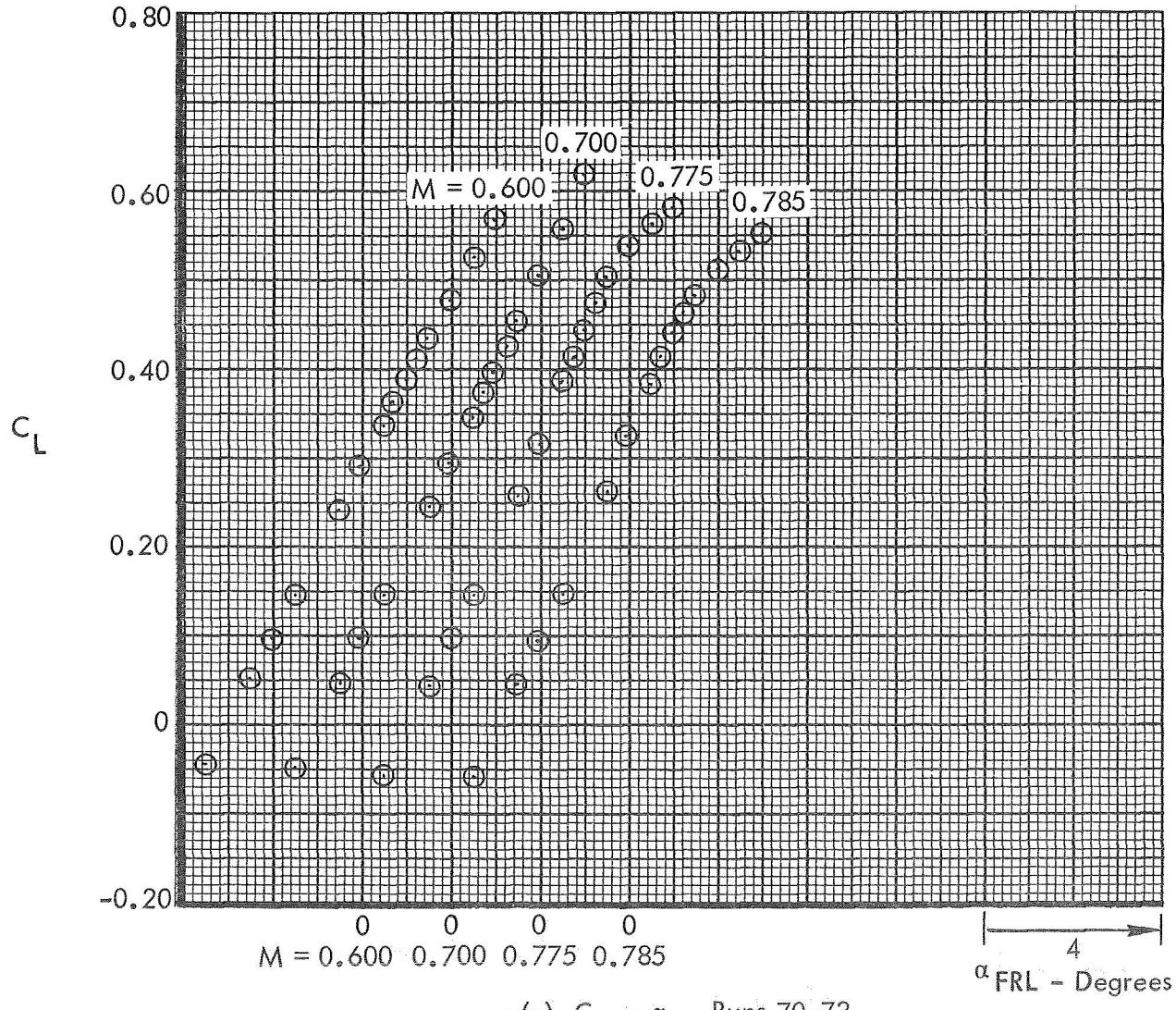
(d) $C_L - C_D$. Runs 57-59.

Figure 27. Continued.



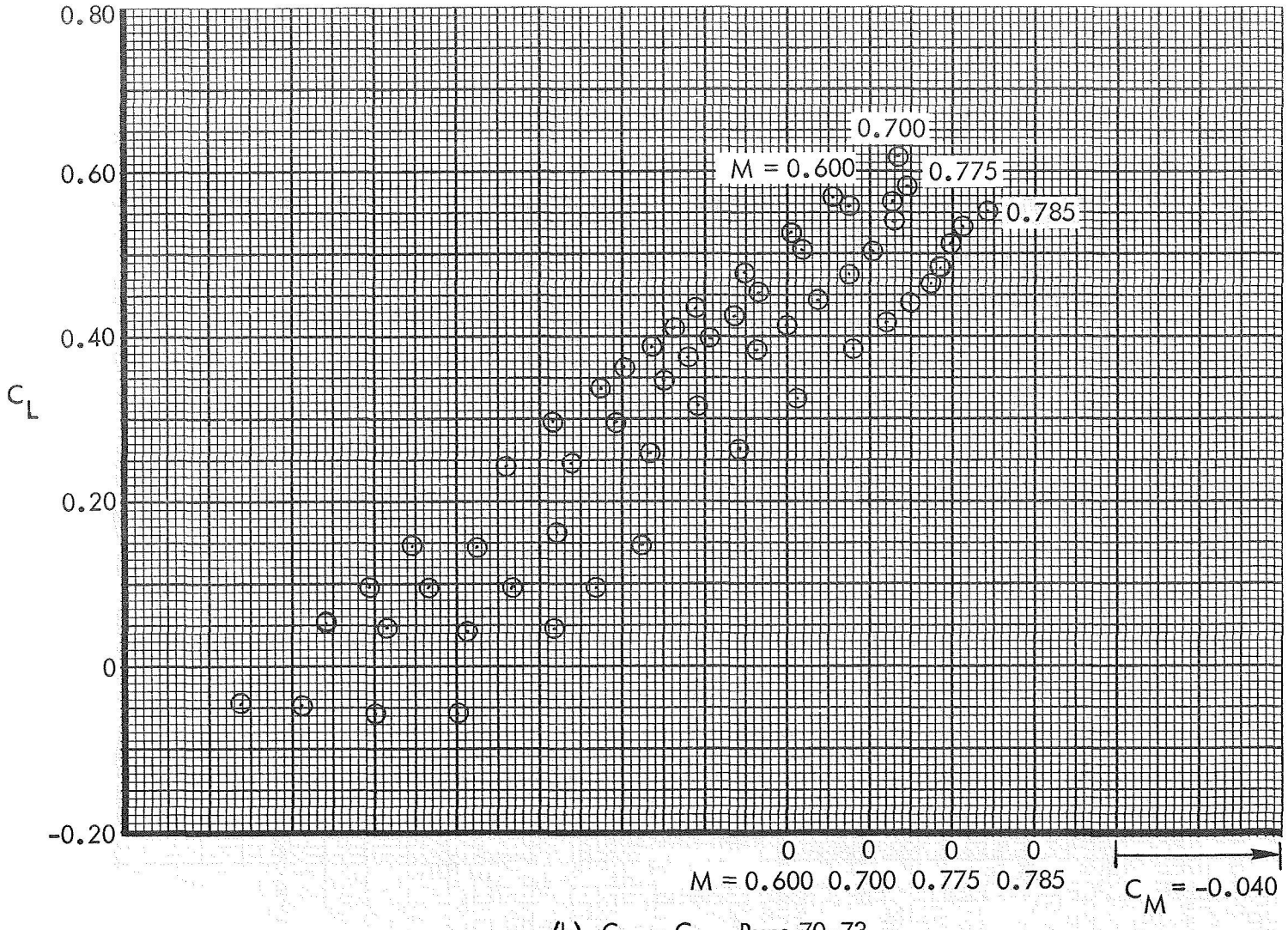
(e) $C_L - C_D$. Run 56.

Figure 27. Concluded.



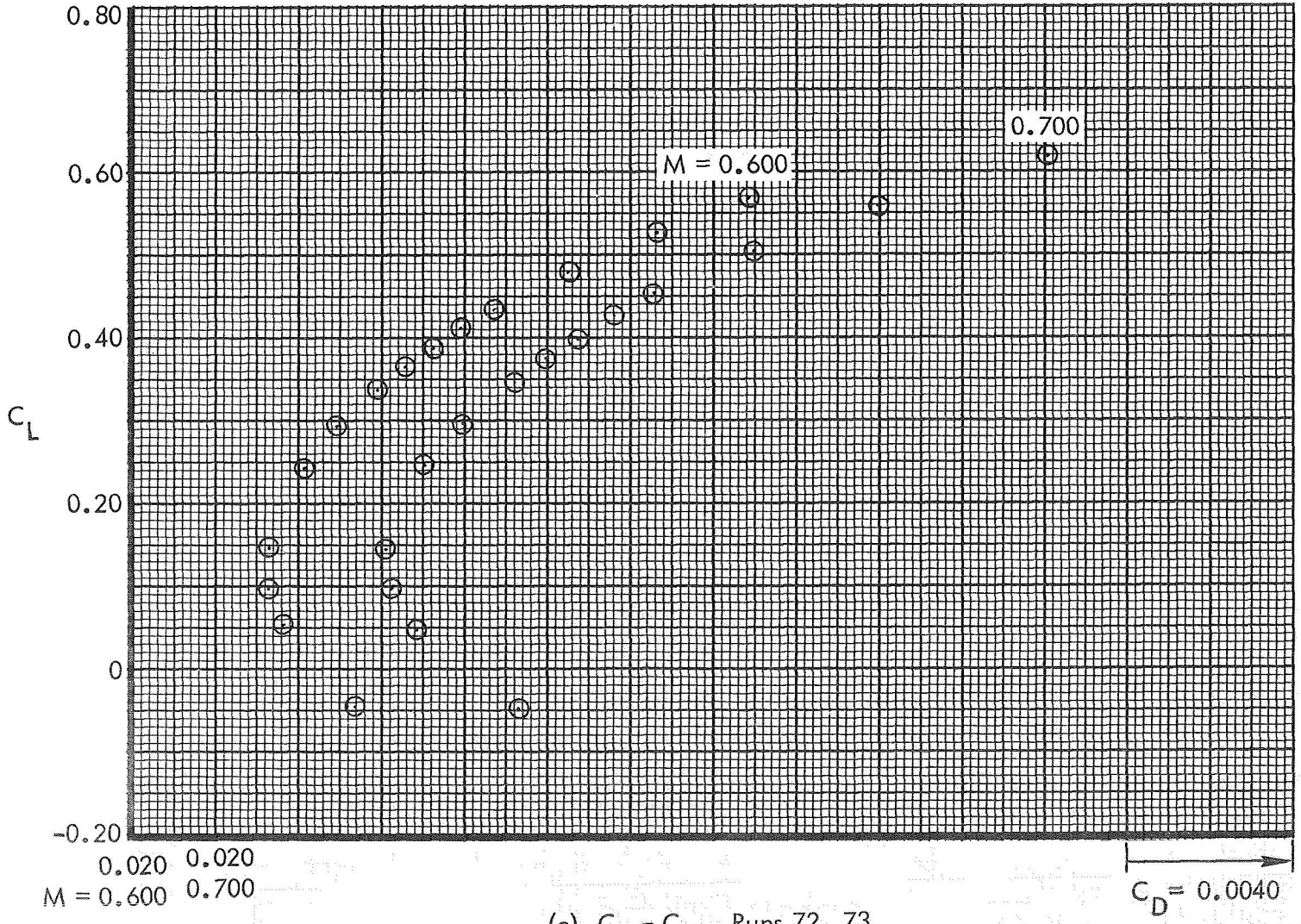
(a) C_L - α . Runs 70-73.

Figure 28. Reynolds Number Effects. i_H -1°. Test 591. $R_N = 5 \times 10^6$/foot



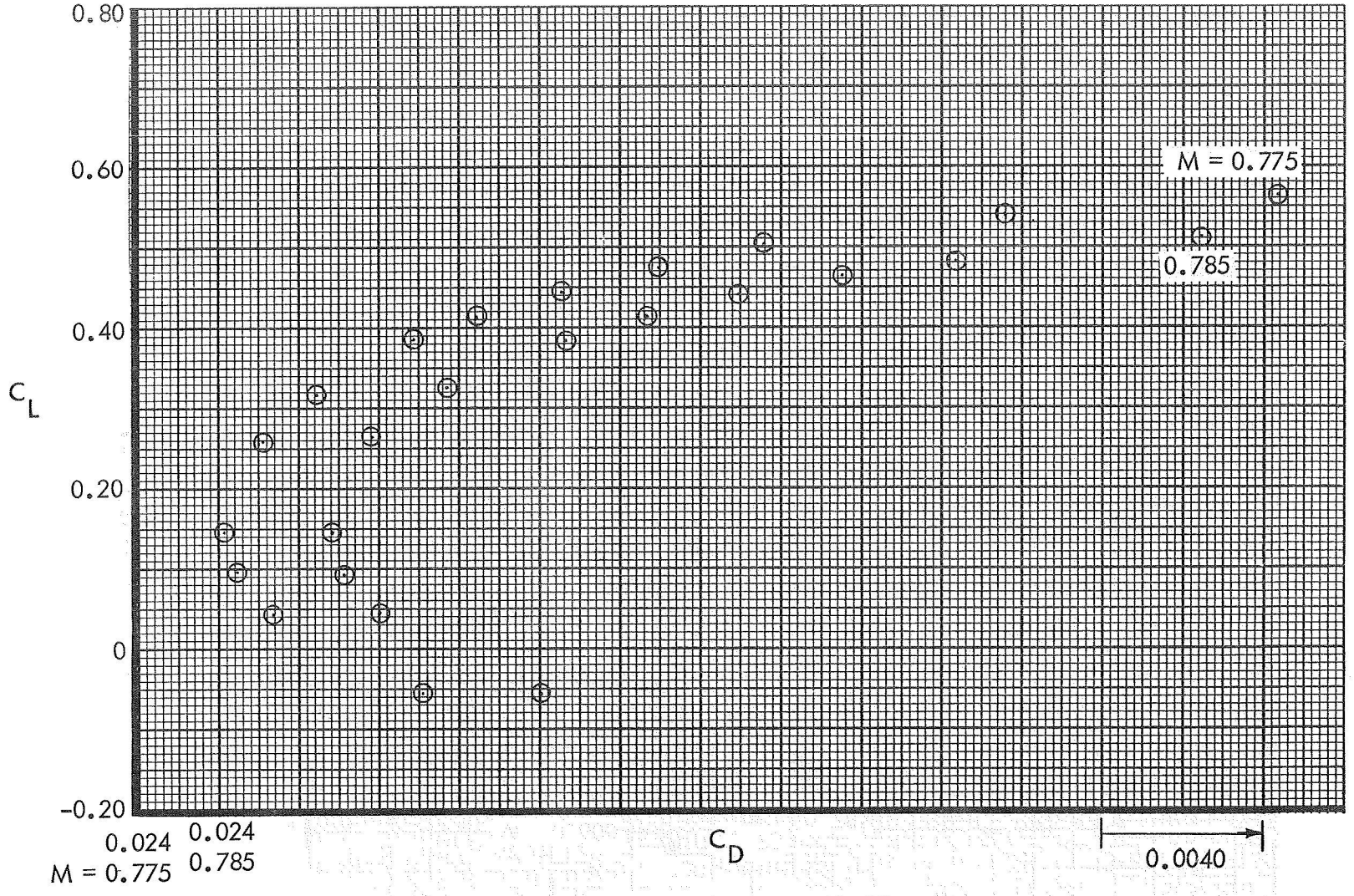
(b) $C_M - C_L$. Runs 70-73.

Figure 28. Continued.



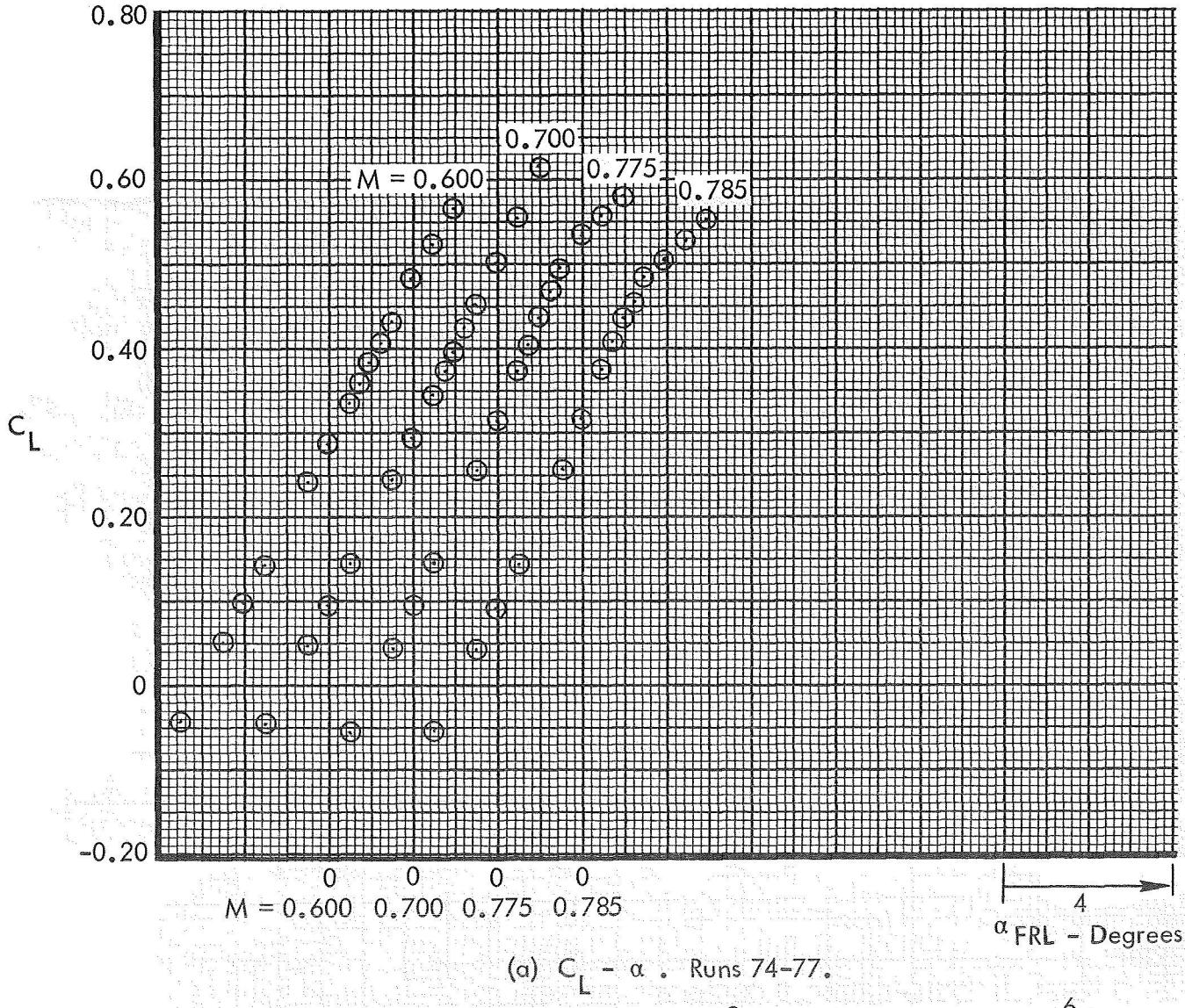
(c) $C_L - C_D$. Runs 72, 73.

Figure 28. Continued.



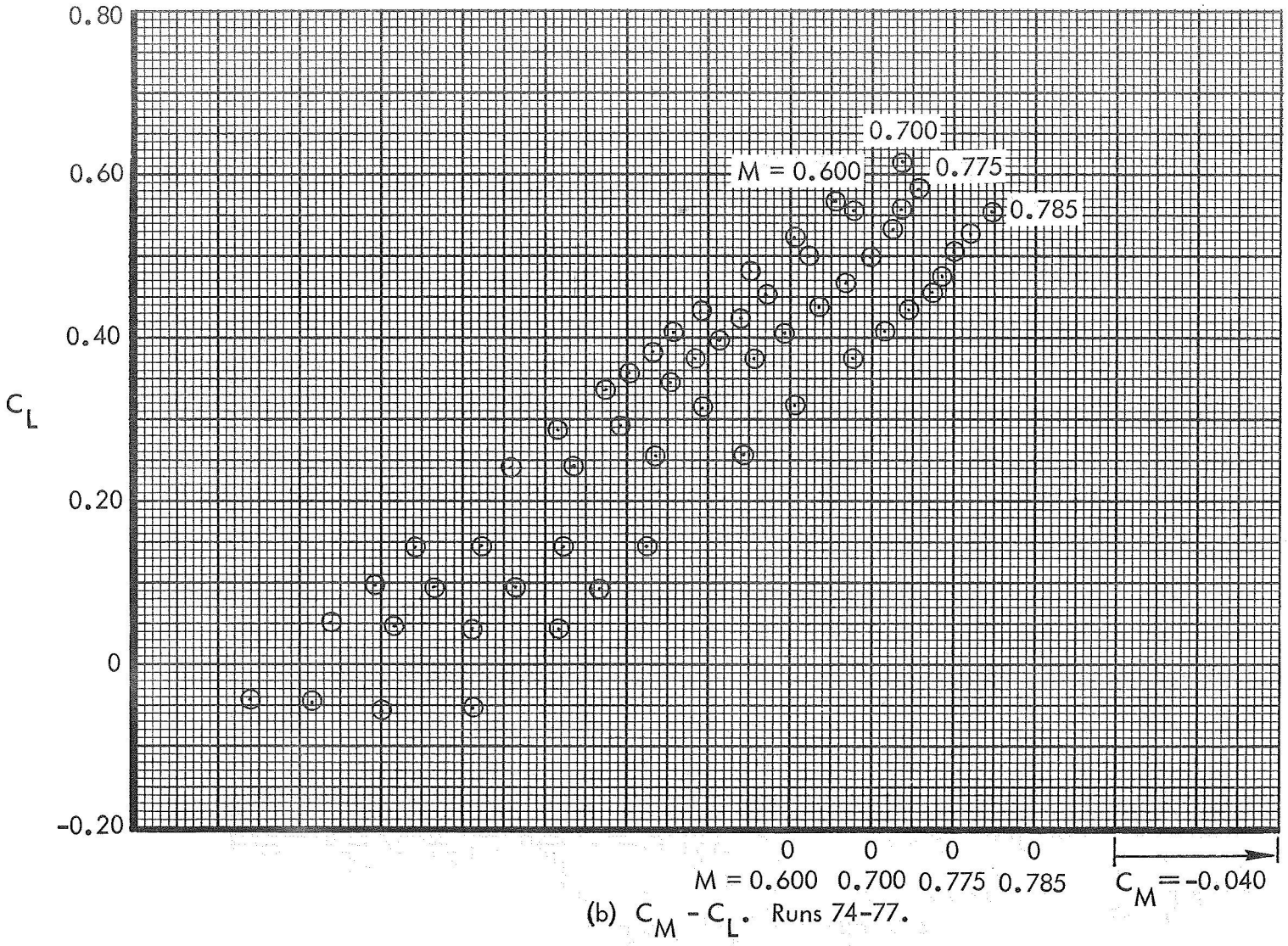
(d) $C_L - C_D$. Runs 70, 71.

Figure 28. Concluded.



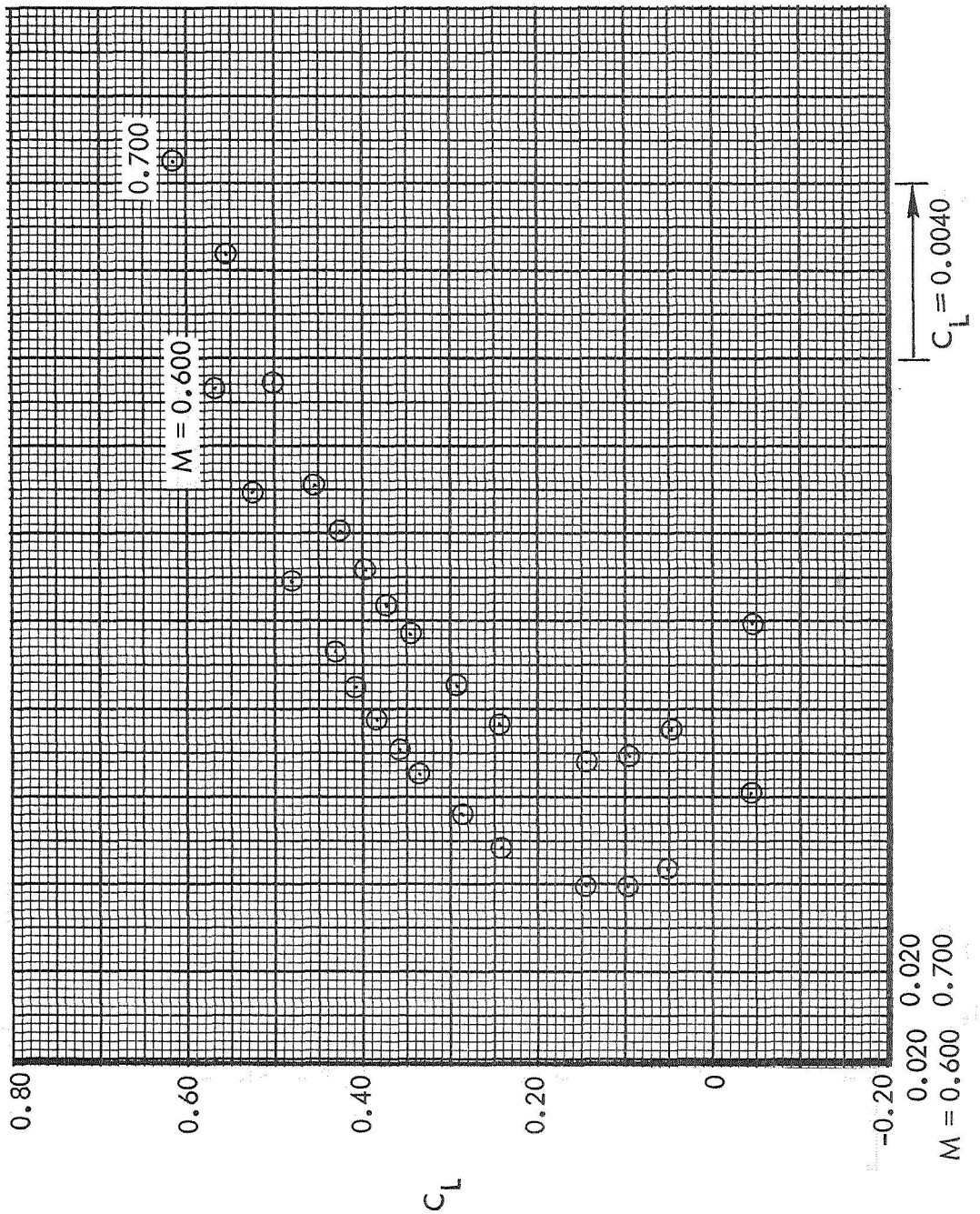
(a) C_L - α . Runs 74-77.

Figure 29. Reynolds Number Effects. $i_H = -1^\circ$. Test 591. $R_N = 4 \times 10^6$/foot



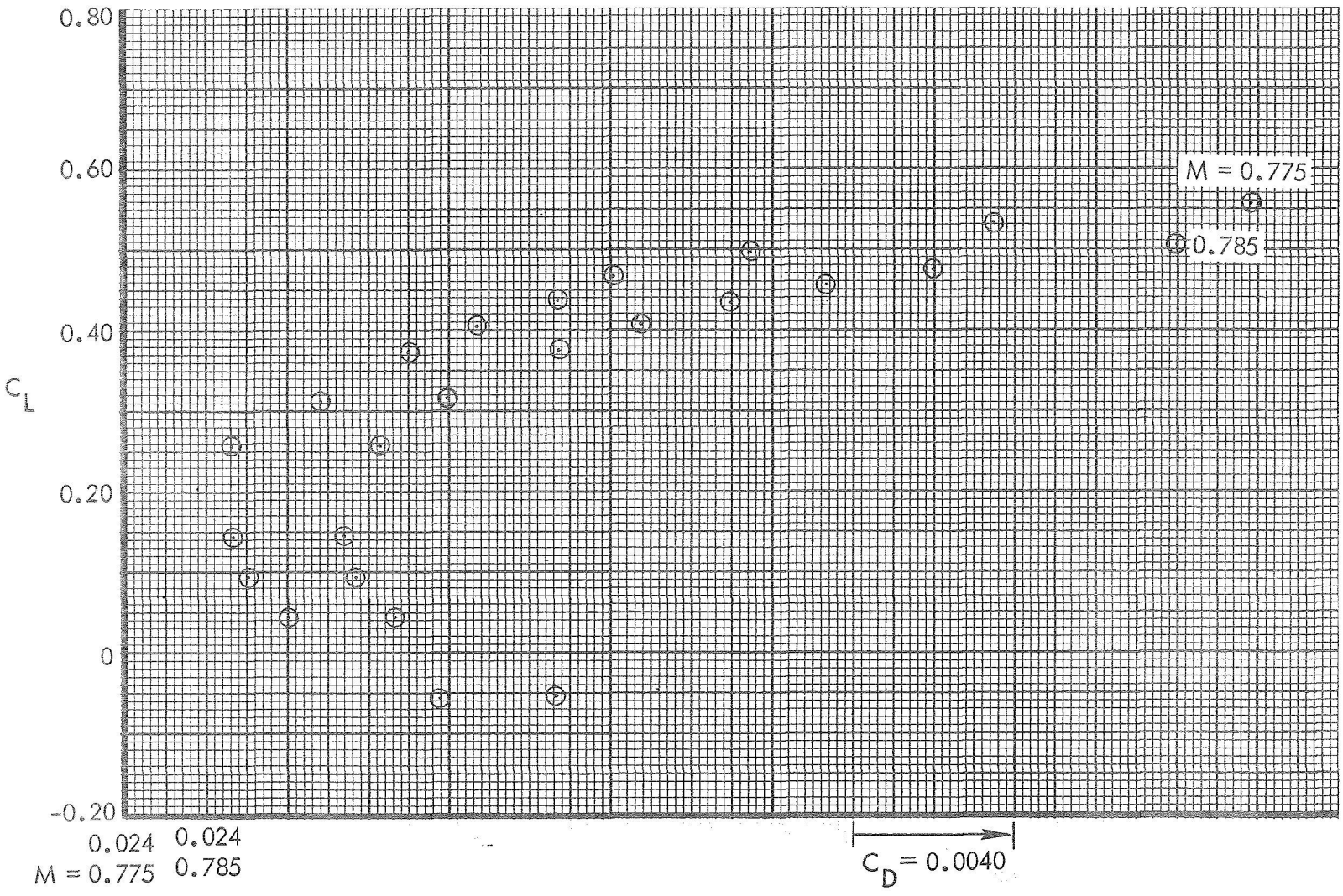
(b) $C_M - C_L$. Runs 74-77.

Figure 29. Continued.



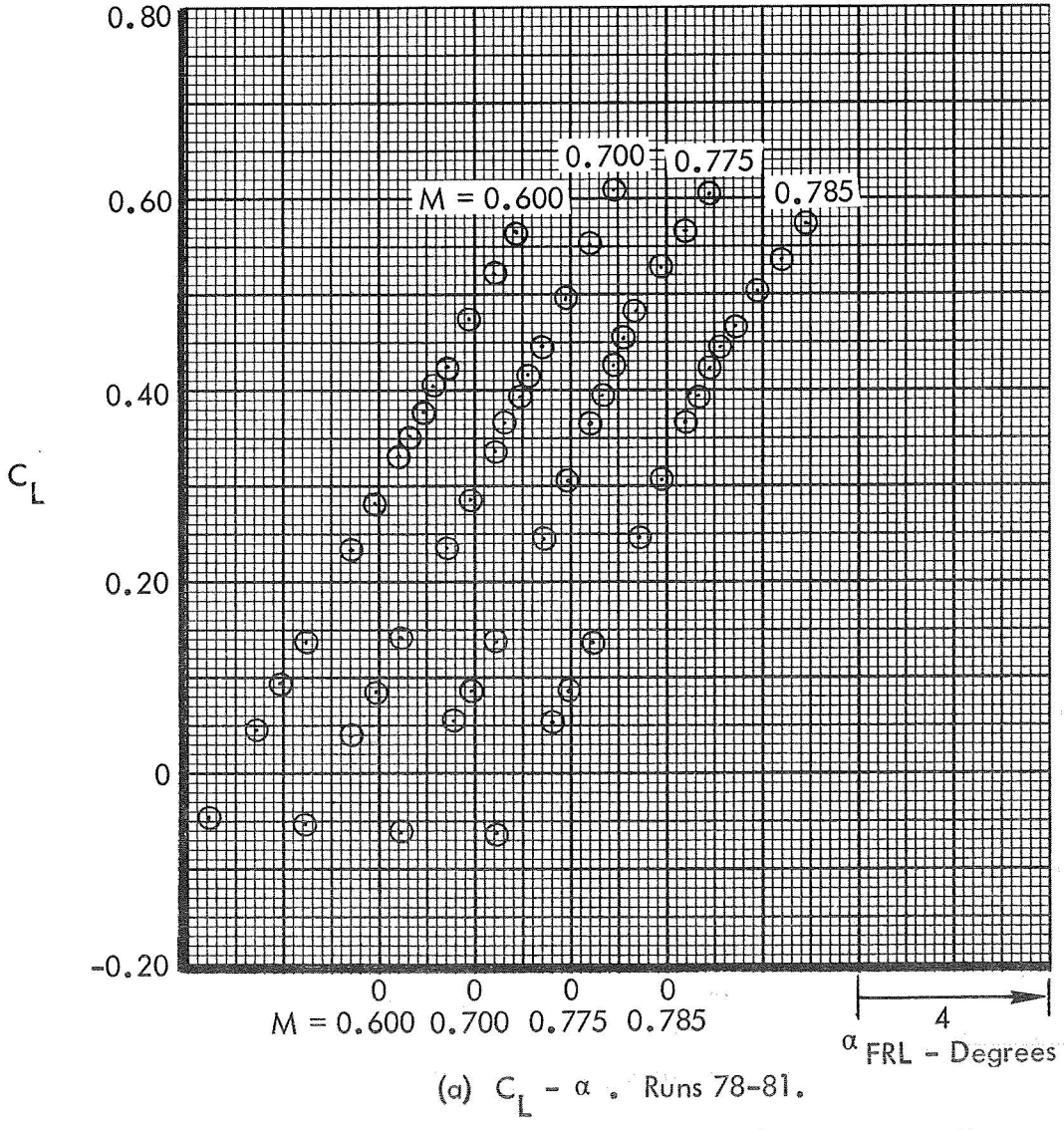
(c) $C_L - C_D$. Runs 74, 75.

Figure 29. Continued.



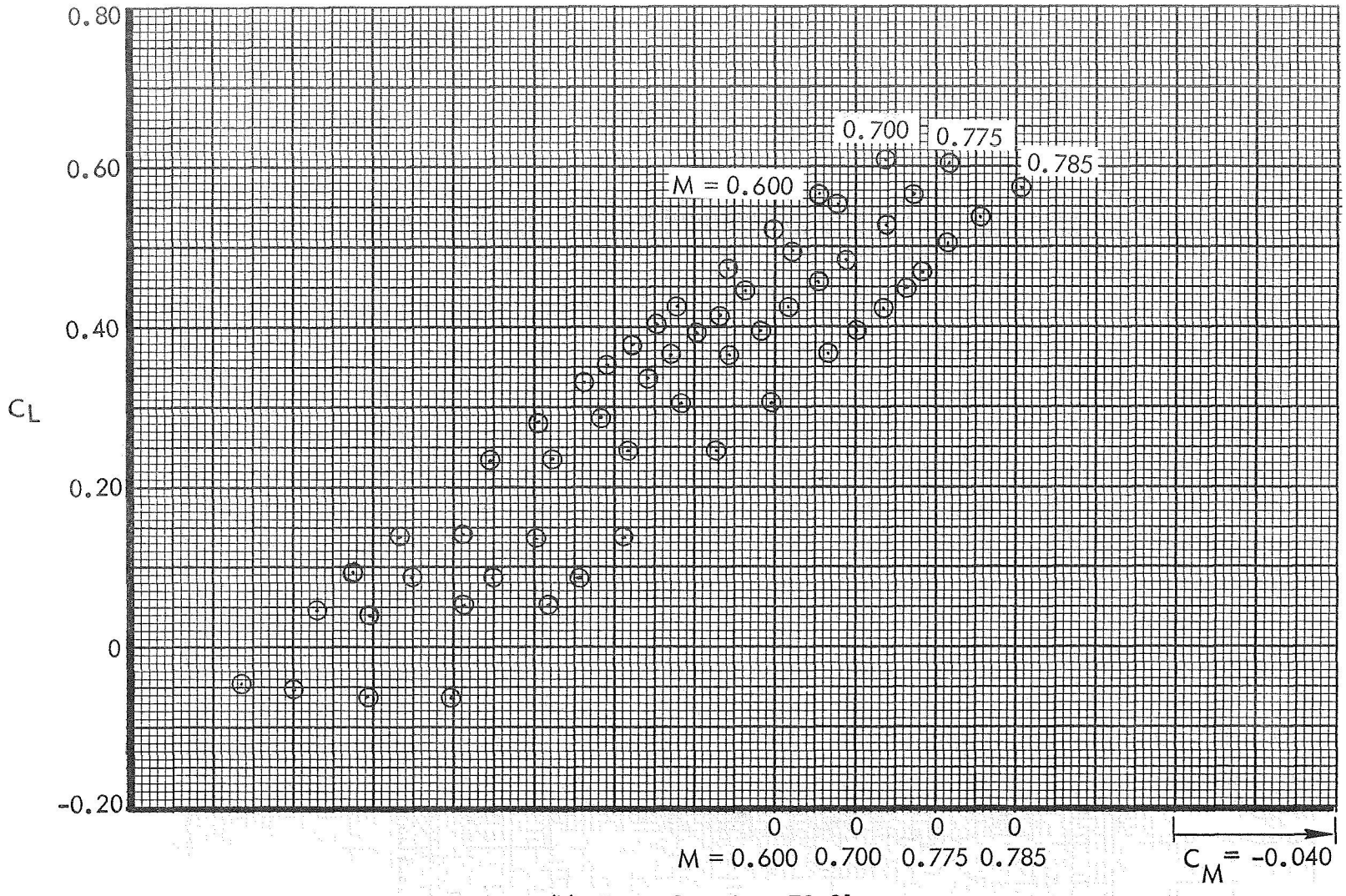
(d) $C_L - C_D$. Runs 76, 77.

Figure 29. Concluded.



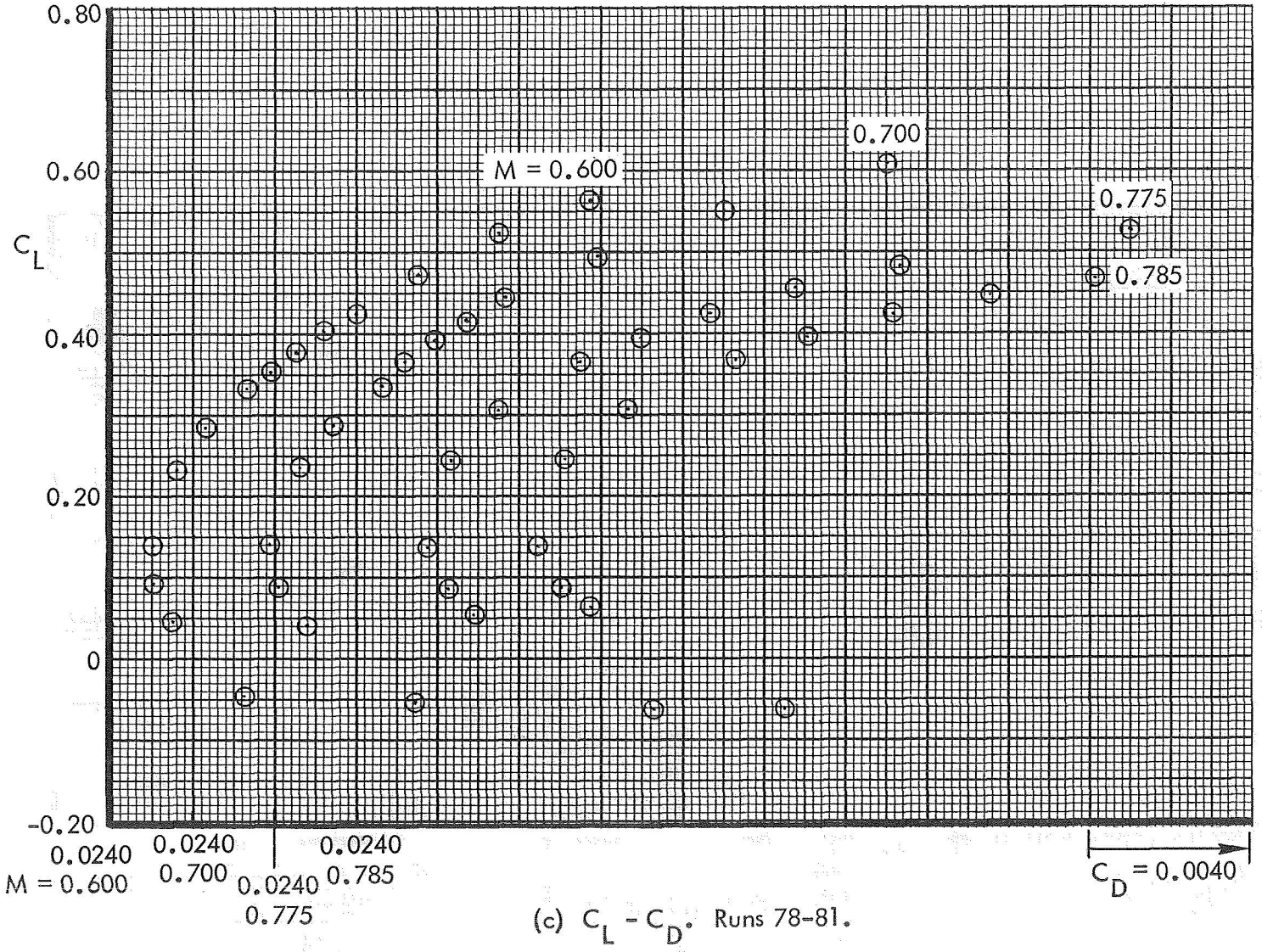
(a) $C_L - \alpha$. Runs 78-81.

Figure 30. Reynolds Number Effects. $i_H = -1^\circ$. Test 591. $R_N = 3 \times 10^6$/foot



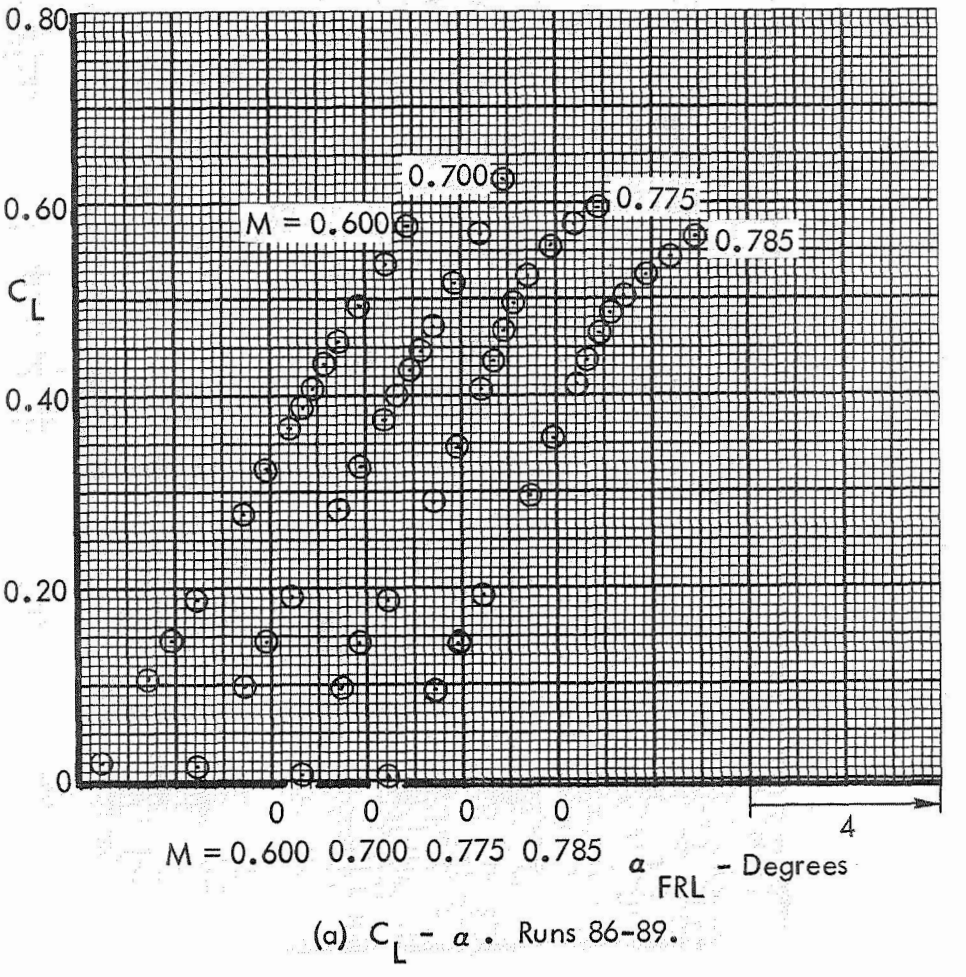
(b) $C_M - C_L$. Runs 78-81.

Figure 30. Continued.



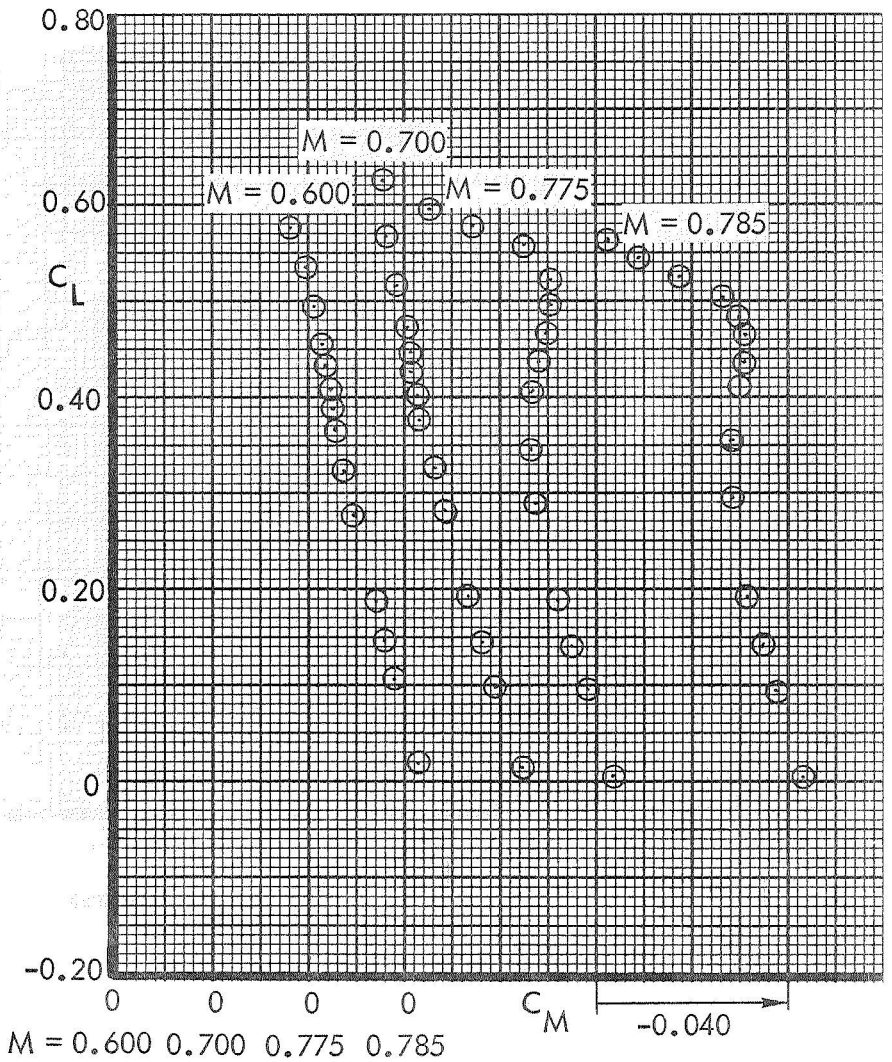
(c) $C_L - C_D$. Runs 78-81.

Figure 30. Concluded.



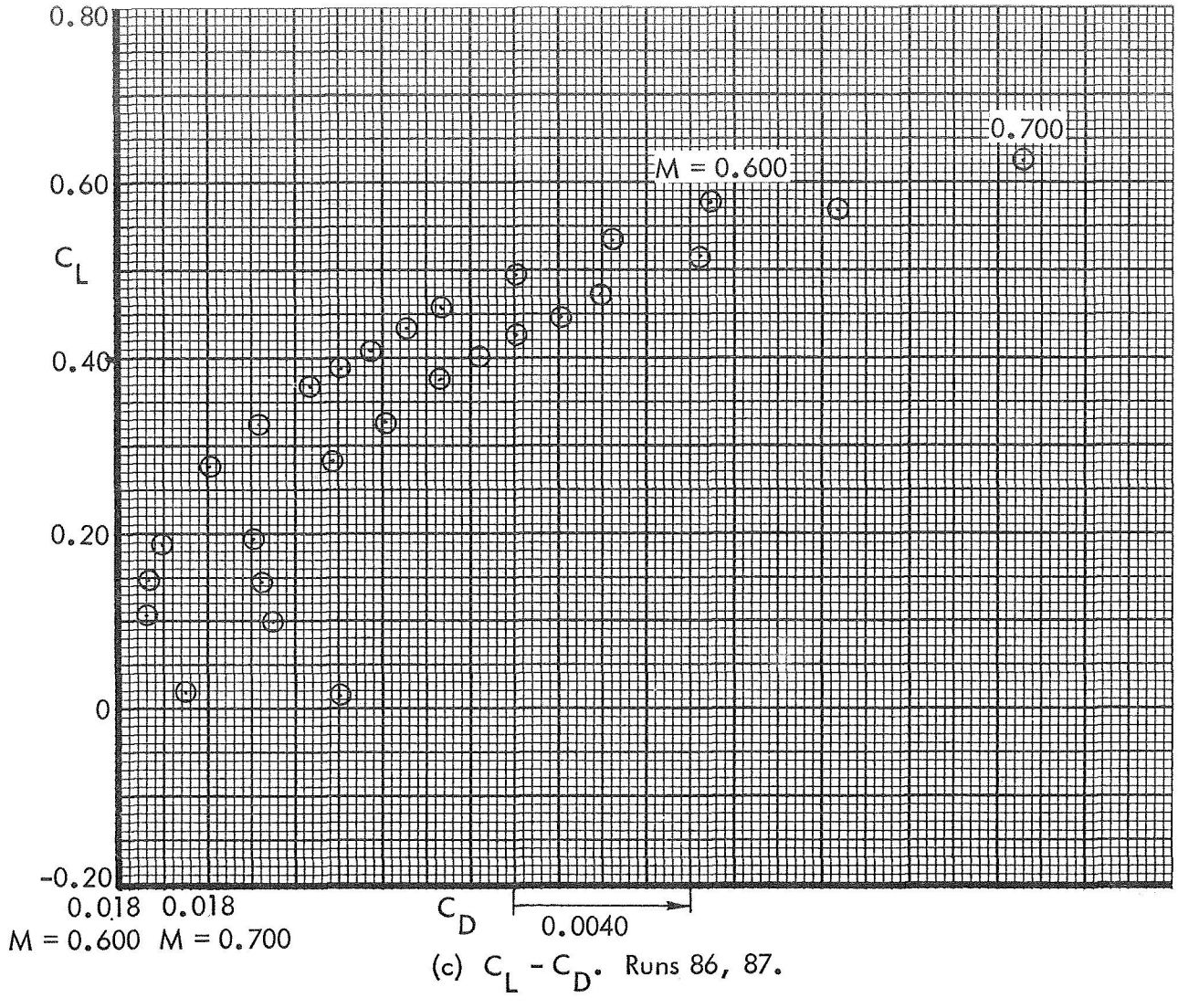
(a) $C_L - \alpha$. Runs 86-89.

Figure 31. Basic Aerodynamic Data. Tail-off. Test 591.
$R_N = 5 \times 10^6$/foot



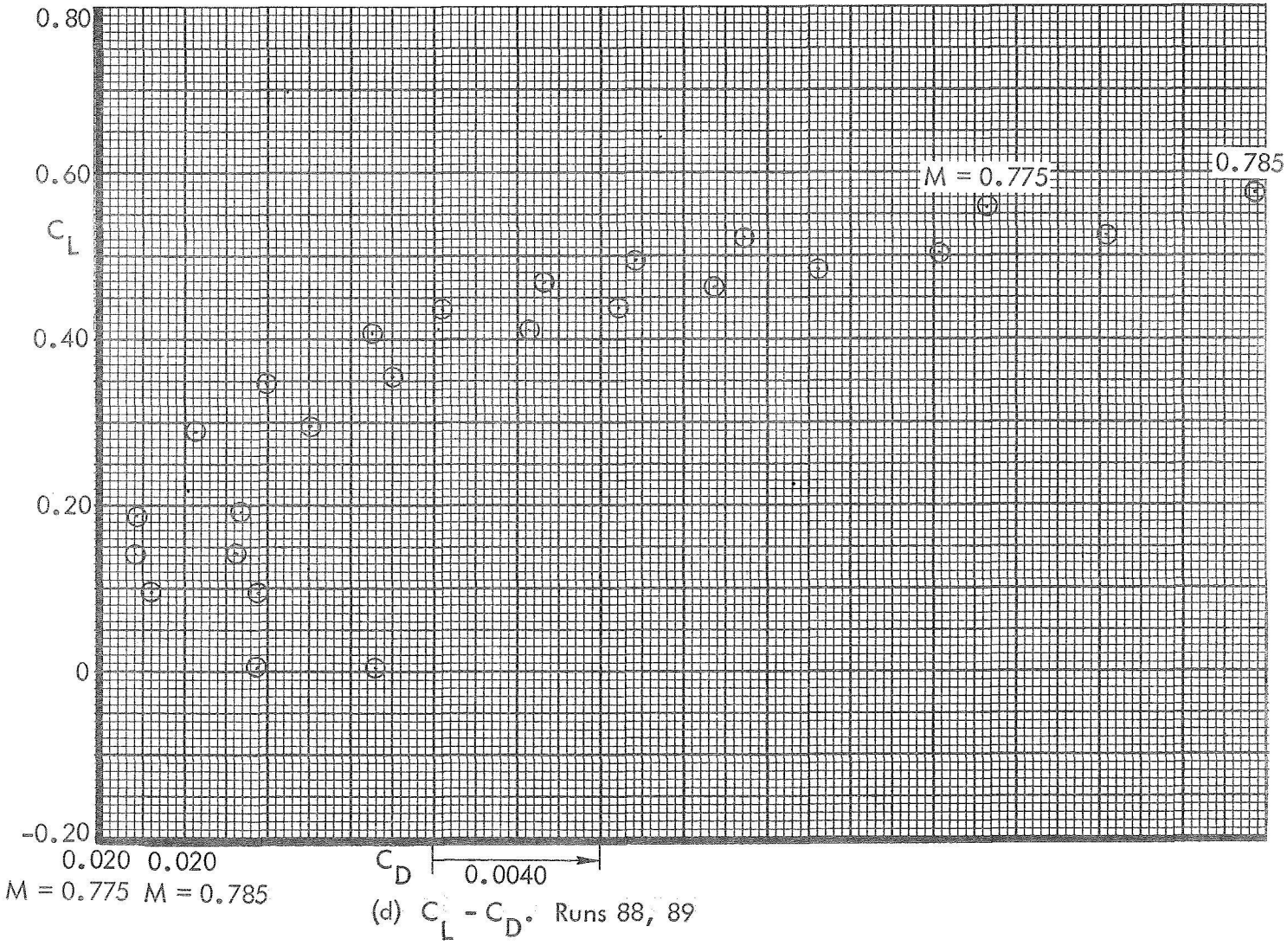
(b) $C_M - C_L$. Runs 86-89.

Figure 31. Continued.



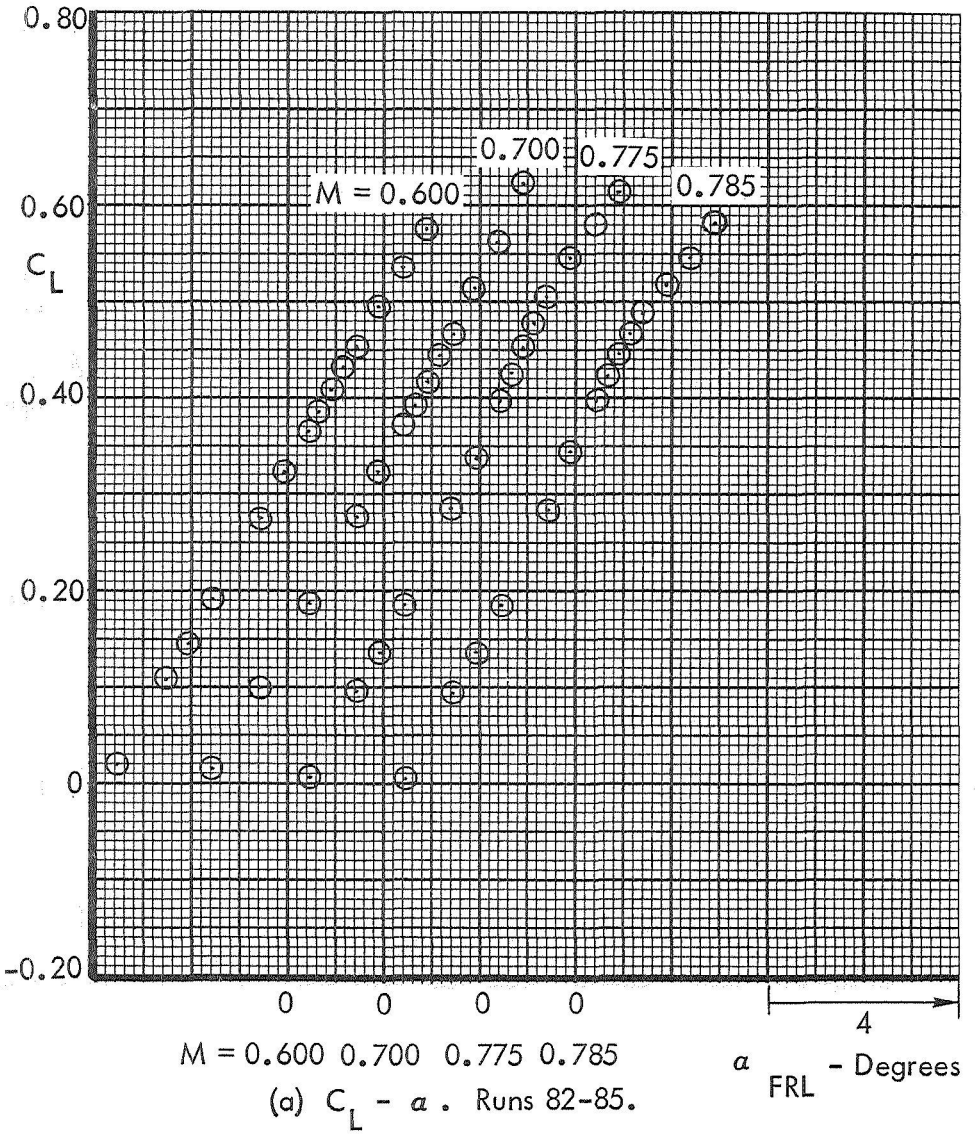
(c) $C_L - C_D$. Runs 86, 87.

Figure 31. Continued.



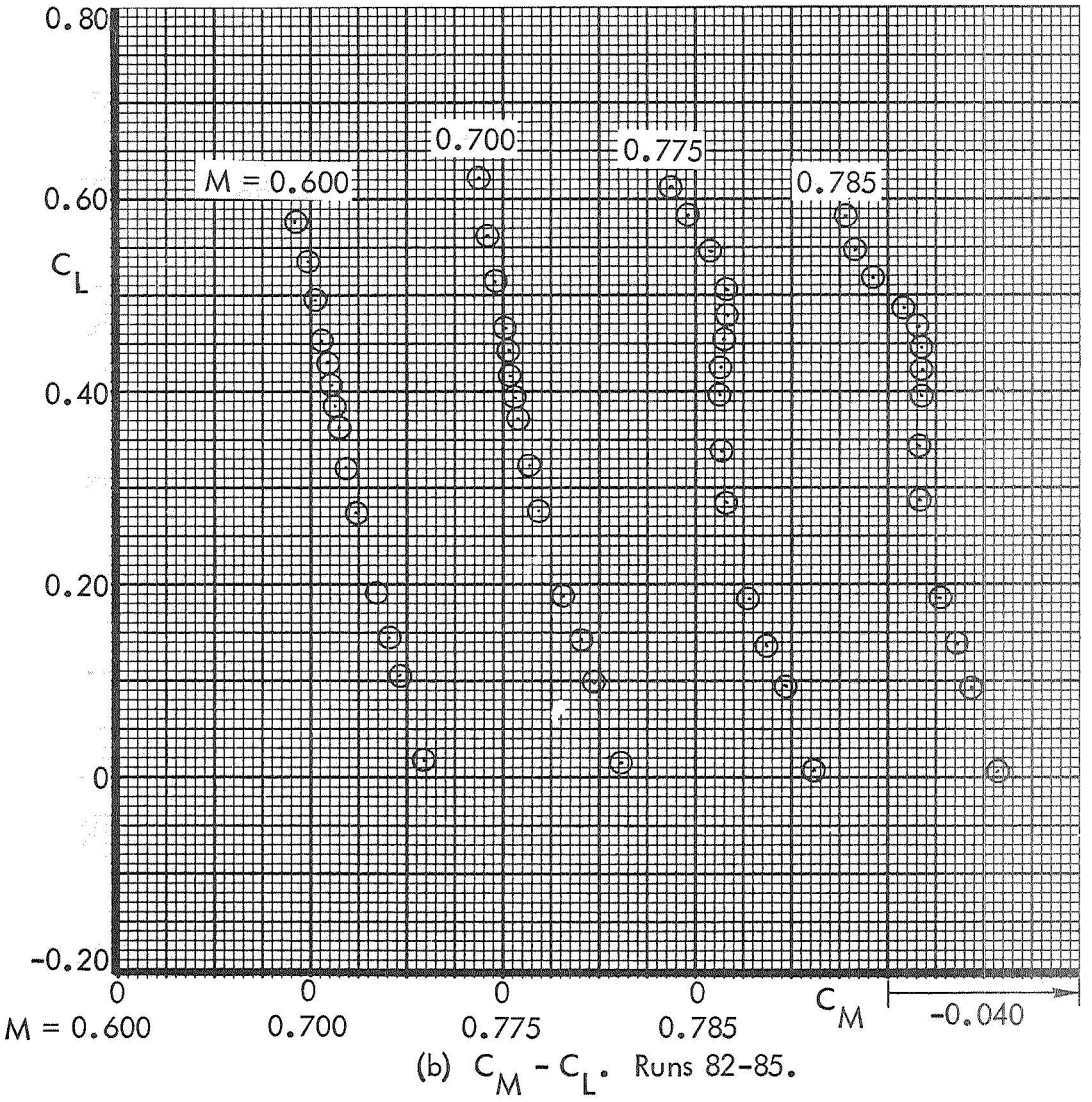
(d) $C_L - C_D$. Runs 88, 89

Figure 31. Continued.



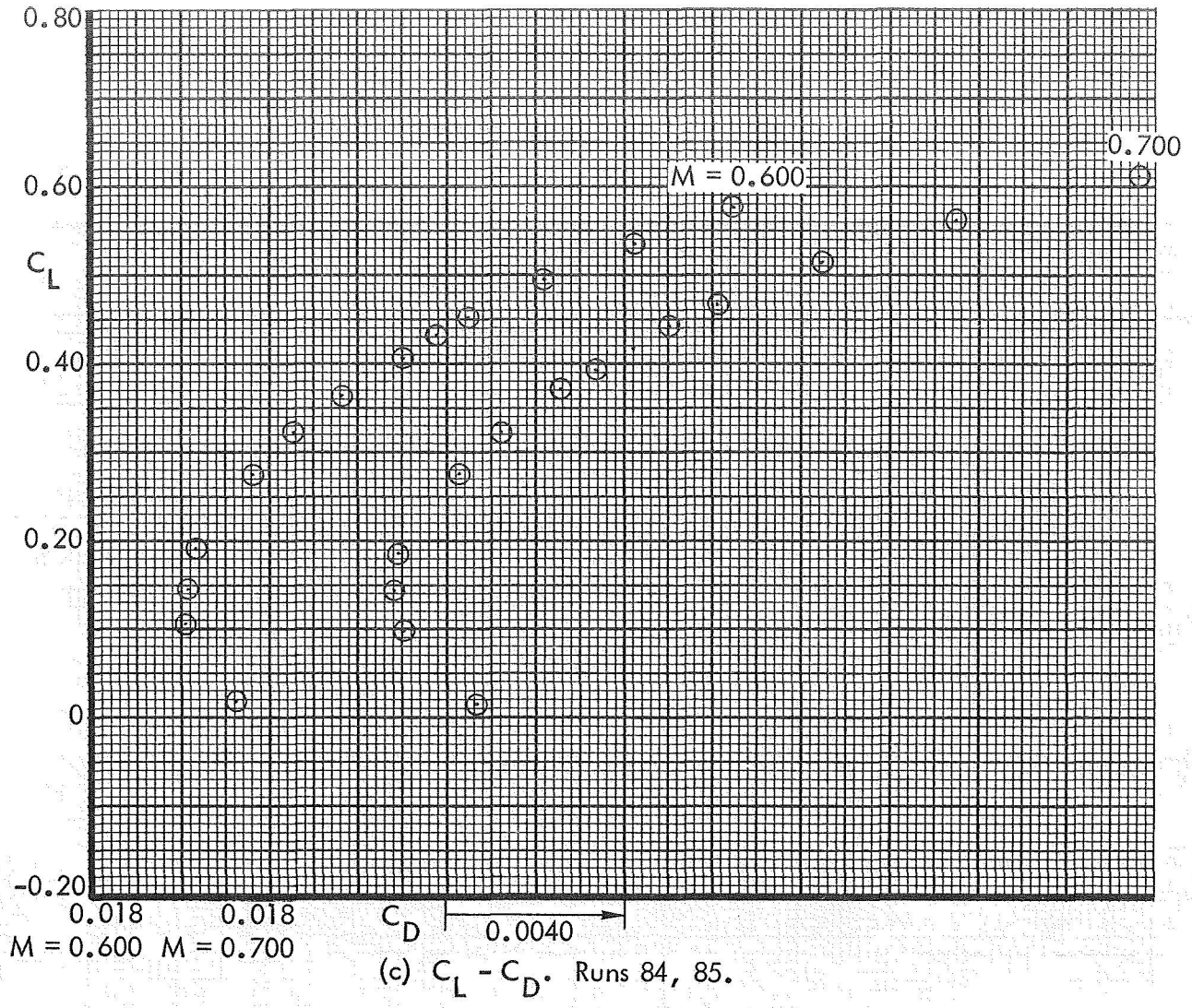
(a) $C_L - \alpha$. Runs 82-85.

Figure 32. Basic Aerodynamic Data. Tail-Off. Test 591.
$R_N = 3 \times 10^6$/foot



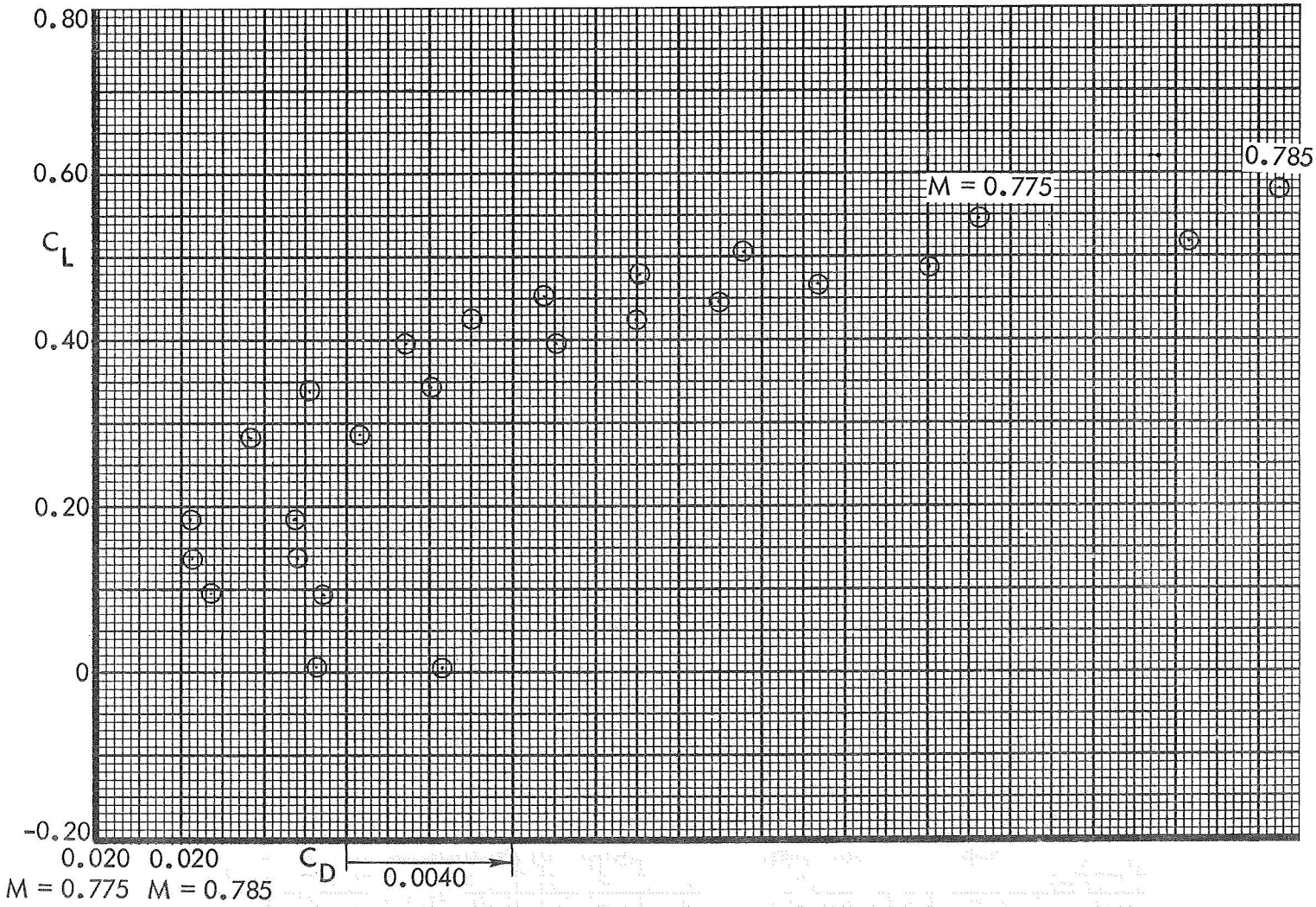
(b) $C_M - C_L$. Runs 82-85.

Figure 32. Continued.



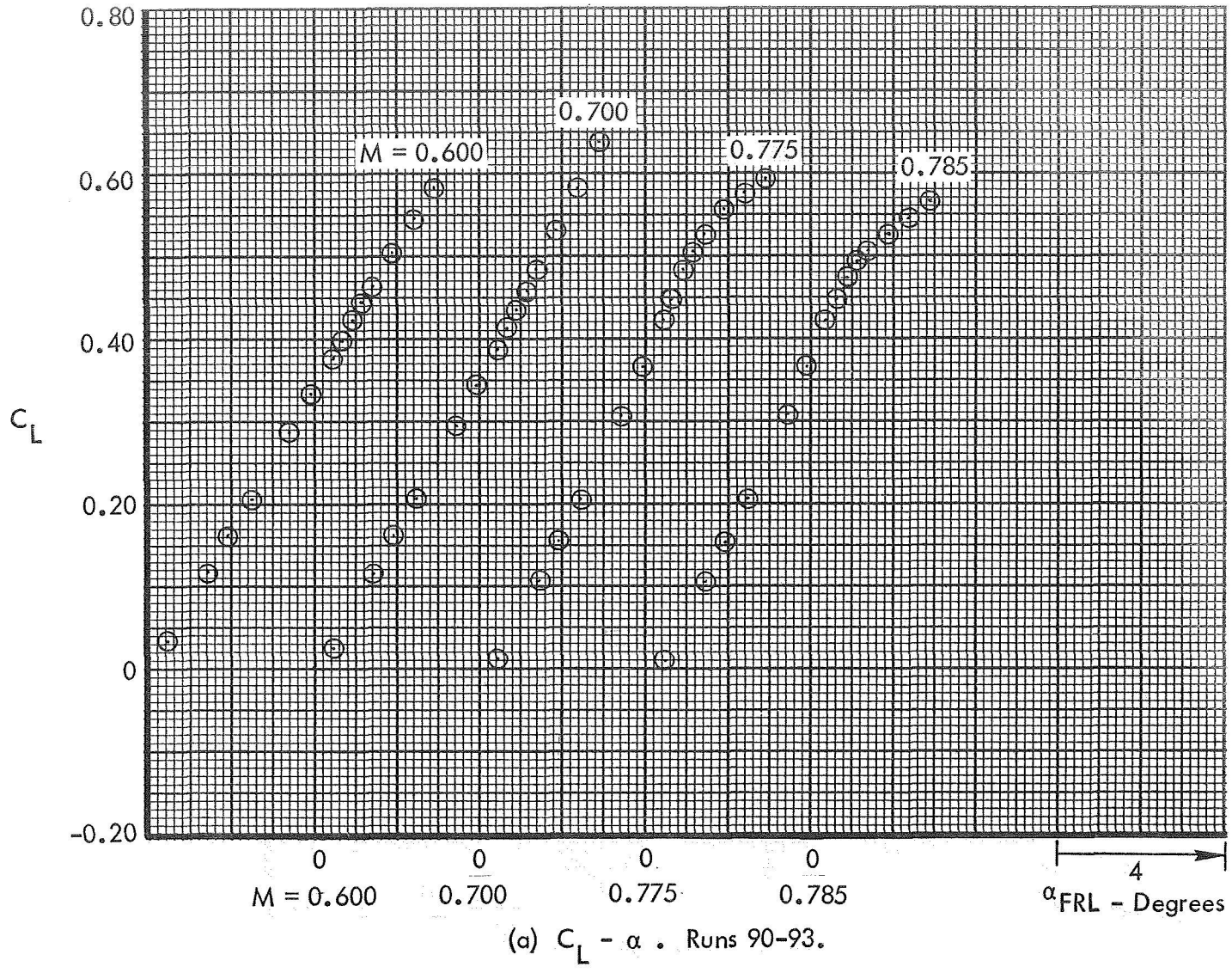
(c) $C_L - C_D$. Runs 84, 85.

Figure 32. Continued.



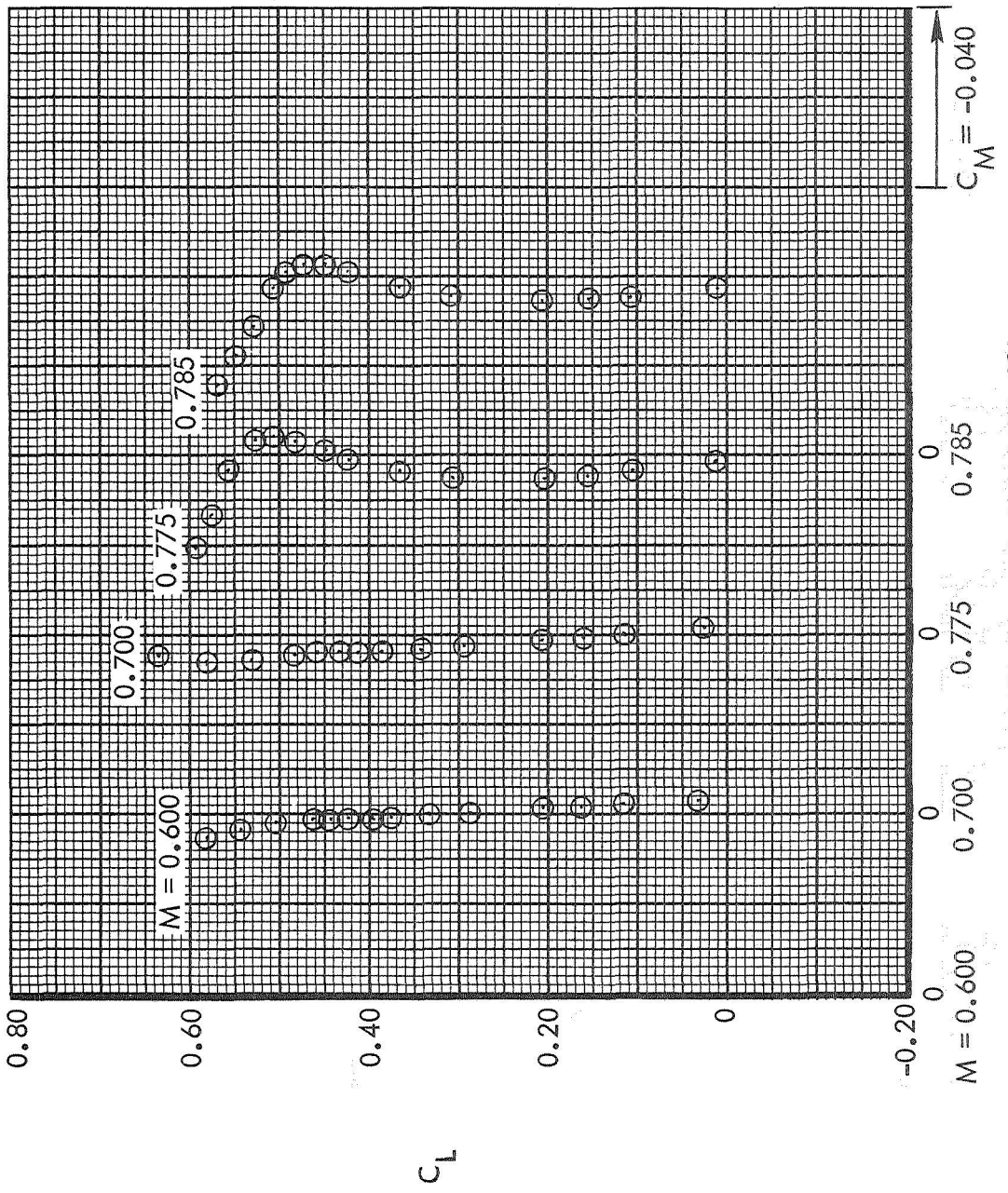
(d) $C_L - C_D$. Runs 82, 83.

Figure 32. Concluded.



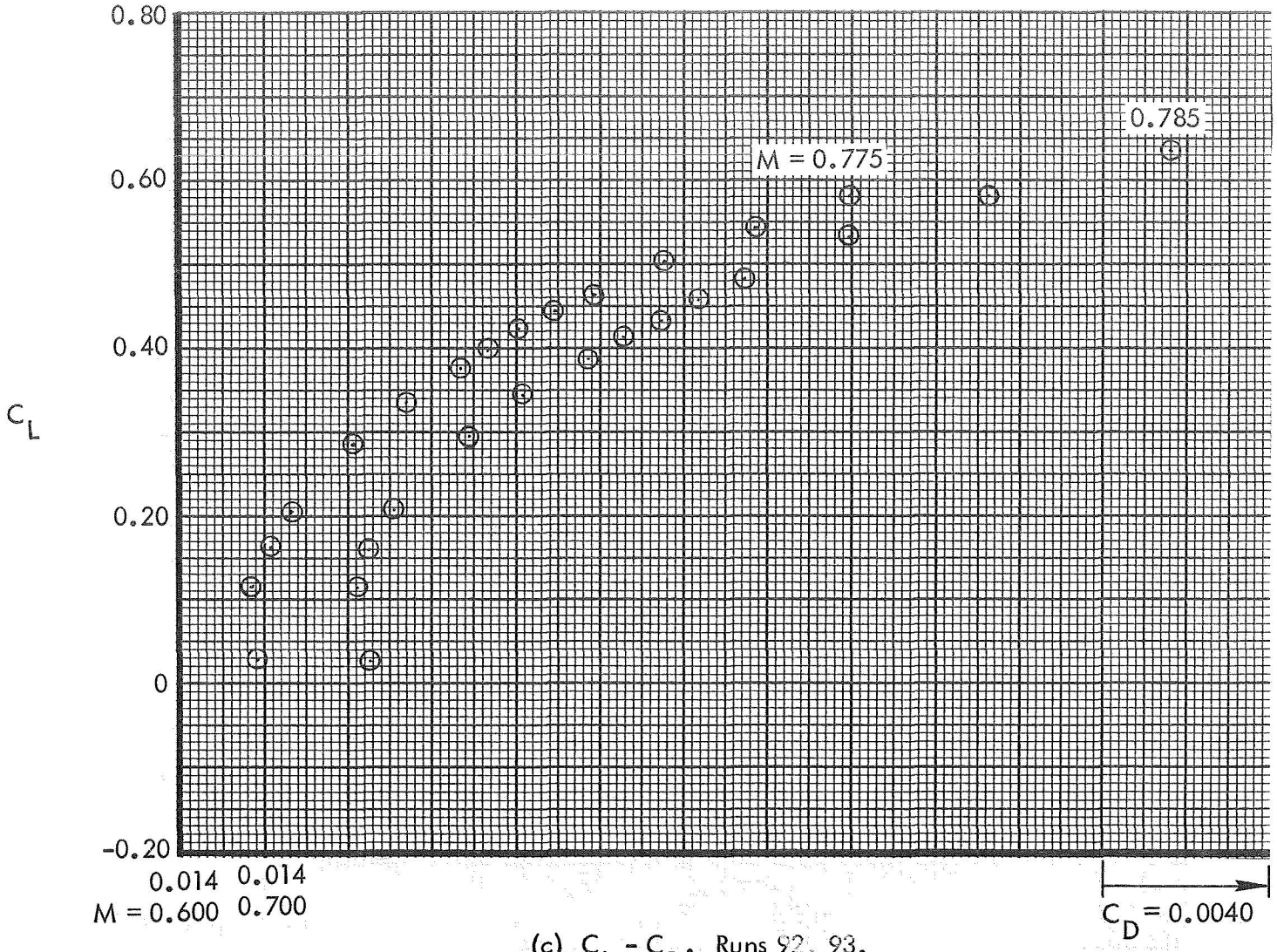
(a) $C_L - \alpha$. Runs 90-93.

Figure 33. Basic Aerodynamic Data. Tail-Off. Pylon/Nacelles-Off. Test 591.



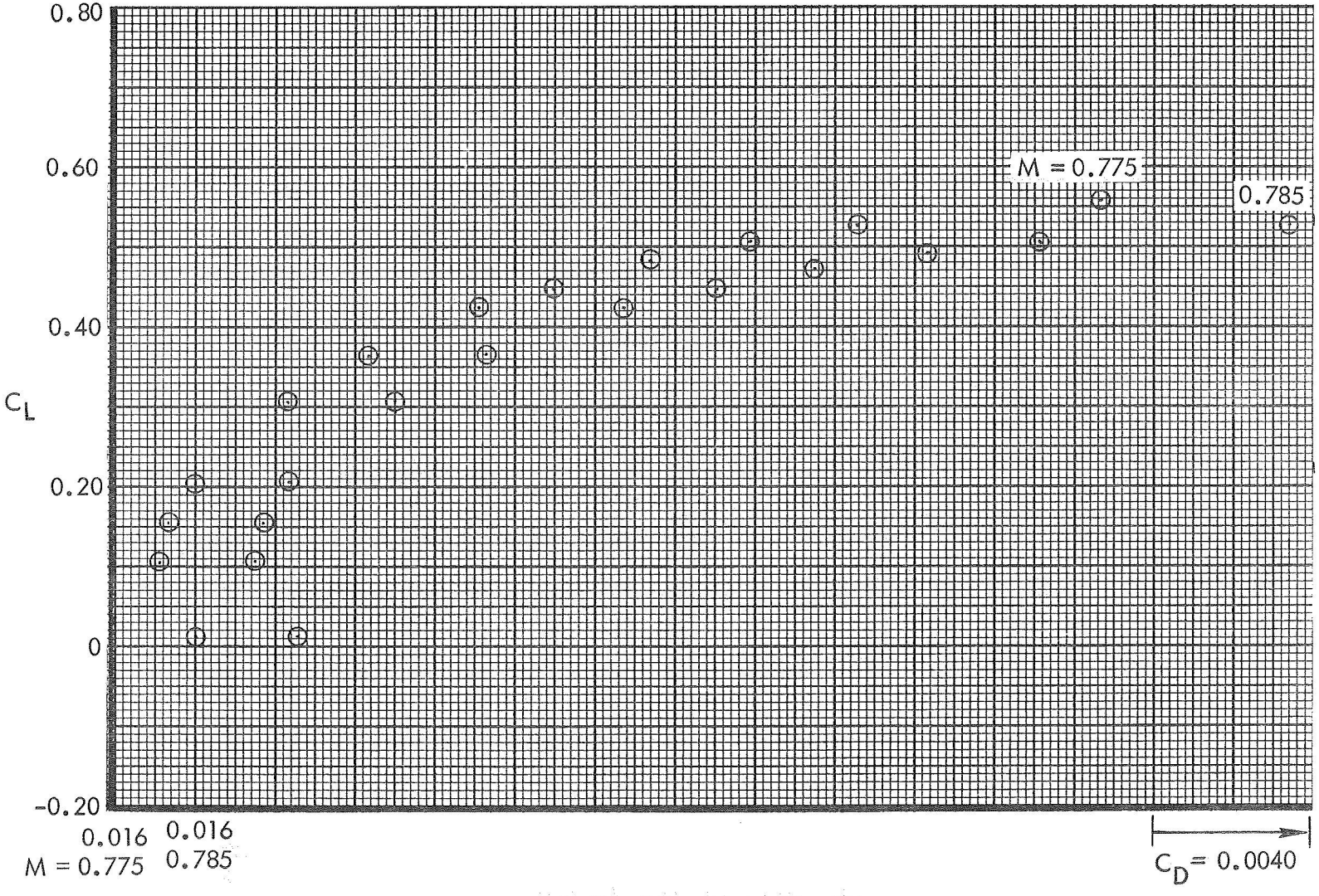
(b) $C_M - C_L$. Runs 90-93.

Figure 33. Continued.



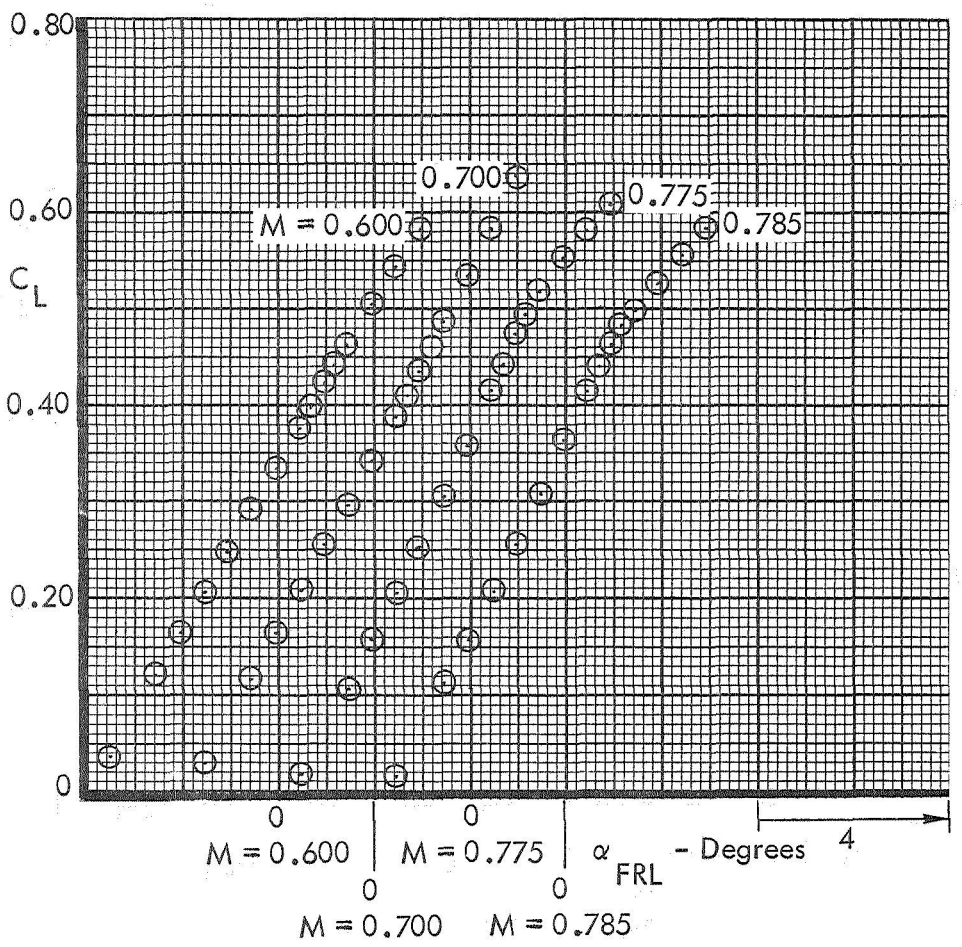
(c) $C_L - C_D$. Runs 92, 93.

Figure 33. Continued.



(d) $C_L - C_D$. Runs 90, 91.

Figure 33. Concluded.



(a) C_L - α Runs 70 - 73

Figure 34. Basic Aerodynamic Data
Wing + Fuselage + Wheel Fairings Test 617

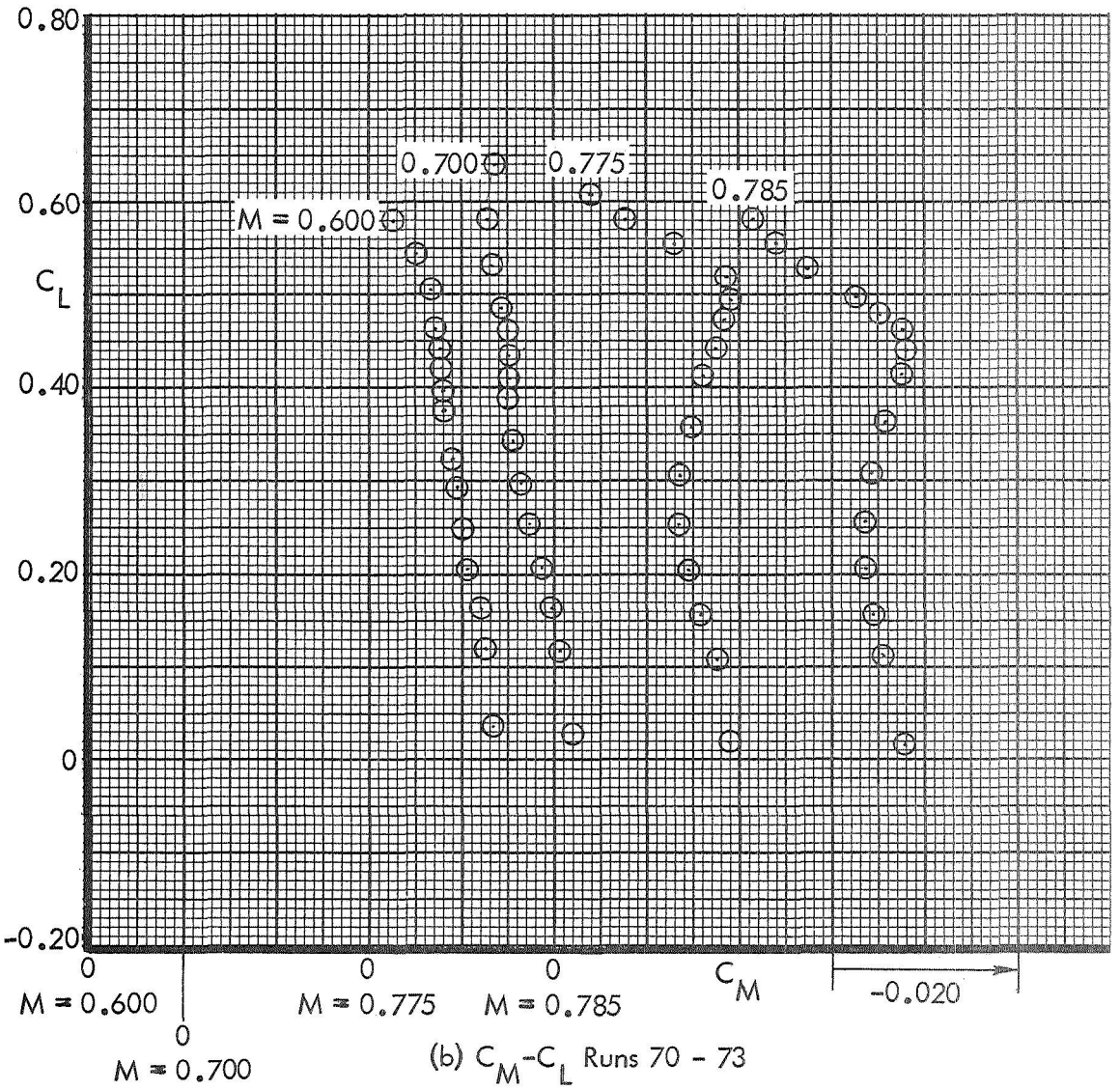


Figure 34. Continued

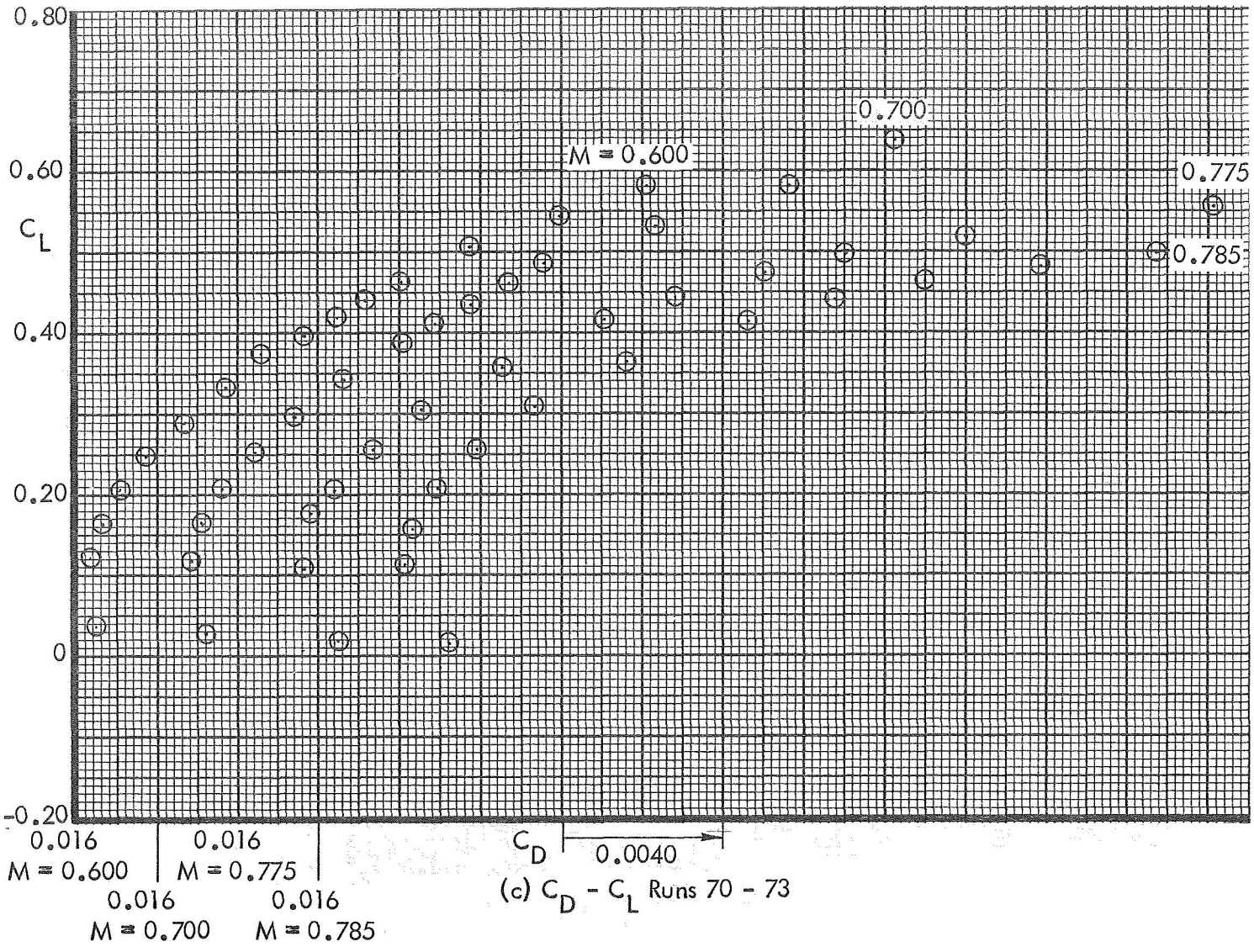
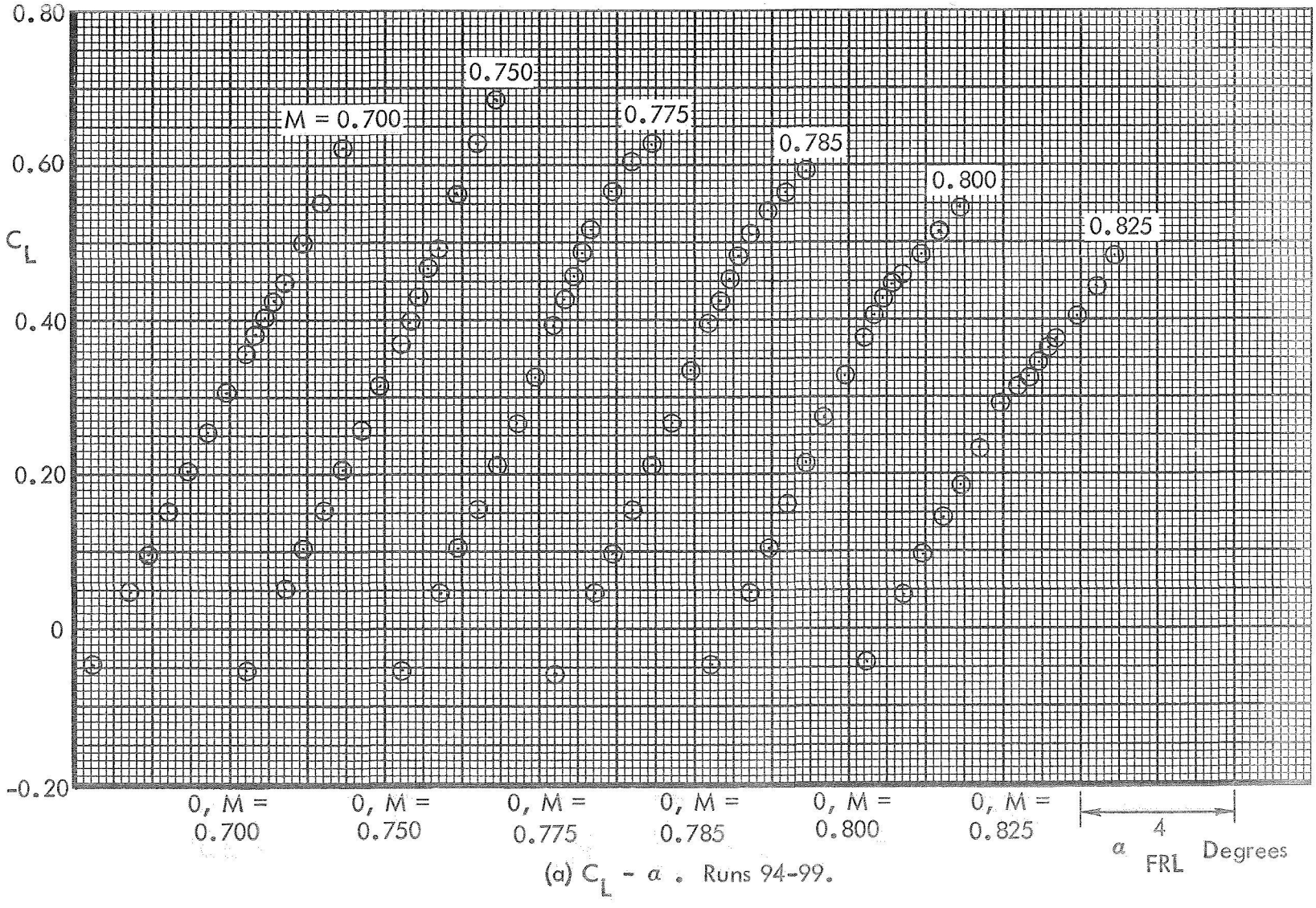
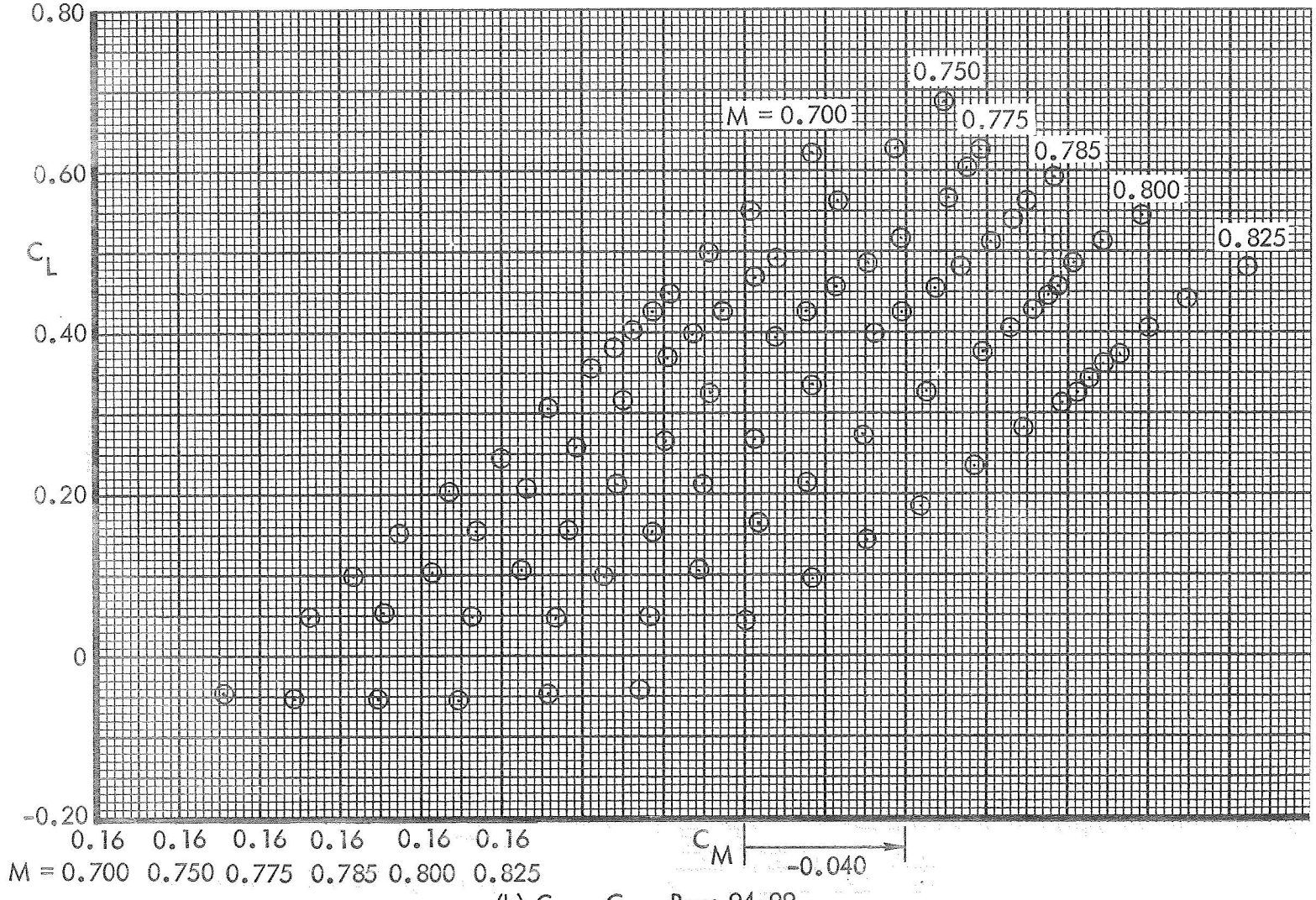


Figure 34. Concluded



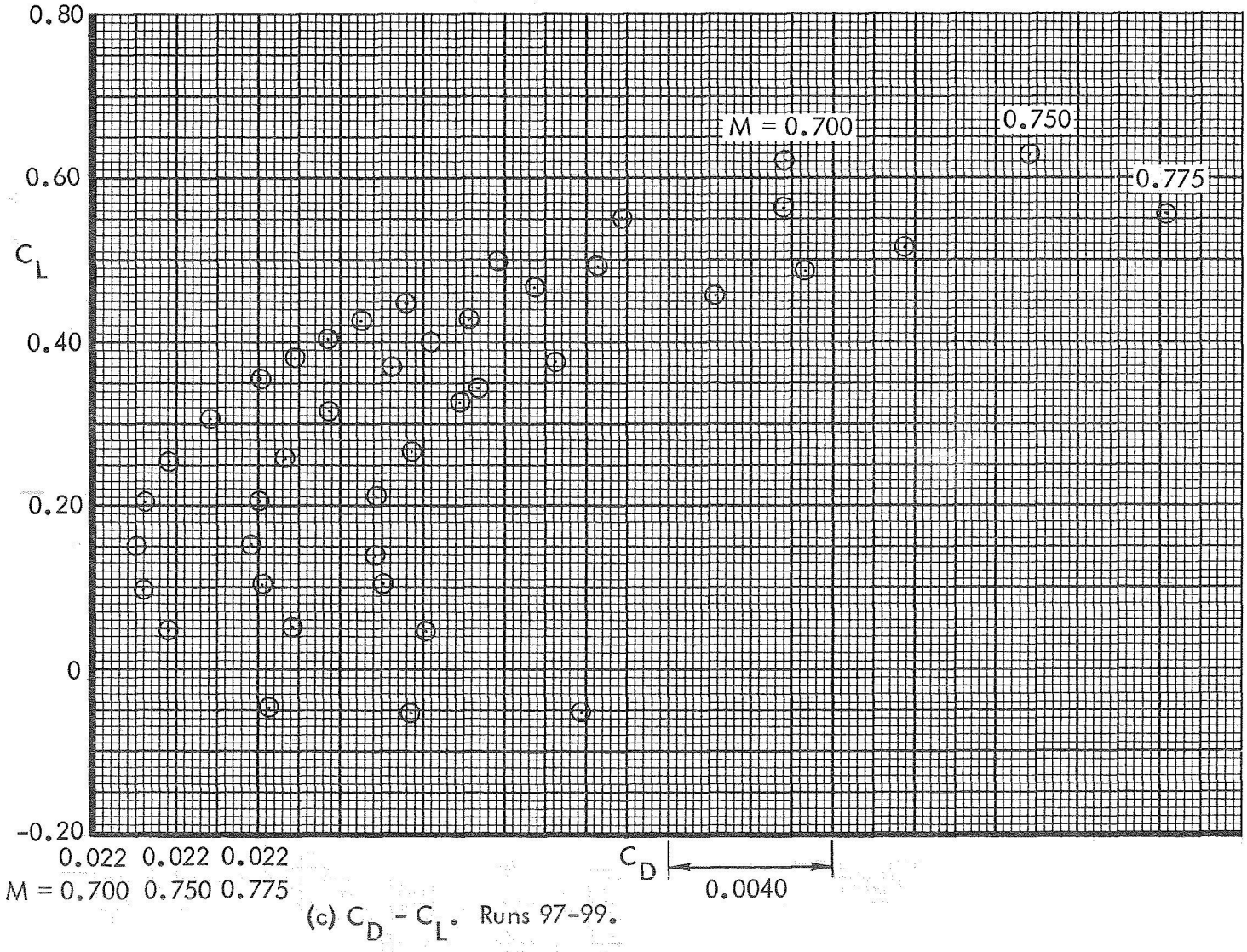
(a) $C_L - \alpha$. Runs 94-99.

Figure 35. Basic Aerodynamic Data. Aft Located Transition. $i_H = -1°$. Test 617.



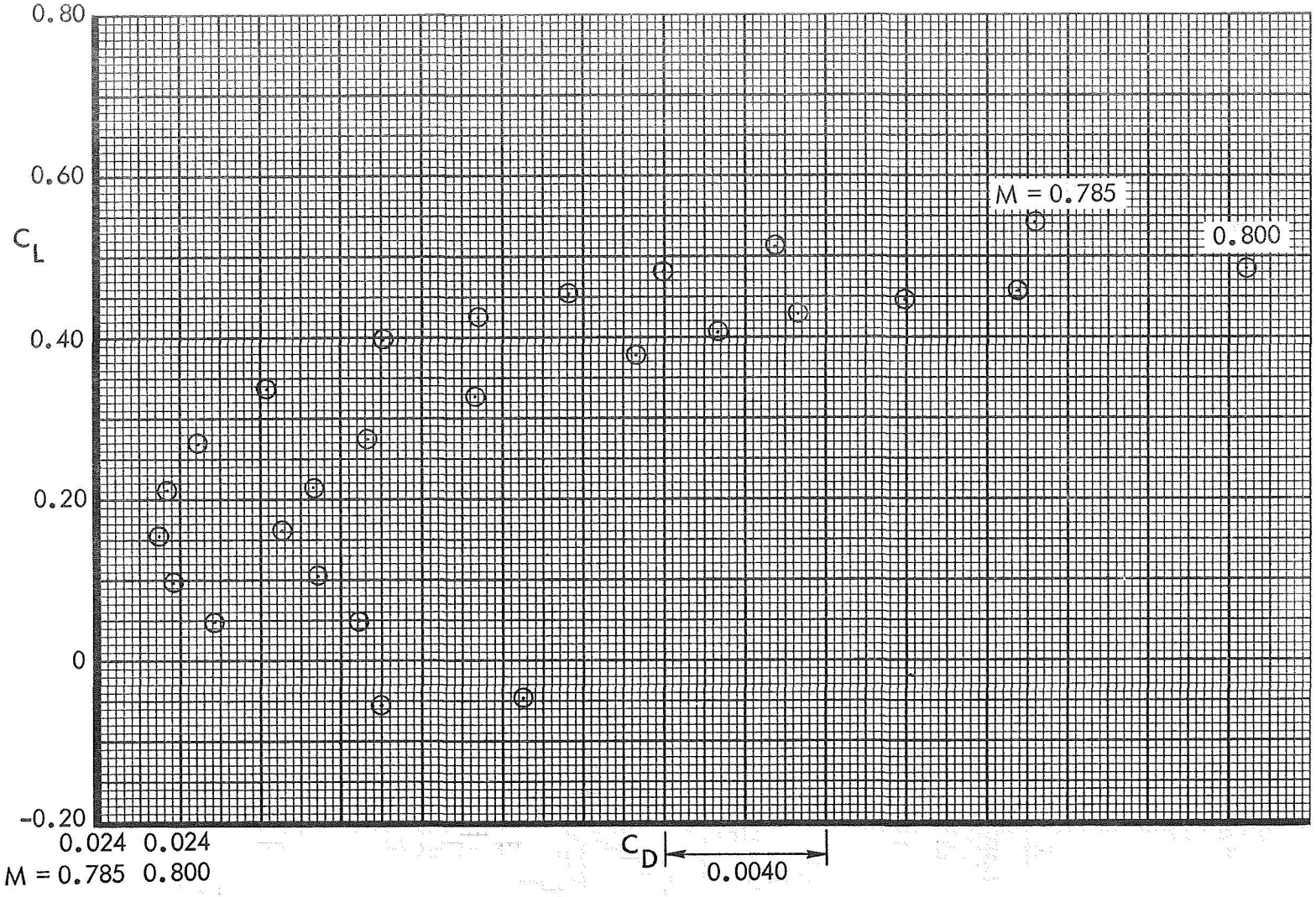
(b) $C_M - C_L$. Runs 94-99.

Figure 35. Continued.



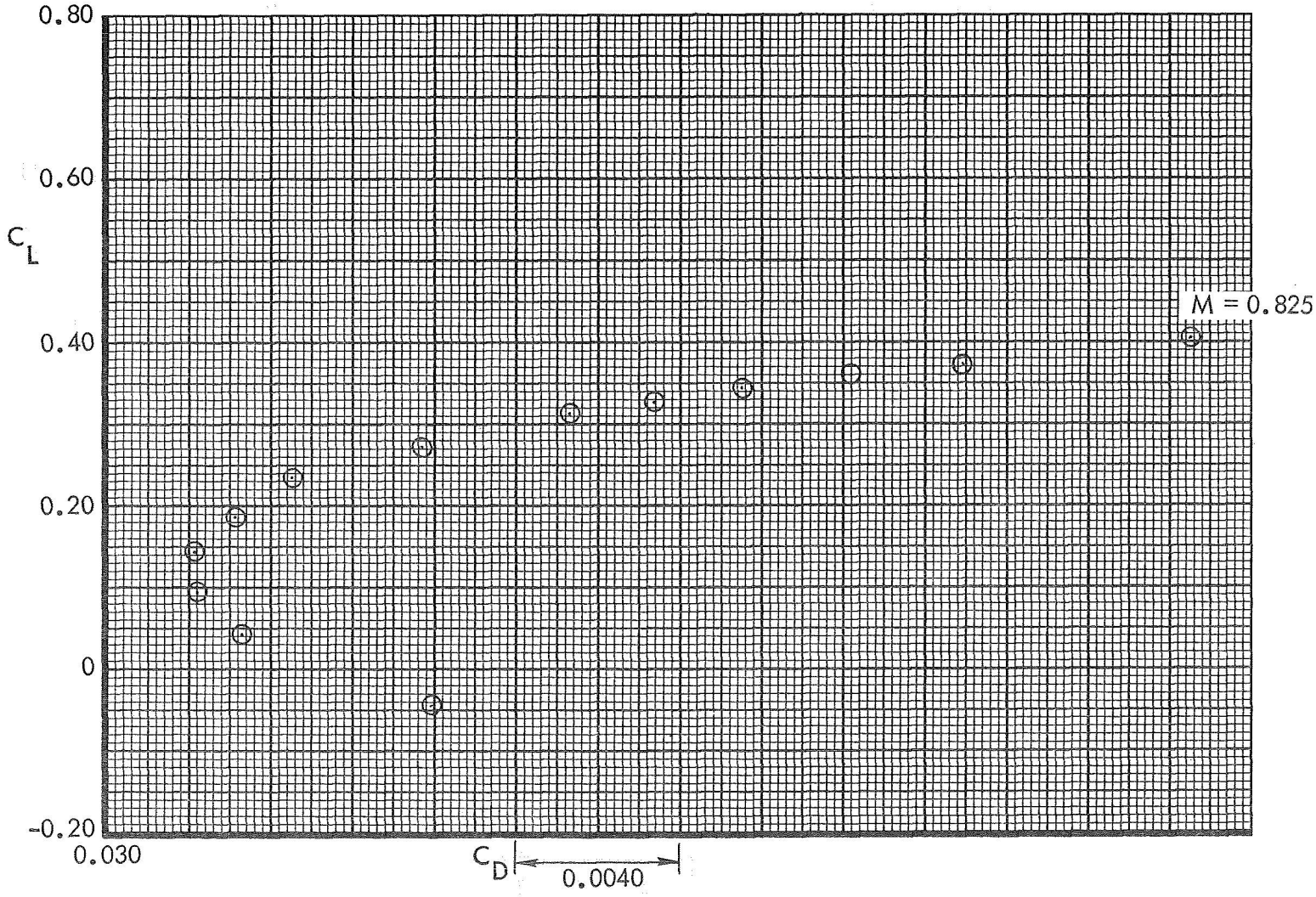
(c) $C_D - C_L$. Runs 97-99.

Figure 35. Continued.



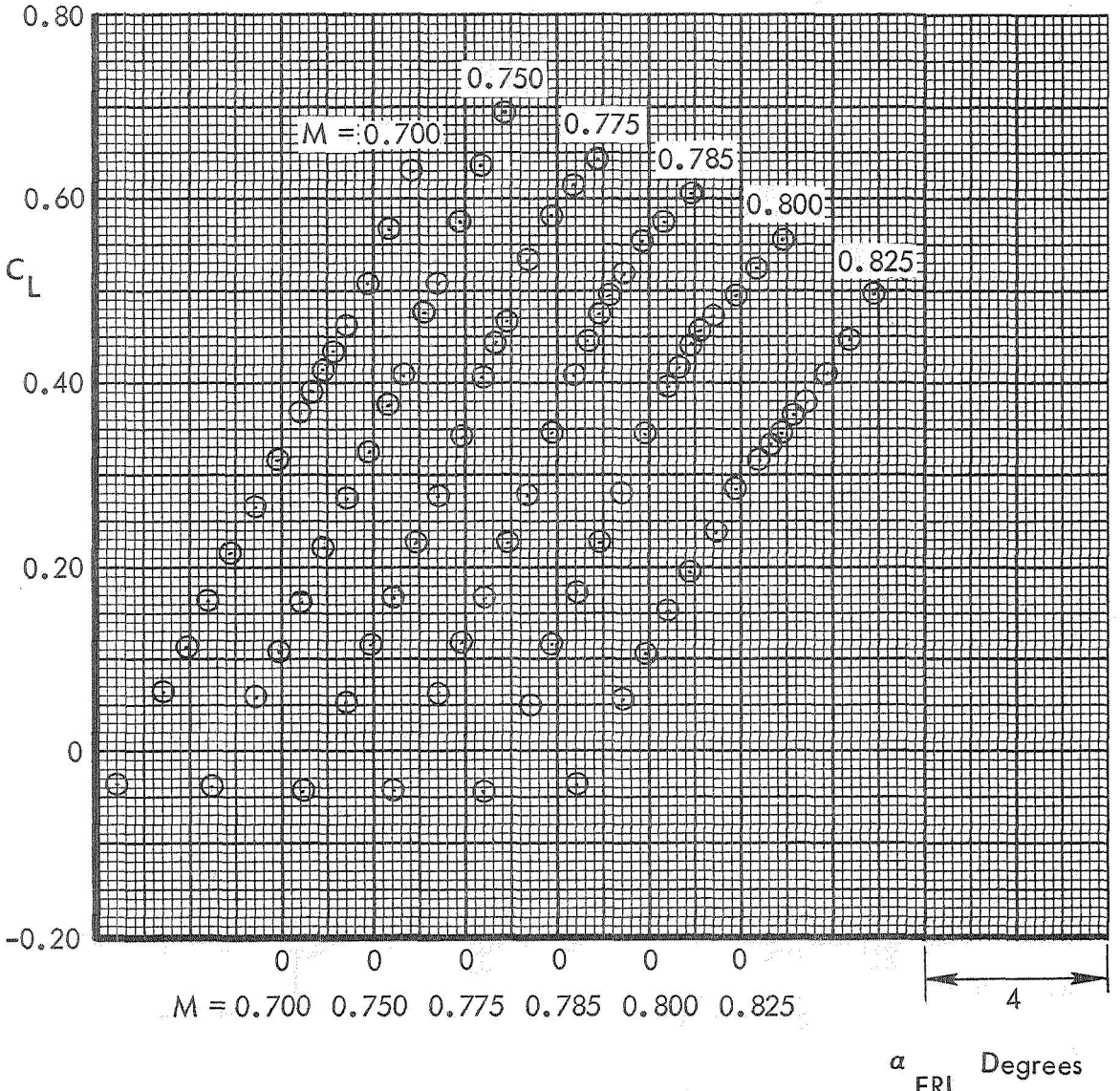
(d) $C_D - C_L$. Runs 95, 96.

Figure 35. Continued.



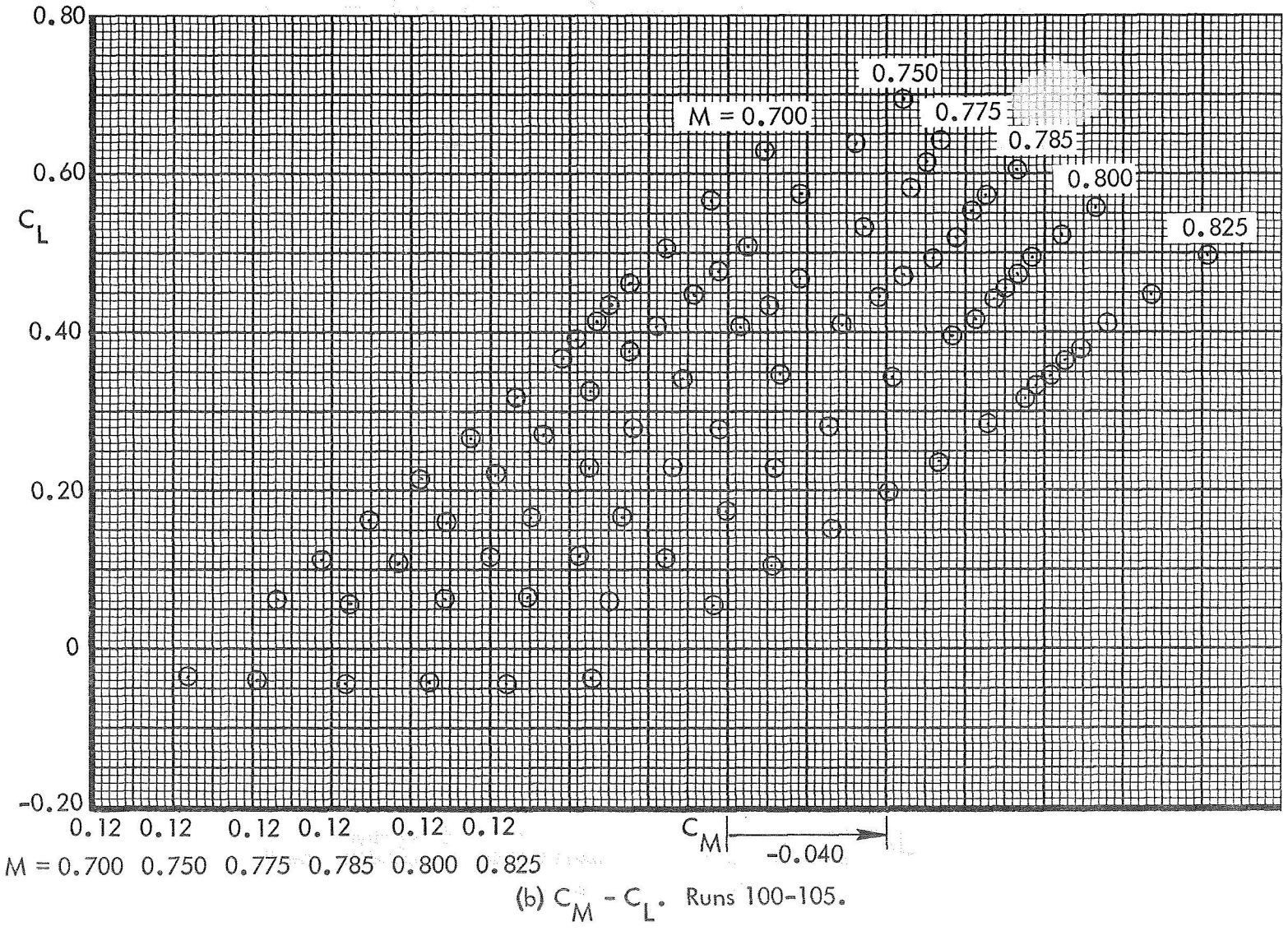
(e) $C_D - C_L$. Run 94.

Figure 35. Concluded.



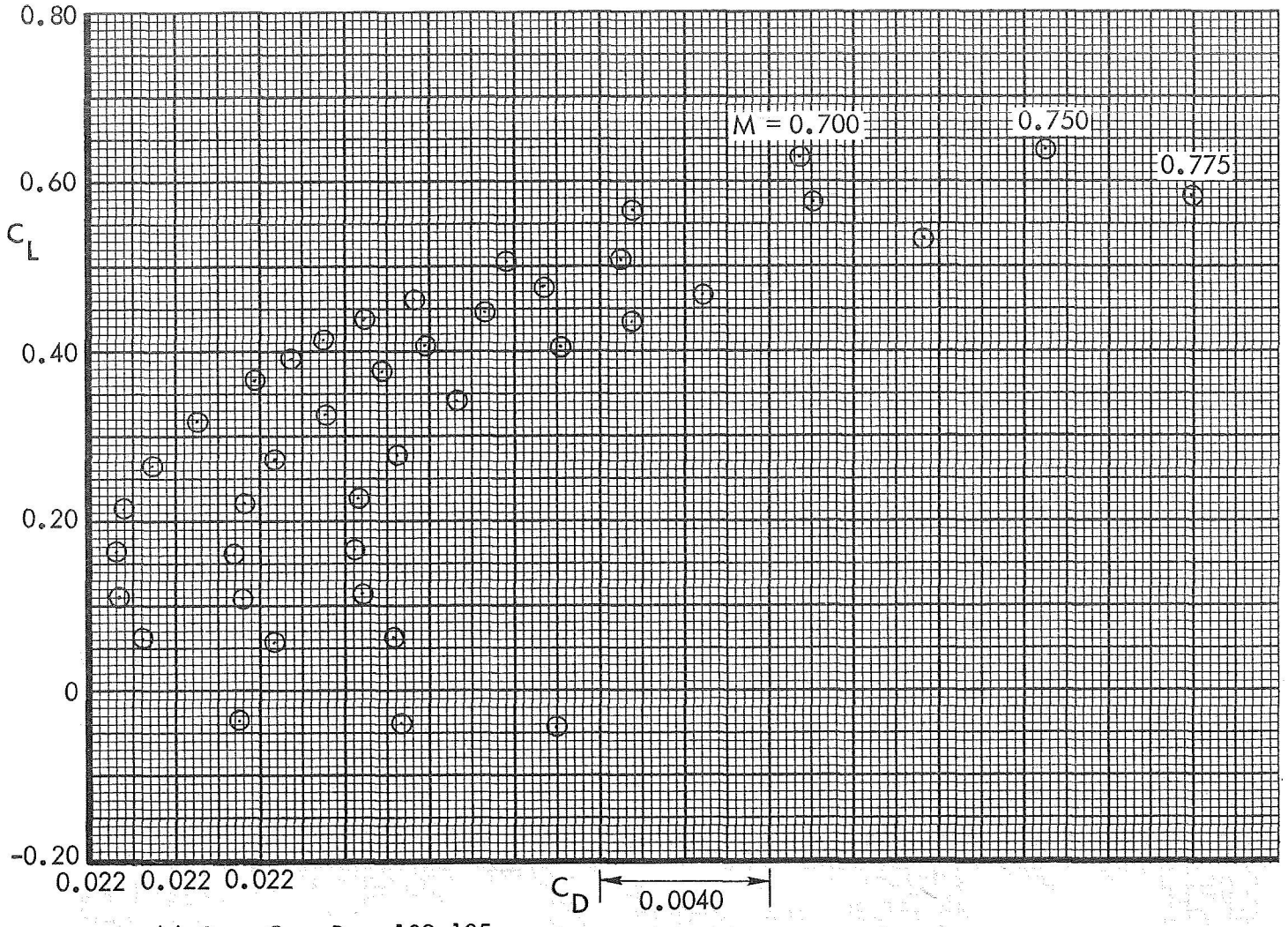
(a) $C_L - \alpha$. Runs 100-105.

Figure 36. Basic Aerodynamic Data. Aft Located Transition. $i_H = 0$. Test 617.



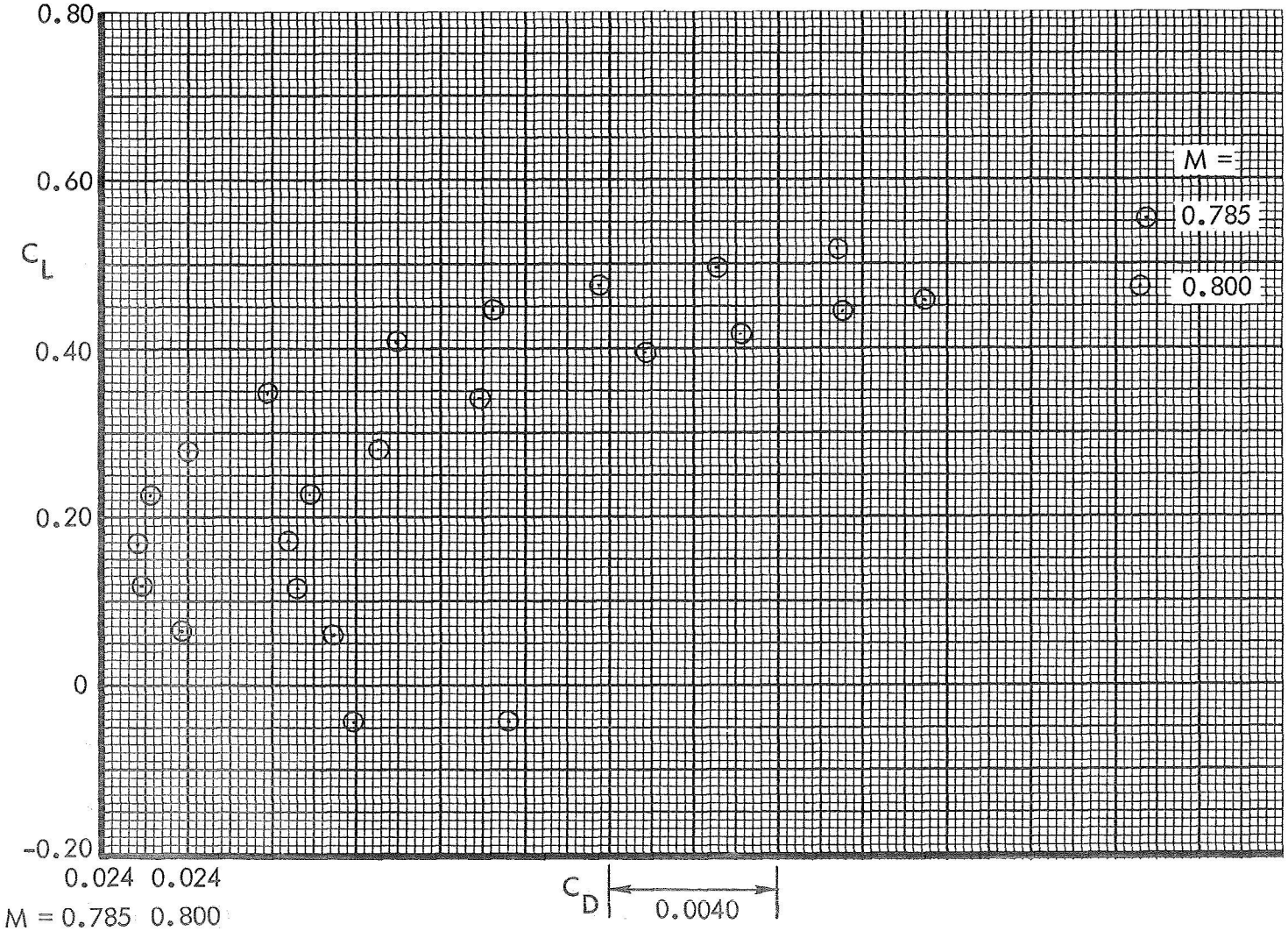
(b) $C_M - C_L$. Runs 100-105.

Figure 36. Continued.



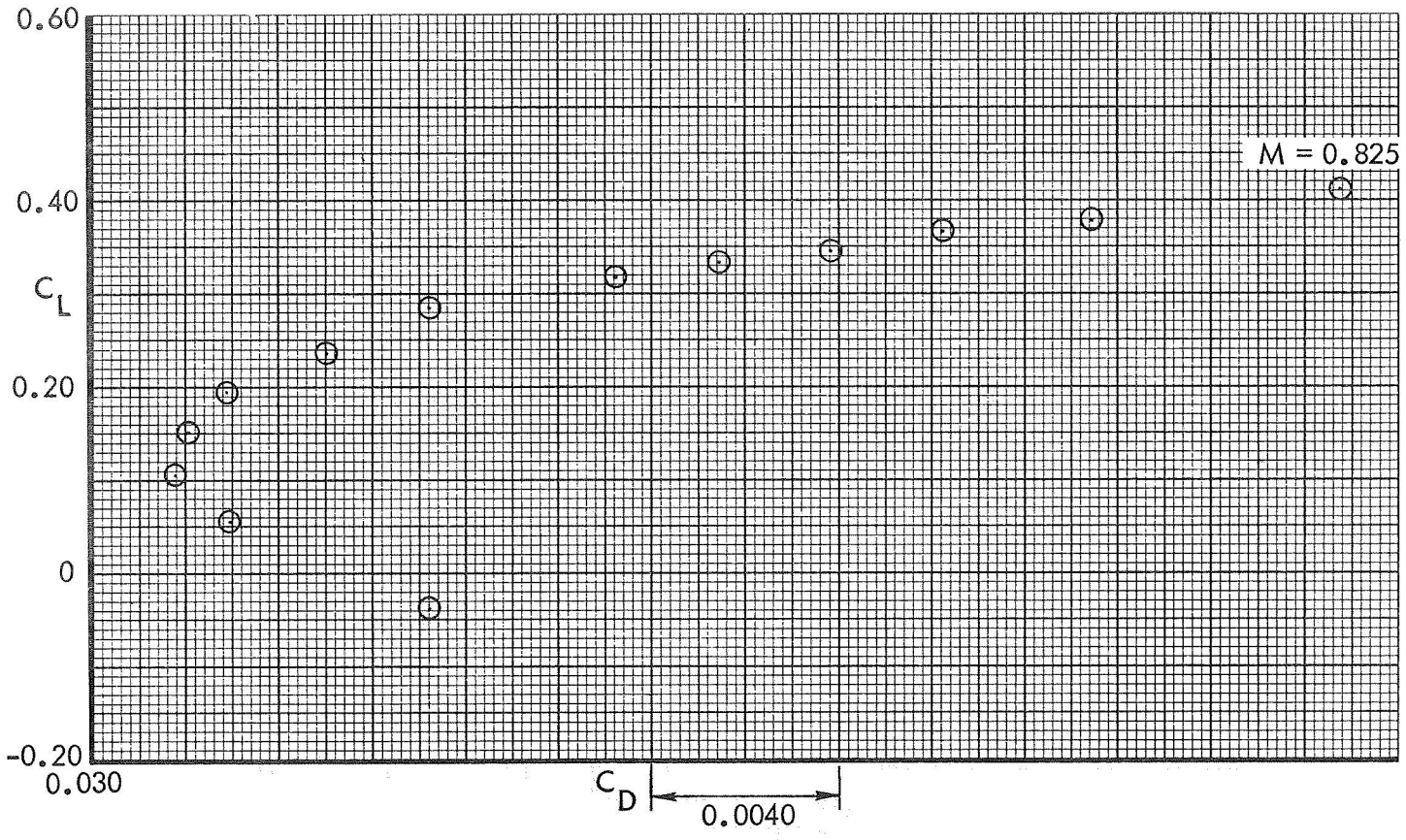
(c) $C_D - C_L$. Runs 103-105.

Figure 36. Continued.



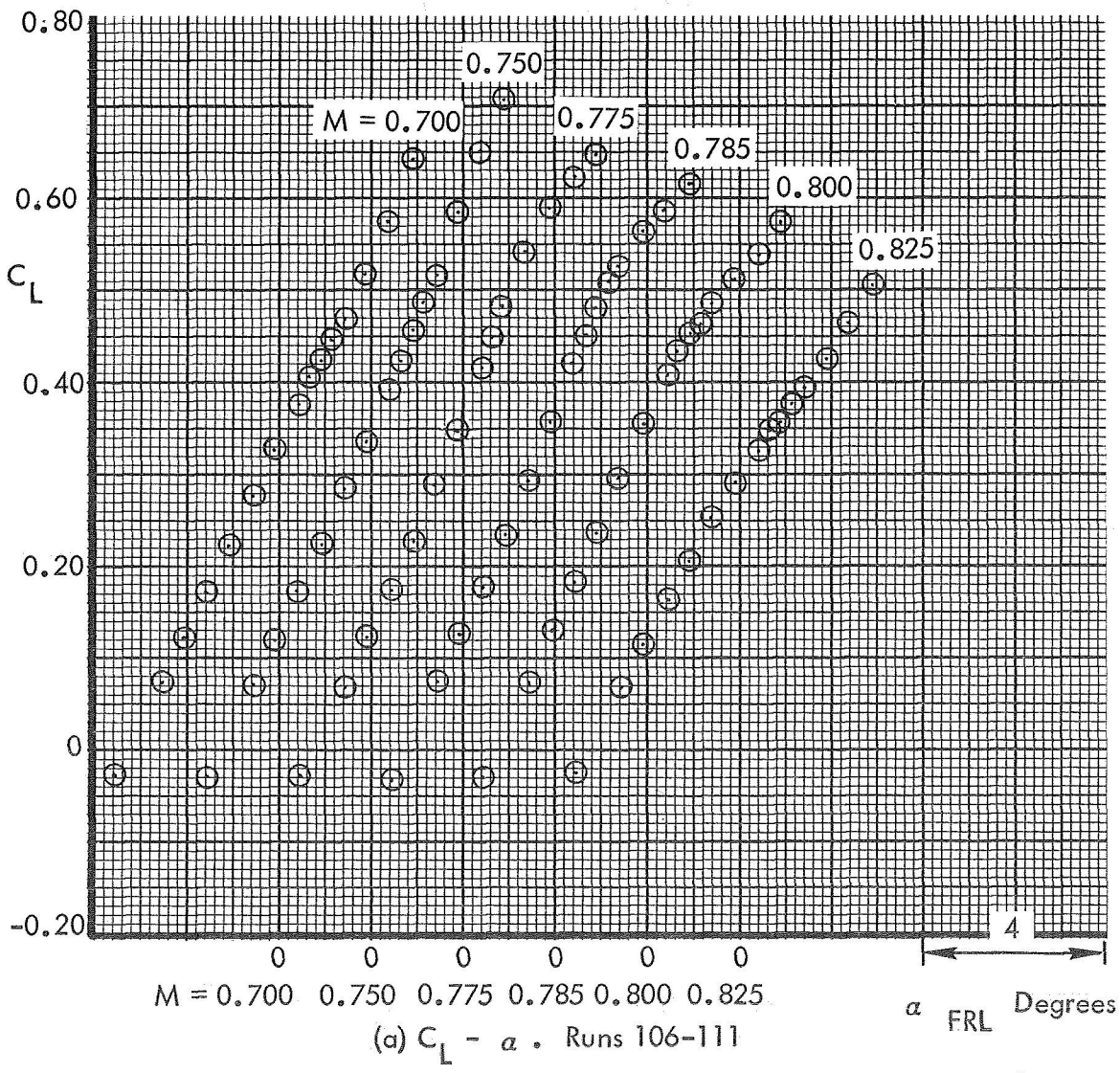
(d) $C_D - C_L$. Runs 101, 102.

Figure 36. Continued.



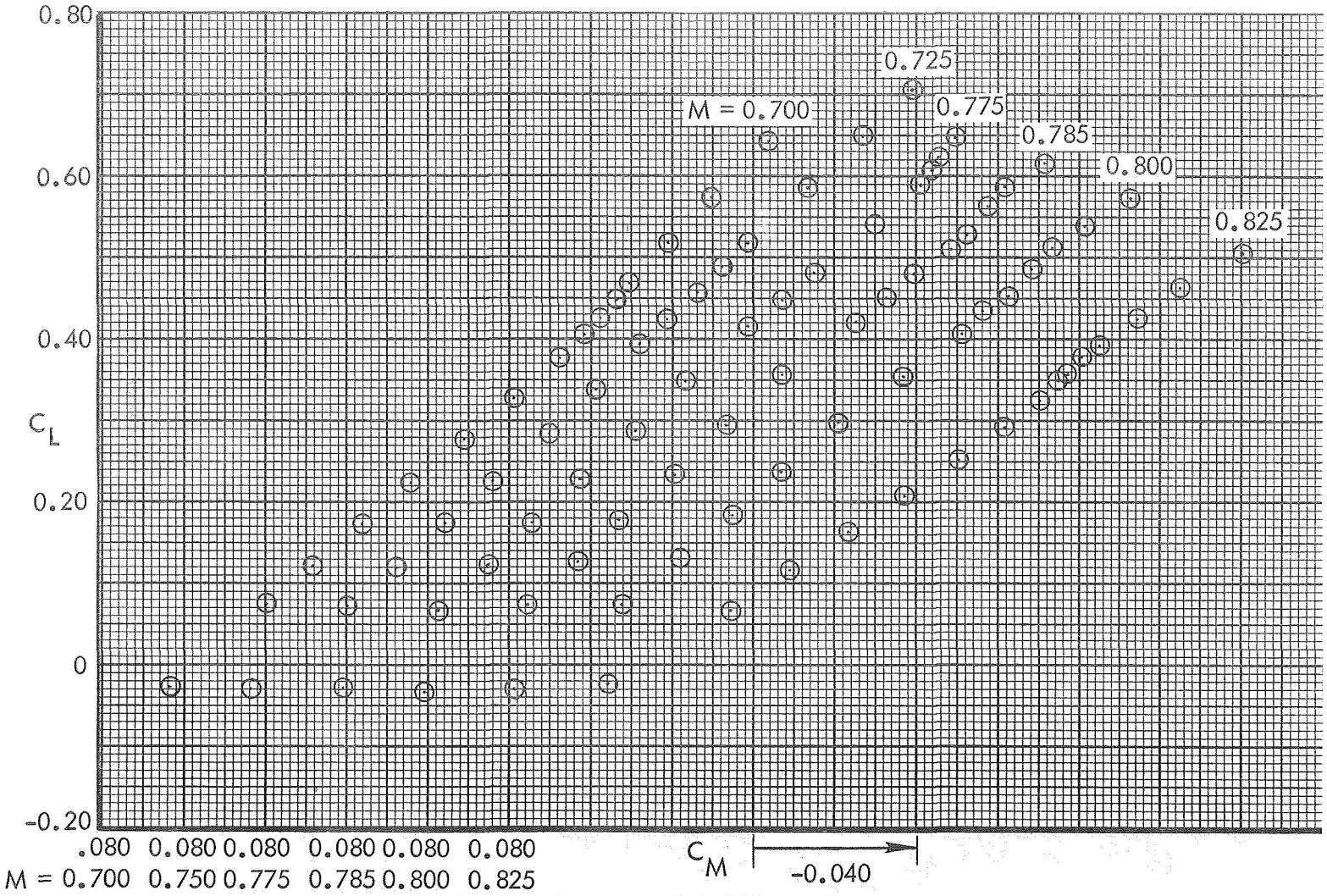
(e) $C_D - C_L$. Run 100.

Figure 36. Concluded.



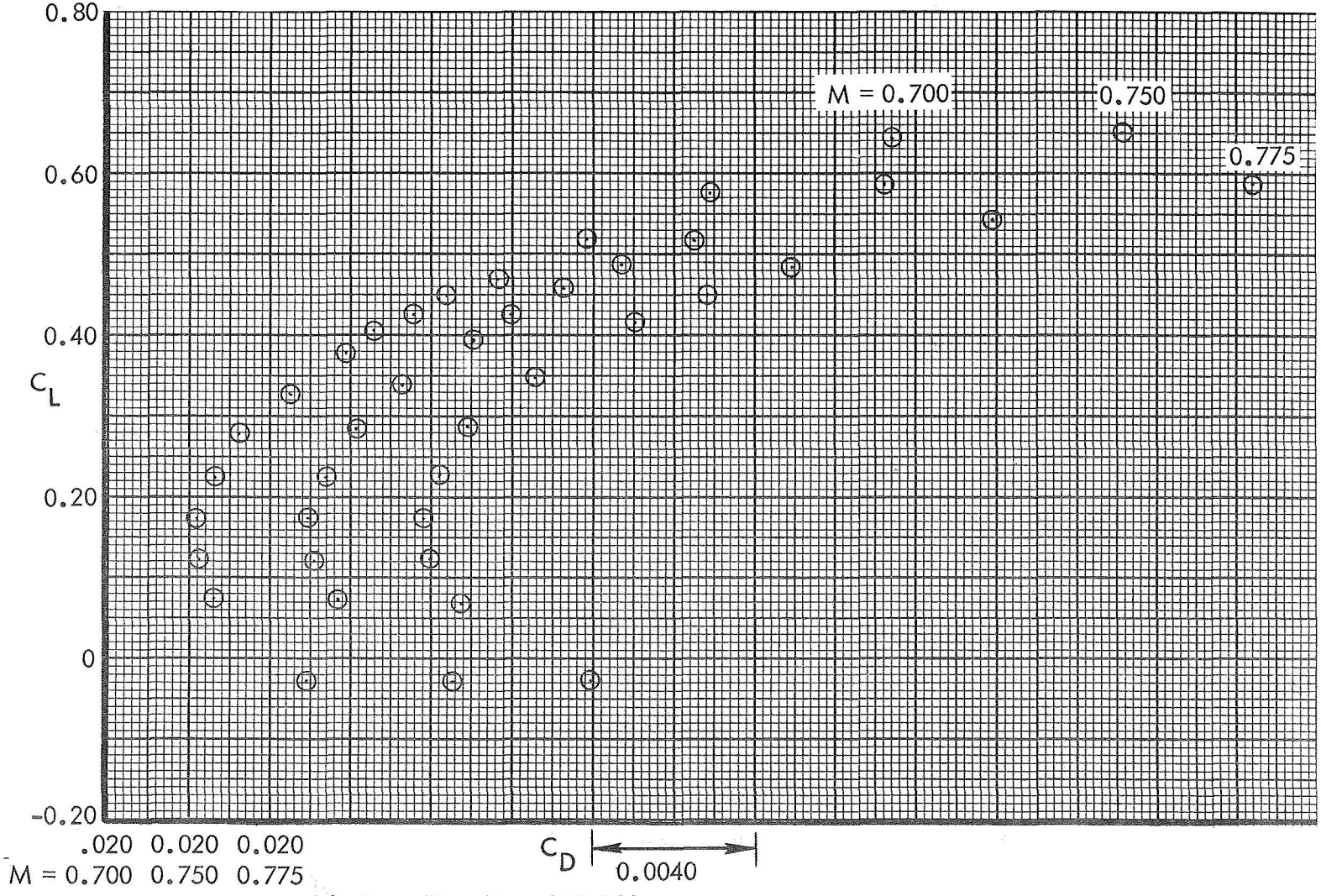
(a) $C_L - \alpha$. Runs 106-111

Figure 37. Basic Aerodynamic Data. Aft Located Transition, $i_H = +1^\circ$. Test 617.



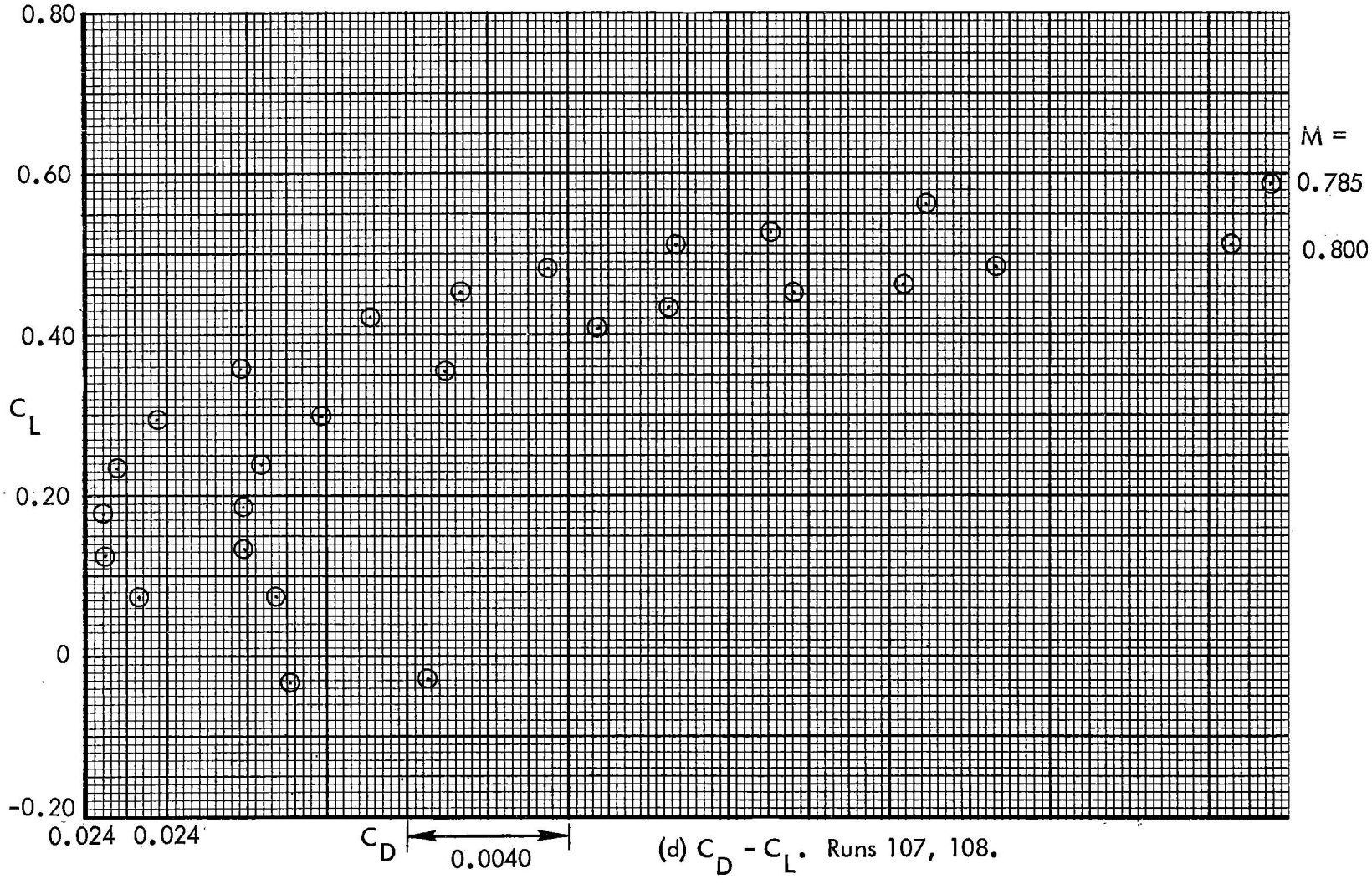
(b) $C_M - C_L$. Runs 106-111.

Figure 37. Continued.



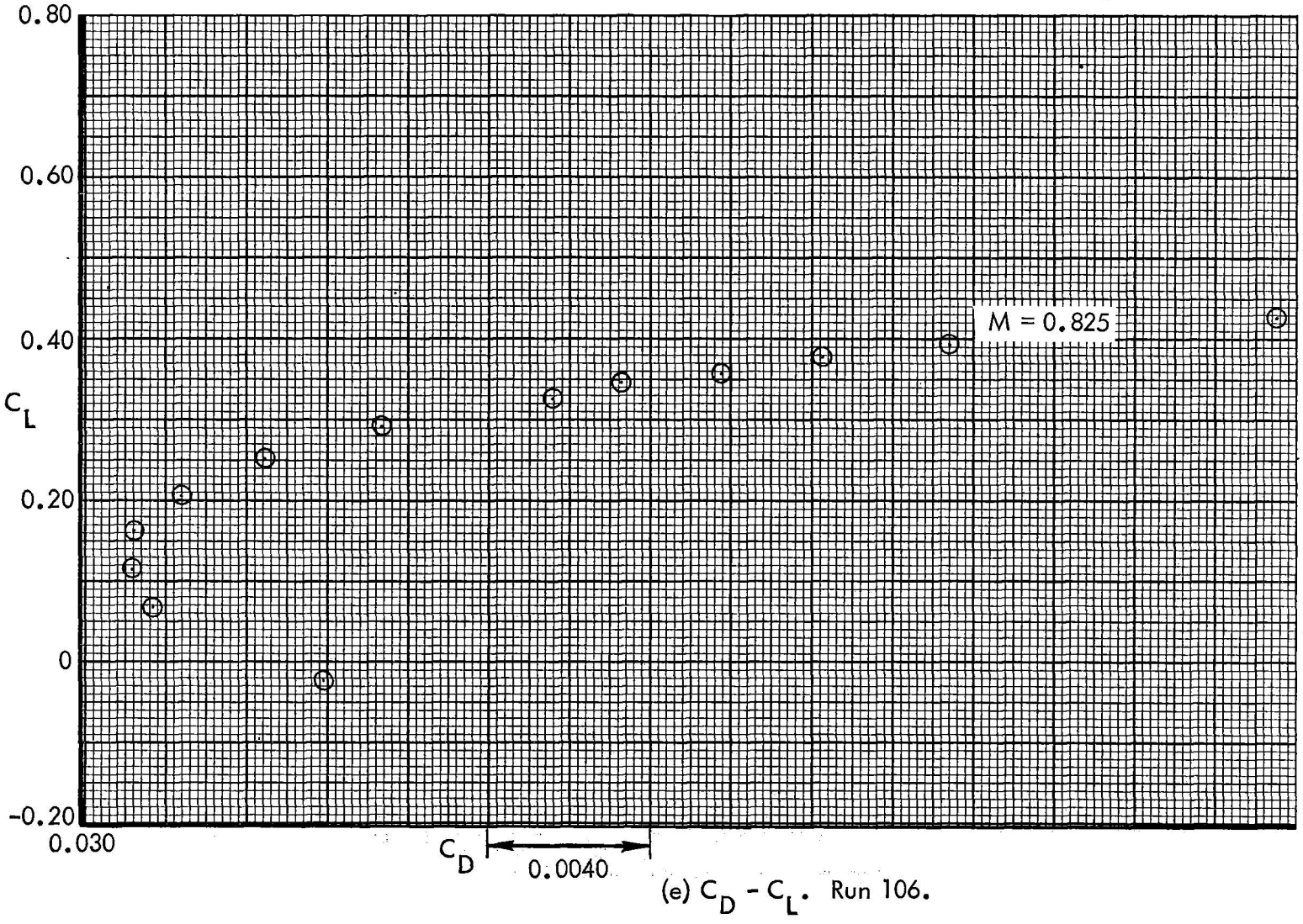
(c) $C_D - C_L$. Runs 109-111.

Figure 37. Continued.



(d) $C_D - C_L$. Runs 107, 108.

Figure 37. Continued.



(e) $C_D - C_L$. Run 106.

Figure 37. Concluded.

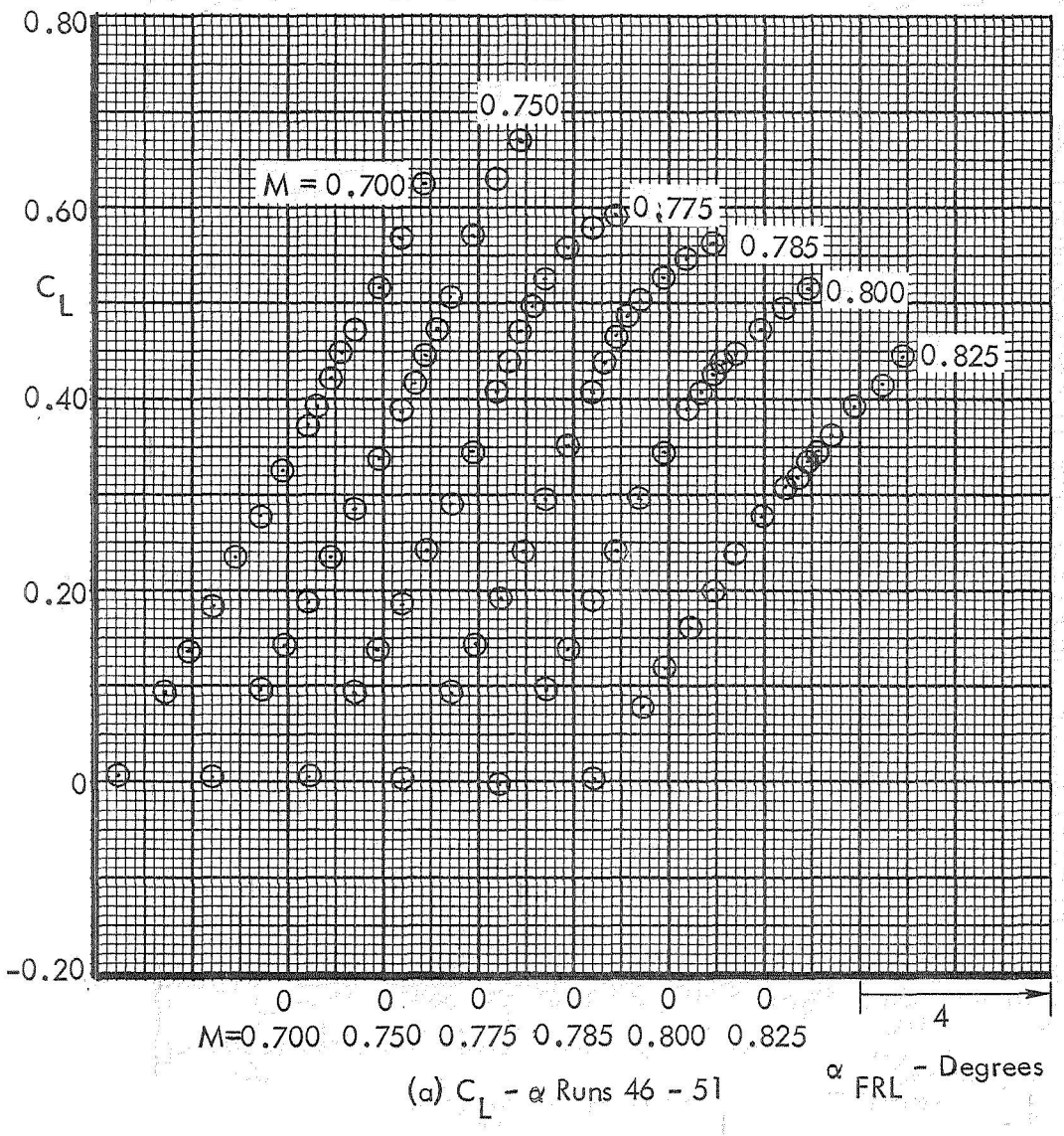


Figure 38. Basic Aerodynamic Data. Tail-Off Test 617
Sting Configuration 2.

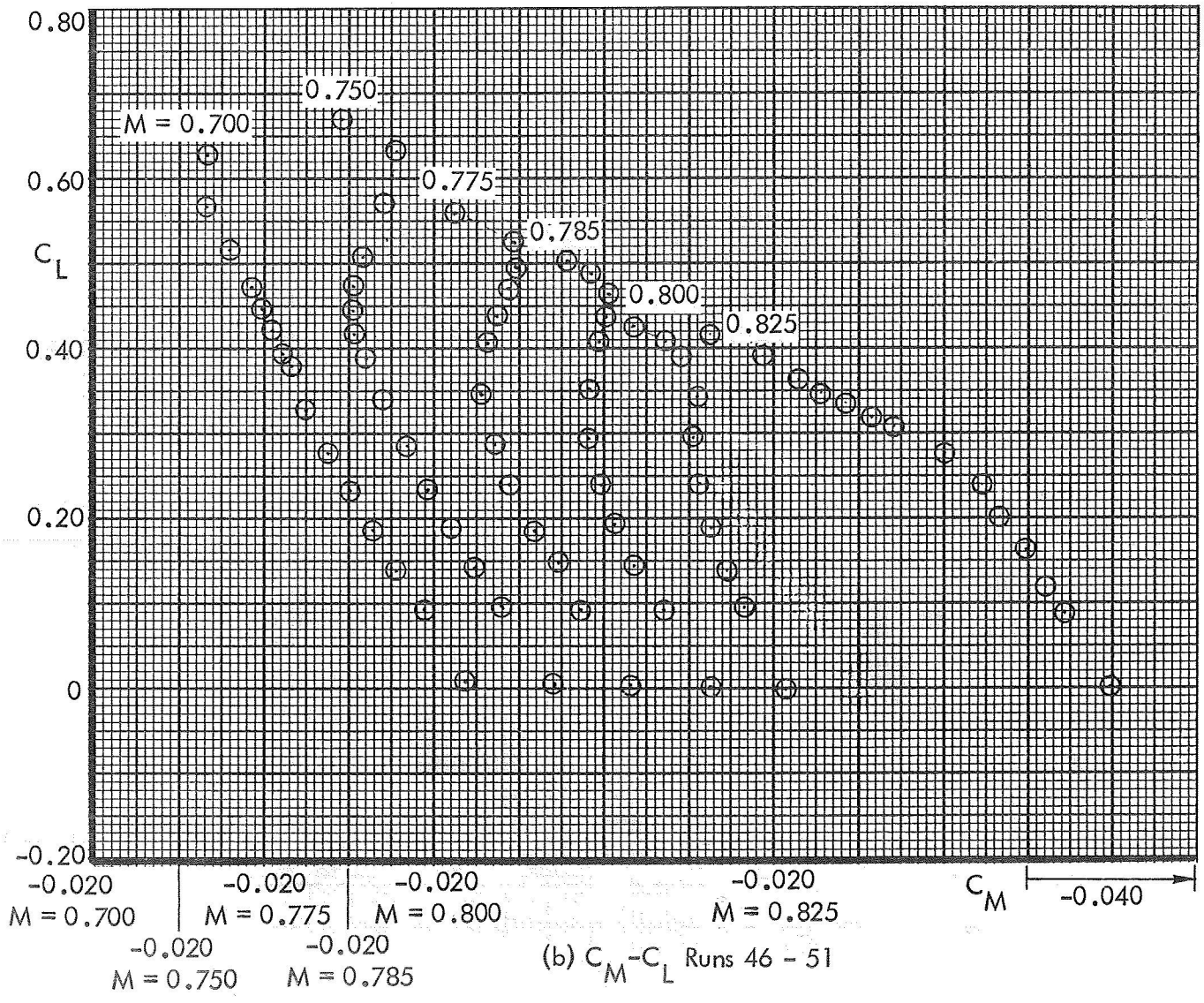
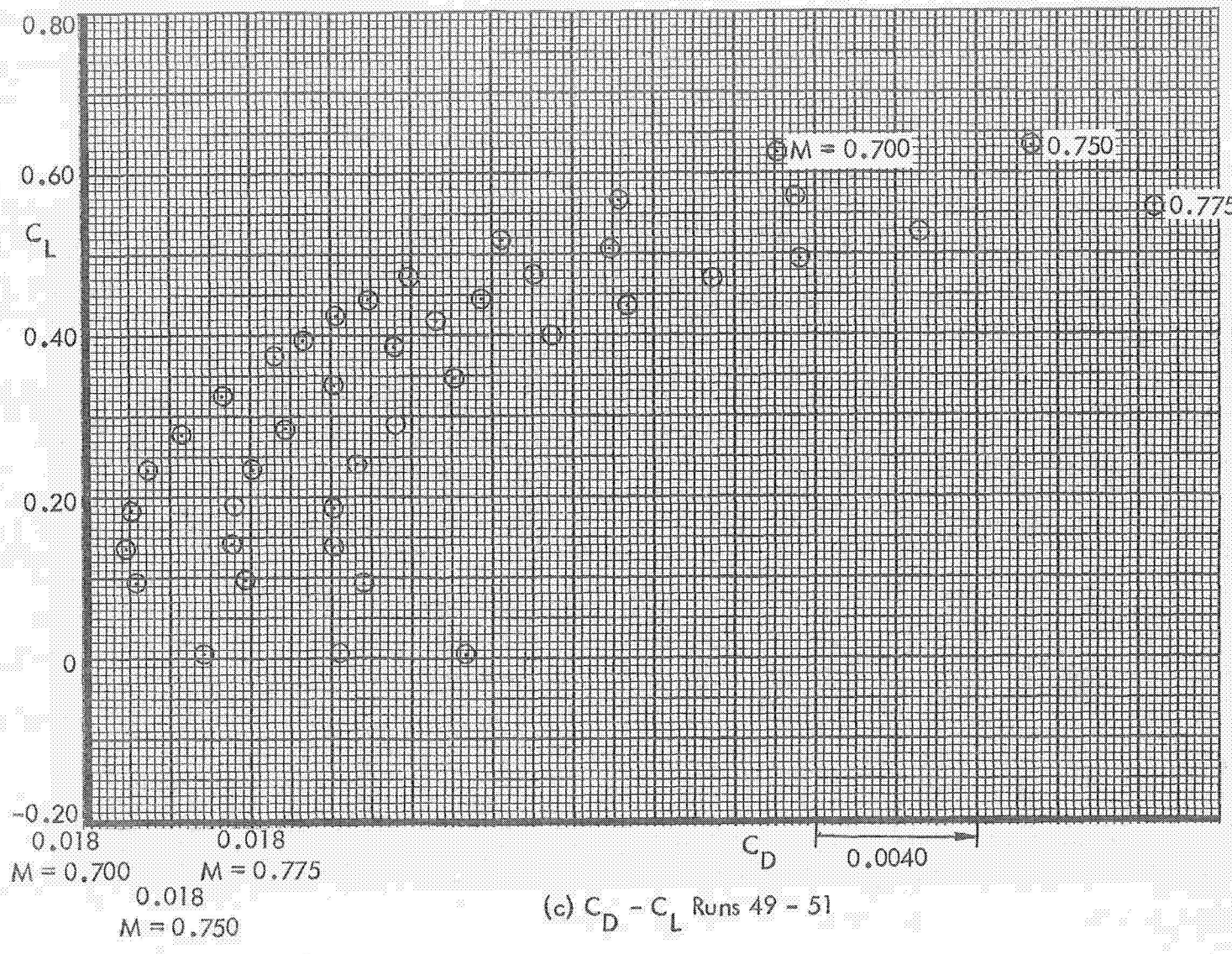
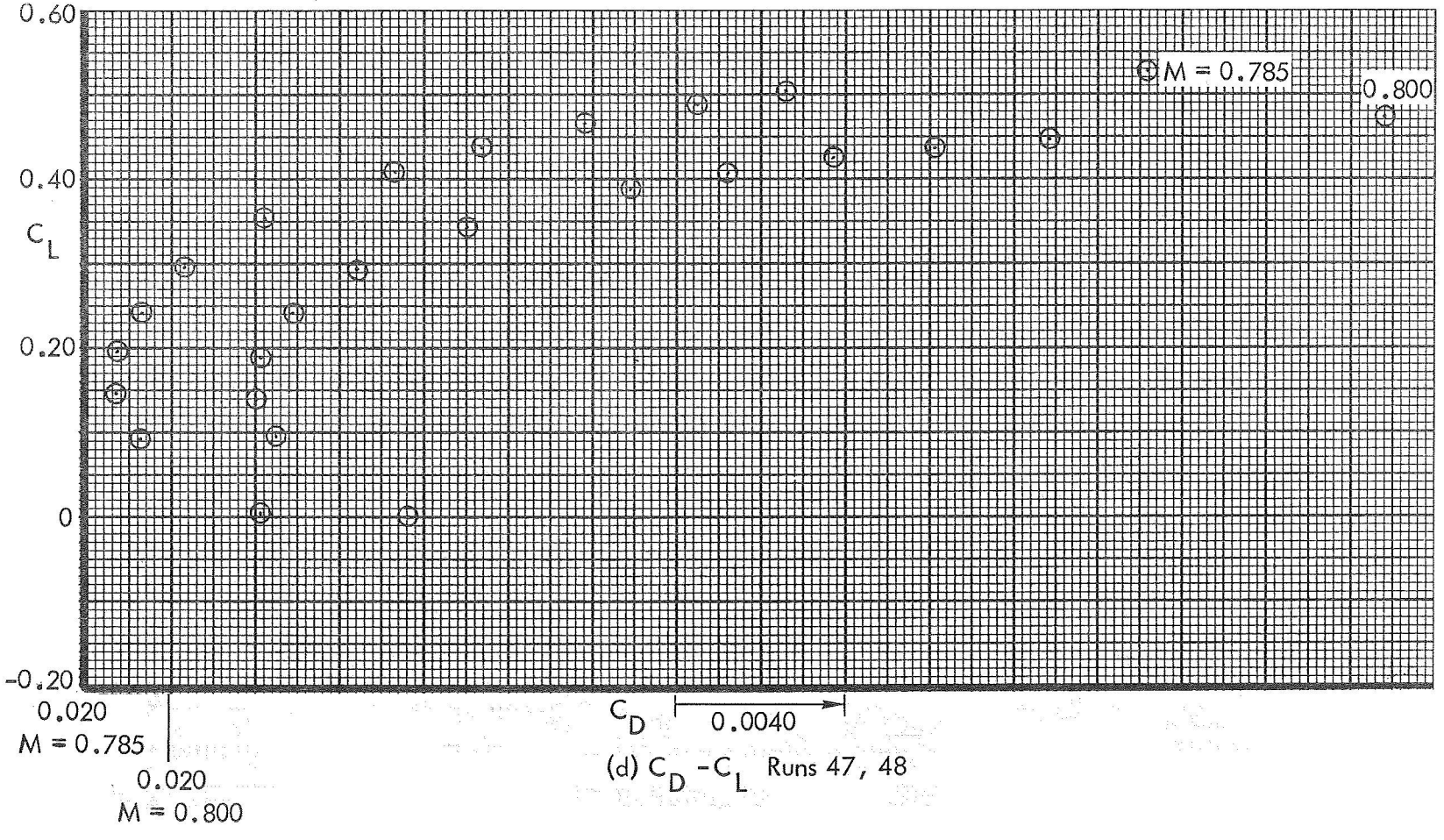


Figure 38. Continued



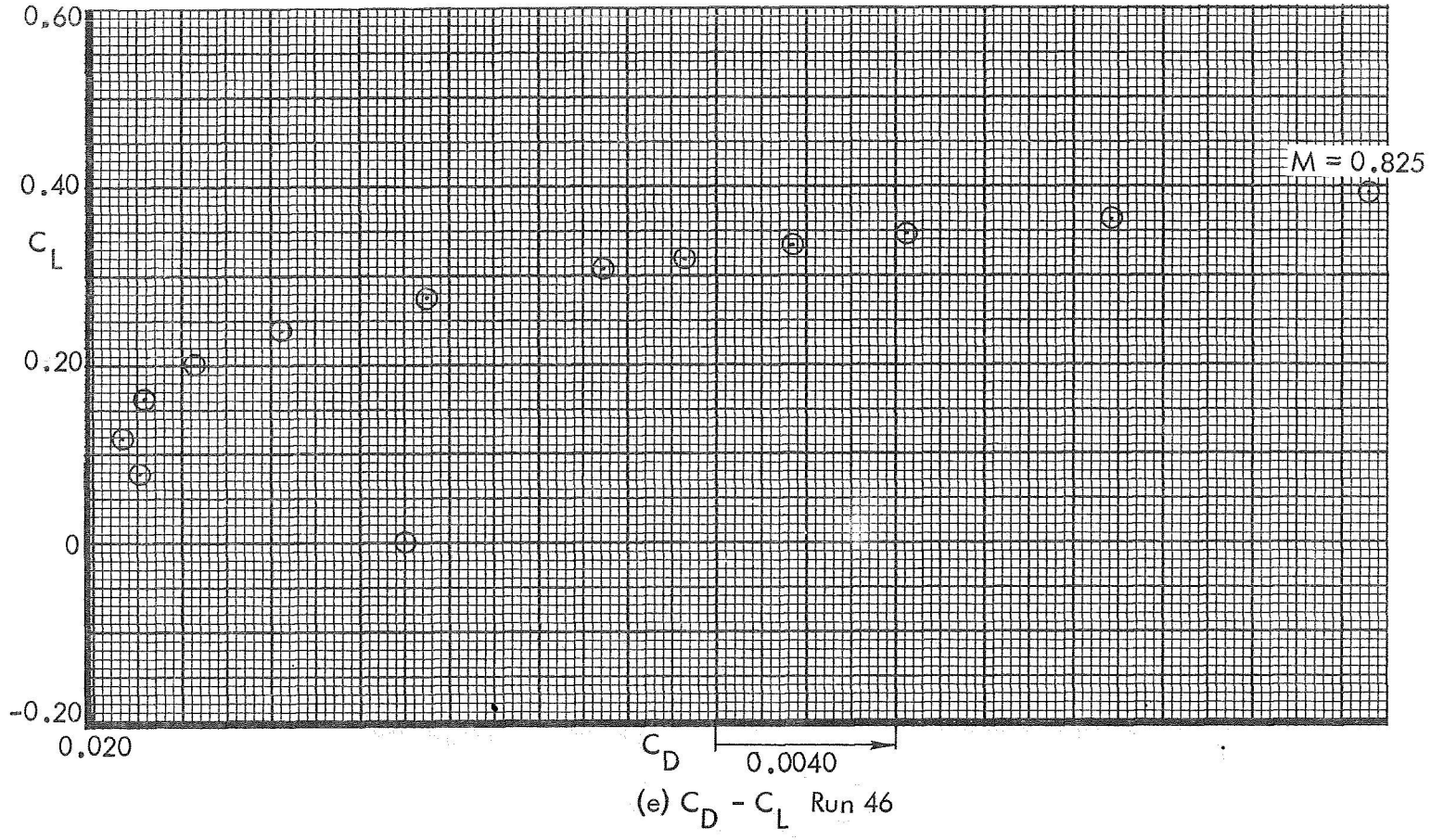
(c) $C_D - C_L$ Runs 49 - 51

Figure 38. Continued



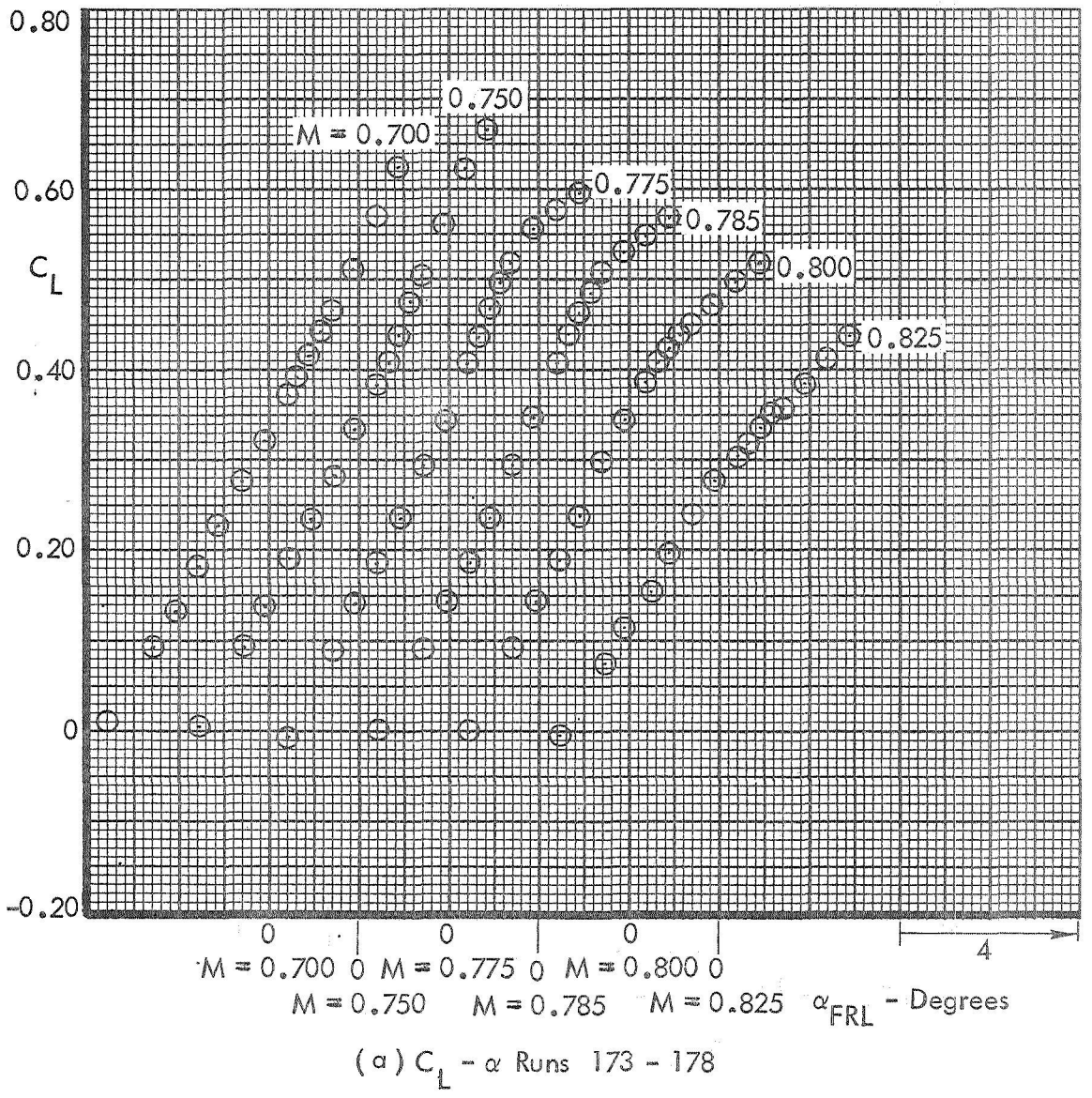
(d) C_D - C_L Runs 47, 48

Figure 38. Continued



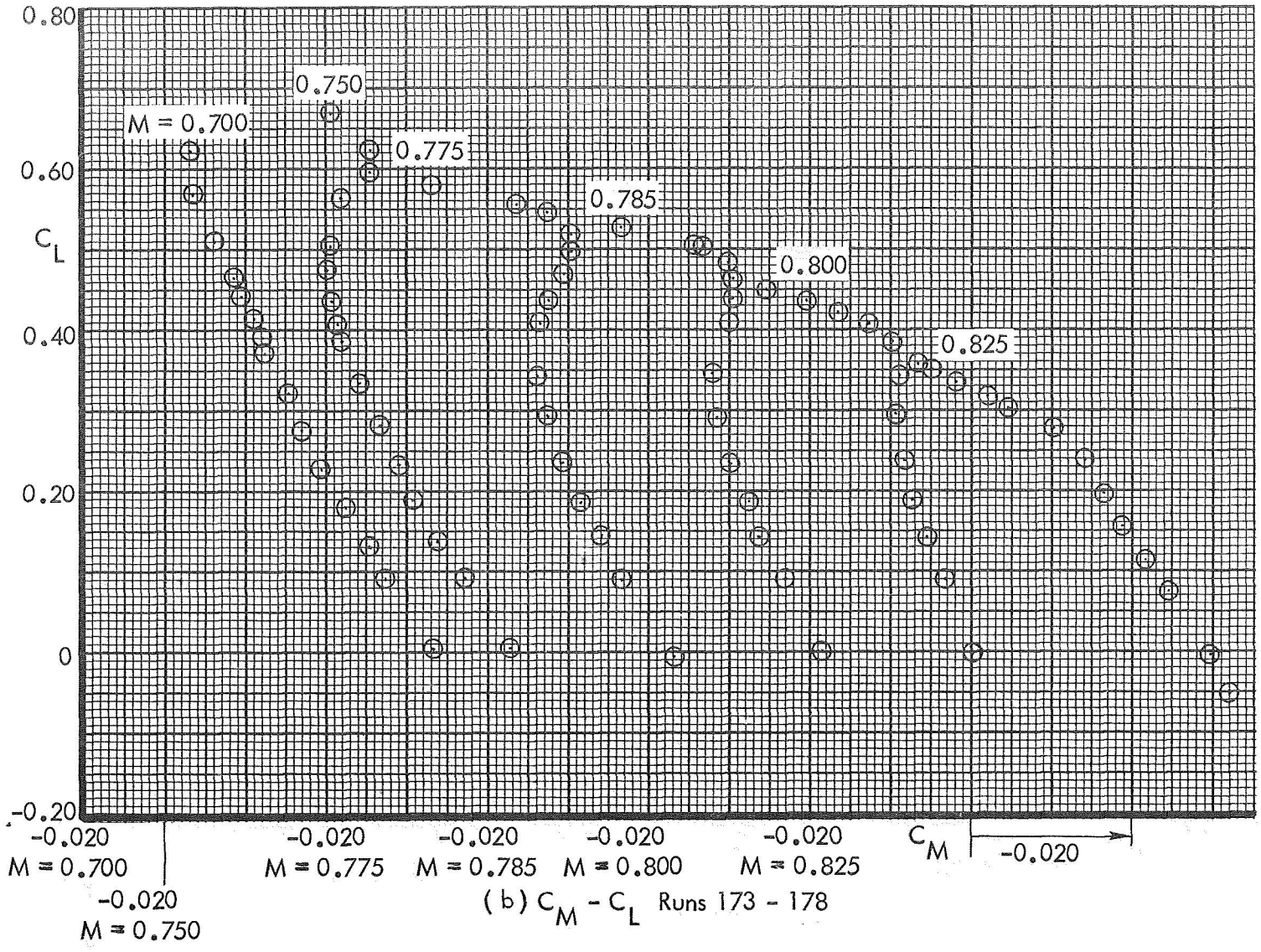
(e) $C_D - C_L$ Run 46

Figure 38. Concluded



(a) C_L - α Runs 173 - 178

Figure 39. Basic Aerodynamic Data. Tail-Off
Sting Configuration 1 Test 617



(b) $C_M - C_L$ Runs 173 - 178

Figure 39. Continued

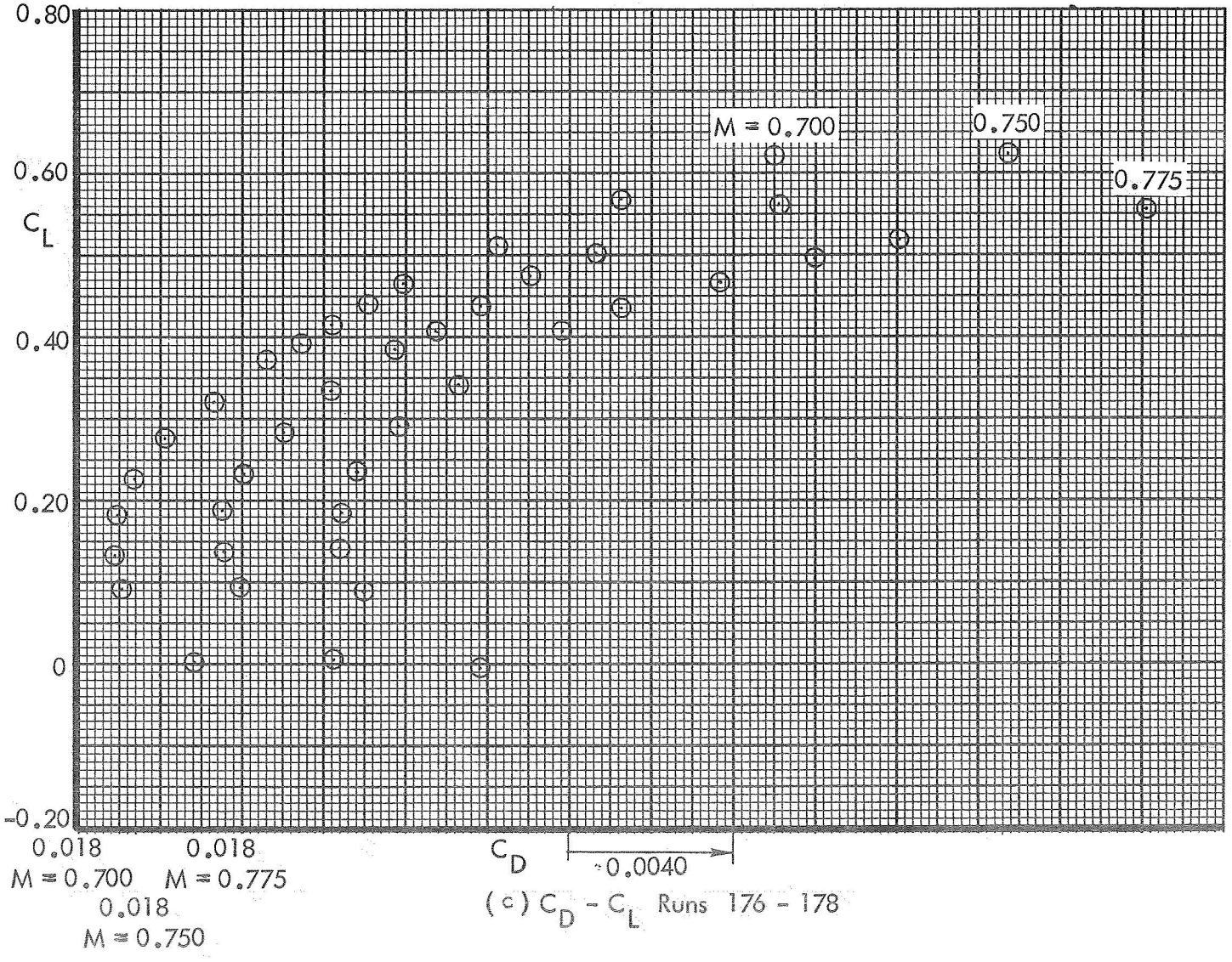
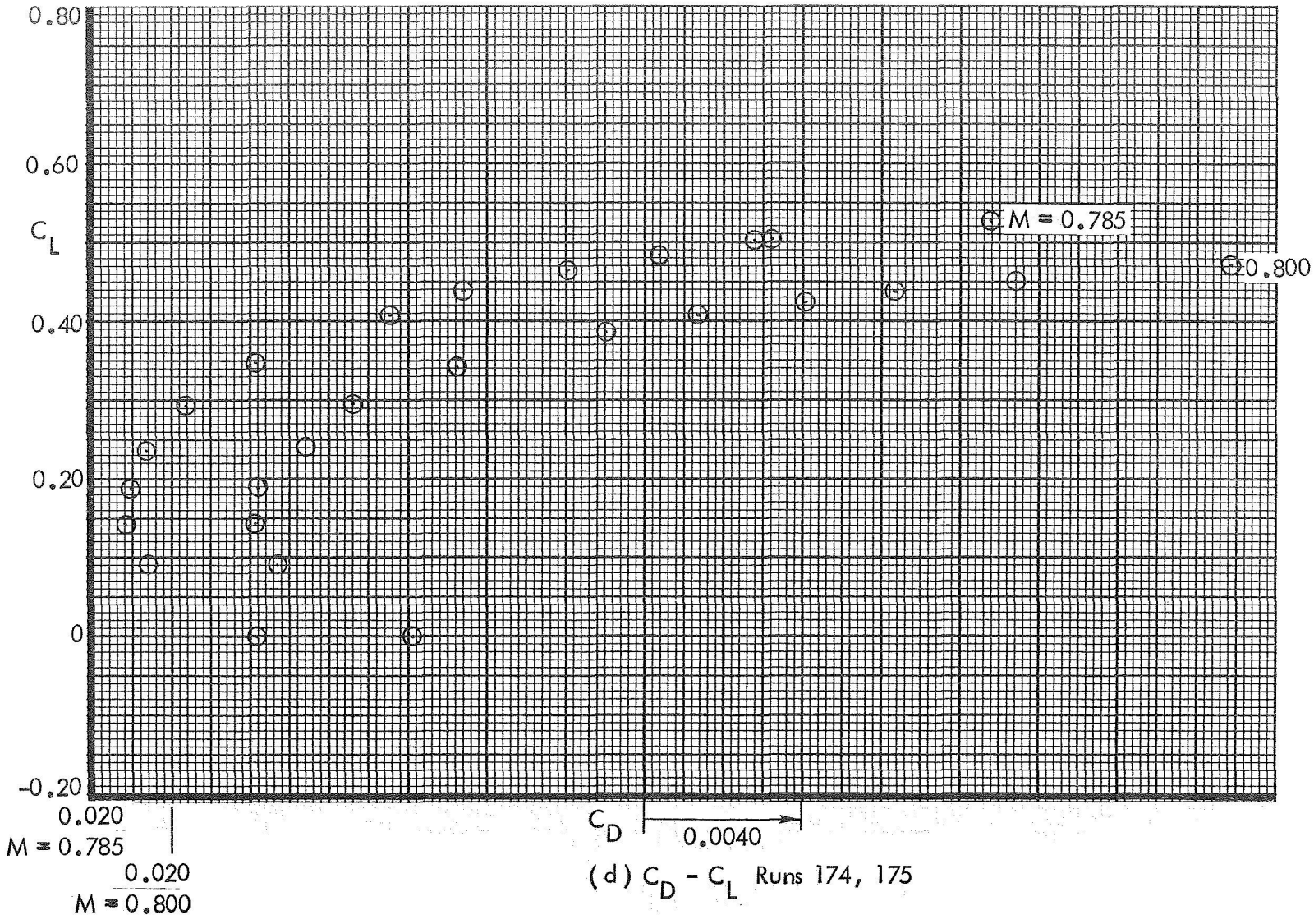
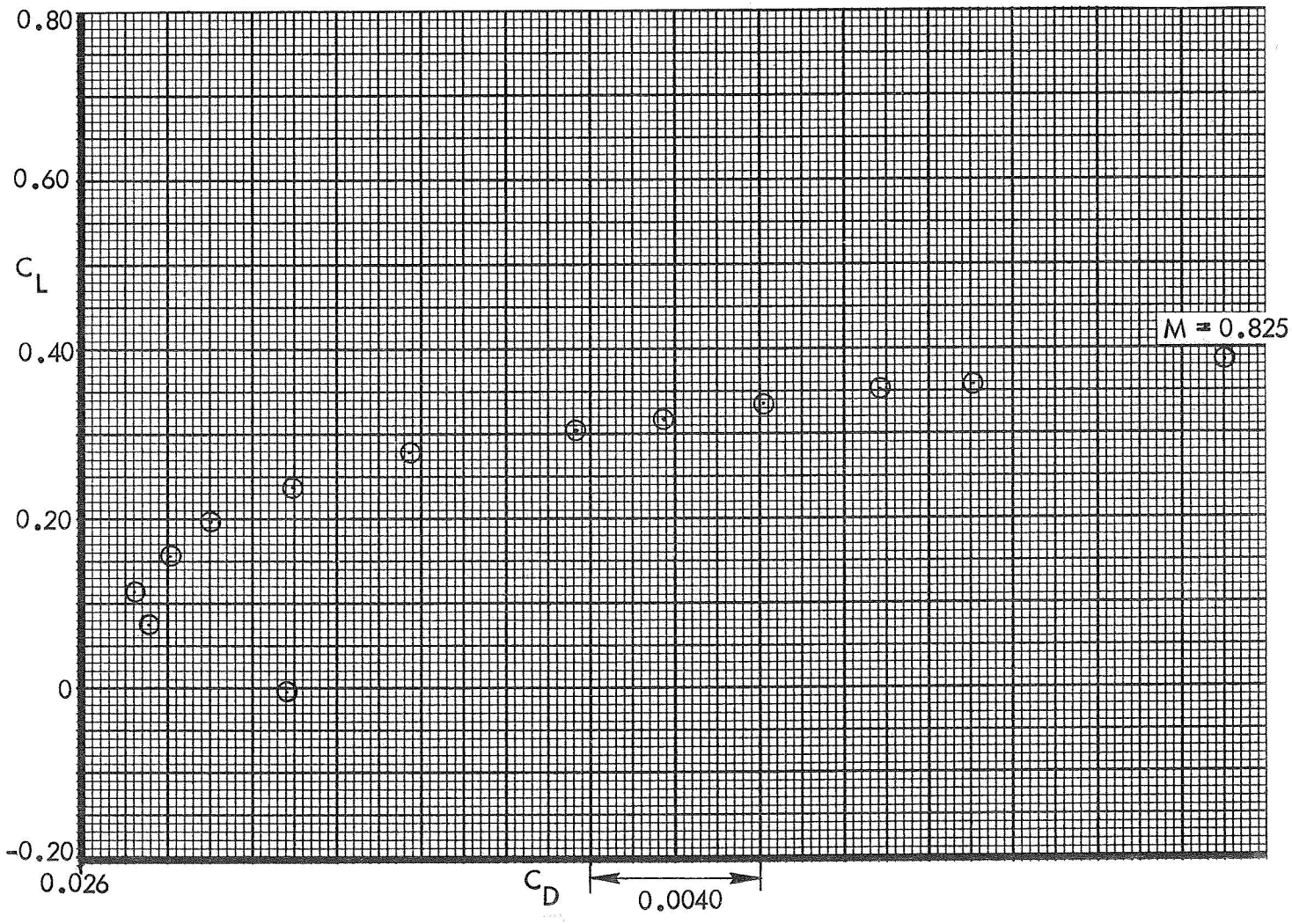


Figure 39. Continued



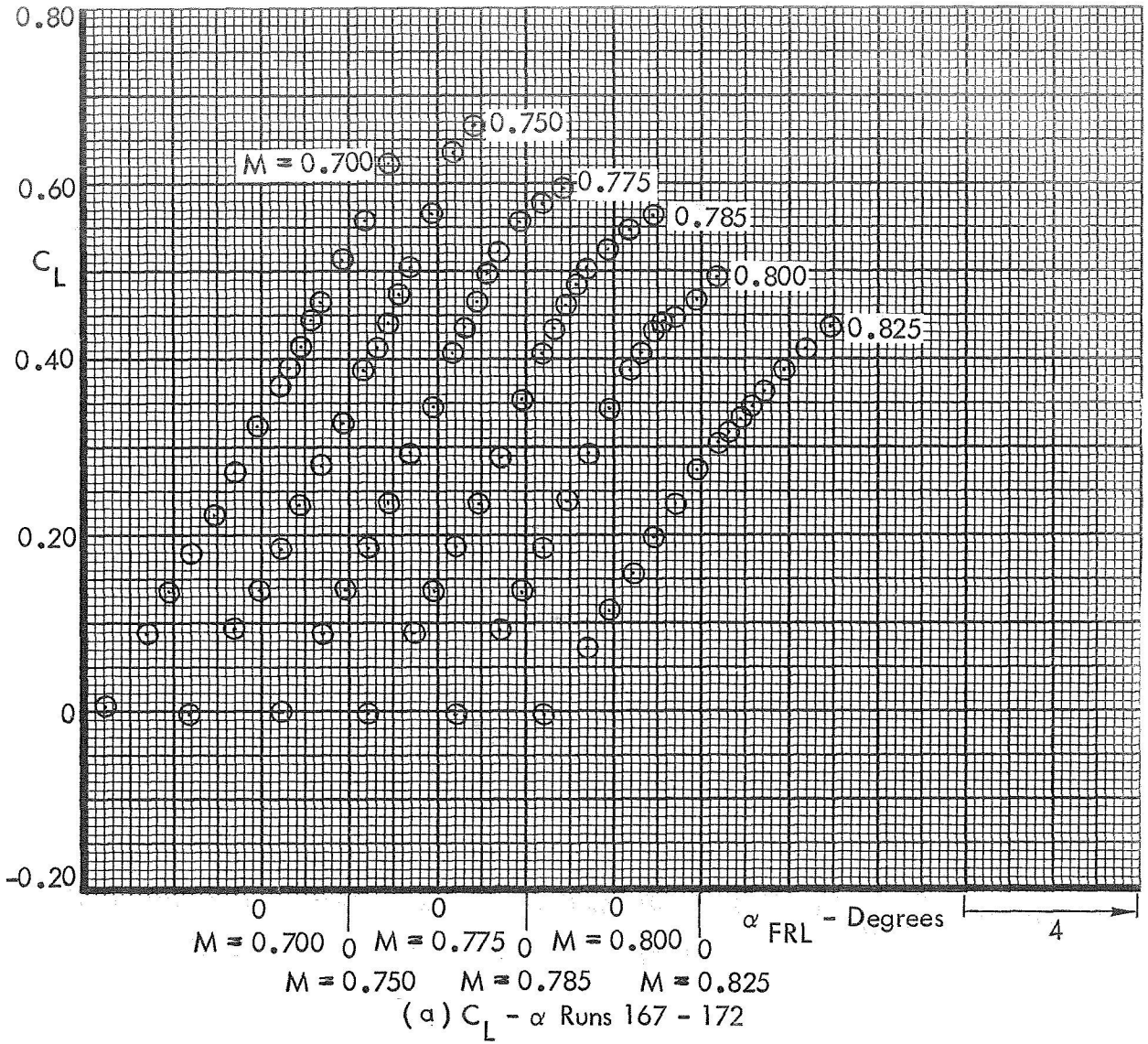
(d) C_D - C_L Runs 174, 175

Figure 39. Continued



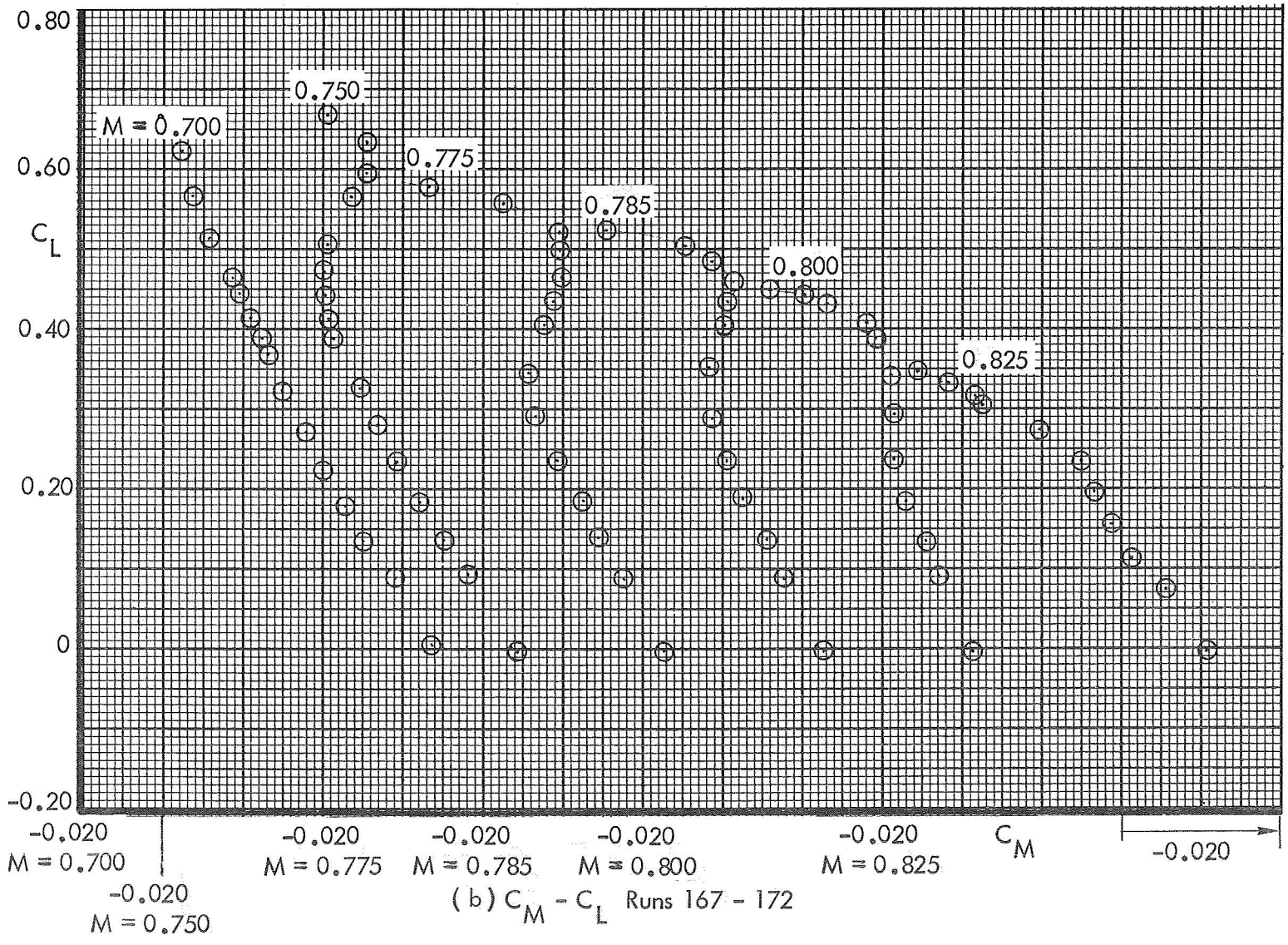
(e) $C_D - C_L$ Run 173

Figure 39. Concluded



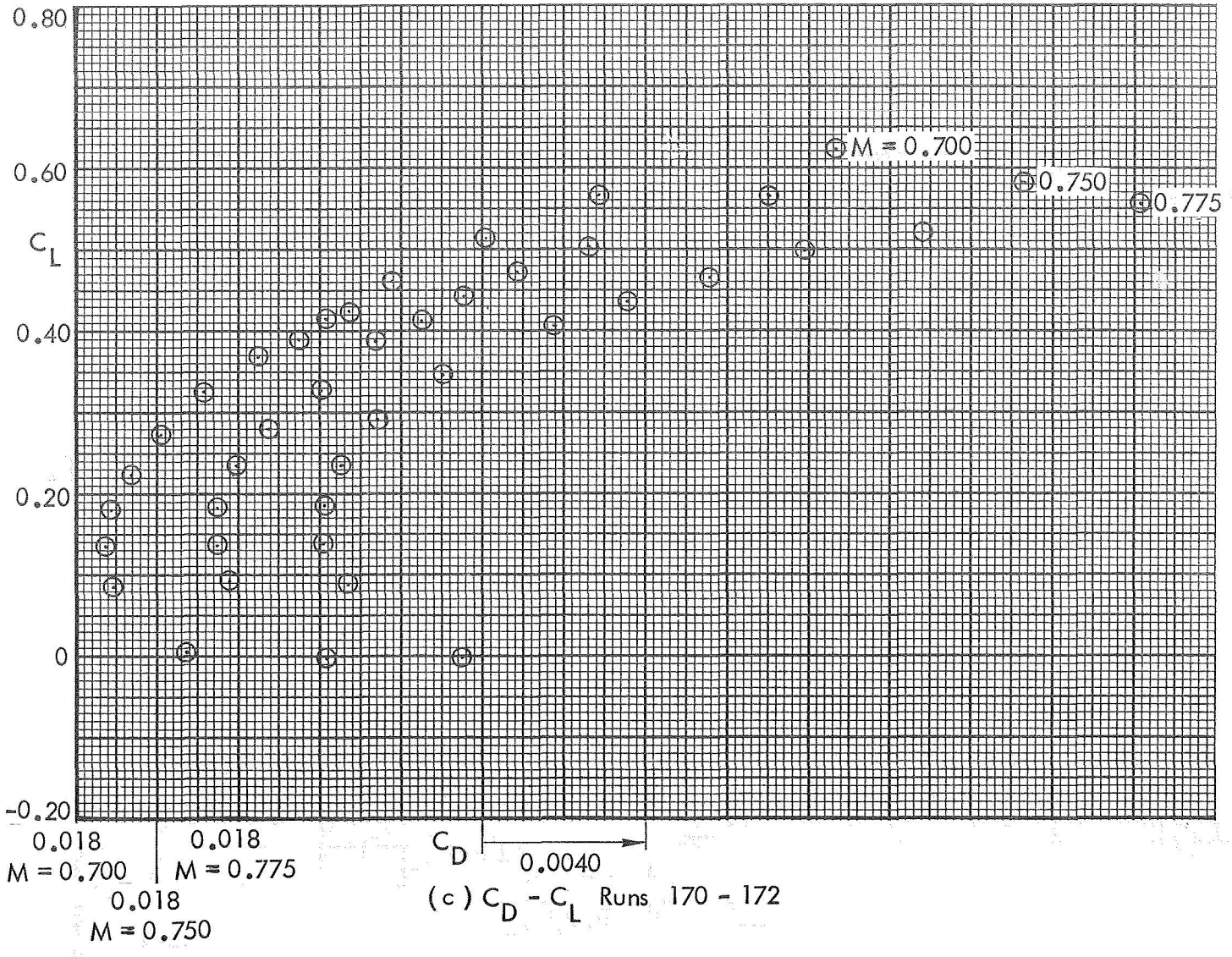
(a) C_L - α Runs 167 - 172

Figure 40. Basic Aerodynamic Data. Tail-Off
Sting Configuration 2. Test 617



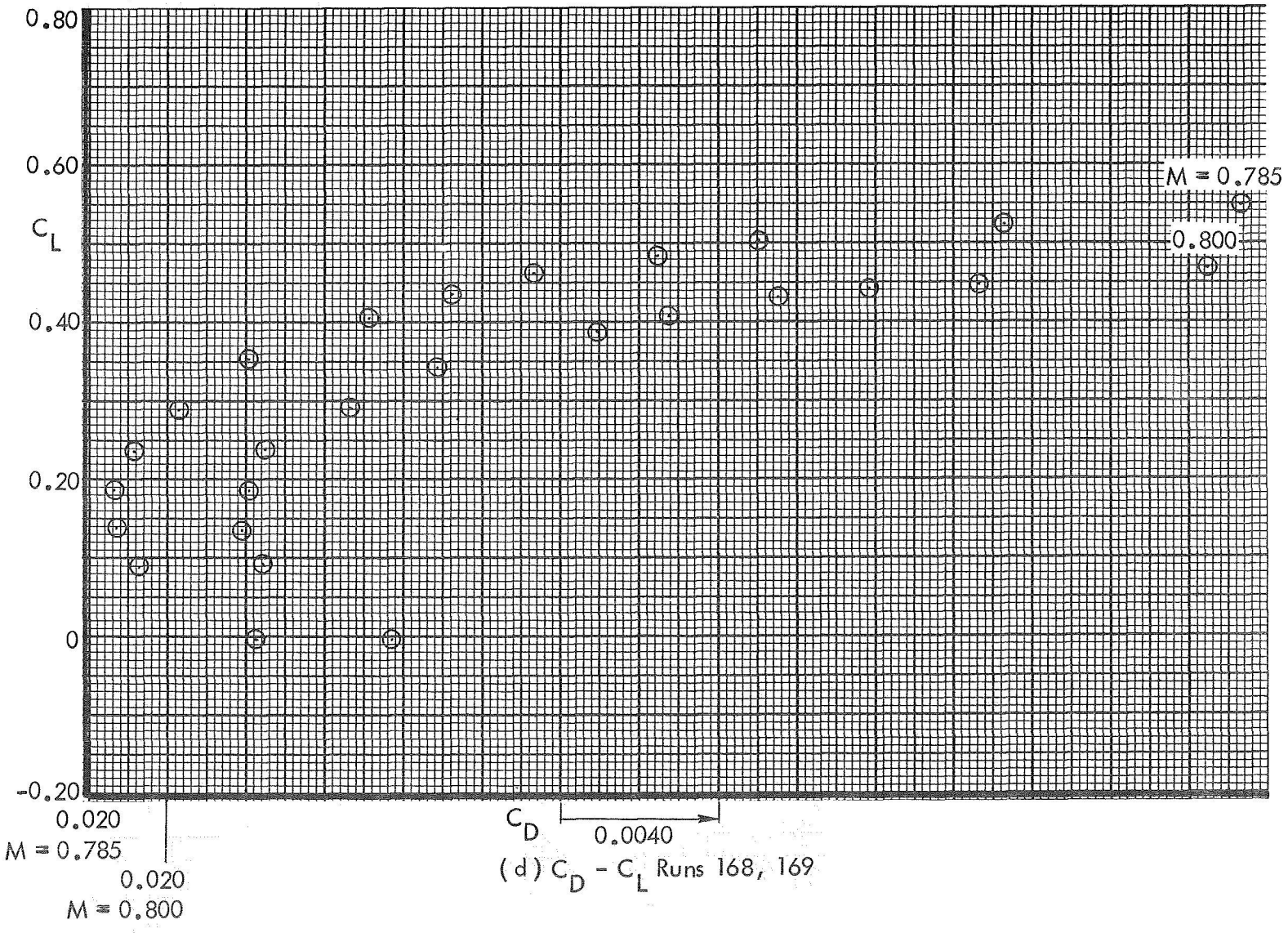
(b) $C_M - C_L$ Runs 167 - 172

Figure 40. Continued



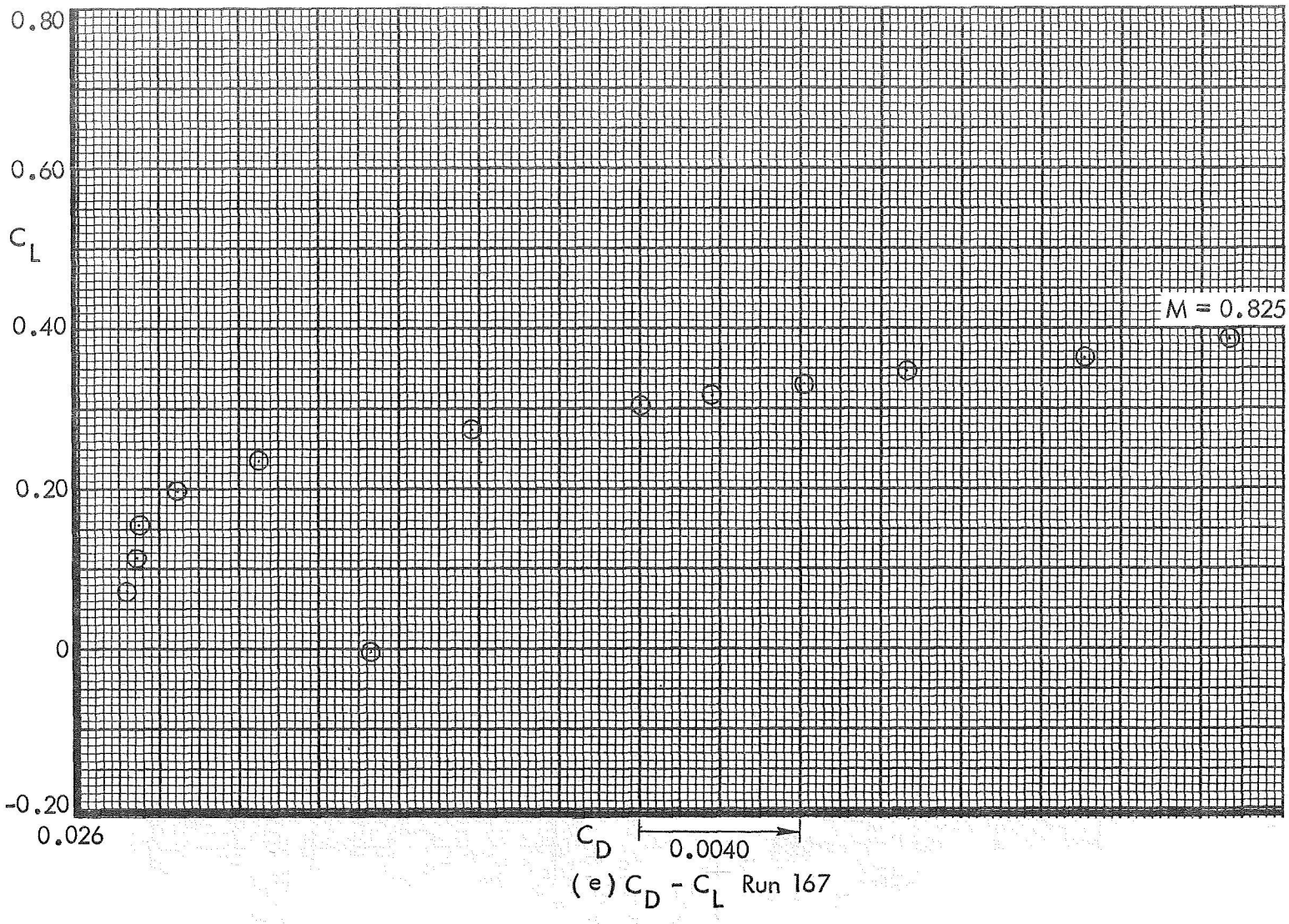
(c) C_D - C_L Runs 170 - 172

Figure 40. Continued



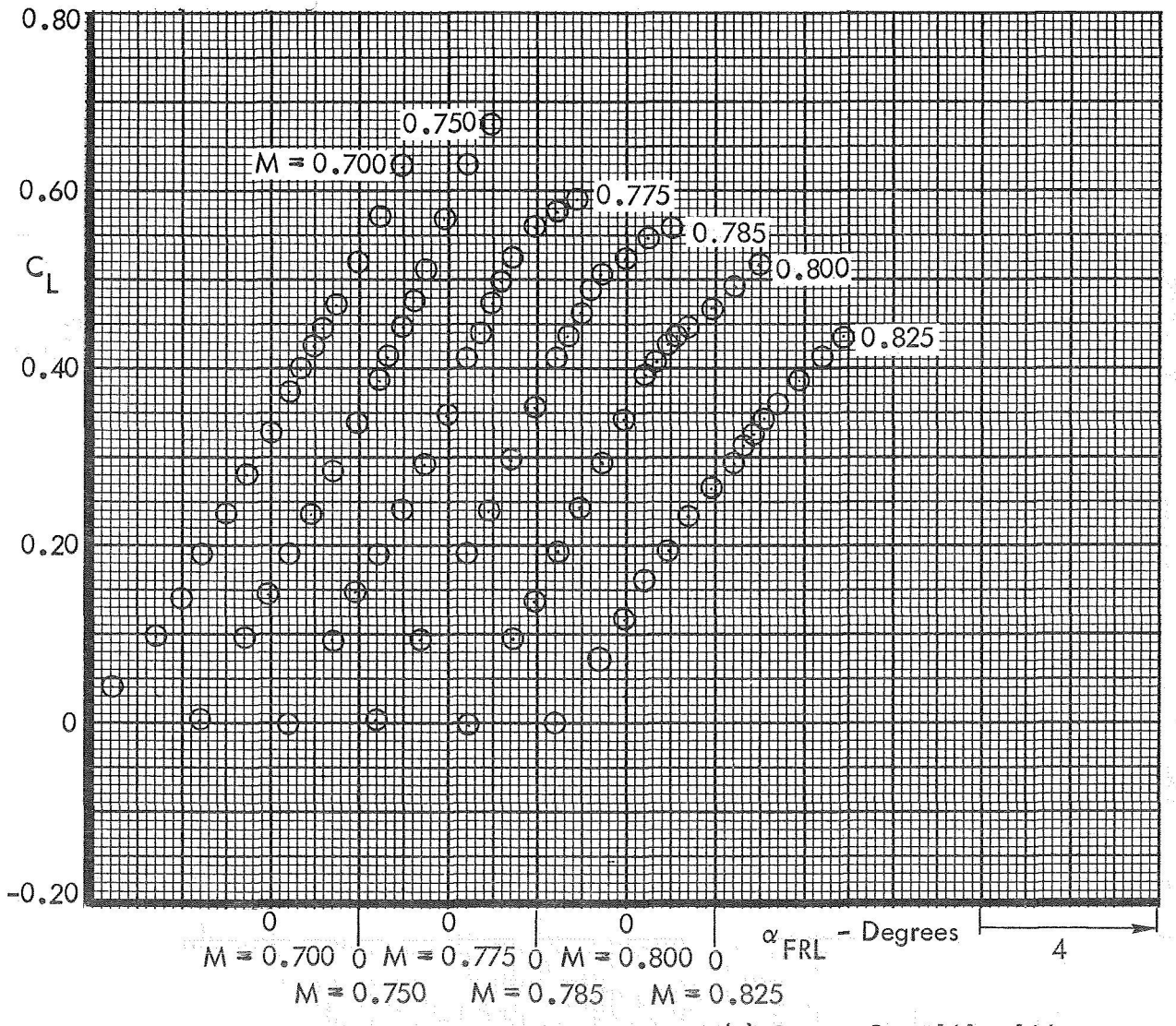
(d) C_D - C_L Runs 168, 169

Figure 40. Continued



(e) C_D - C_L Run 167

Figure 40. Concluded



(a) $C_L - \alpha$ Runs 161 - 166

Figure 41. Basic Aerodynamic Data. Tail-Off Sting Configuration 3. Test 617

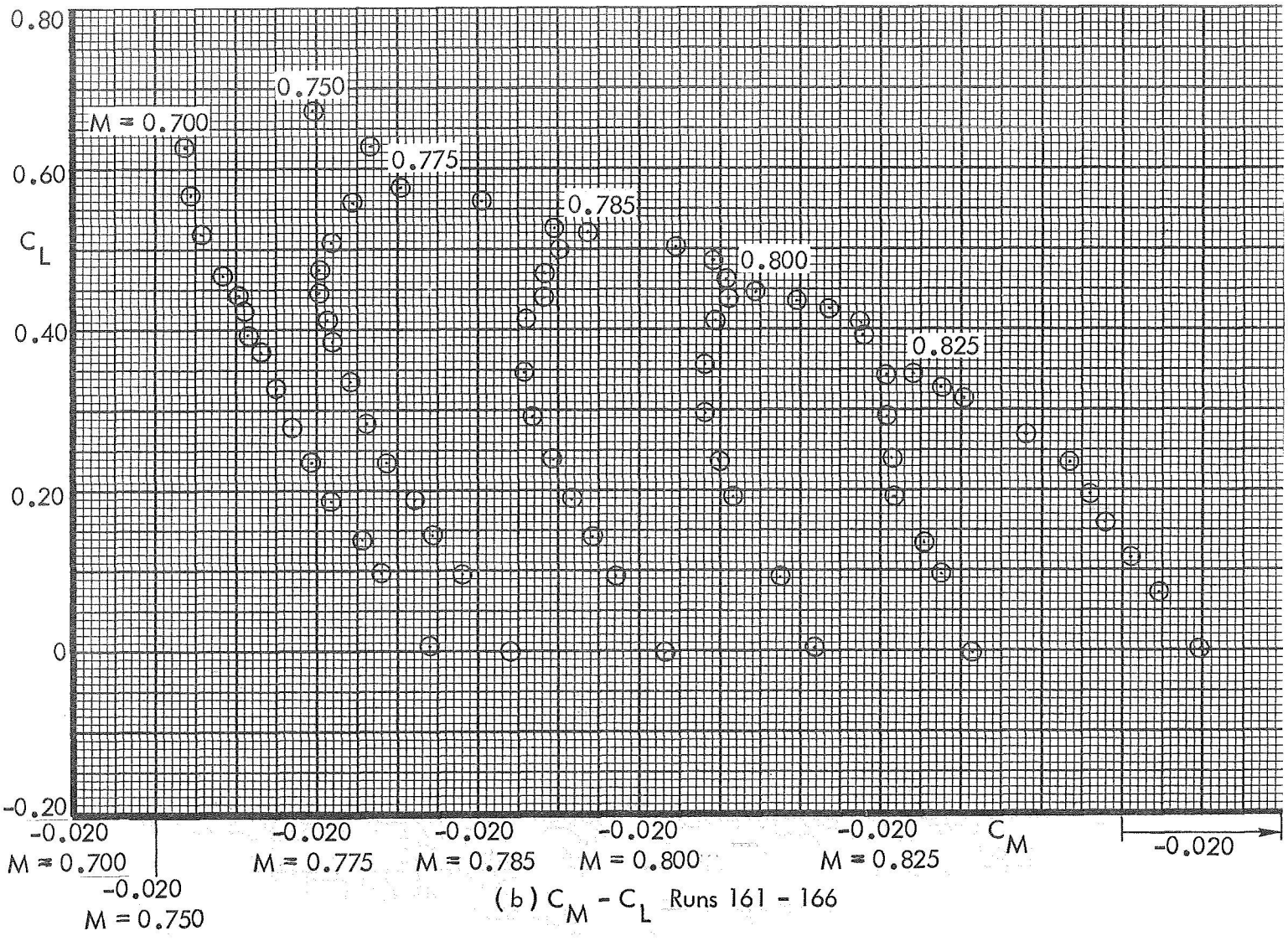
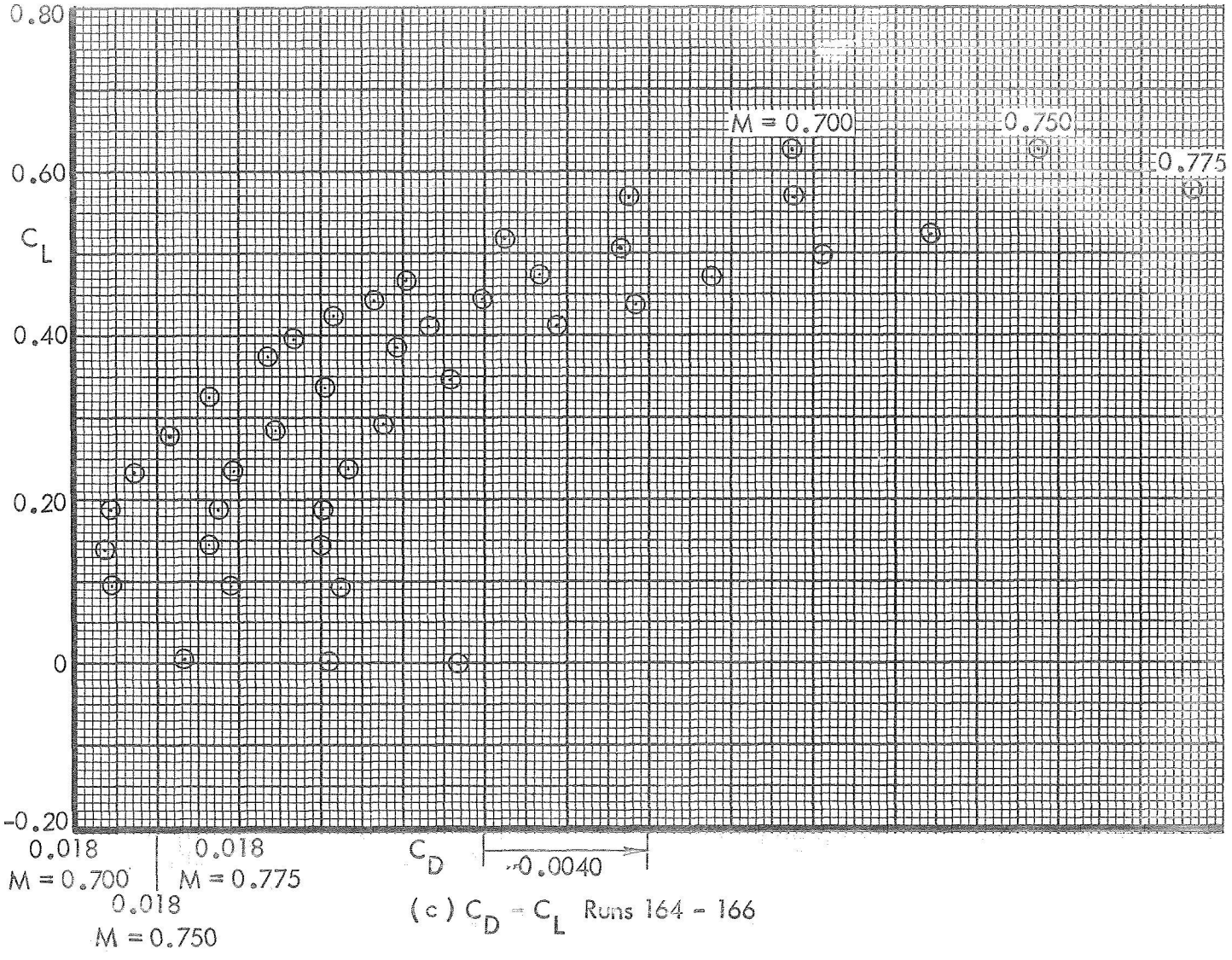
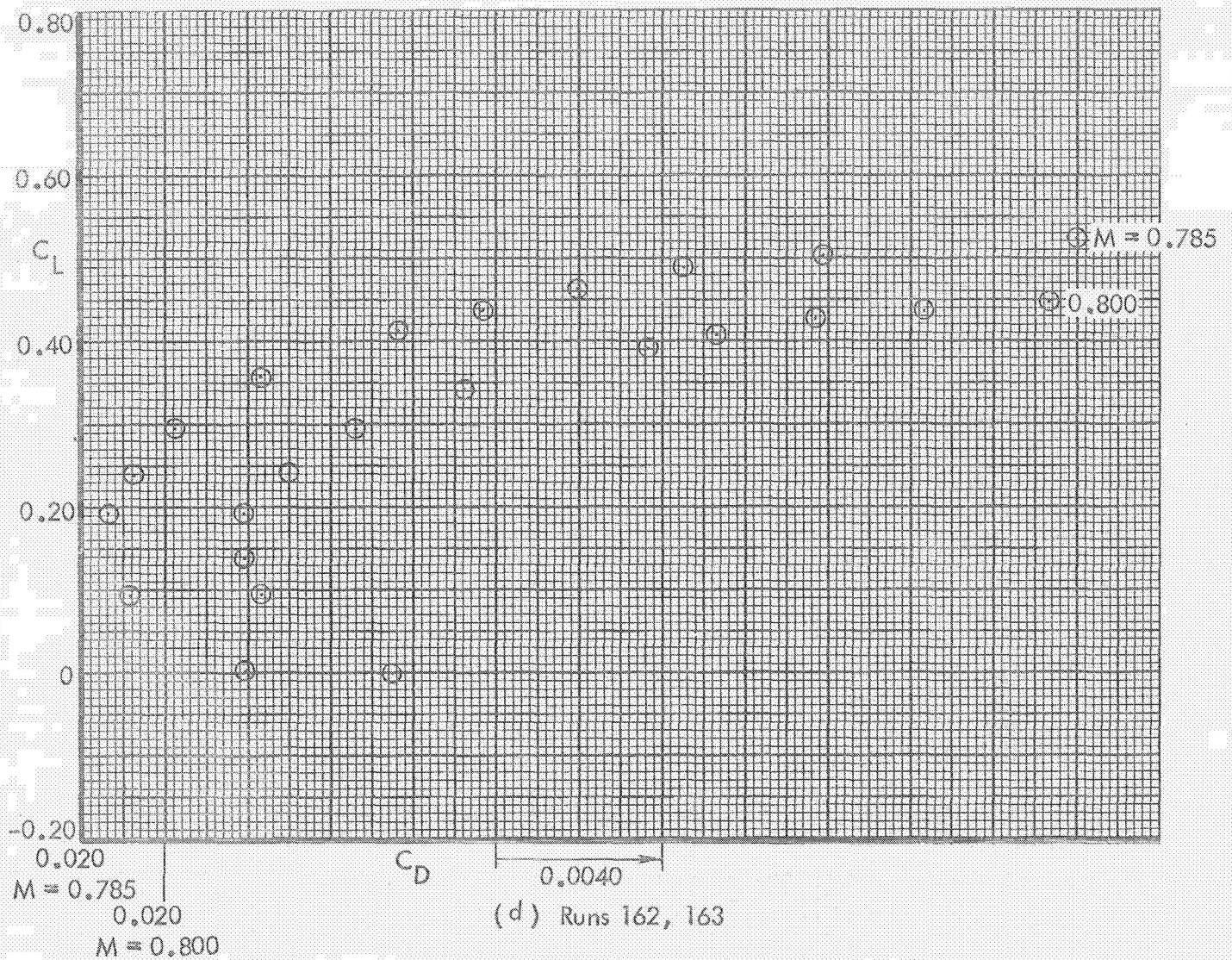


Figure 41. Continued



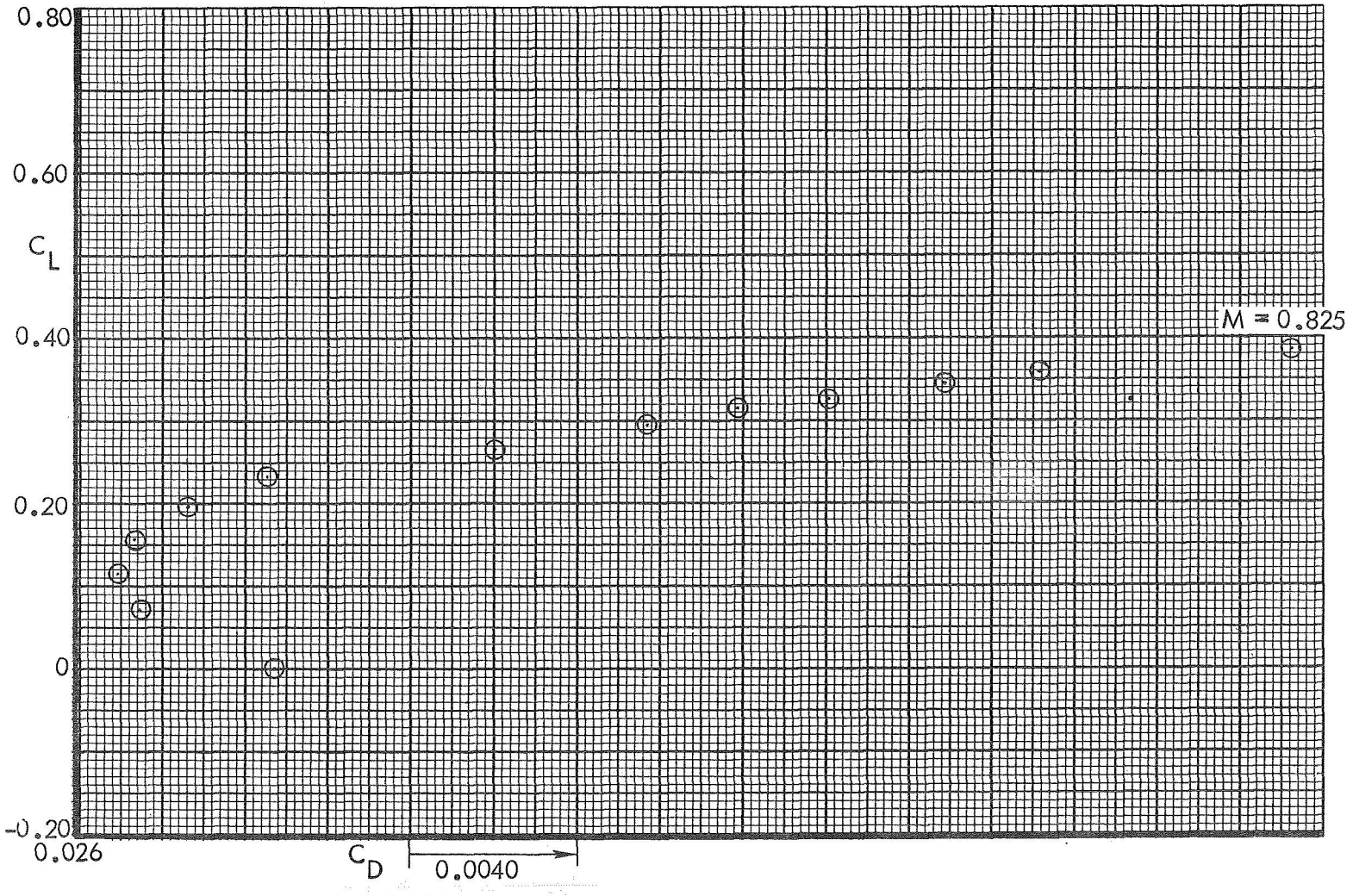
(c) $C_D - C_L$ Runs 164 - 166

Figure 41. Continued



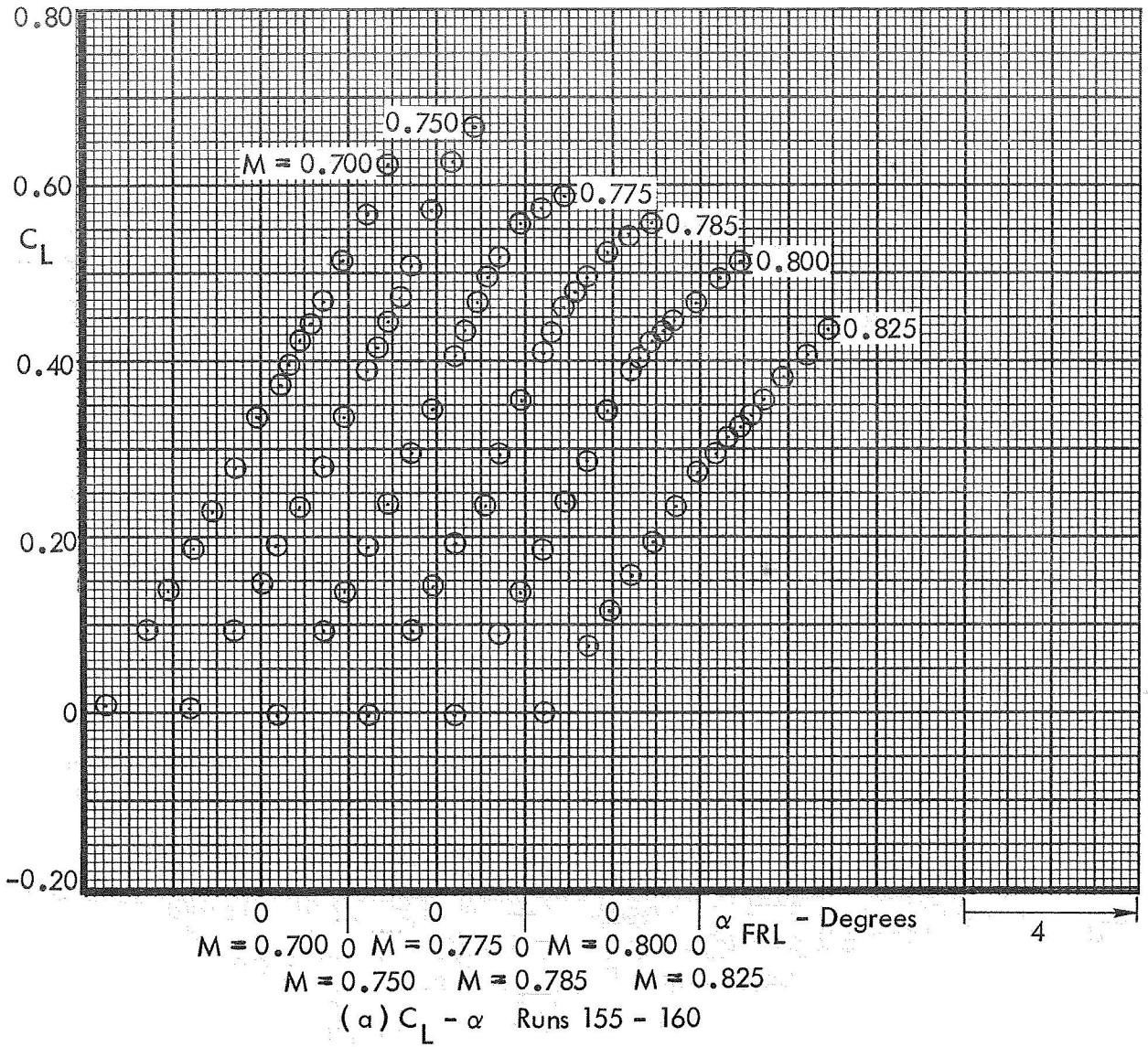
(d) Runs 162, 163

Figure 41. Continued



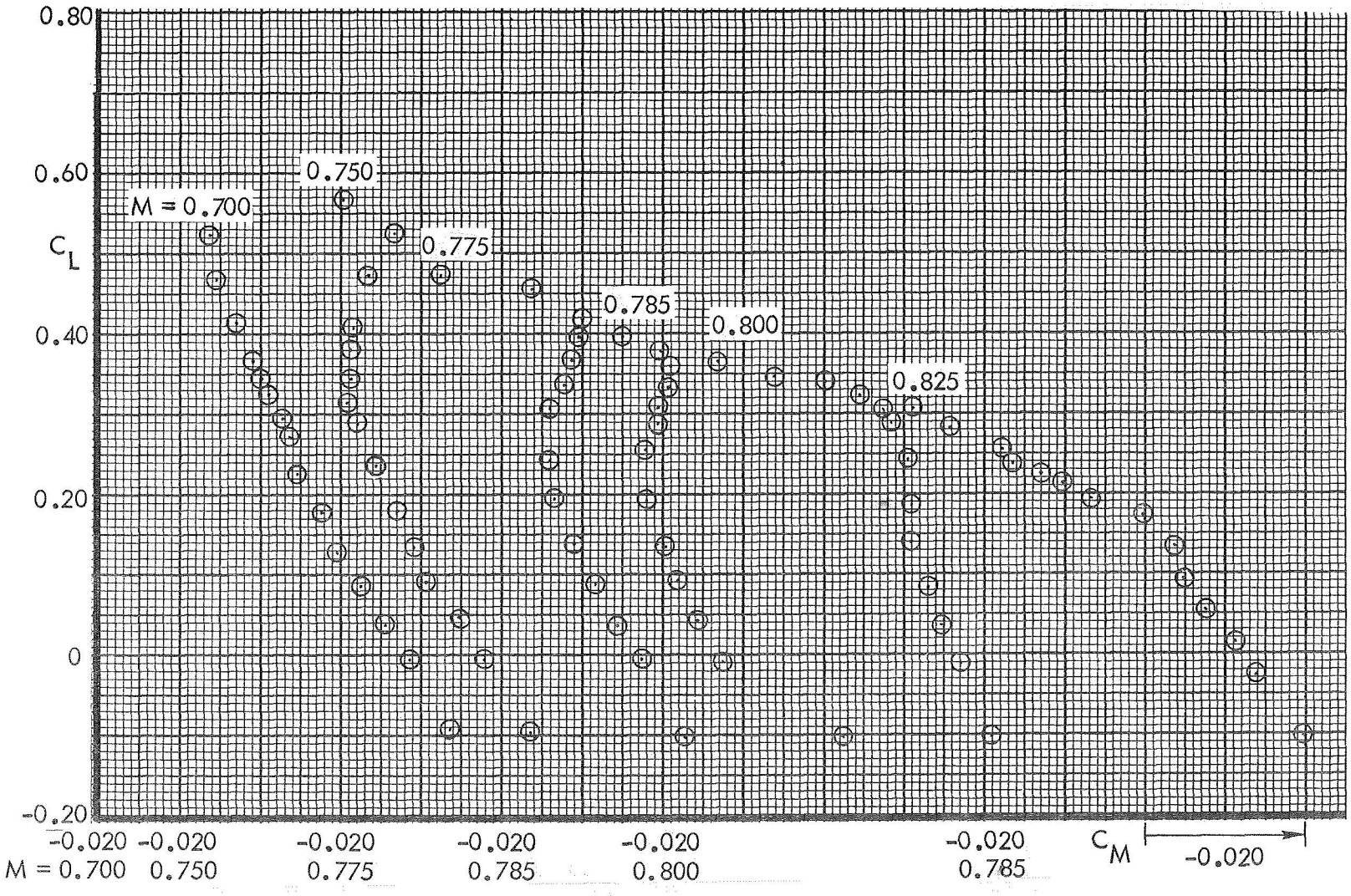
(e) Run 161

Figure 41. Concluded



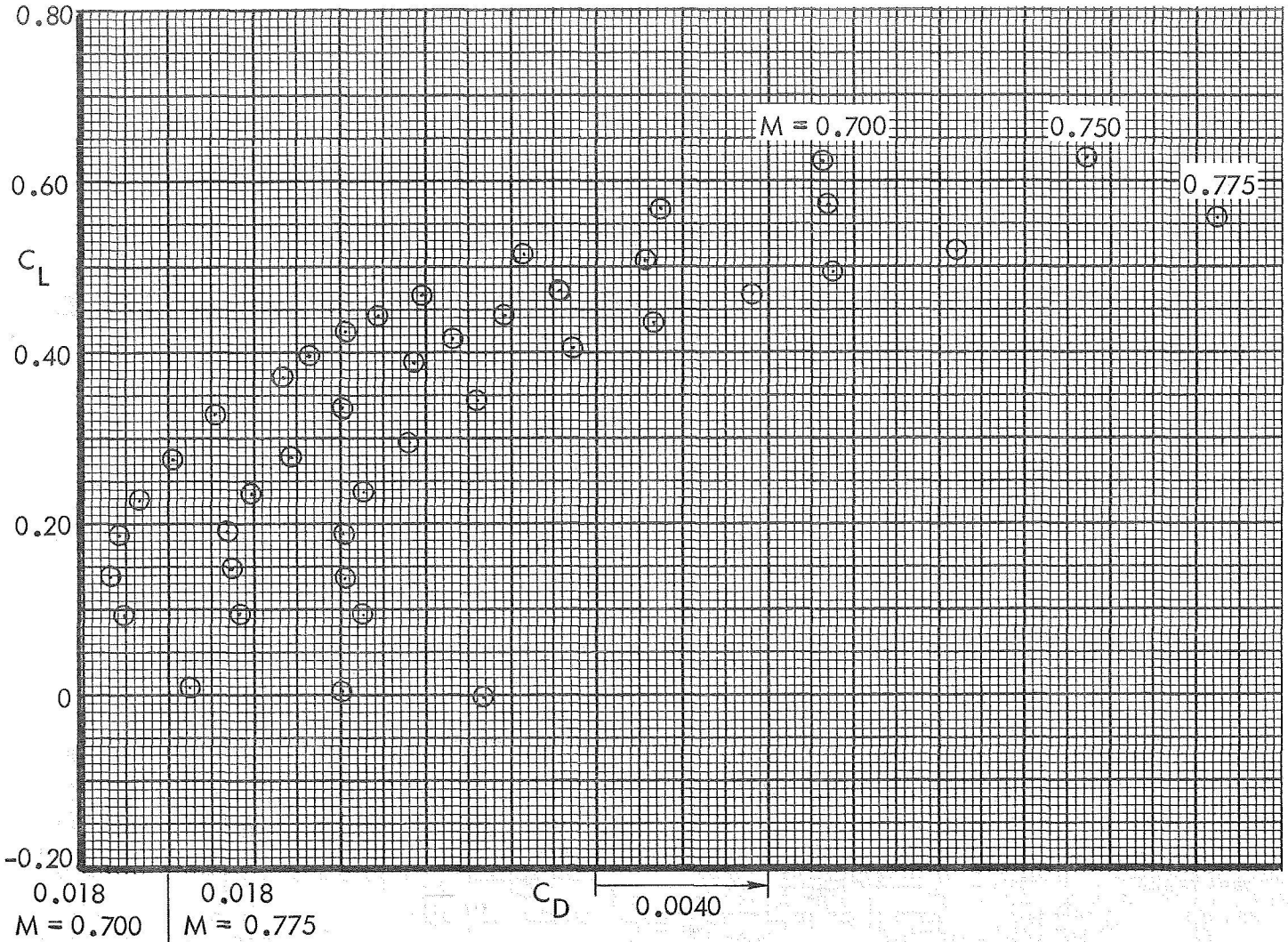
(a) $C_L - \alpha$ Runs 155 - 160

Figure 42. Basic Aerodynamic Data. Tail-off
Sting Configuration 4. Test 617



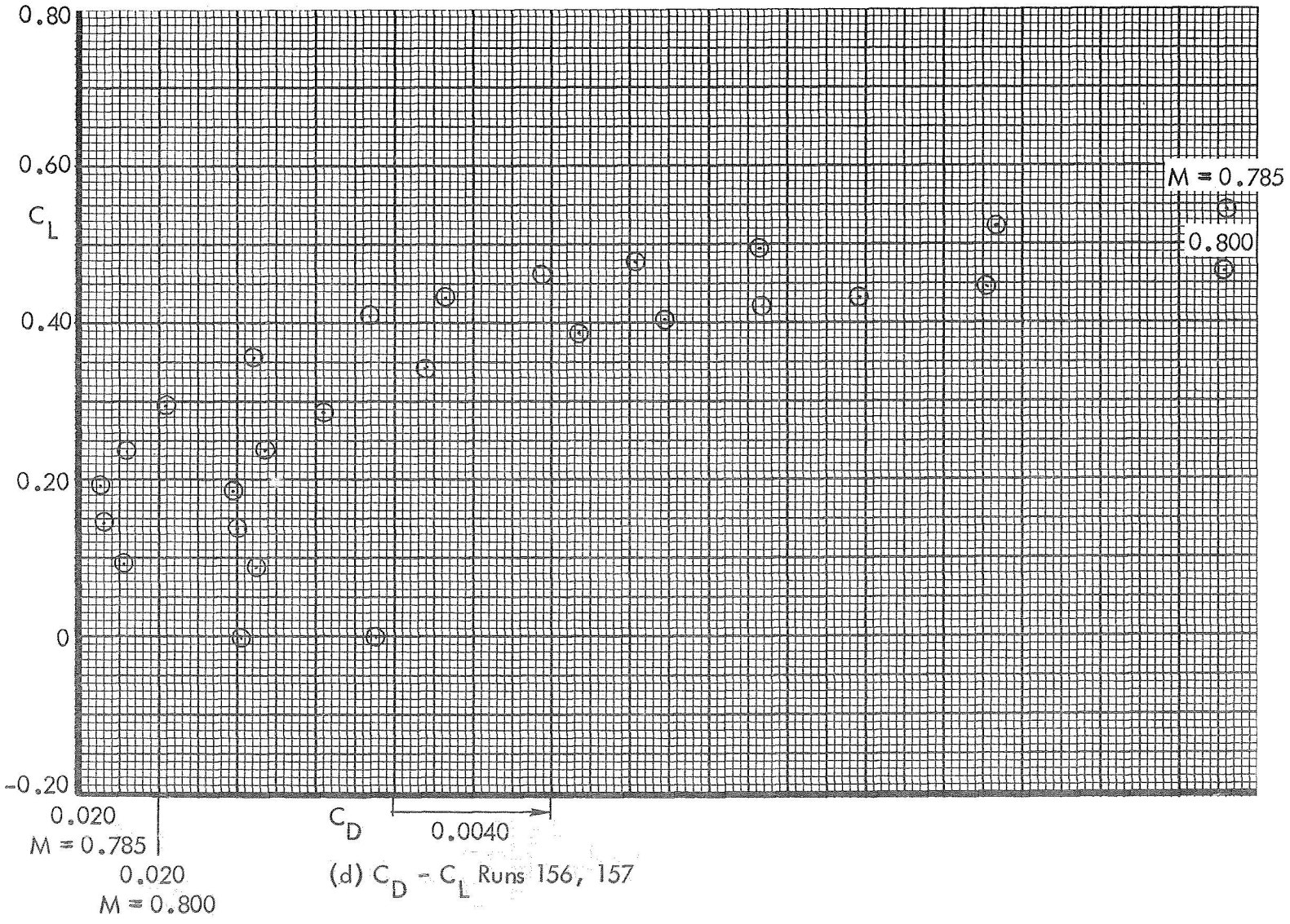
(b) $C_M - C_L$ Runs 155 - 160

Figure 42. Continued



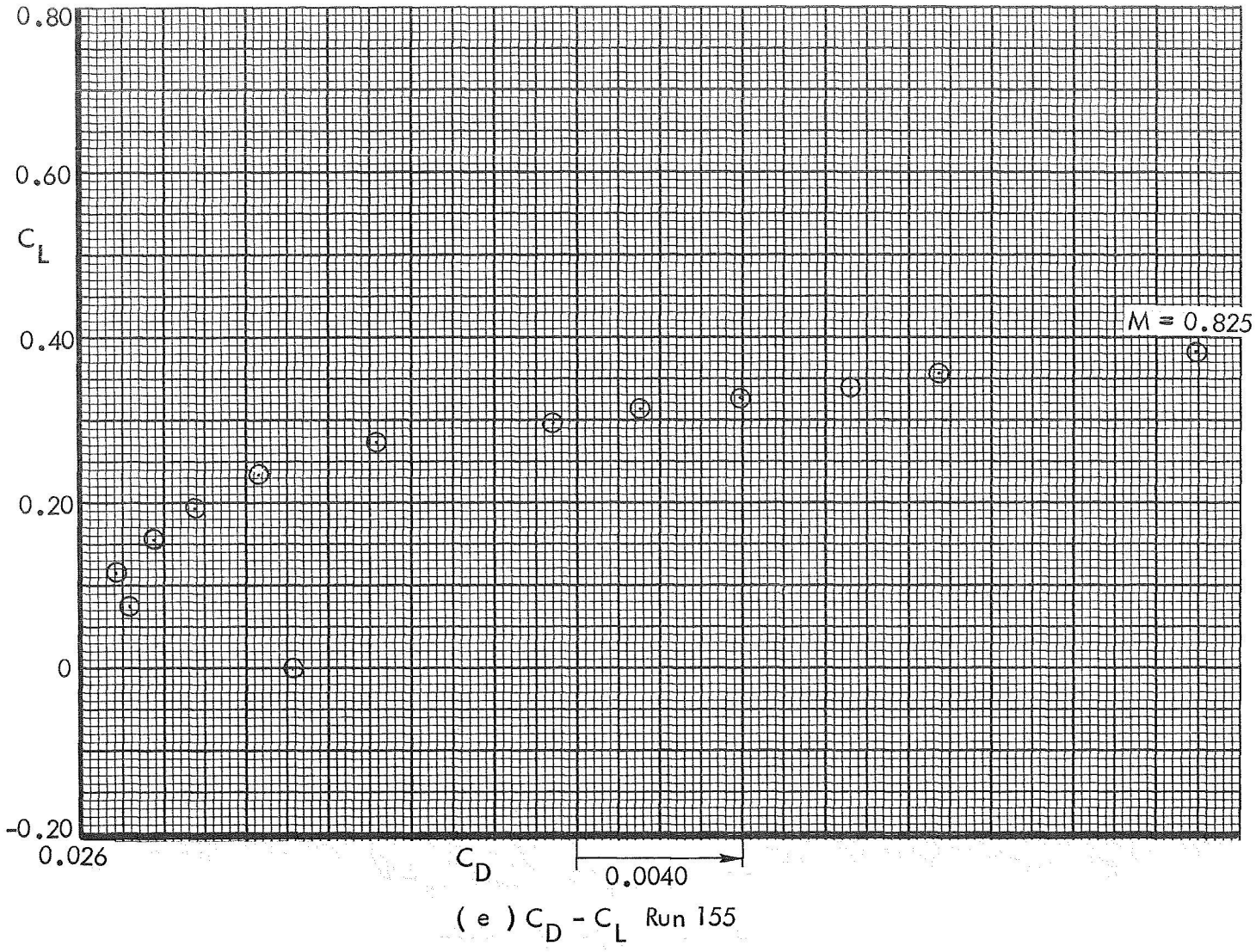
(c) C_D - C_L Runs 158 - 160

Figure 42. Continued



(d) $C_D - C_L$ Runs 156, 157

Figure 42. Continued



(e) C_D - C_L Run 155

Figure 42. Concluded

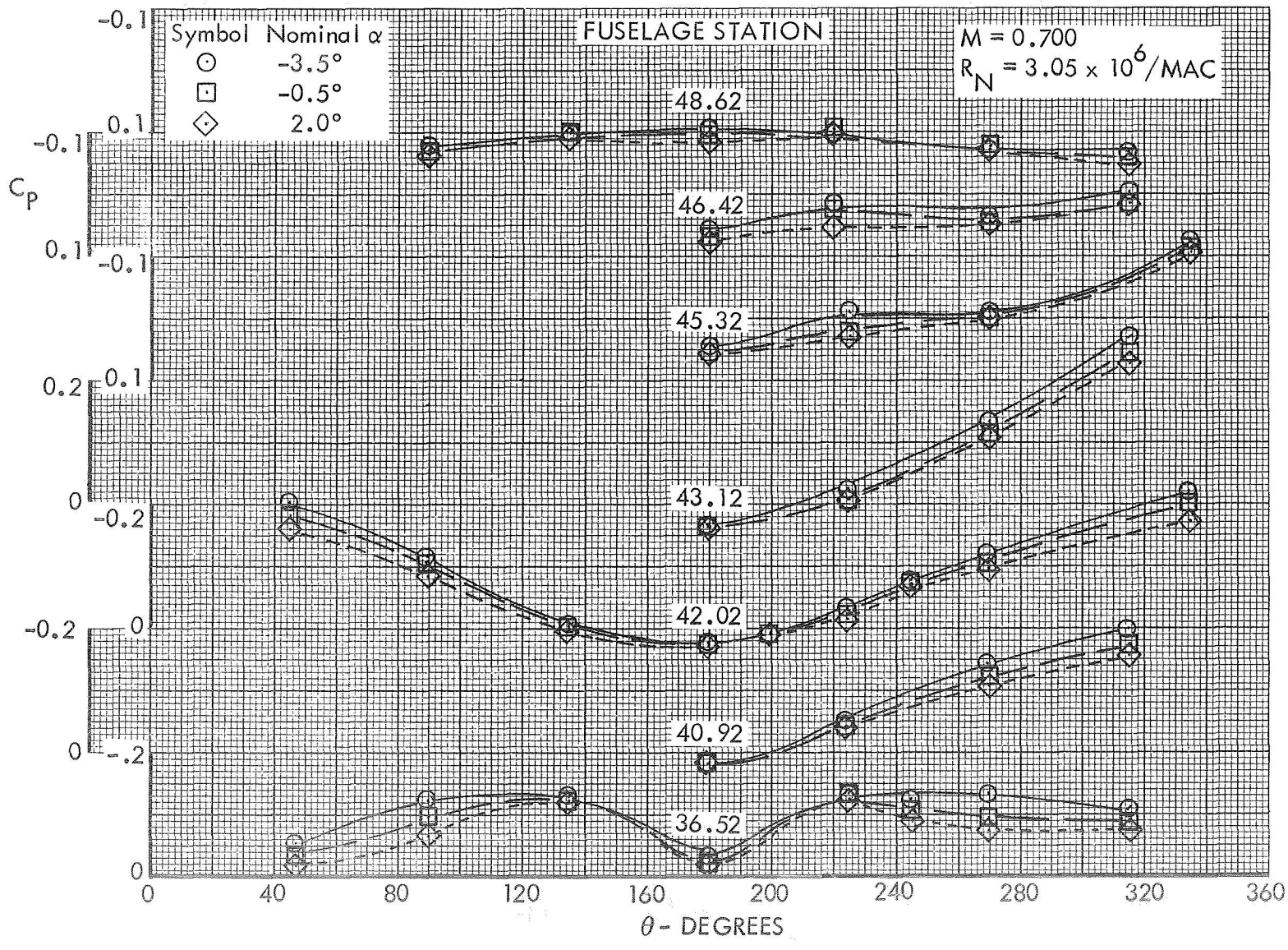


Figure 43. Afterbody Pressures. Test 617, Run 32, Dorsal Mounted with Dummy Lower Blade.

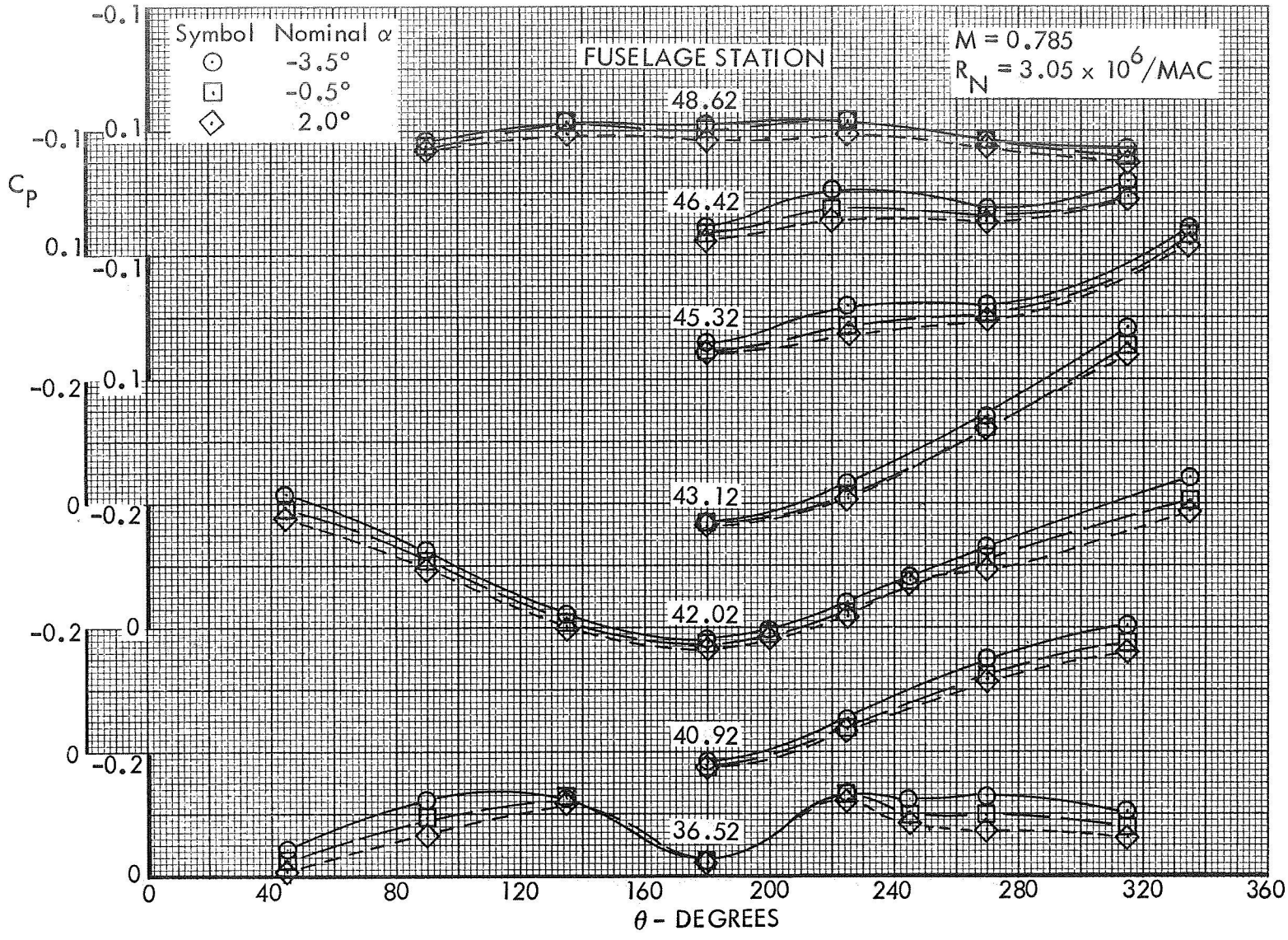


Figure 44. Afterbody Pressures. Test 617, Run 29, Dorsal Mounted with Dummy Lower Blade.

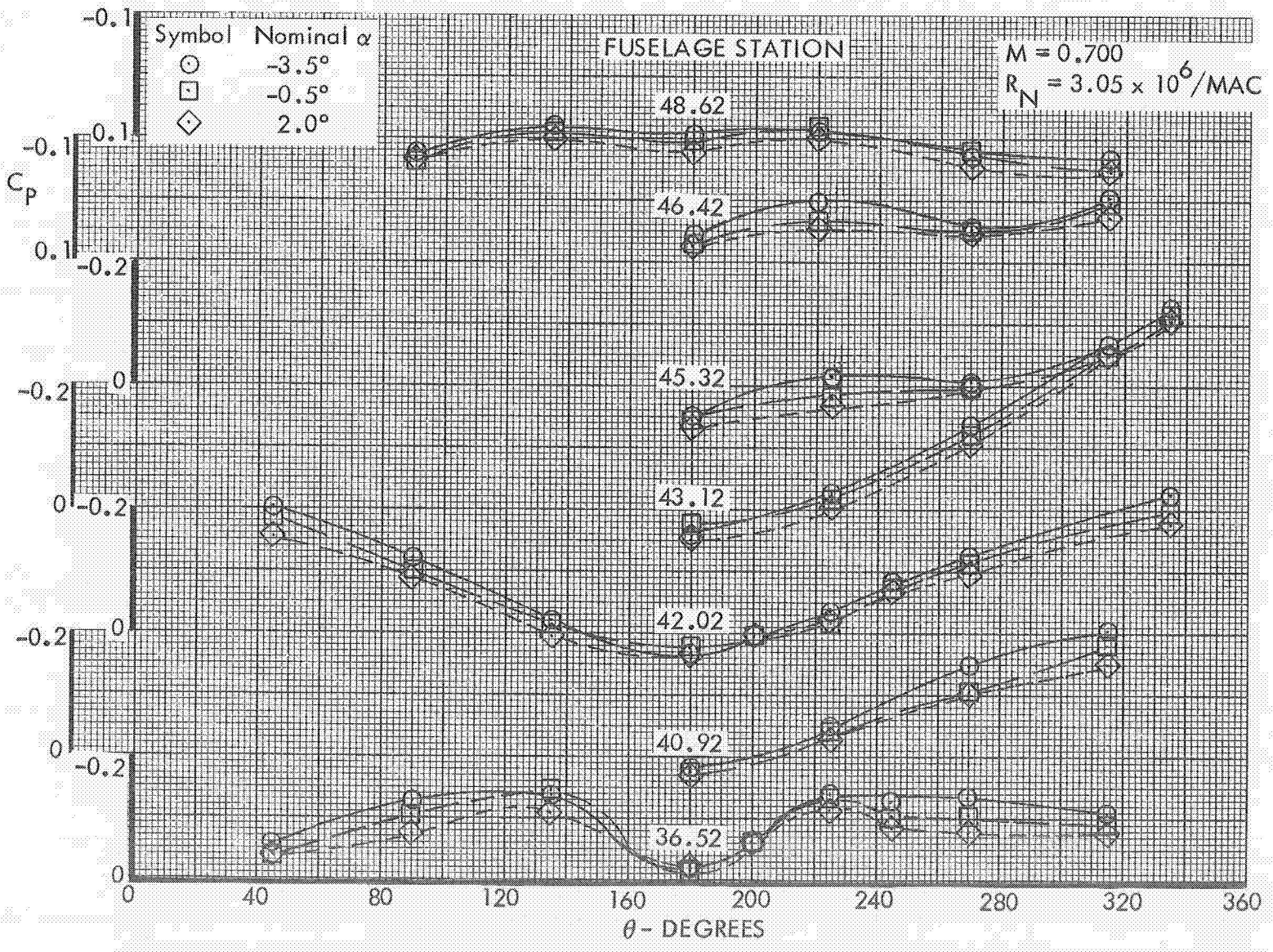


Figure 45. Afterbody Pressures. Test 617, Run 39, Dorsal Mounted with Dummy Lower Sting Only.

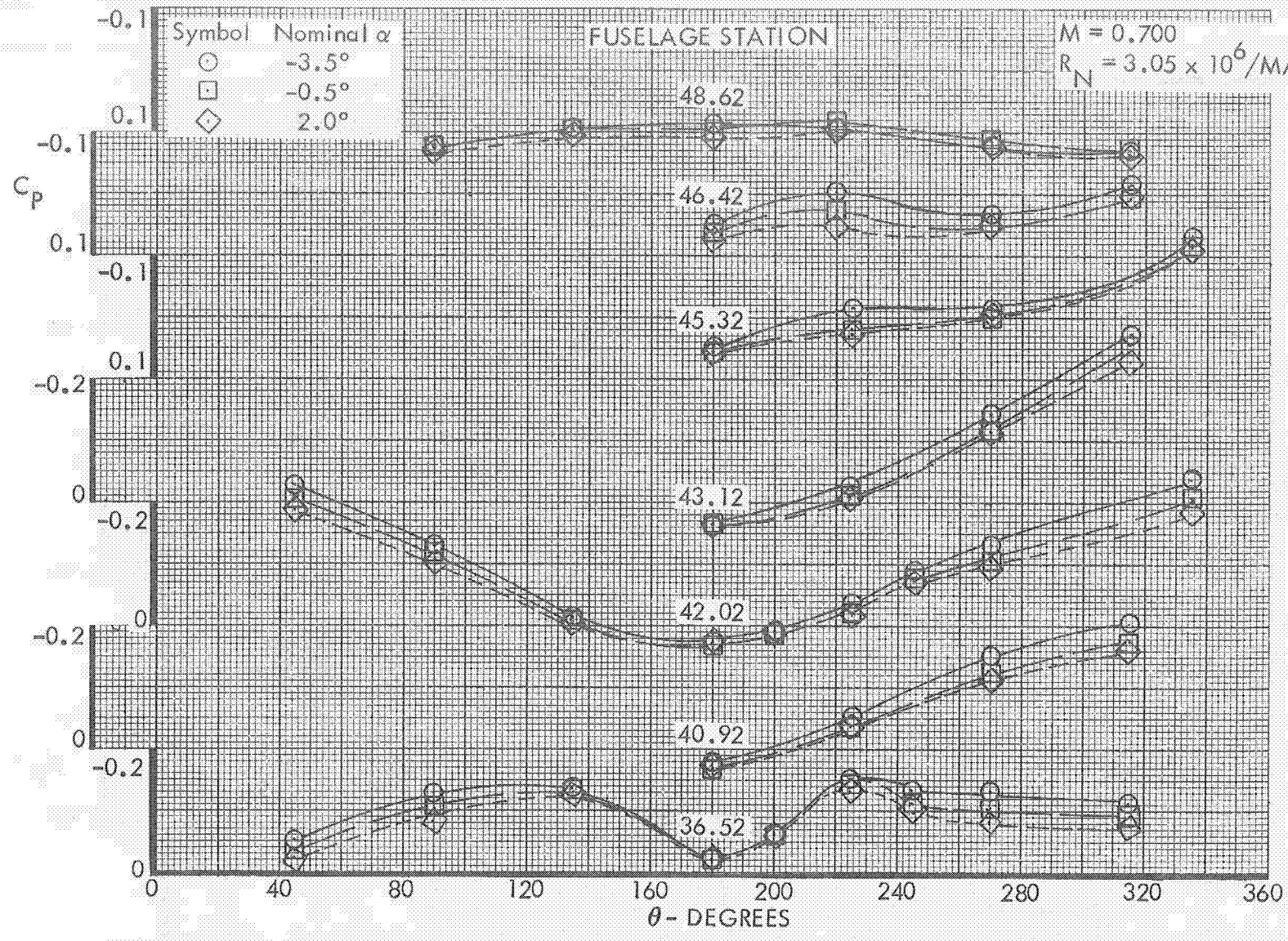


Figure 46. Afterbody Pressures. Test 617, Run 25, Dorsal Mounted with No Lower Dummy Supports.

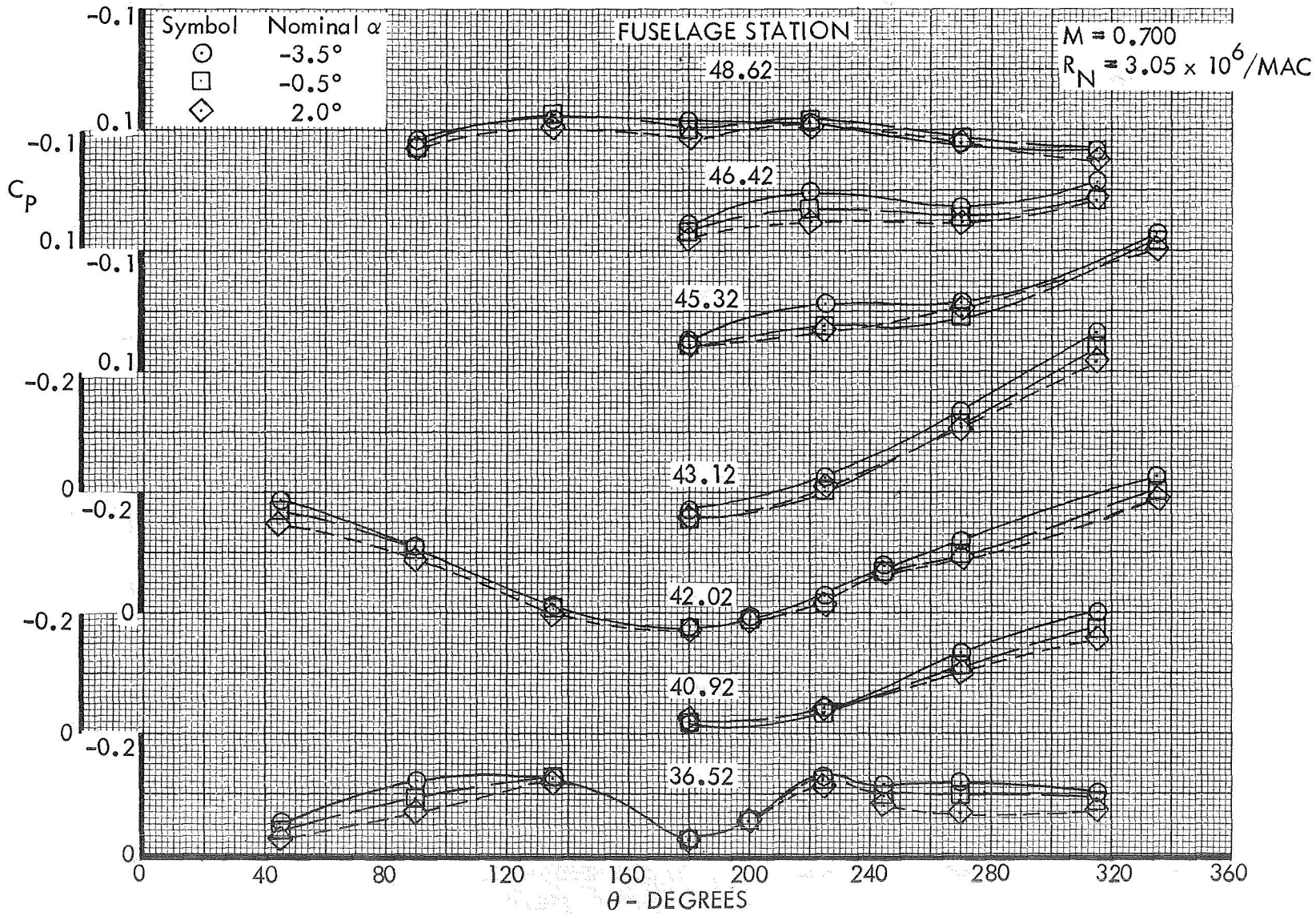


Figure 47. Afterbody Pressures. Test 617, Run 18, Dorsal Mounted with Dummy Lower Blade and Sting.

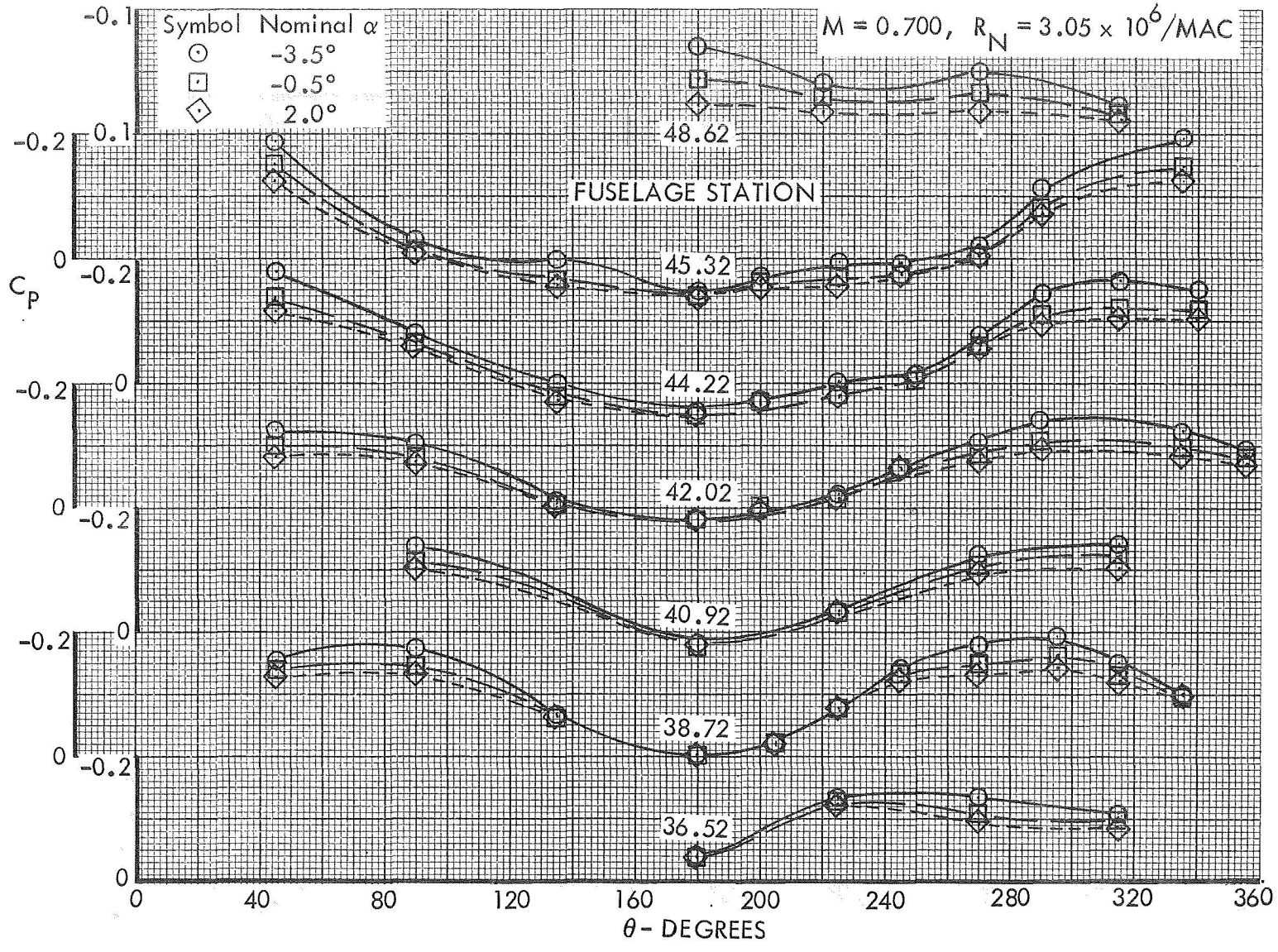


Figure 48. Afterbody Pressures. Test 617, Run 134, Model at Sting Position No. 1

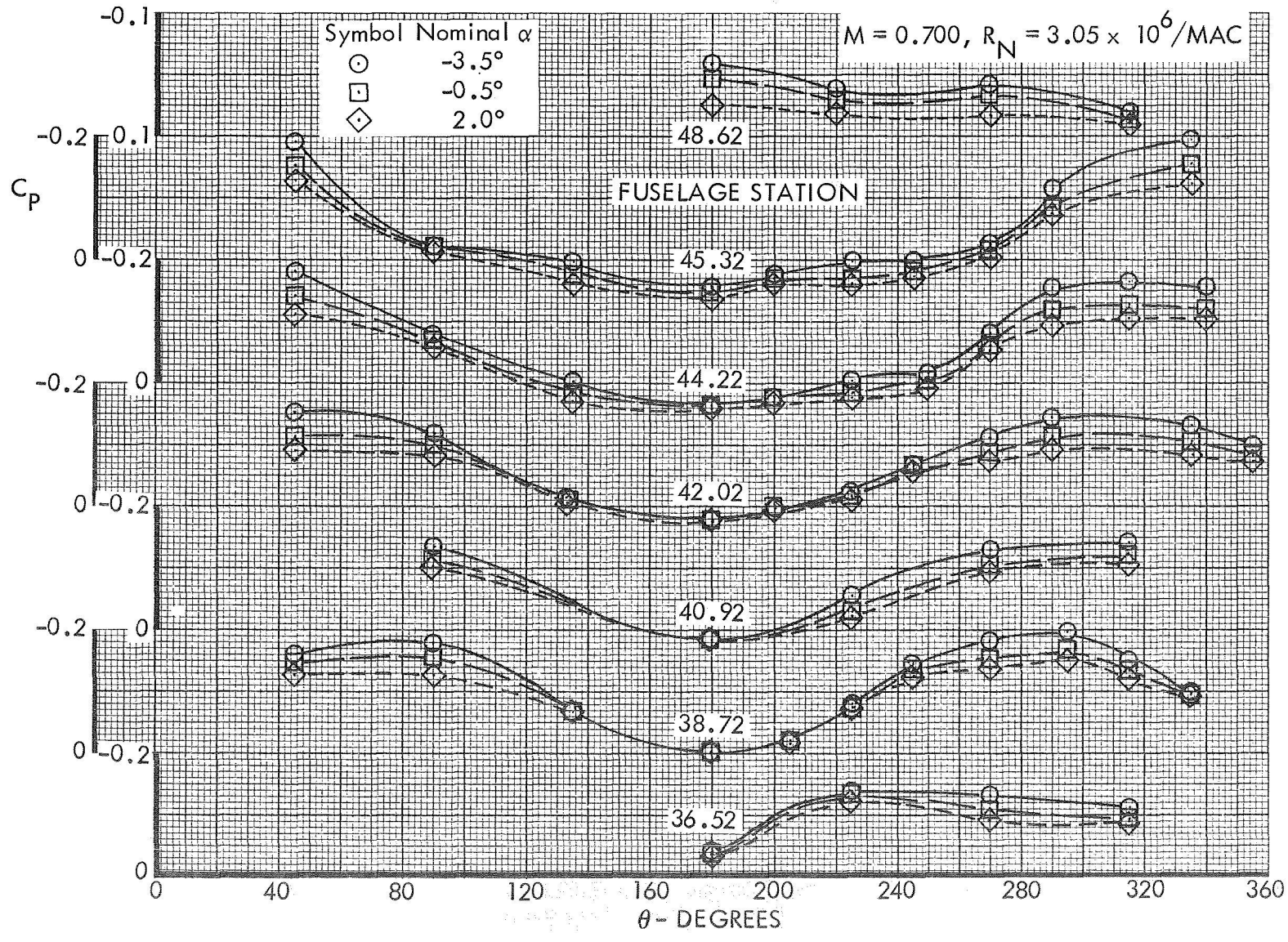


Figure 49. Afterbody Pressures. Test 617, Run 137, Model at Sting Position No. 2

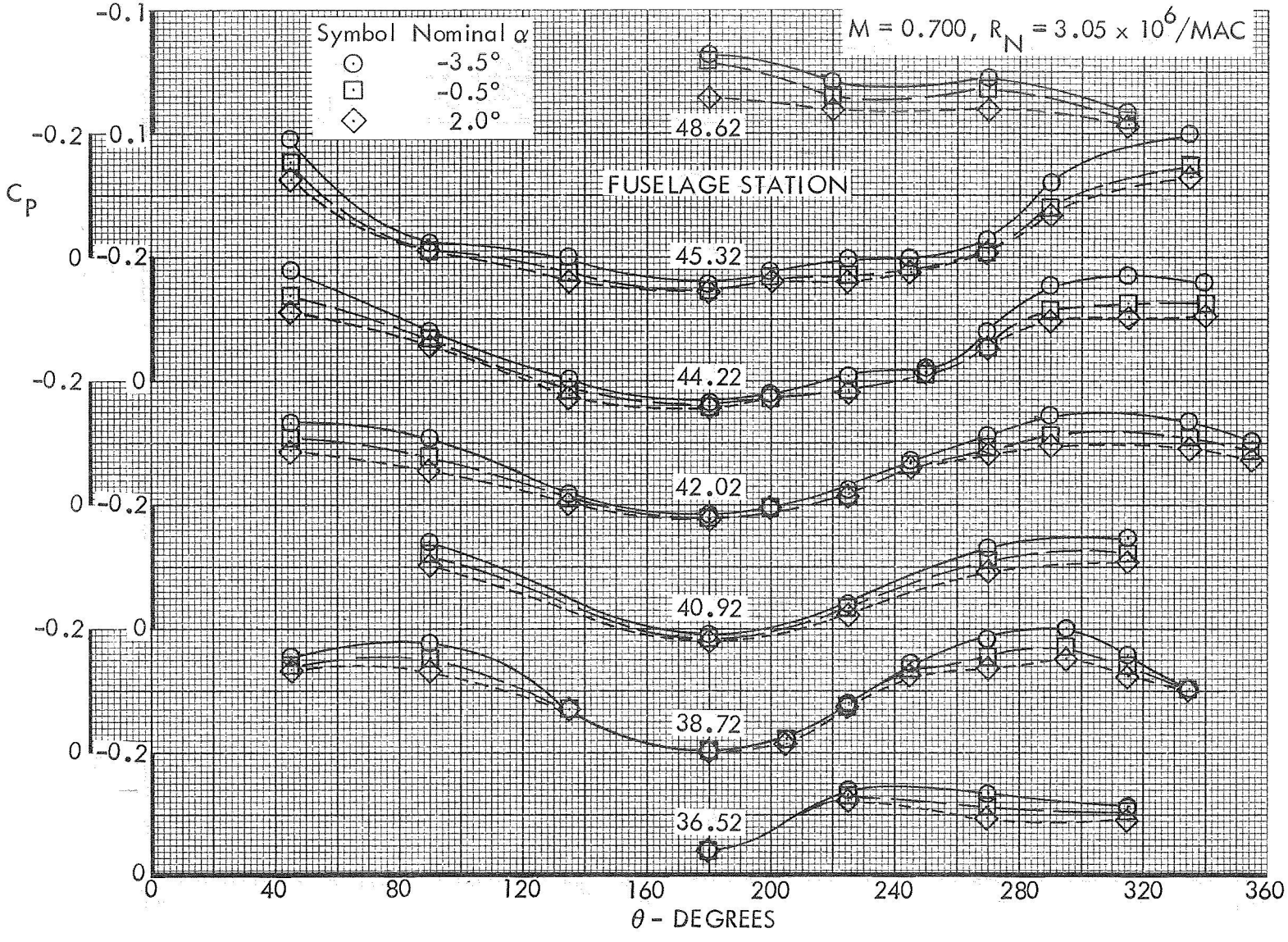


Figure 50. Afterbody Pressures. Test 617, Run 140, Model at Sting Position No. 3

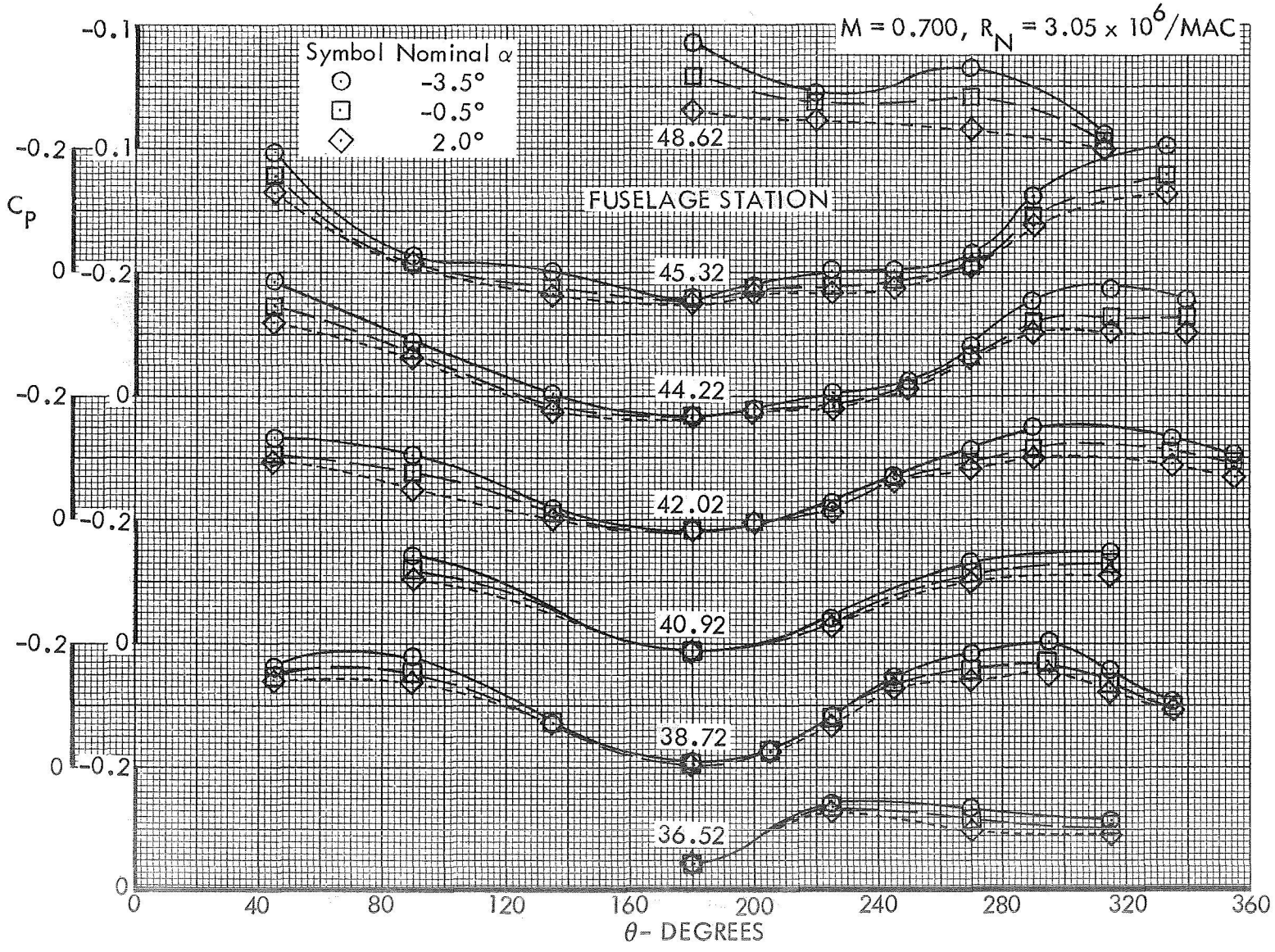


Figure 51. Afterbody Pressures. Test 617, Run 143, Model at Sting Position No. 4.

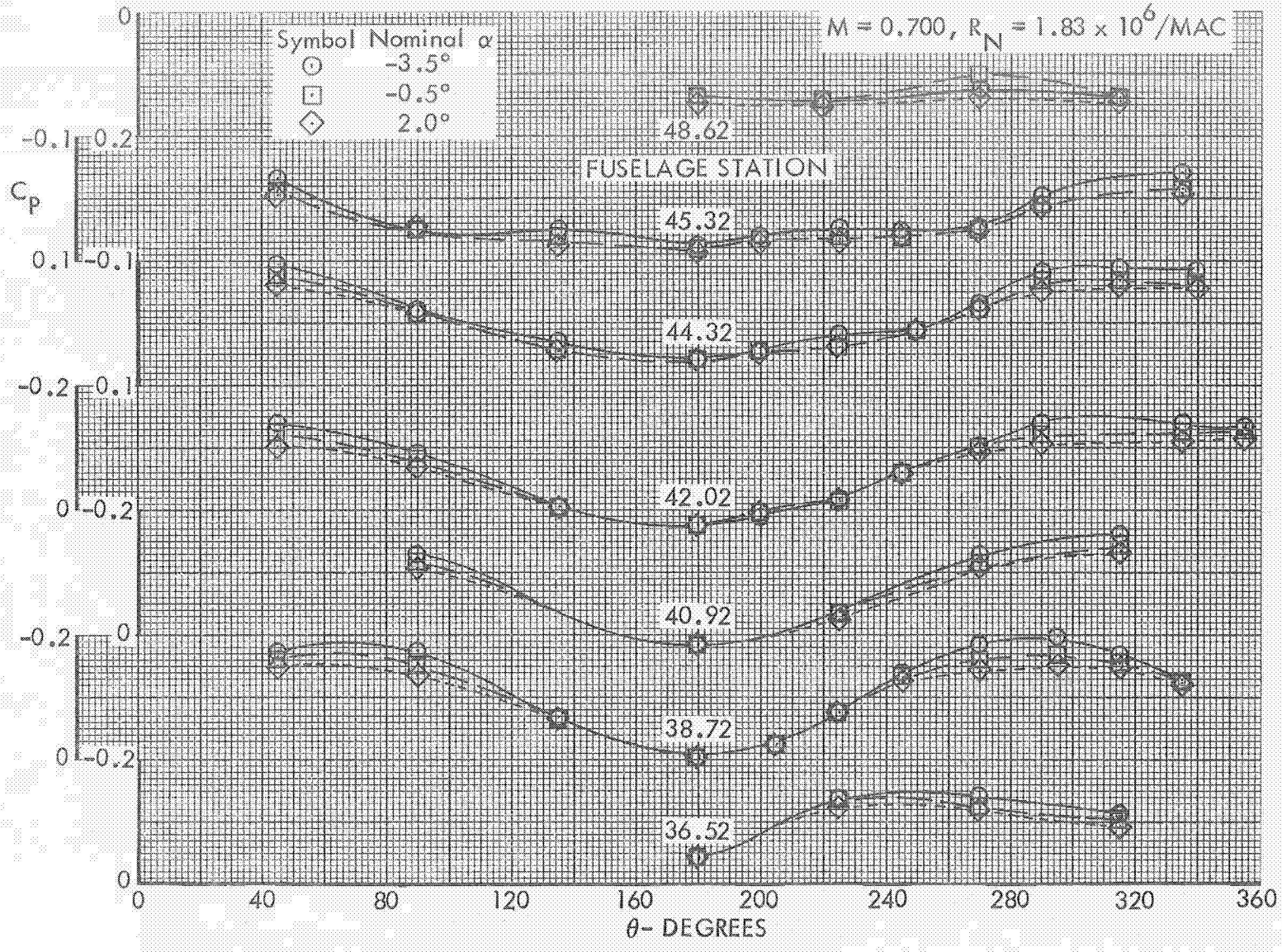


Figure 52. Afterbody Pressures. Test 617, Run 72, Fuselage + Wheel Wells + Wing

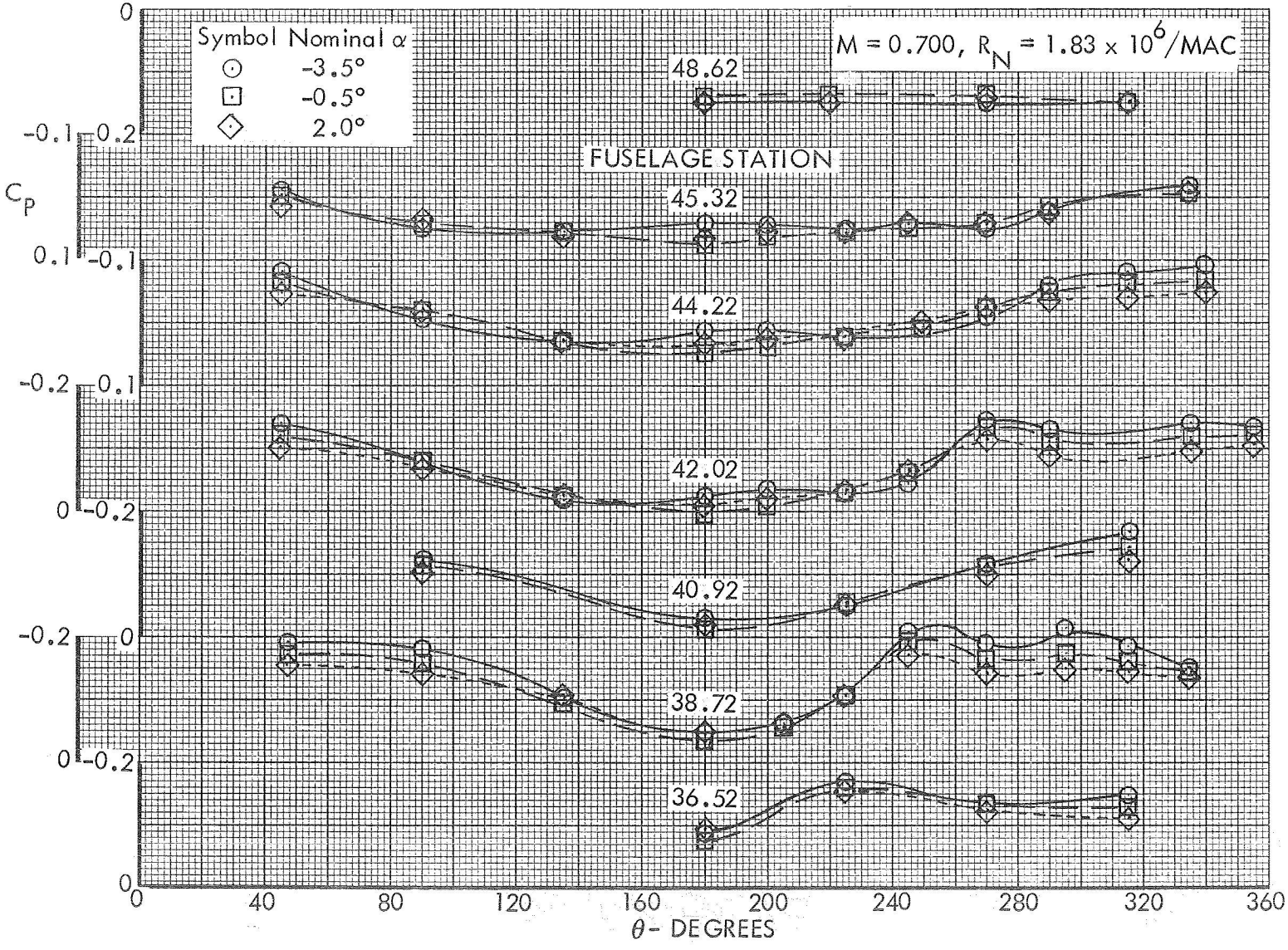


Figure 53. Afterbody Pressures. Test 617, Run 76, Fuselage = Wheel Wells

*U.S. GOVERNMENT PRINTING OFFICE: 1974-739-157/92

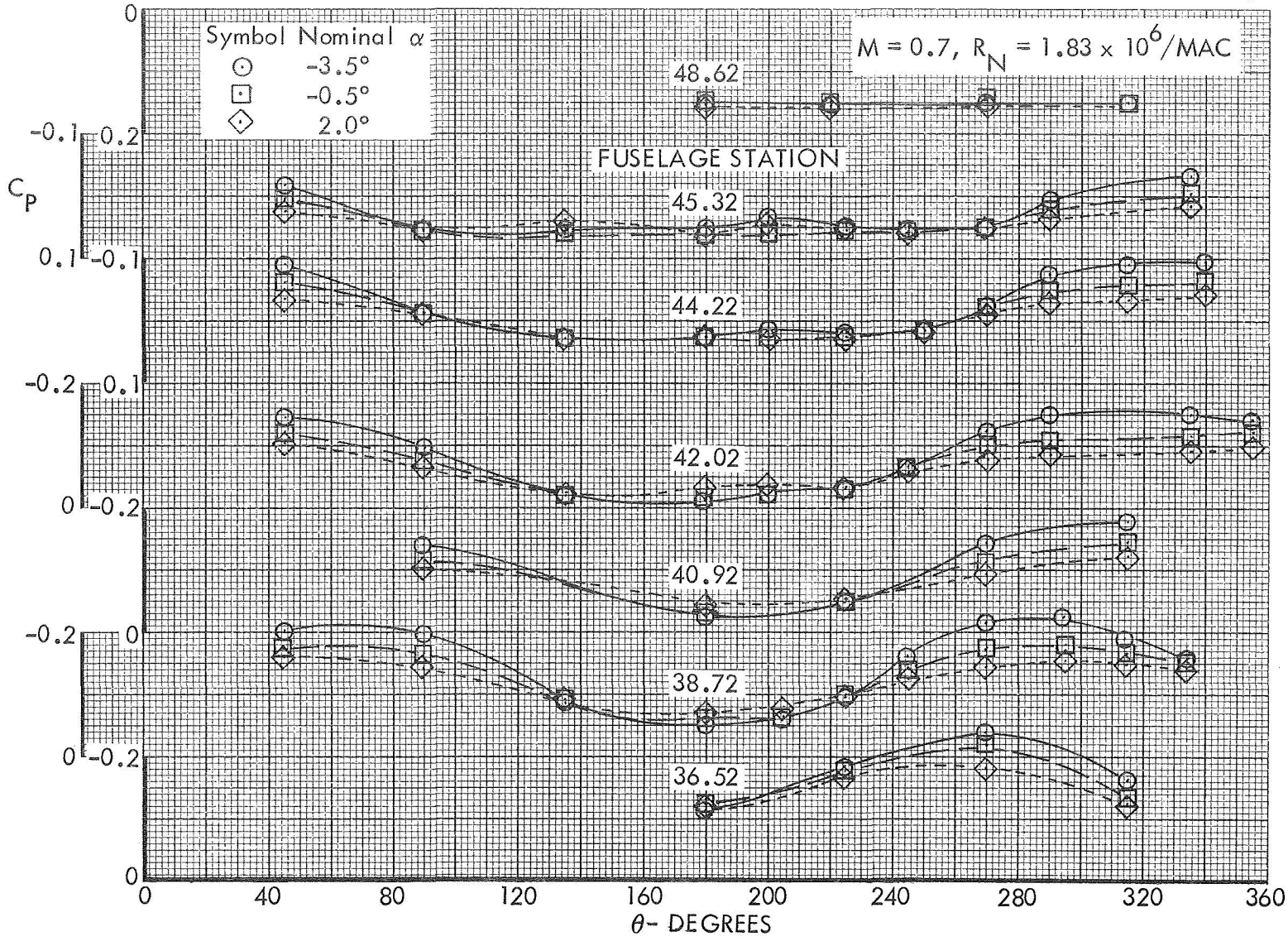


Figure 54. Afterbody Pressures. Test 617, Run 81, Fuselage Alone.

NATIONAL AERONAUTICS AND SPACE ADMINISTRATION
WASHINGTON, D.C. 20546

OFFICIAL BUSINESS
PENALTY FOR PRIVATE USE $300

SPECIAL FOURTH-CLASS RATE BOOK

POSTAGE AND FEES PAID
NATIONAL AERONAUTICS AND SPACE ADMINISTRATION
451

U.S.MAIL

POSTMASTER: If Undeliverable (Section 158 Postal Manual) Do Not Return

"The aeronautical and space activities of the United States shall be conducted so as to contribute . . . to the expansion of human knowledge of phenomena in the atmosphere and space. The Administration shall provide for the widest practicable and appropriate dissemination of information concerning its activities and the results thereof."

—NATIONAL AERONAUTICS AND SPACE ACT OF 1958

NASA SCIENTIFIC AND TECHNICAL PUBLICATIONS

TECHNICAL REPORTS: Scientific and technical information considered important, complete, and a lasting contribution to existing knowledge.

TECHNICAL NOTES: Information less broad in scope but nevertheless of importance as a contribution to existing knowledge.

TECHNICAL MEMORANDUMS: Information receiving limited distribution because of preliminary data, security classification, or other reasons. Also includes conference proceedings with either limited or unlimited distribution.

CONTRACTOR REPORTS: Scientific and technical information generated under a NASA contract or grant and considered an important contribution to existing knowledge.

TECHNICAL TRANSLATIONS: Information published in a foreign language considered to merit NASA distribution in English.

SPECIAL PUBLICATIONS: Information derived from or of value to NASA activities. Publications include final reports of major projects, monographs, data compilations, handbooks, sourcebooks, and special bibliographies.

TECHNOLOGY UTILIZATION PUBLICATIONS: Information on technology used by NASA that may be of particular interest in commercial and other non-aerospace applications. Publications include Tech Briefs, Technology Utilization Reports and Technology Surveys.

Details on the availability of these publications may be obtained from:

SCIENTIFIC AND TECHNICAL INFORMATION OFFICE

NATIONAL AERONAUTICS AND SPACE ADMINISTRATION

Washington, D.C. 20546